Doctorate Program in Molecular Oncology and Endocrinology
Doctorate School in Molecular Medicine

XXVII cycle - 2011–2014
Coordinator: Prof. Massimo Santoro

"Glucose-induced gene expression changes in breast cancer cells: a putative role in Tamoxifen responsiveness"

Maria Rosaria Ambrosio

University of Naples Federico II
Dipartimento di Medicina Molecolare e Biotecnologie Mediche

Administrative Location

Dipartimento di Medicina Molecolare e Biotecnologie Mediche
Università degli Studi di Napoli Federico II

Partner Institutions

Italian Institutions

Università degli Studi di Napoli "Federico II", Naples, Italy
Istituto di Endocrinologia ed Oncologia Sperimentale "G. Salvatore", CNR, Naples, Italy
Seconda Università di Napoli, Naples, Italy
Università degli Studi di Napoli "Parthenope", Naples, Italy

Foreign Institutions

Université Libre de Bruxelles, Bruxelles, Belgium
Universidade Federal de Sao Paulo, Brazil
University of Turku, Turku, Finland
University of Madras, Chennai, India
University Pavol Jozef Šafàrik, Kosice, Slovakia

Supporting Institutions

Dipartimento di Medicina Molecolare e Biotecnologie Mediche, Università degli Studi di Napoli "Federico II", Naples
Istituto di Endocrinologia ed Oncologia Sperimentale "G. Salvatore", CNR, Naples
Istituto Superiore di Oncologia
Regione Campania

Italian Faculty

Francesco Beguinot
Roberto Bianco
Bernadette Biondi
Francesca Carlomagno
Maria Domenica Castellone
Gabriella Castoria
Angela Celetti
Annamaria Cirafici
Annamaria Colao
Gerolama Condorelli
Valentina De Falco
Vittorio De Franciscis
Sabino De Placido
Gabriella De Vita
Monica Fedele
Pietro Formisano
Alfredo Fusco
Fabrizio Gentile
Domenico Grieco
Michele Grieco
Maddalena Illario
Paolo Laccetti
Antonio Leonardi
Paolo Emidio Macchia
Rosa Marina Melillo
Claudia Miele
Nunzia Montuori
Roberto Pacelli
Giuseppe Palumbo
Giovanna Maria Pierantoni
Rosario Pivonello
Giuseppe Portella
Maria Fiammetta Romano
Giuliana Salvatore
Massimo Santoro
Donatella Tramontano
Giancarlo Troncone
Giancarlo Vecchio
Mario Vitale

“Glucose-induced gene expression changes in breast cancer cells: a putative role in Tamoxifen responsiveness”

TABLE OF CONTENTS

LIST OF PUBLICATIONS

This dissertation is based upon the following publications:

1. Ciccodicola A, **Ambrosio MR**, Scarpato M, Costa V. *Non-coding RNA in Neurodegeneration.* Current Translational Geriatrics & Experimental Gerontology Reports, 2012; 1:219-228.

2. Scarpato M, Esposito R, Evangelista D, Aprile M, **Ambrosio MR**, Angelini C, Ciccodicola A, Costa V. *AnaLysis of Expression on human chromosome 21, ALE-HSA21: a pilot integrated web resource*. Database (Oxford), 2014; 25;2014.

3. Aprile M, **Ambrosio MR**, D'Esposito V, Beguinot F, Formisano P, Costa V, Ciccodicola A. *PPARG in Human Adipogenesis: Differential Contribution of Canonical Transcripts and Dominant Negative Isoforms*. PPAR Res. 2014; 2014:537865.

4. D'Esposito V, Passaretti F, Perruolo G, **Ambrosio MR**, Valentino R, Oriente F, Raciti G, Nigro C, Miele C, Sammartino G, Beguinot F, Formisano P. *Platelet-Rich Plasma increases growth and motility of adipose tissue-derived mesenchymal stem cells and controls adipocyte survival and secretory function*. Manuscript in revision.

5. Catanzano O, D'Esposito V, Acierno S, De Caro C, Avagliano C, **Ambrosio MR**, Russo P, Russo R, Miro A, Ungaro F, Calignano A, Formisano P, Quaglia F. *AlginateHyaluronan composite hydrogels promote wound healing process*. Manuscipt in revision.

6. D'Esposito V, Liguoro D, **Ambrosio MR**, Cantile M, Collina F, Beguinot F, Di Bonito M, Franco R, Formisano P. *Glucose-induced ccl5 release by human adipocytes promotes breast cancer invasiveness and distant metastasis.* Manuscript in preparation.

7. Aprile M, **Ambrosio MR**, D'Esposito V, Formisano P, Ciccodicola A, Costa V. *New insights into PPARG regulation: the unexplored impact of alternative splicing on its function*. Manuscript in preparation.

LIST OF ABBREVIATIONS

Ad-MSCs: adipose derived mesenchymal stem cells

AT: adipose tissue

CTGF: connective tissue growth factor

CYR61: cysteine rich 61

DEGs: differentially expressed genes

E_2: estradiol

ER: estrogen receptor

EREs: estrogen responsive elements

hADIPO-CM: adipocyte conditioned medium

HG: high glucose

IGF1: insulin-like growth factor

IGFBP: insulin-like growth factor binding proteins

IL6: interleukin 6

LG: low glucose

NGS: next generation sequencing

RQI: RNA quality indicator

SHBG: sex hormone binding globulin

SVF: stromal vascular fraction

T1D: type 1 diabetes

T2D: type 2 diabetes

TNFα: tumor necrosis factor

4-OHT: 4-hydroxy-tamoxifen

ABSTRACT

Diabetes is one of the most challenging and growing health problems worldwide. Diabetes (mainly type 2; T2D) is an independent risk factor for development of several types of cancer. A great number of epidemiological studies have reported that T2D patients have an increased risk of breast cancer, and up to 16 % of breast cancer patients suffer from T2D or impaired glucose tolerance. The presence of T2D, as cancer-associated comorbidity, is linked to poorer prognosis and survival in breast cancer post-menopausal women. Hyperglycemia, the most important feature of T2D, is known to affect breast cancer cell proliferation. Little is known about the contribution of glucose on breast cancer cell drug resistance. Besides acting on cancer cells, glucose may affect surrounding cells as well as distant cells, which in turn may interfere with anti-cancer drug response. Breast cancer cell growth and/or metastasis predominantly occur as a result of the adipocyte-rich microenvironment in which breast cancer cells are embedded, and reflect a role for adipocytes in tumour maintenance and progression. Adipocytes secrete a variety of adipokines and proinflammatory cytokines that may contribute to drug resistance. Therefore, the aim of this work is to investigate whether and how hyperglycaemia and adipose-derived factors may affect cellular response of breast cancer cell to Tamoxifen, an antagonist of the estrogen receptor (ER), widely used as hormonal treatment of estrogen dependent breast cancer. It was observed that Tamoxifen reduced MCF7 breast cancer (ER^+) cell viability by about 50 % when cells were cultured in glucose concentration corresponding to normal fasting glucose levels in humans (5.5 mM; Low Glucose-LG). Conversely, MCF7 cell sensitivity to Tamoxifen of was 2-fold reduced when cells were cultured in glucose concentration resembling hyperglycaemia in humans (25 mM; High Glucose-HG). Interestingly, shifting MCF7 cells from HG to LG medium restored their drug sensitivity, whereas the shift from LG to HG medium reduced their responsiveness to Tamoxifen. In addition, MCF7 cell response to Tamoxifen in HG medium was worsened in presence of adipocyte-released factors. Notably, RNA-Sequencing revealed that glucose significantly deregulated gene expression and that 70 cell cycle-related genes were significantly down-regulated when MCF7 cells were shifted from HG to LG medium. Among those genes, *CTGF* and *CYR61* were significantly reduced. Consistently, experimental evidences showed that both genes were overexpressed in MCF7 exposed to HG concentrations or to adipocytes released factors in HG concentrations. On the opposite, *CTGF* and *CYR61* gene expression was reduced in MCF7 cells shifted from HG to LG concentrations. Interestingly, *CTGF*, while not *CYR61*, gene silencing significantly increased Tamoxifen sensitivity of MCF7 cells in HG medium. Hence, CTGF may be a novel diabetes associated predictive marker for chemo-sensitivity and may represent a potential therapeutic target to overcome Tamoxifen resistance, improving survival of T2D patients affected by breast cancer.

1. BACKGROUND

1.1 Diabetes

Diabetes mellitus is a group of metabolic diseases characterized by hyperglycemia resulting from defects in insulin secretion, insulin action, or both (Aronson 2008). Several pathogenic processes are involved in the development of diabetes. These range from autoimmune destruction of the β-cells of the pancreas with consequent insulin deficiency to abnormalities that result in resistance to insulin action. Deficient insulin action results from inadequate insulin secretion and/or diminished tissue responses to insulin at one or more points in the complex pathways of hormone action. Impairment of insulin secretion and defects in insulin action frequently coexist in the same patient, and it is often unclear which abnormality, if either alone, is the primary cause of the hyperglycemia. According to the classification recommended by the American Diabetes Association (2008), the vast majority of cases of diabetes fall into two broad etiopathogenetic categories. In one category, type 1 diabetes (T1D), the cause is an absolute deficiency of insulin secretion, making necessary insulin injection for survival. Individuals with increased risk of developing this type of diabetes can often be identified by serological evidence of an autoimmune pathologic process occurring in the pancreatic islets and by genetic markers. In the much more prevalent category, type 2 diabetes (T2D), the cause is a combination of resistance to insulin action in peripheral tissue, an inadequate compensatory insulin secretory response and excessive hepatic glucose production (Harrison 2009). In this category, a degree of hyperglycemia sufficient to cause pathologic and functional changes in various target tissues, but without clinical symptoms, may be present for a long period of time before diabetes is detected. People with T2D are not dependent on exogenous insulin, but may require the hormone for the control of glucose homeostasis if this is not achieved with diet alone or with oral hypoglycaemic agents. The etiology of T2D is multifactorial and genetically based, but it also has strong behavioral components. Several risk factors have been associated with T2D, including family history of diabetes, overweight, unhealthy diet, physical inactivity, increasing age, high blood pressure, ethnicity, impaired glucose tolerance. In addiction, diabetic patients have an increased risk of developing a number of other serious health problems. The chronic hyperglycemia can lead to long-term damage, dysfunction, and failure of various organs especially the eyes, kidneys, nerves, heart, and blood vessels. Therefore, long-term complications of diabetes include retinopathy with potential loss of vision; nephropathy leading to renal failure; peripheral neuropathy with risk of foot ulcers, amputations, and Charcot joints; and autonomic neuropathy causing gastrointestinal, genitourinary, and cardiovascular symptoms and sexual dysfunction. Patients with diabetes have

also an increased incidence of atherosclerotic cardiovascular, peripheral arterial, and cerebrovascular disease. Hypertension and abnormalities of lipoprotein metabolism are often found in people with diabetes. Impairment of growth and susceptibility to certain infections may also accompany chronic hyperglycemia (IDF Diabetes ATLAS 2013). Notably, the metabolic dysregulation and the chronic hyperglycemia associated with diabetes can potentially influence cancer both directly contributing to cancer risk on a molecular level both indirectly affecting cancer because of associated end organ damage that may influence screening and treatment choices, affect treatment toxicities, and lead to worse outcomes (Renehan et al. 2012; Srokowski et al. 2009).

1.2 The global implications of diabetes and cancer

The past two decades have seen an explosive increase in the number of people diagnosed with diabetes worldwide. Pronounced changes in the human environment, and in human behaviour and lifestyle, have resulted in escalating rates of diabetes. The diabetes epidemic relates particularly to T2D, and is taking place both in developed and developing nations (Zimmet et al. 2001). The International Diabetes Federation has projected that the number of people with diabetes in the world will increase from 387 million in 2014 to 592 million in 2035 (Shi and Hu 2014) (Figure 1).

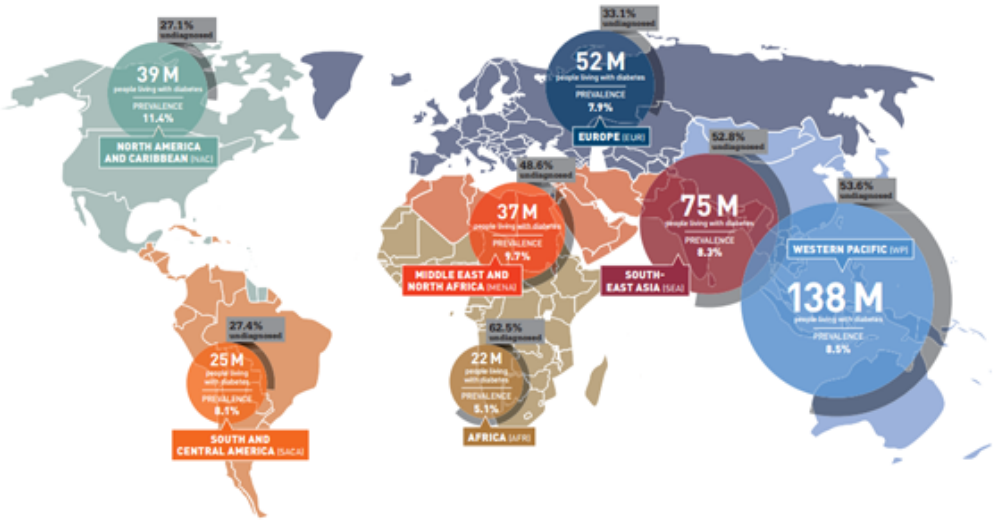

Figure 1: Prevalence of diabetes worldwide (according to the International Diabetes Federation, 2014)

A considerable challenge to the clinical and research communities is the recent surge of attention to the relationship between diabetes and cancer (Johnson and

Pollak 2010). Diabetes and cancer have been closely linked to each other both epidemiologically and biologically. Convincing evidences indicate that diabetes – mainly T2D - is associated with increased risk for developing cancer (Noto et al. 2010; Wotton et al. 2011). Meta-analyses have recognized that T2D increases the risk of site-specific cancers of the bladder (Larsson et al. 2006), liver (El-Serag et al. 2006), colorectum (Larsson et al. 2005), pancreas (Huxley et al. 2005), endometrium (Friberg et al. 2007) and breast (Larsson et al. 2007). Moreover, strong evidence exists about the association between T2D and increased risk of mortality from liver, pancreatic, ovary, colorectum, lung, bladder and breast cancer (Seshasai et al. 2011). In addition to an increase in incidence and mortality, diabetes is associated with an increase in distant metastases in breast cancer patient, as well as with a greater chance of recurrence in lung, colorectum and breast cancer patients (Gallagher et al. 2013). Furthermore, diabetes and cancer are frequently diagnosed in the same individuals, supporting the hypothesis that those two diseases share common risk factors and pathophysiological mechanisms (Ryu et al. 2014).

1.3 Proposed biological mechanisms linking diabetes and cancer

In diabetic patients, cancer may be favored by: i) general mechanisms that promote cancer initiation or progression in any organ because they are due to alterations that affect all tissues, and ii) site-specific mechanisms affecting carcinogenesis of a particular organ (Vignieri et al. 2009). Cancer cells originate from noncancer cells and exhibit very distinctive metabolic hallmarks, such as increased proliferation, survival, invasion and migration, and accumulation of mutations in DNA (Hanahan and Weinberg 2011). Potential biological explanations for the increased cancer risk in the diabetic population concern various i) hormonal, ii) immunological, or iii) metabolic characteristics of the disease and iv) antidiabetic treatments (Figure 2).

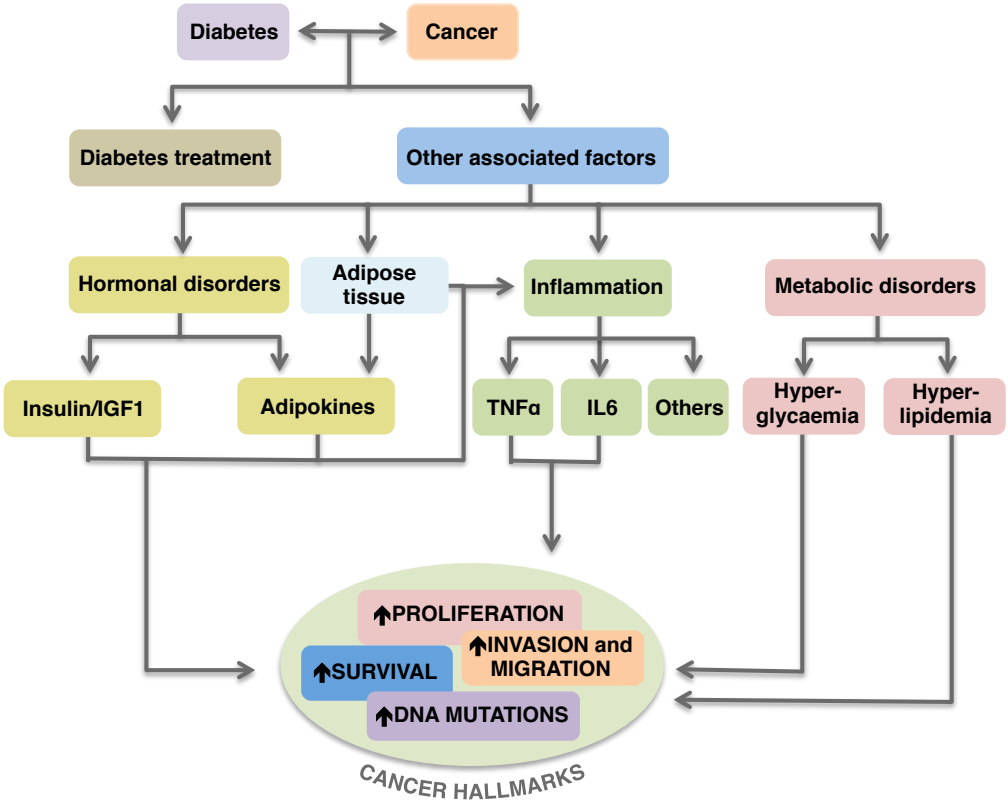

Figure 2: Potential biological link between diabetes and cancer. *Summary of potential biological mechanisms contributing to increased cancer risk in diabetic population. Adapted from García-Jiménez et al. (2013).*

The major **hormonal disorders** occurring in diabetes are hyperinsulinemia and the associated increase in insulin-like growth factor 1 (IGF1) signaling. Hyperinsulinemia develops early in T2D as a physiological response to lower the increasingly high glucose levels in the blood. Insulin is a growth factor that can have direct tumorigenic effect thought activation of insulin receptors in tissues. It might also exert indirect influence thought increased bioactive IGF1, which has potential mitogenic actions on pre-neoplastic and neoplastic cells (Shi and Hu 2014). IGF1 exerts its action by interacting with IGF1 receptor, and this interaction is regulated by a group of specific binding proteins (IGFBPs). IGFBPs have many functions, including the stabilization of a large pool of circulating IGF1 and thus the regulation of IGF1 availability for binding to its receptor (Clemmons 1998). Chronically increased insulin concentrations lead to reduce synthesis and blood levels of IGFBP that in turn determine an increase in free bioavailable IGF1 levels and concomitant changes in cellular environment that promote tumor development (Calle and Kaaks 2004). Moreover, increased insulin and IGF1 concentrations in diabetes down-regulate the production of sex hormone binding globulin (SHBG), which increase free estradiol and testosterone (in women). Increased concentrations

of sex hormones, particularly estrogen, are strongly associated with endometrial and postmenopausal breast cancer (Seshasai et al. 2011). Diabetes is also characterized by unbalanced adipokines secretion (Khandekar et al. 2011) that strongly contributes to **a chronic inflammatory state** (similar to what occurs within the tumor environment) that induces an activation of monocytes and macrophages increasing the circulating inflammatory cytokines and chemokines (McCall et al. 1992). Moreover, in a subset of tumours, cancer growth and/or metastasis predominantly occur as a result of the adipocyte-rich microenvironments in which these tumours are embedded, and reflect a role for adipocytes in tumour maintenance and progression. **Adipocytes** secrete a large variety of adipokines and proinflammatory cytokines that may contribute to cancer phenotypes (Park J et al. 2011). For instance, tumor necrosis factor alpha (TNFα) and interleukin 6 (IL6) have been implicated in the pathogenesis of ovarian, prostate, colon and breast cancer and in the development of breast cancer metastasis by promoting the epithelial-mesenchymal transition (Gallagher et al. 2013). Leptin has been shown to promote proliferation in colorectal, prostate and breast cancer in vitro. In addition, TNFα and IL6 as well as leptin, stimulate estrogen biosynthesis by the way of aromatase induction (García-Jiménez et al. 2013). Moreover, adipocyte released factors provide a chemotactic gradient that attracts monocytes which in turn secrete their own chemokines, attracting additional macrophages and setting up a feed-forward inflammatory process (Osborn and Olefsky 2012). Another aspect of diabetes and cancer' pathophysiology is represented by diabetes-associated **metabolic alterations**, such as increased circulating levels of lipids and sugar represent. Increased levels of triglycerides have been correlated to a higher risk of overall cancer (Borena et al. 2011) and hyperglycemia, the best characterized metabolic alteration in all types of diabetes, has been associated with a higher proportion of patients with active cancer than patients in remission (Feng et al. 2011). Finally, the influence of specific **antidiabetic medications** on cancer risk is an area of active research. Epidemiological studies have reported an increased cancer risk associated with the diabetes medication such as the use of insulin and insulin analogs. Conversely, metformin and thiazolidinediones, which decrease insulin resistance and indirectly circulating insulin levels, have been associated with a decreased incidence of and mortality owing to breast cancer (Seshasai et al. 2011). Thus, the exact mechanisms underlying the relationship between T2D, medications for T2D, and cancer have not been fully elucidated (Onitilo et al. 2012).

1.3.1 Proposed mechanisms relating hyperglycaemia and cancer

Plausible connections between diabetes and cancer consist of hyperinsulinemia, higher levels of IGF1, insulin resistance, chronic inflammation, oxidative stress, and hyperglycemia. All of these factors

potentially promote tumor progression in various ways. Nevertheless, the impact of insulin, IGF1, and chronic inflammation in cancer progression has been extensively studied (Novosyadlyy and LeRoith 2010; Djiogue et al. 2013) whereas effects of hyperglycemia on cancer have received less attention, although hyperglycemia is one of the most widely studied metabolic changes in diabetes (Ryu et al. 2014). Over the last century, cancer patients have been reported to exhibit signs of early glucose intolerance and insulin insensitivity. On the other hand, enhanced glucose uptake is a well-known metabolic hallmark of cancer cells (Hanahan and Weinberg 2011). Thus, the relationship between hyperglycemia and cancer appears bidirectional: cancer can cause hyperglycemia, and hyperglycemia may facilitate cancer appearance and growth. Cancer cells acquire higher proliferation rates and migratory capacity coupled to senescence and apoptosis bypass. Moreover, enhanced angiogenesis in response to factors secreted by the tumor drives the genesis of new blood vessels that increase the supply of energetic substrates and building blocks needed to make new cells (García-Jiménez et al. 2013). The anabolic urge of tumor cells drives them to adapt with profound metabolic changes, among which the most remarkable is the switch from oxidative phosphorylation pathways toward aerobic glycolysis, known since 1956 as the 'Warburg effect' (O'Mahony et al. 2012). The recent resurgence of interest in this hypothesis and cancer energetics emphasizes the dependence of many cancers on glycolysis for energy (Giovannucci et al., 2010), strongly supporting the hypothesis that glucose could be a relevant mediator in the complexity of interactions between diabetes and cancer. The advantage of glycolytic metabolism is the production of glycolytic intermediates that can be used in anabolic pathways that allow synthesis of proteins, nucleic acids, and lipids needed for proliferation. An increase in glucose availability will generally speed up the metabolism, including oxidative phosphorylation. Cancer cells increase their glucose uptake and utilization but keep a reduced oxidative phosphorylation rate that in turn declines ROS production leading to increased cell survival and contributing to sustain pluripotency (García-Jiménez et al. 2013). Thus, hyperglycemia may improve cancer through several cooperative mechanisms (Figure 3), both direct and indirect, that converge on cancer hallmarks.

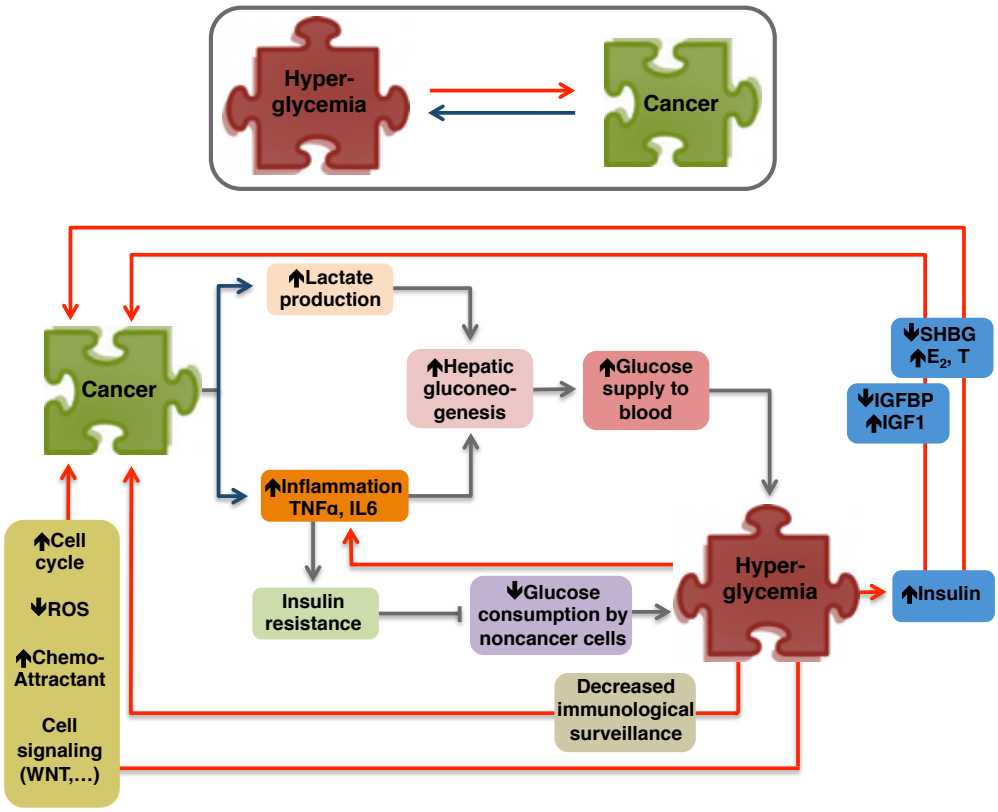

Figure 3: Bidirectional relationship between hyperglycaemia and cancer. *Summary of the bidirectional relationship between hyperglycaemia and cancer: cancer cells ensure high glucose supply (blue arrow) enhanced hyperglycaemia and hyperglycaemia favours tumor growth (red arrow). Adapted from García-Jiménez et al. (2013).*

The **direct effects** of high glucose on tumor cells include: i) increased growth factor signaling and accelerated cell cycle through the change in the expression of critical genes such as *E2F* and *cyclins A* and *E* (Masur et al. 2011), ii) reduced ROS production to ensure survival (García-Jiménez et al. 2013), iii) up regulation of chemo-attractants that promote invasion and migration (Masur et al. 2011) and iv) modified cancer-associated signaling pathways such as WNT signaling (Chocarro-Calvo et al. 2013) (Figure 3). Hyperglycemia also exerts **indirect effects** favouring tumor growth at the organism level: i) increased circulating levels of insulin, that in turn causes the reduction of IGFBP and SHBG synthesis and the increase of bioavailable IGF1, free estradiol and testosterone, ii) reduced immune surveillance, and iii) increased circulating inflammatory cytokines, such as TNFα and IL6, known to cause insulin resistance (Makino et al. 1998) that diminishes glucose consumption (by noncancer cells) thus contributing to hyperglycemia. On the other hand, cancer supports and enhances hyperglycemia in various ways: i) the metabolic switch in cancer cells drives increased glycolytic flux and lactate production, ii) tumor

growth induces an acute inflammatory response with increased production of inflammatory cytokines. Both the inflammatory state and the increased production of lactate increase hepatic glyconeogenesis. The reduced uptake of glucose from the blood and the increase supply from the liver strongly contribute to hyperglycemia (García-Jiménez et al. 2013).

1.3.2 Hyperglycaemia and breast cancer

Breast cancer is the most common female malignant neoplasia with the highest incidence in the industrialized world (Maccio et al. 2009). A great number of cohort (Weiderpass et al. 1997; Wideroff et al. 1997; Michels et al. 2003; Coughlin et al. 2004; Silvera et al. 2005) and case–control studies (Talamini et al. 1997; Baron et al. 2001) have reported that patients with T2D have an increased risk of breast cancer (Larsson et al. 2007), and up to 16 % of breast cancer patients suffer from T2D or impaired glucose tolerance (Coebergh et al. 1999; Yancik et al. 2001). A number of epidemiological studies have also shown a direct association between breast cancer risk and the consumption of sweet foods with high glycaemic index (Lubin et al. 1981; Landa et al. 1994; Potischman et al. 2002; Tavani et al. 2006). Of note, animal models of diabetes have shown an increase in susceptibility to chemically induced mammary tumours (Shafie and Grantham 1981). Moreover, breast cancer is the fifth most common cause of cancer death in women (Yi et al. 2013). It has been provided evidence that high carbohydrate intake is associated with poorer survival after diagnosis for early breast cancer (Krone and Ely 2005). Consistently, cancer mortality is geographically correlated with the level of dietary sugar intake; countries with the greatest sugar intake exhibit the highest rates of breast cancer mortality independent of other variables (Carroll 1977; Hems 1978). Although breast cancer is the most common cancer form in women (Youlden et al. 2012), and a numbers of studies strongly support the association of diabetes with an higher risk and a poor prognosis in women with breast cancer (Zeng et al. 2010), the direct or indirect effects of glucose on cancer cell is relatively unexplored, and more needs to be learned about which signaling pathways are involved and how they are controlled (Ryu et al. 2014).

1.4 The emerging role of tumor microenvironment

Cancers are not just masses of malignant cells but complex ‘rogue’ organs, to which many other cells are recruited and can be corrupted by the transformed cells. Interactions between malignant and non-transformed cells create the tumor microenvironment (Balkwill et al. 2012). The bidirectional communication between cells and their microenvironment is critical for both

normal tissue homeostasis and tumor growth. In particular, interactions between tumor cells and the associated stroma represent a powerful relationship that influences disease initiation, progression and patient prognosis (Quail and Joyce 2013). In cancer, the coordinated intercellular interactions present in normal adult tissues are disrupted as the tumor acquires the capacity to chronically circumvent normalizing cues from the microenvironment, and in turn, the microenvironment evolves to accommodate the growing tumor Thus, the non-malignant cells of tumor microenvironment have a dynamic and often tumor-promoting function at all stages of carcinogenesis (Bissell and Hines 2011). However, the complexity of the interactions between neoplastic tumor cells and their microenvironment has become increasingly apparent, and at the same time, the number of agents entering clinical trials that specifically target interactive pathways between neoplastic and stromal cells has increased (Balkwill et al. 2012). About breast, it is a very heterogeneous tissue, characterized by a number of different cell types. Epithelial cells make up the parenchyma of the tissue, forming the ducts and glands involved in milk production, storage, and secretion. However, a highly relevant component of tumor microenvironment in mammary gland is represented by adipose tissue (AT).

1.4.1 Adipose tissue

AT is a type of loose connective tissue characterized by a marked cellular heterogeneity. Overall, fat tissue consists of approximately one-third of mature adipocytes. The remaining two-thirds contains the stromal-vascular fraction (SVF), a combination of mesenchymal stem cells (Ad-MSCs), T regulatory cells, endothelial precursor cells, fibroblasts, smooth muscle cells, pericytes, macrophages and preadipocytes in various stages of development. Preadipocytes have the ability to proliferate and differentiate into mature adipocytes, conferring AT a constant functional plasticity, which determines its ability to expand throughout the entire lifespan (Moreno-Navarrete and Fernández-Real 2012; Niemelä 2008; Zuk et al. 2002). AT has been traditionally regarded as an insulating and mechanically supportive site of energy storage, which is mobilized for peripheral organs during times of increased energy demand. However, over the past decade the traditional role of AT has evolved to a fully functioning endocrine organ, capable of regulating systemic energy and metabolic homeostasis through a complex network of endocrine, paracrine, and autocrine signals (Nieman et al. 2013; Poulos et al. 2010; Galic et al. 2010). Indeed, adipocytes express and secrete various factors known to play a role in immunological responses, vascular diseases and appetite regulation (Figure 4).

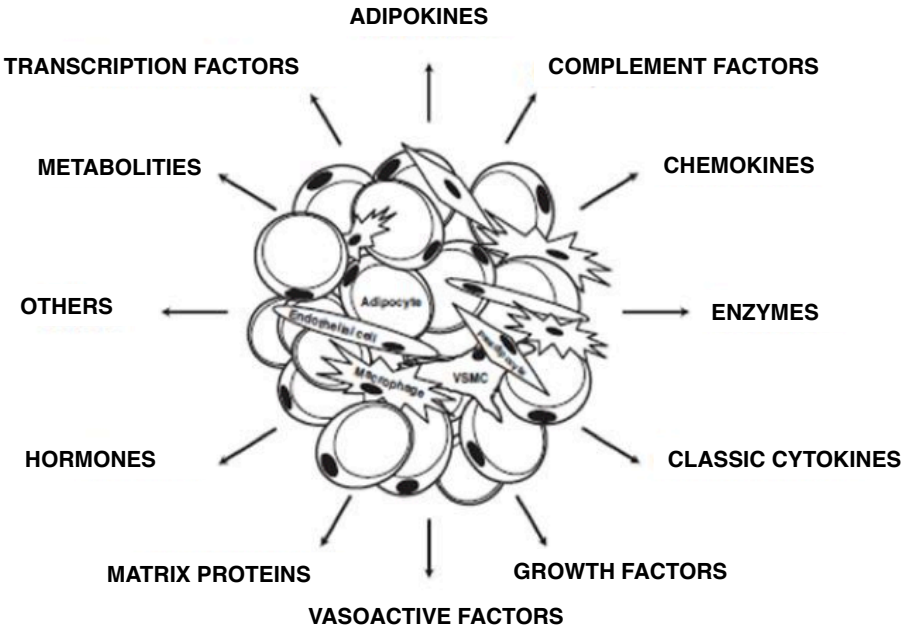

Figure 4: Adipose tissue*. Schematic representation of multicellularity of adipose tissue and its multiple adipose-derived factors.*

Among adipose-derived factors, leptin is made and secreted by mature adipocytes, and it has various biological activities, including effects on appetite, food intake and body weight regulation, fertility, reproduction and hematopoiesis (Flier 1998; Kim and Moustaid-Moussa 2000). AT is also an important site for estrogen biosynthesis and steroid hormone storage. In addition, AT secretes a variety of peptides, cytokines and complement factors, which act in autocrine and paracrine manner to regulate adipocyte metabolism and growth, as well as endocrine signals to regulate energy homeostasis

1.4.2 Adipose tissue as mediator of indirect effect of glucose on breast cancer

Although AT is vitally important to various normal processes of the human body, it has also many implications for human disease states. The excess of adiposity characterizes obesity, one of the most challenging and growing health problems worldwide and considered a major risk factor for T2D. Of note, similarly to diabetes, obesity has been associated to some types of cancer, including breast (Niemelä 2008). The role of AT, and more specifically of adipocytes, in tumor initiation, growth, and metastasis, is a relatively new area of investigation. AT may contribute to tumor phenotypes by either acting as an energy reservoir for embedded cancer cells either

through the secretion of signaling molecules such as adipokines, proinflammatory cytokines, chemokines, growth factors, hormones, proangiogenic factors and extracellular matrix constituents (Park J et al. 2014). Considering that breast cancer cells grow and metastasize to a predominantly adipocyte-dominated host environment (Calle and Kaaks 2004), virtually all of the adipocyte factors may be envisioned as contributing factors for cancer onset and/or progression. In this regard, it has been demonstrated that adipocytes may integrate inputs from the metabolic environment and promote growth of breast cancer cells (D'Esposito V et al. 2012). Since adipocytes respond to energy and nutrient metabolism through a complex network of signals (Rajala and Scherer 2003; Frühbeck et al. 2001), they are able to influence the function of mammary epithelial cells contributing to the stromal-ductal epithelial cell-cell interaction within the mammary microenvironment (Iyengar et al. 2003). Consequently, it can not be excluded that adipocytes may integrate metabolic derangements characterizing T2D, such as hyperglycaemia influencing on several aspects of tumorigenesis, from inducing cell proliferation to promoting local invasion, angiogenesis, metastasis and drug resistance (Figure 5).

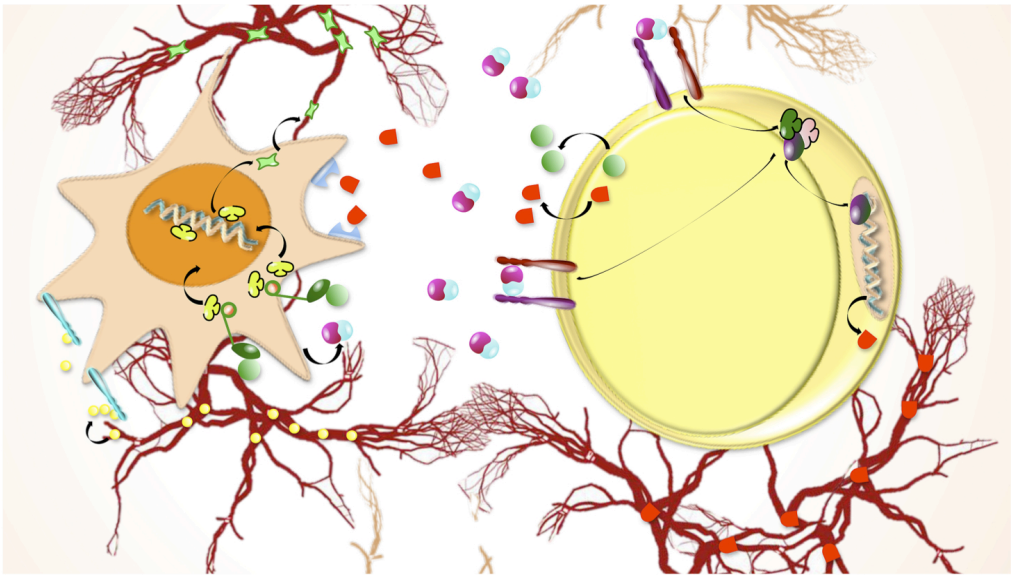

Figure 5: Breast cancer cells and adipose tissue inter-relations. *Graphic representation of breast cancer cells and adipose tissue inter-relation in the tumour microenvironment.*

1.5 Tamoxifen therapy in estrogen sensitive breast cancer

The development of chemotherapy resistance continues to be a major problem in the treatment of cancer patients. It can occur prior to drug treatment (primary or innate resistance) or may develop over time following exposure (Giaccone and Pinedo 1996). Moreover, chemotherapy has a wide range of acute and long-term side effects that substantially affect the patient's quality of life (Yi et al. 2013). In women younger than 50 years with breast cancer, chemotherapy increases the 15-year survival rate by 10 %, whereas the increase is only 3 % in older women. Newer agents, whether chemotherapeutic or targeted, are constantly being developed. Although most anticancer therapies will alter tumor growth, in most cases the effect is not long lasting and their failure impacts the survival of breast cancer patients.

About 70 % of breast cancers are estrogen receptor (ER)-positive and depend on oestrogen to grow and proliferate (Peifer and Alessi 2009). Estradiol is mitogenic in up to 50 % of de novo breast cancers, causing recruitment of quiescent cells into G1 and shortening the G1-to-S phase interval (Cariou et al. 2000). The binding of estrogen to ERs induces conformational changes in protein structure that allow for receptor dimerization, interaction with co-activator molecules, and subsequent transcriptional activation of genes directly, through the interaction with estrogen response elements (EREs) in gene promoters, or indirectly through the binding to other transcription factors such as AP1, SP1 or NFκB. The efficacy of the activated receptor is regulated by several mechanisms, and the balance of these mechanisms could determine the tissue-specific activity of the receptor. In addition, a range of studies revealed ‘non-genomic’, ‘non-nuclear’ or ‘non- transcriptional’ actions of ER. Non-transcriptional functions of ER in the cytoplasm are characterized by fast and transient signal outputs that could potentially lead to a convergence of oestrogen signalling with other cellular signalling transduction pathways (Shang 2006; Bartella et al. 2012). A specific antagonist to the estrogen action or its deprivation must be considered as the most rational therapeutic approach for the prevention and treatment of hormone-dependent breast cancer (Maccio et al. 2009). Tamoxifen is one of the most widely prescribed antiestrogen drugs for the treatment of ER-positive breast cancer patients (Mojarrad et al. 2010). It is a pro-drug - metabolized in the liver to its active metabolite, 4-hydroxy-tamoxifen (4-OHT) - that acts as selective estrogen receptor modulator competitively interacting with ER. Thus, it blocks the effects of estrogen producing a non-functional complex that fails to stimulate transcription (Peifer and Alessi 2009) and lead to a G0/G1 arrest in susceptible ER-positive breast cancer cells (Cariou et al. 2000) (Figure 6).

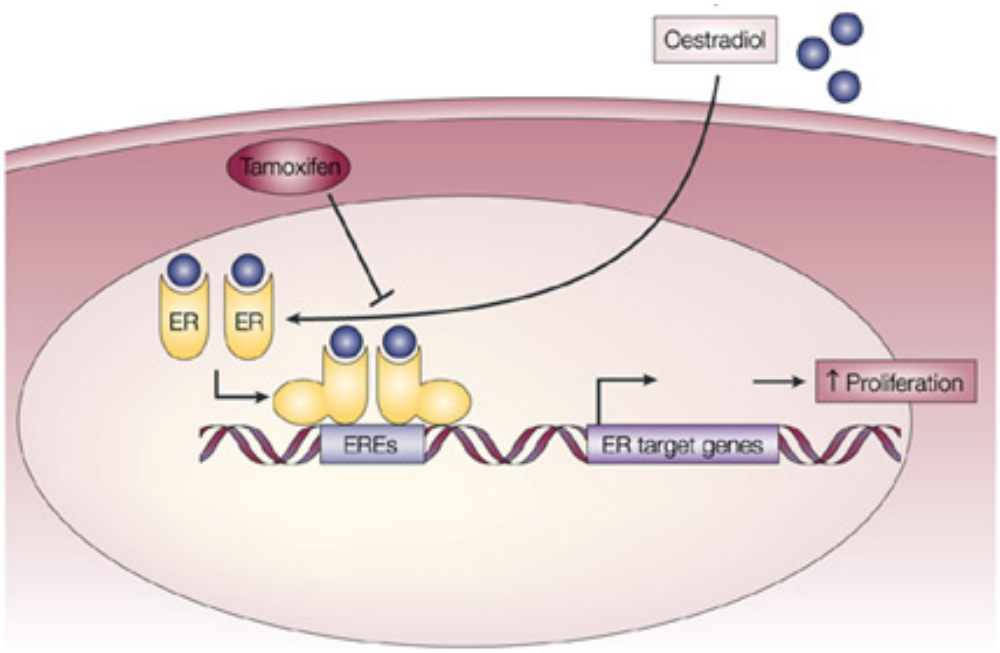

Figure 6: Tamoxifen mechanism of action. *Tamoxifen competes with estrogen in binding to estrogen receptor. It determines a production of a complex that fails to stimulate transcription and in turn induces a cell cycle arrest. Adapted from Johnston and Dowsett (2003).*

Undoubtedly, the significant reduction in breast cancer mortality during the last decade is thought to be attributable to the widespread use of Tamoxifen (Yi et al. 2013). It has been shown to greatly prolong disease-free survival and induce remission in more than half of all patients with ER-positive metastatic disease (Knowlden et al. 2003; Gutierrez et al. 2005). Unfortunately, although 70 % of breast cancers express ER, almost 25 % of ER-positive breast cancer patients do not respond to Tamoxifen (Mojarrad et al. 2010). Moreover, approximately one-third of early-stage breast cancer patients will become resistant to Tamoxifen over the 5-year treatment period, making resistance to Tamoxifen treatment one of the major obstacles to the successful treatment of breast cancer (Peifer and Alessi 2009). Thus, despite the its indisputable benefits, resistance to Tamoxifen is the underlying cause of treatment failure in a significant number of patients with breast cancer, also contributing to an enhanced aggressive tumor phenotype and transition toward a mesenchymal phenotype (Yi et al. 2013). To be able to overcome cancer chemoresistance it is necessary to acquire a complete understanding of the molecular processes that make possible this effect. In this way, several studies have already revealed a number of mechanisms of Tamoxifen resistance, such as increased metabolism of Tamoxifen, loss or alterations of ERs expression, estrogen hypersensitivity, altered expression of co-regulators, and microRNA interference. Nevertheless, a more comprehensive understanding of the

molecular mechanisms and pathways underlying intrinsic and acquired resistance to Tamoxifen is of huge clinical importance and could result in novel strategies to overcome Tamoxifen resistance, further improving survival of breast cancer patients (Peifer and Alessi 2009; Mojarrad et al. 2010; Huber-Keener et al. 2012).

2. AIM OF THE STUDY

T2D is an independent risk factor and worsen the prognosis of multiple types of cancer. Indeed, a number of cancers such as pancreatic, liver, breast, and female reproductive cancers have shown an increased prevalence and a higher mortality rate in diabetic patients compared to healthy subjects (Ryu et al. 2014). The presence of T2D, as cancer-associated comorbidity, is linked to poorer prognosis and survival, particularly in breast cancer post-menopausal women. Nowadays, breast cancer is the most common cancer type in women (Youlden et al. 2012). Unfortunately, the development of chemotherapy resistance constitutes a major problem in the treatment of this type of cancer. T2D is a metabolic disorder characterized by chronic hyperglycemia due to insulin deficiency or insulin resistance. Hyperglycaemia, is known to affect breast cancer cell proliferation. Little is known about the contribute of glucose to the progression of the malignant phenotype of breast cancer cells, and particularly to drug resistance. Another important determinant of the responsiveness of cancer cells to anti-neoplastic drugs is the tumor microenvironment. The common features of tumor microenvironment in different cancer types suggest that targeting the non-malignant cells, or the mediators of their communication (e.g. secreted molecules), is a promising avenue to treat different tumor types as it may represent a valid adjuvant treatment option (Balkwill et al. 2012). Adipocytes represent one of the most abundant cell type in breast tumor microenvironment. Over the past decade, the adipose tissue has been demonstrated to be an active source of endocrine and metabolic activity playing a more dynamic role than previously recognized in many physiological processes (Niemelä 2008). In this *scenario*, understanding how T2D-associated metabolic perturbations may affect cellular response to anti-cancer agents is of crucial importance to identify novel biomarkers and to tailor targeted strategies to overcome chemoresistance. The increased concentrations of glucose, typical of T2D patients, may either directly or indirectly affect cancer cell phenotypes. Indeed, besides acting on cancer cells, glucose may simultaneously act on surrounding and distant cells, thus interfering with anti-cancer drug response. Therefore, the aim of this project is to investigate whether and how T2D-associated metabolic perturbations (i.e. Hyperglycaemia) and tumor microenvironment (i.e. Adipose tissue) may affect cellular response to breast cancer cell sensitivity to Tamoxifen, the chemotherapic agent commonly used as adjuvant hormonal treatment of estrogen dependent breast cancer.

3. MATERIALS AND METHODS

3.1 Cell Culture

MCF7 human breast cancer cells (ER-positive), available in host laboratory, were cultured in Dulbecco's modified Eagle's medium (DMEM) supplemented with 10 % fetal bovine serum (FBS), 2 mM glutamine, 100 units/ml penicillin and 100 units/ml streptomycin. 48 hours before the induction of the experiments, MCF7 cells were shifted to RPMI-1640 without phenol red supplemented with 10 % Charcoal Stripped (C/S) FBS, 2 mM glutamine, 100 units/ml penicillin and 100 units/ml streptomycin.
Adipose derived human Mesenchymal Stem Cells (Ad-MSCs) were obtained by abdominal biopsy. Briefly, adipose tissue was cut in small pieces and treated with 1 mg/ml collagenase in DMEM and Ham's F12 (1:1) supplemented with 10 % FBS, 2 mM glutamine, 100 units/ml penicillin, and 100 µM streptavidin, for 45 minutes at 37°C. The isolated cells were filtered through a 250 µm nylon mesh and incubated at room temperature until to observe the separation of two phases: the upper phase consisting of adipocytes, and the lower phase containing the stromal vascular fraction (SVF). The SVF fraction, containing Ad-MSCs, was collected and washed twice before seeding in T25 Flask in culture medium DMEM-F12 (1:1) supplemented with 10 % FBS, glutamine and antibiotics.
Cultures were maintained in a humidified atmosphere of 95 % air and 5 % CO_2 at 37°C. Media, sera and antibiotics for cell cultures were from Lonza (Basel, Switzerland).

3.2 Adipocyte differentiation and Oil-Red O staining

Adipocyte differentiation was achieved as described by Isakson and colleagues (Isakson et al. 2009). Briefly, Ad-MSCs were seeded ($2x10^5$) and cultured in six-well plates until confluence. Adipocyte differentiation was induced with a differentiation cocktail consisting of 850 nmol/l insulin, 10 µmol/l dexamethasone, 0.5 mM isobutylmethylxanthine, 10 µM pioglitazone, 33 µM biotin and 17 µM pantothenate in DMEM-F12 (1:1) supplemented with 3 % FBS, 2 mM glutamine and antibiotics. After 3 days, the medium was changed to a medium containing only insulin and pioglitazone in DMEM-F12 (1:1) supplemented with 10 % FBS, glutamine and antibiotics. Culture medium was then changed every 2 days for another 8 days up to obtain a complete adipocyte differentiation of Ad-MSCs. Lipid accumulation was determined by Oil red O staining as described by Isakson and colleagues (Isakson et al. 2009). Briefly, cells were fixed with 10 % formalin for 20 minutes and then stained with Oil red O for 60 minutes. After a careful wash of the stained cells, optical density for Oil red O was determined by the addiction of isopropanol to each

well and the incubation at room temperature for 10 minutes. Optical density was measured at 510 nm. The absorbance of cells that had undergone differentiation was then related to that of undifferentiated cells.

3.3 Cell viability/sulforhodamine assay

MCF7 cells ($2x10^3$) were seeded into 96-well microplates in complete medium. The cells were stimulated with 100 nM Estradiol (E_2) and/or different concentrations of 4-idrossi-Tamoxifen (4-OHT) in RPMI 10 % C/S FBS containing 5.5 mM glucose (Low Glucose; LG) or 25 mM glucose (High Glucose; HG). After 4 days, cell viability was assessed by sulforhodamine assay (Chiba et al. 1998). Briefly, the cells were fixed with 50 % trichloroacetic acid for at least 2 hours at 4°C. Then, cells were washed 5 times with distilled and de-ionized water. After air-drying, cells were stained for 30 minutes with 100 µl 0.4 % sulforhodamine B dissolved in 1 % acetic acid. Unbound dye was removed by five washes with 1 % acetic acid. After air-drying, 10 mM Tris solution (pH 7.5) was added to dissolve the protein-bound dye. Cell survival was assessed by optical density determination at 510 nm using a microplate reader. Three replicate wells were used for each data point. Each experiment was performed three times. E_2 (dissolved in ethanol), 4-OHT (dissolved in dimethyl sulfoxide) and all reagents for sulforhodamine assay were from Sigma-Aldrich (St. Louis, MO).

3.4 Conditioned media system

Ad-MSCs were differentiated in mature adipocytes as described in Paragraph 3.2. Differentiated Ad-MSCs were washed two times with sterile phosphate-buffered saline (PBS) before the incubation with serum-free RPMI (HG) supplemented with 0,25 % albumin bovine serum (BSA). After 8 hours, the conditioned medium was collected and centrifuged to remove cellular debris. Then, it was applied on serum-starved MCF7 cells, seeded into 96-well microplates ($2x10^3$), and treated with 5 µM 4-OHT and/or 100 nM E_2. After 4 days, cell viability was assessed by sulforhodamine assay (see Paragraph 3.3). Three replicate wells were used for each data point. Each experiment was performed three times.

3.5 Co-Culture system

Ad-MSCs ($4x10^4$) were seeded and differentiated (see Paragraph 3.2) on the bottom of a 12-transwell chamber. MCF7 cells ($2x10^4$) were seeded in the upper chamber of the transwell culture system and treated with 5 µM 4-

OHT and/or 100 nM E_2 in presence or absence of differentiated adipocytes. After 24 hours, cell viability was assessed by crystal violet. Briefly, cells were fixed with 11 % glutaraldehyde for 15 minutes at room temperature, washed three times with PBS, and stained with 0.1 % crystal violet-20 % methanol for 20 minutes at room temperature. After three PBS washes and complete drying at room temperature, crystal violet was solubilized by the immersion of the filters in 10 % acetic acid. The concentration of the solubilized crystal violet was evaluated by optical density determination at 540 nm using a microplate reader. Each experiment was performed three times.

3.6 RNA isolation and quantitative/qualitative analysis

MCF7 cells ($15x10^4$) were seeded into 100 mm dishes in complete medium. The cells were stimulated with 100 nM E_2 in RPMI 10 % C/S FBS LG or HG. After 4 days, total RNA was isolated from cells, using TRIzol solution (Life Technologies, Carlsbad, CA, USA) according to the manufacturer's instructions. All RNA samples were quantified by measuring the absorbance at 260 nm and 280 nm (NanoDrop spectrophotometer, Life Technologies, Carlsbad, CA, USA). Integrity of RNA samples was further analyzed by using the digital electrophoresis system Experion with the "RNA StdSens Kit" (Biorad, Hercules, CA, USA), following the manufacturer's instructions. Briefly, the Experion automated electrophoresis system performs electrophoresis of samples within a microfluidic chip. Within each chip, a series of microchannels connects the sample wells to a separation channel and buffer wells. A set of electrodes in the electrophoresis station applies a voltage across the microchannels, causing charged molecules in the samples to migrate into and through the separation channel. The run and result analysis were performed by the Experion software. RNA samples with a RNA Quality Indicator (RQI) value ≥ 9 were considered good for the further analyses (Figure 7).

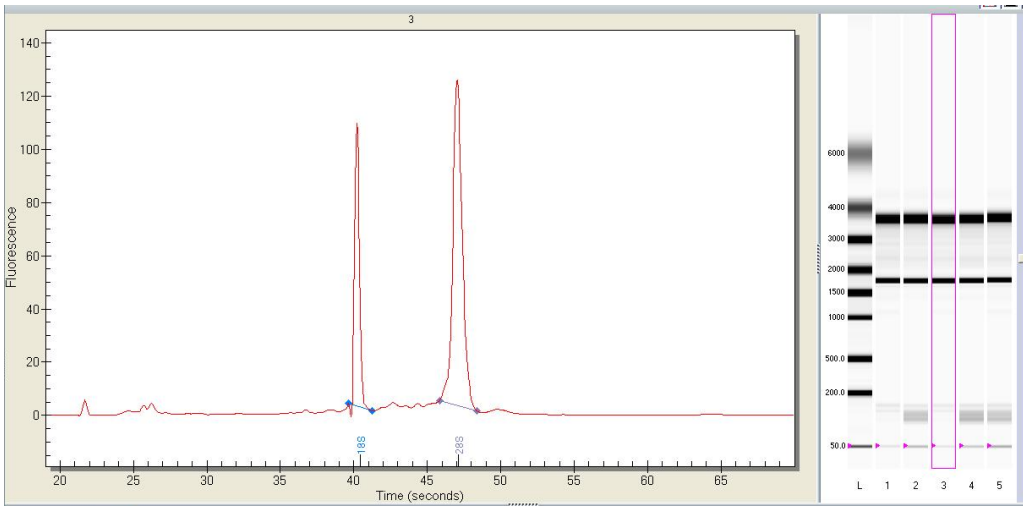

Figure 7: RNA samples Experion profile. *RNA samples integrity was evaluated based on RNA Quality Indicator (RQI) value obtained by using the Experion system.*

3.7 Preparation of paired-end cDNA libraries for RNA-Sequencing

Paired-end cDNA libraries were prepared for Next Generation Sequencing (NGS) on the Illumina Hi-Seq 2000 platform using "TruSeq RNA Sample Preparation kit" (Illumina). According to manufacturer's protocol, oligo-dT attached magnetic beads were used to capture polyA mRNA molecules from 4 µg of isolated total RNA. Resulting polyA RNA was fragmented and reverse transcribed - using random hexamers - into first and second strand cDNA. The overhangs resulting from fragmentation were converted into blunt ends - by end repair process - before the adenylation of 3' ends with a single 'A' nucleotide preventing the ligation between fragments. Subsequently, multiple indexing adapters were ligated to the ends of the dsDNA; a single 'T' nucleotide on the 3' end of the adapters provides a complementary overhang for ligating to the adenylated fragments. Finally, enrichment of dsDNA fragments with adapter molecules on both ends was performed by PCR amplification using a primer cocktail annealing to the ends of the adapters. Yield of purified PCR products was assessed by using the "Qubit dsDNA HS (High Sensitivity) Assay Kit" on Qubit Fluorometer (Life Technologies, Carlsbad, CA, USA). For each cDNA library, size distribution of fragments and sample purity were evaluated by using "Experion DNA 1K Analysis Kit" (Biorad, Hercules, CA, USA) and the Experion system. The electrophoresis run and the subsequent data analysis were carried out using the Experion software. In particular, peak median values were determined at approximately 200-260 bp. Sample concentration and peak median values were used to calculate molar concentration of cDNA libraries. Given that for each

sample a different index was used, one pool of cDNA libraries was attached on the flow cell (a multi-lane glass-based substrate) in the cluster station and amplified to form clusters for sequencing. Subsequently, one strand was selectively linearized and blocked to prevent the sequencing of non-specific sites. After strand denaturation and hybridization of the first sequencing primer, the flow cell was mounted on the Illumina Hi-Seq 2000 platform and subjected to 36 cycles of "sequencing-by-synthesis". Subsequently, the extended sequencing primer was removed and, after strand linearization, blocking and denaturation, the second primer was hybridized. Thus, further 36 cycles of sequencing were performed, reaching a read length of 2 x 70 nucleotides. Hi-Seq data collection was carried out by line scanning mode and four camera system that detects the intensities of all four bases simultaneously. The sequencing run in paired-end mode of the samples required about one week (Figure 8).

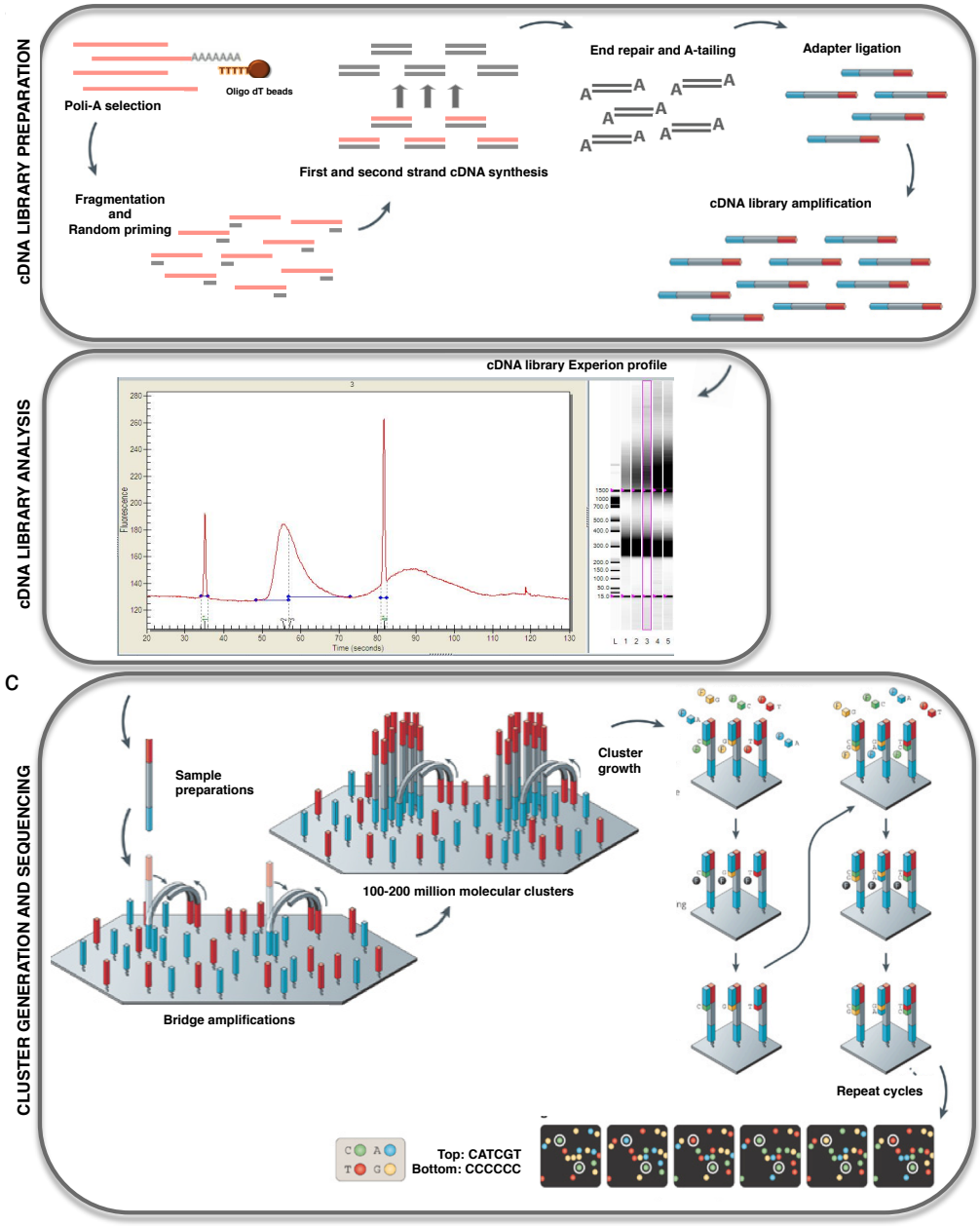

Figure 8: RNA-Sequencing. *The polyadenilated fractions of total RNA isolated from MCF7-HG and MCF7-HG→LG have been used to create cDNA libraries (a). For each cDNA library, size distribution of fragments and sample purity were evaluated by using the Experion system (b). cDNA libraries were used for "cluster generation" and subsequent sequencing at high depth of coverage on the Illumina HiSeq 2000 (c).*

3.8 RNA-Seq data processing, visualization and gene expression analysis

Quality of sequenced reads was assessed using the quality control tool "FastQC" (http://www.bioinformatics.babraham.ac.uk/projects/fastqc/). Subsequently, the TopHat software (version 2.0.10) was used to map the reads against the reference human genome (hg19, Genome Reference Consortium GRCh37) and the RefSeq human transcripts annotation, with default parameters. RefSeq track was downloaded from Table Browser of UCSC Genome Browser (http://genome.ucsc.edu) in GTF format, selecting protein coding gene annotation. Only uniquely mapped reads (about 90 % of sequenced reads) were used for further analyses. SAMTools and BEDTools were used to convert file formats (.sam/.bam/.bed). Precisely, coverage files in bedgraph format were produced using BED Tools. Visual inspection of filtered reads and coverage files on UCSC was used to assess the overall quality of the RNA-Seq experiment and to inspect gene-specific features. Quantification of gene expression, and analysis of differential expression were carried out using the "RNASeqGUI" (http://bioinfo.na.iac.cnr.it/RNASeqGUI; Russo and Angelini, 2014), an open source graphical user interface for the differentially expression analysis of RNA-Seq data. The analysis was carried out in five steps: (1) the exploration of the bam files, (2) the counting process of the mapped reads against the gene annotation file, (3) the exploration of count-data and on pre-processing of the data, including the normalization procedures, (4) the identification of the differentially expressed genes by "NOISeq" method and (5) the inspection of the results and the quantitative comparison among them. In particular, by using the R Bioconductor package NOISeq (Tarazona et al. 2011), it was exploited the non-parametric approach NOISeq-real, optimized for technical replicates. Low count features were filtered has by Wilcoxon test. For each gene a "probability of differential expression" (Pr) was attributed. Genes with Pr≥0.7 were considered as differentially expressed (DEGs) (Figure 9).

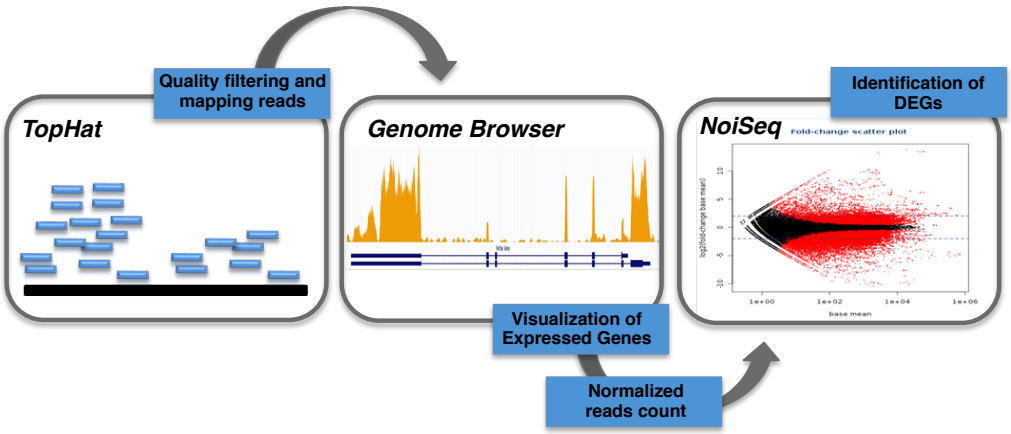

Figure 9: Schematic workflow of the RNA-Seq computational analysis. *In the left panel, the reads' mapping schema is shown. After quality filtering, visual inspection on a genomic browser (e.g. UCSC Genome Browser) of RNA-Seq data is used to qualitatively evaluate the bona fide of the experiment (center panel). Example of a plot showing differentially expressed genes of a typical RNA-Seq experiment.*

Finally, pathway and gene ontology analysis was performed using the "Protein ANalysis THrough Evolutionary Relationships" (PANTHER) (http://www.pantherdb.org).

3.9 RT-PCR and Quantitative Real-Time PCR assays

Previously isolated RNA samples (1 μg), were reverse transcribed using SuperScript II Reverse Transcriptase with oligo dT primers (Invitrogen, Carlsbad, CA, USA) according to the manufacturer's instructions. To check the amplifiable template RNA/cDNA, RT-PCR amplification of a housekeeping gene (hypoxanthine guanine phosphoribosyl transferase; *HPRT*) was performed in all samples. For each data point, as negative control, a sample without reverse transcriptase was amplified under the same conditions than the reverse transcribed RNA. Each amplification reaction was set-up using AmpliTaq Gold (Life Technologies, Carlsbad, CA, USA) and specific primer pairs, designed using Oligo 4.0 and listed in Table 1.

Table 1: Primer pairs used in RT-PCR and qReal-Time PCR analysis

GENE	Primer Forward	T_m F	Primer Reverse	T_m R	Product Size
CYR61	TGCGGCTGCTGTAAGGTC	58°C	ACAGAGGAATGCAGCCCAC	60°C	253 bp
EGR3	AAGCTGCCGGTGACCATGA	60°C	GTAGGTCACGGTCTTGTTGC	62°C	234 bp
EGR1	CAGCAGCAGCACCTTCAAC	60°C	GTGGGTGCCGCTGAGTAAA	60°C	381 bp
JUN	TCCAGCAACGGGCACATCA	60°C	GTTGCTGAGGTTTGCGTAGA	60°C	279 bp
FOS	ACTCACCCGCAGACTCCTT	60°C	GGGCTCTGGTCTGCGATG	60°C	186 bp
EGR2	CCCCTTTGACCAGATGAAC	58°C	TGGATGAGGCTGTGGTTGA	58°C	266 bp
ATF3	CATCACAAAAGCCGAGGTAG	60°C	CACTCCGTCTTCTCCTTCTT	60°C	114 bp
E2F2	CCTCTCCCCTCTACCTCCA	62°C	CAGGTCCCCAAGGTCGTAG	62°C	354 bp
FOSB	TCCTTCGGCAGTCCACCCA	62°C	TGGAAGAGATGAGGGTGGG	60°C	145 bp
E2F7	CAGGTCCCCAAGGTCGTAG	60°C	GGGACAGTCGGGTTCAGAG	62°C	303 bp
CTGF	GGGAAATGCTGCGAGGAGT	58°C	GATAGGCTTGGAGATTTTGG	58°C	237 bp

PCR products were analyzed by electrophoresis on agarose gel and Sanger sequencing. Then, cDNAs obtained were used as template for Quantitive Real-Time PCRs (qReal-Time PCR) performed by iTaq Universal SYBR Green Supermix (Biorad, Hercules, CA, USA), according to the manufacturer's instructions for the CFX Connect Real Time system (Biorad, Hercules, CA, USA). Relative quantification of gene expression was measured by using

$2^{-\Delta\Delta Ct}$ method. Expression levels were normalized for the reference sample (MCF7-HG) using *HPRT* as housekeeping gene. Each assay was performed in triplicate in all samples.

3.10 Gene silencing/RNA interference

MCF7 cells ($2x10^4$) were seeded in 24-well microplates. The following day, the cells at about 70 % confluence were transfected with Dicer-substrate RNAs (DsiRNAs, IDT Coralville, Iowa, USA) recognizing *CTGF* or *CYR61* genes. For each gene, three different DsiRNAs were tested. In detail, to optimize transfection conditions, the cells were transfected with DsiRNA control or each DsiRNA, in different conditions (doses and times). The transfection was carried out by Lipofectamine 3000 (Life Technologies, Carlsbad, CA, USA), in RPMI without antibiotics and serum, according to manufacturer's instructions. After 6 hours, the cells were feed with RPMI 10 % C/S FBS, removing the transfection medium. Transfected cells were stimulated with 100 nM E_2 and/or 4-OHT, and incubated for further 24 hours. Therefore (after 30 hours of transfection) sulforhodamine assay was performed to assess cell viability (see Paragraph 3.3). Simultaneously, gene silencing was checked analyzing the expression of *CTGF* or *CYR61* genes by qReal-Time PCR (see Paragraphs 3.9) using as reference sample the cells transfected with DsiRNA control. Each experiment was performed three times.

4. RESULTS

4.1 Glucose directly modifies MCF7 breast cancer cell responsiveness to 4-OHT.

To investigate the effect of glucose on MCF7 response to 4-OHT treatment, the cells have been cultured in 5.5 mM glucose (MCF7-LG) - a concentration corresponding to normal fasting glucose levels in humans - or in 25 mM glucose (MCF7-HG) - corresponding to the regular culture condition for this cell line, but resembling hyperglycaemia in humans – for one month. MCF7-HG and MCF7-LG have been treated with 100 nM E_2 and raising concentrations of 4-OHT (100 nM, 1 µM and 5 µM) in RPMI 10 % C/S FBS for 4 days. Next, cell viability has been assessed by sulforhodamine assay (see Paragraph 3.2.). As control, MCF7 cells have been incubated with RPMI 10 % C/S FBS (negative control) or treated with E_2 alone (positive control). As expected, E_2 was able to increase cell viability of MCF7 cells both in HG and in LG medium (data not shown). Interestingly, 100 nM and 1 µM 4-OHT treatment significantly reduced MCF7 viability in LG medium of about 25 %, whereas it did not determine the same effect on cells grown in HG medium. The increase of 4-OHT concentration (5 µM) did not induce a further reduction of MCF7-LG viability whereas it significantly reduced of about 20 % the number of viable MCF7 cells in HG medium. These results indicate that glucose concentration modifies MCF7 breast cancer cells' sensitivity to 4-OHT (Figure 10).

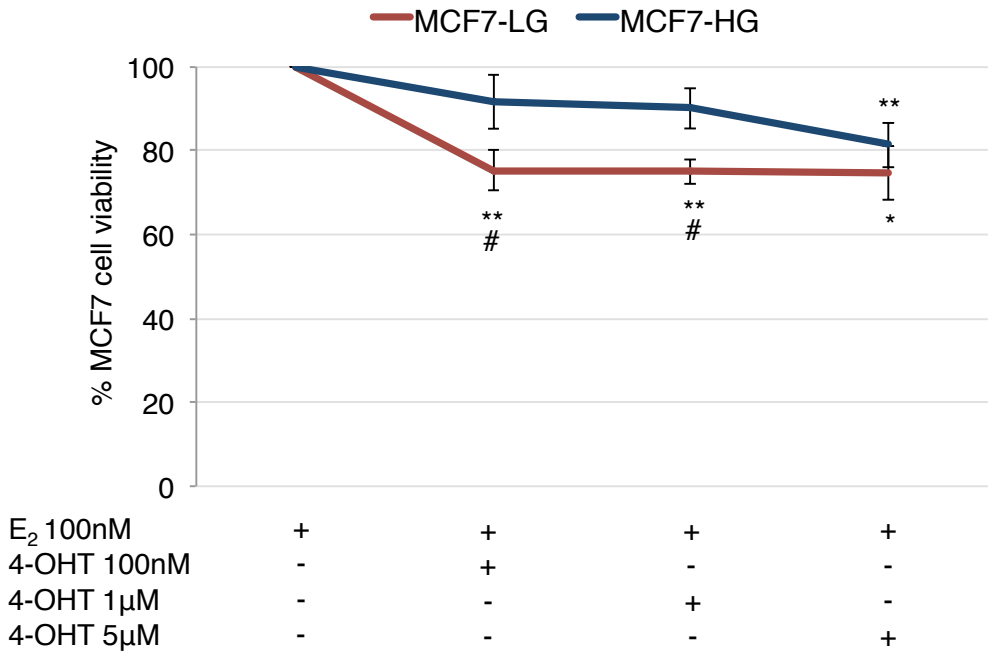

Figure 10: Effect of glucose concentration on MCF7 cells' responsiveness to 4-OHT treatment. *MCF7-HG and MCF7-LG cells have been cultured in RPMI 10 % C/S FBS red phenol free for 48 hours before treatment with 100 nM, 1 µM or 5 µM 4-OHT in presence of 100 nM E_2. After 4 days cell viability has been analyzed by sulforhodamine assay. The results have been reported as percentage of viable cells compared to cells treated with E_2 alone, considered as 100 % viable cells. * $p < 0.05$, ** $p < 0.001$ denote statistically significant values compared to positive control; # $p < 0.05$ indicates statistically significant value compared to MCF7-HG.*

Subsequently, to evaluate the effect of increasing glucose concentration on 4-OHT responsiveness, MCF7-LG cells have been shifted from 5.5 mM to 25 mM glucose concentration (MCF7-LG→HG) and treated with 100 nM 4-OHT for 4 days. As previously reported (Figure 10), the treatment with 100 nM 4-OHT was able to reduce of about 25 % cell viability of MCF7-LG. Interestingly, 4-OHT treatment did not affect cell viability of MCF7 cells shifted to higher glucose concentrations (MCF7-LG→HG), indicating that increasing glucose concentration impairs cell responsiveness to 4-OHT (Figure 11).

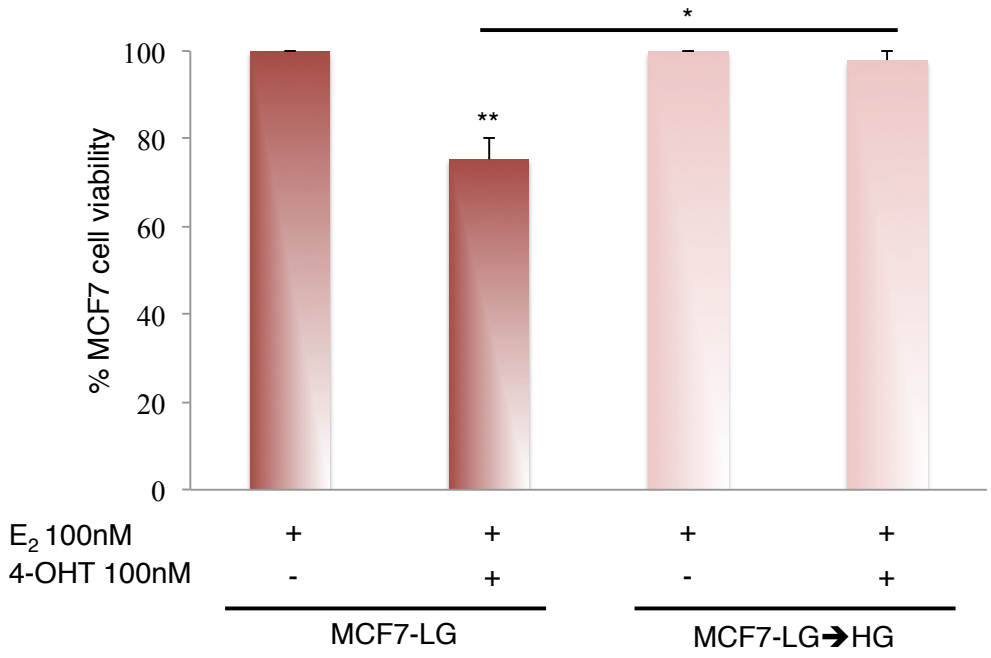

FIGURE 11: Effect of increasing glucose concentration on MCF7 cells' responsiveness to 4-OHT. *MCF7-LG cells have been cultured in RPMI 10 % C/S FBS red phenol free for 48 hours. They have been shifted in HG medium (MCF7-LG→HG) when treated with 100nM 4-OHT in presence of 100 nM E_2. After 4 days, cell viability has been assessed by sulforhodamine assay. The*

results have been reported as percentage of viable cells compared with cells treated with E_2 alone, considered as 100 % viable cells. Asterisks denote statistically significant values ($p < 0.05$; ** $p < 0.001$).*

Similarly, to evaluate the response of MCF7-HG to 4-OHT in presence of reduced glucose concentrations, cells have been shifted from 25mM to 5.5mM glucose (MCF7-HG→LG) and treated with 5µM 4-OHT. As previously shown (Figure 10), the treatment with 5µM 4-OHT reduced cell viability of MCF7-HG of about 20 %. Of note, 4-OHT treatment significantly reduced the percentage of viable MCF7-HG cells - shifted to LG - of about 50 %. These data indicate that reducing glucose concentration significantly ameliorates MCF7-HG sensitivity to 4-OHT (Figure 12).

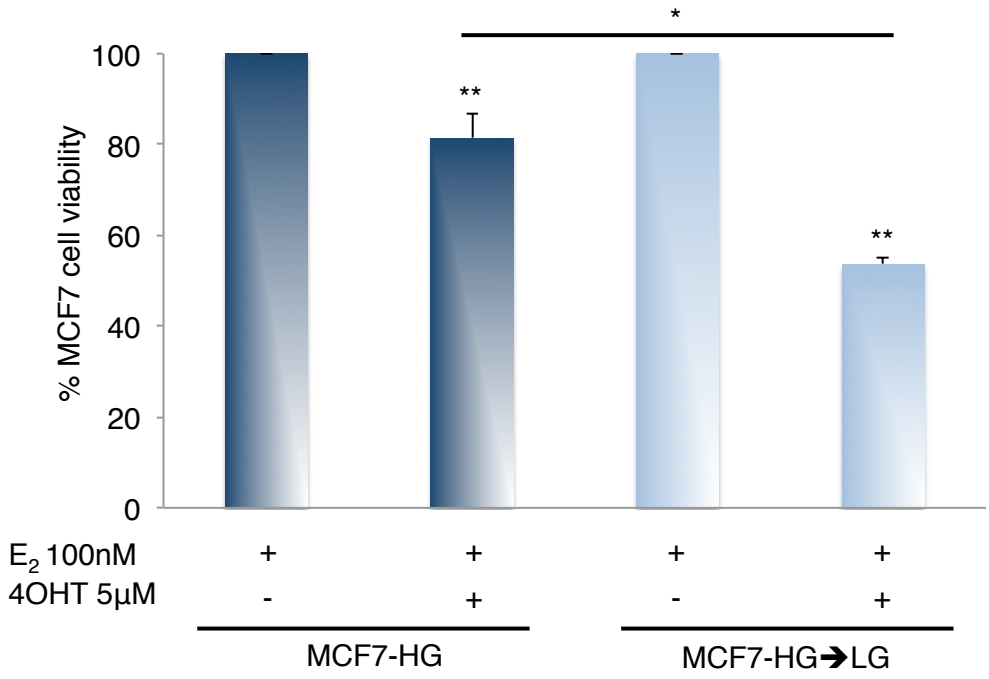

FIGURE 12: Effect of reducing glucose concentration on MCF7 cells' responsiveness to 4-OHT. *MCF7-HG cells have been cultured in RPMI 10 % C/S FBS red phenol free for 48 hours. Then, they have been shifted in LG medium (MCF7-HG→LG) when treated with 5 µM 4-OHT in presence of 100 nM E_2. After 4 days, cell viability has been assessed by sulforhodamine assay. The results have been reported as percentage of viable cells compared with cells treated with E_2 alone, considered as 100 % viable cells. Asterisks denote statistically significant values (* $p < 0.05$; ** $p < 0.001$).*

4.2 Adipocyte released factors impairs MCF7 breast cancer cell responsiveness to 4-OHT.

It has been demonstrated that glucose enhances the ability of adipocytes to produce factors involved in the control of cancer cell phenotypes (D'Esposito et al. 2012). Therefore, to investigate whether adipose-derived factors may affect MCF7 response to 4-OHT treatment in HG medium, Ad-MSC cells, an established model of differentiating adipocyte, have been isolated from adipose tissue (see Paragraph 3.1) and differentiated in mature adipocytes (see Paragraph 3.2) (Figure 13).

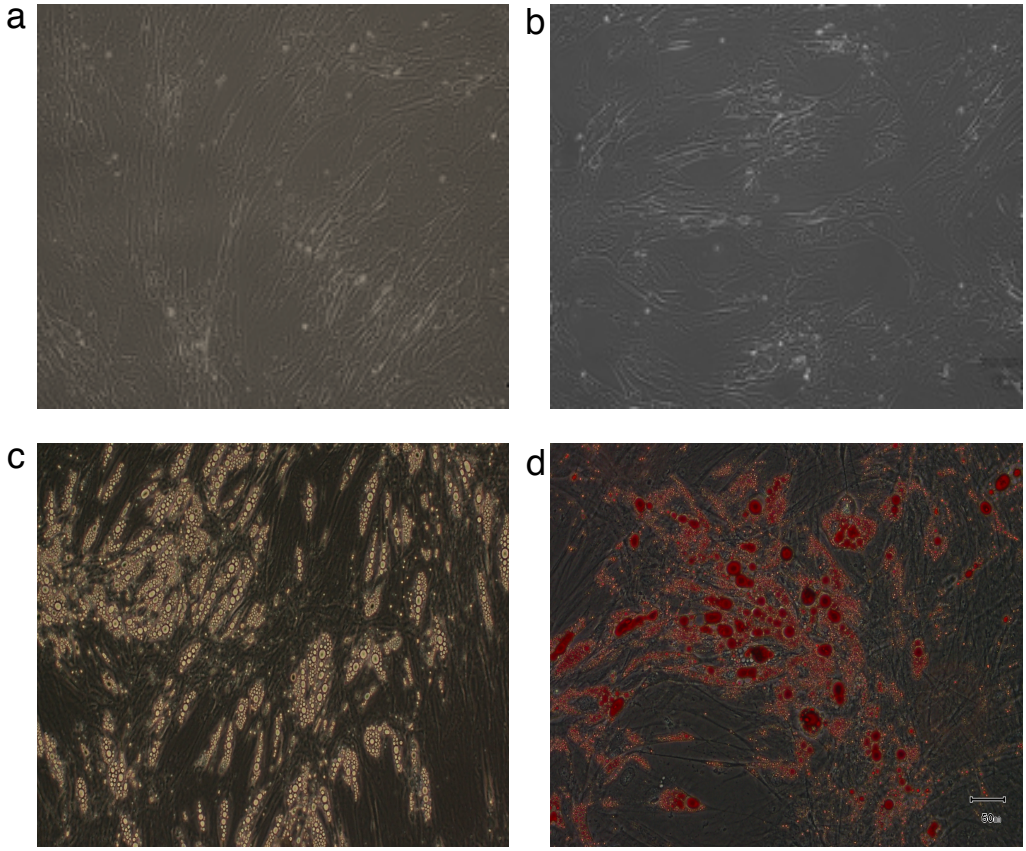

FIGURE 13: Adipocyte differentiation of Ad-MSCs. *Ad-MSCs (a) have been cultured in DMEM-F12 (1:1) 10 % FBS until confluence. Adipocyte differentiation has been inducted with a differentiation cocktail consisting of 850 nM insulin, 10 µmol/l dexamethasone, 0.5 mM isobutylmethylxanthine, 10 µM pioglitazone, 33 µM biotin and 17 µM pantothenate in DMEM-F12 (1:1) 3 % FBS. After 3 days (b), the medium was changed to a medium containing only insulin and pioglitazone in DMEM-F12 (1:1) supplemented with 10 % FBS, glutamine and antibiotics. Culture medium was then changed every 2 days for another 8 days up to obtain a complete adipocyte differentiation of hMSCs (c). Lipid accumulation was determined by Oil red O staining (d).*

Conditioned media from differentiated adipocytes (hAdipo-CM) have been applied onto serum-starved MCF7-HG cells during the treatment with 5µM 4-OHT. After 4 days, cell viability has been assessed by sulforhodamine assay (see Paragraph 3.3). As described in Paragraph 3.4, hAdipo-CM have been collected by using RPMI (HG) 0,25 % BSA without serum. Therefore, and differently to the experiments reported in Paragraph 4.1, MCF7 cells have been incubated with serum-free RPMI 0,25 % BSA as negative control. As positive control the cells have been treated with E_2. As expected, E_2 increased cell viability of MCF7 cells both in presence and in absence of hAdipo-CM (Figure 14). As shown, conditioned media from Ad-MSCs were able to significantly increase MCF7 cell viability (compared to negative control), reaching the levels observed for cells treated with E_2 (positive control). Interestingly, 4-OHT treatment reduced the percentage of viable MCF7-HG cells of about 50 % whereas, in presence of hAdipo-CM, the effect of 4-OHT is reduced to about 30 %, suggesting that adipocyte released factors interferes with MCF7 responsiveness to 4-OHT (Figure 14).

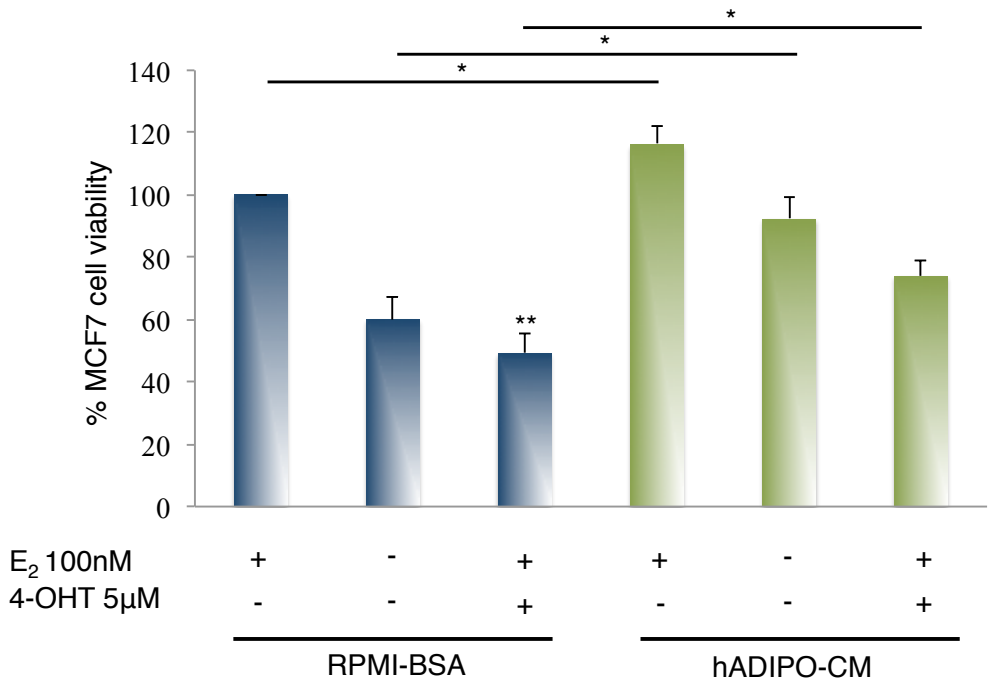

FIGURE 14: Effect of adipocyte conditioned media on MCF7 cells' responsiveness to 4-OHT. *MCF7-HG cells have been cultured in RPMI 10 % C/S FBS red phenol free for 48h. Then, they have been incubated with RPMI 0,25 % BSA (RPMI-BSA) or adipocyte conditioned medium (hADIPO-CM) when treated with 5 µM 4-OHT in presence of 100 nM E_2. After 4 days, cell viability has been assessed by sulforhodamine assay. The results have been reported as percentage of viable cells compared with cells treated with E_2*

alone, considered as 100 % viable cells. Asterisks denote statistically significant values ($p < 0.05$; ** $p < 0.001$).*

Simultaneously, MCF7 cells have been co-coltured with human adipocytes differentiated in the lower chambers of a transwell system (see Paragraph 3.5) and treated with 5 µM 4-OHT in serum free RPMI 0,25 % BSA. After 24 hours, cell viability has been assessed by crystal violet (see Paragraph 3.5). Similarly to the experiments performed by using hAdipo-CM, MCF7 cells have been incubated with RPMI 0,25 % BSA without serum as negative control, or treated with E_2 as positive control. As previously observed, E_2 was able to increase cell viability of MCF7 cells both in presence and in absence of mature adipocytes (Figure 15). As reported, MCF7 cell viability was significantly increased in presence of mature adipocytes (compared to negative control), reaching similar levels to those observed for cells treated with E_2 (positive control). Interestingly, 4-OHT treatment reduced the percentage of viable MCF7-HG cells of about 40 % whereas, in presence of mature adipocytes, the effect of 4-OHT was reduced to 20 % (Figure 15).

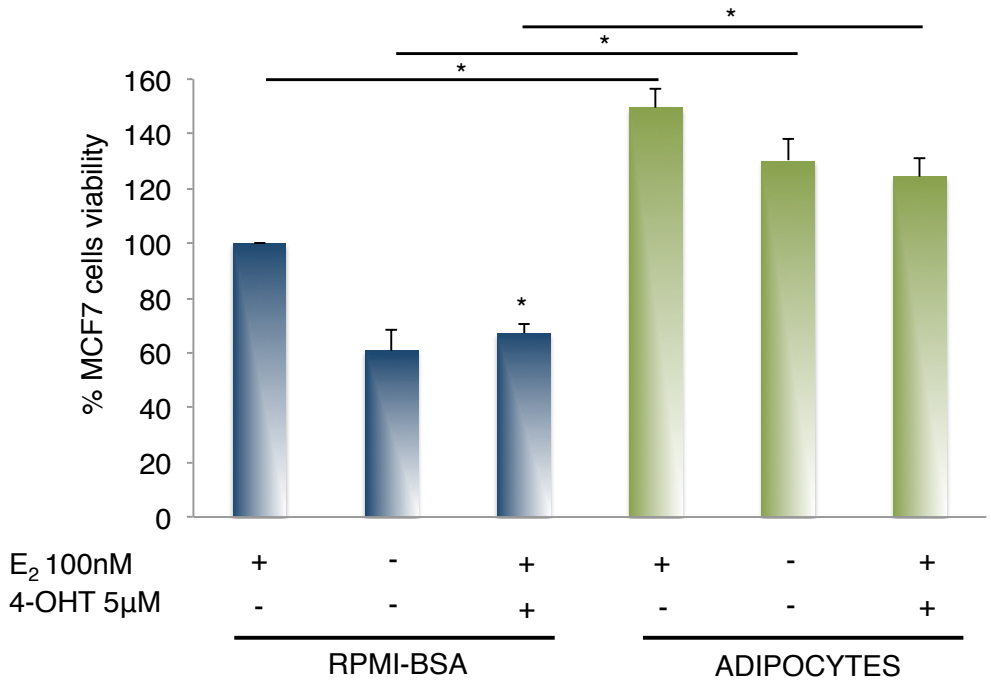

***FIGURE 15: Effect of adipocyte on MCF7 cells' responsiveness to 4-OHT**. MCF7-HG cells have been cultured in RPMI 10 % C/S FBS red phenol free for 48 hours. Then, they have been seeded in the upper chambers of a transwell system in RPMI 0,25 % BSA (RPMI-BSA). Then, treated with E_2 100 nM and/or 5 µM 4-OHT in presence or absence of differentiated adipocytes. After 24 hours, cell viability has been assessed by crystal violet. The results have*

been reported as percentage of viable cells compared with cells treated with E_2 alone, considered as 100 % viable cells. Asterisks denote statistically significant values ($p < 0.05$; ** $p < 0.001$).*

Taken together - data obtained by both conditioned media and co-colture approaches - strongly support the hypothesis that adipocytes' released factors reduce MCF7 cells responsiveness to 4-OHT.

4.3 Glucose modifies the transcriptome of MCF7 breast cancer cells

Since it was observed that MCF7-HG displayed the worst sensitivity to 4-OHT, while the shifting in LG ameliorated their drug sensitivity (see Paragraph 4.1), it has been chosen to investigate whether glucose may induce changes in the expression profile of MCF7. Thus, RNA-Sequencing on a Next Generation Sequencing (NGS) platform has been performed to explore the entire transcriptome of MCF7-HG and MCF7-HG→LG. RNA-Sequencing generated more than 80 million of paired-end reads per sample. The computational analysis of RNA-Seq datasets (see Paragraph 3.8) revealed that 494 genes were differentially expressed (DEGs) between the analyzed conditions (Figure 16).

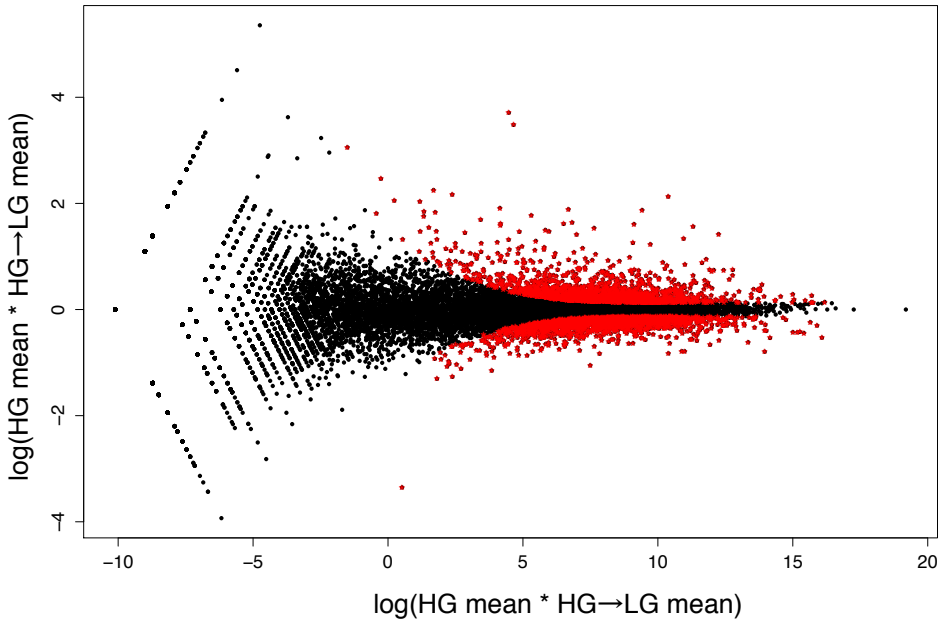

FIGURE 16: MA plot of expressed genes. *MA plot (M means log ratios and A mean average) showing expressed genes (black dots) and differentially expressed genes (red dots). On y axis are reported the normalized expression values indicated as log differences per gene (logHG-logHG→LG). On x axis*

are reported the normalized expression values as log sum per gene (logHG+logHG→LG).

In detail, 310 genes were up-regulated and 184 genes were down-regulated (about 60 % and 40 %, respectively) in MCF7 shifted in LG compared to MCF7-HG. Thus, the reliability of the RNA-Seq experiment was assessed through the validation - by qReal-Time PCR - of randomly selected genes (both not expressed and not differentially expressed; data not shown). Then, functional enrichment analysis performed on DEGs has been carried out using the "Protein ANalysis THrough Evolutionary Relationships" (PANTHER) (http://www.pantherdb.org). This analysis revealed that the most represented pathway was "cell cycle" (70/494 DEGs; FDR < 0.05) (Figure 17).

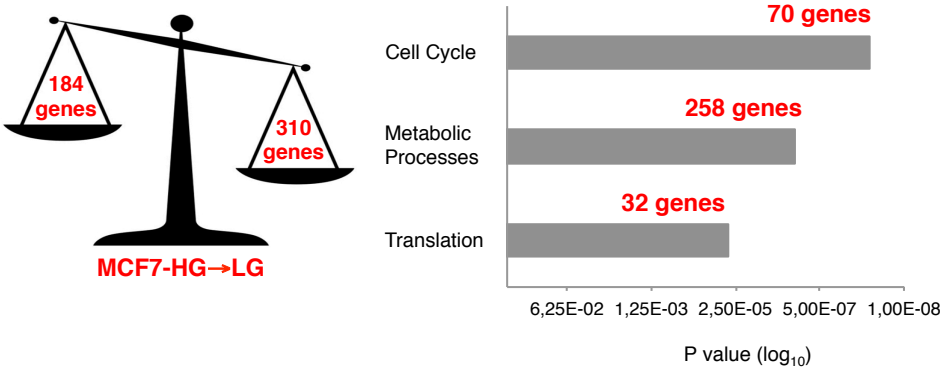

***FIGURE 17: Identification of DEGs**. RNA-Sequencing data analysis revealed that 184 genes were up-regulated and 310 were down-regulated in MCF7-HG→LG compared to MCF7-HG. Pathway enrichment on DEGs has been performed by "Protein ANalysis THrough Evolutionary Relationships" (http://www.pantherdb.org) (Bonferroni correction for multiple testing).*

A more stringent dataset of DEGs was selected by using a posterior probability threshold of 80 % (Pr value ≥ 0.8) (Figure 18a). Using this criterion, 11 out of 70 "cell cycle" genes were selected for further validations. In detail, all these genes were down-regulated when MCF7-HG were shifted in low glucose medium (Figure 18b). Therefore, based on RNA-Seq data analysis, the expression levels of 11 "cell cycle" genes were measured by qReal-Time PCR (as described in Paragraph 3.9). Remarkably, the extent of deregulation for these genes was also confirmed in two independent experiments. These data (Figure 18c) confirmed the previous observations and RNA-seq analysis, except for 2 out of 11 genes selected, and indicated that glucose regulates the expression of at least 9 "cell cycle" genes in MCF7-HG cells. Among them, 7 encoded transcription factors, such as those belonging to the EGR family, whereas two (*CTGF* and *CYR61*) belong to the same growth factor family

(CCN family of immediate-early genes). The latter two genes were selected for further investigations, in order to prove their possible role in MCF7 cells responsiveness to 4-OHT.

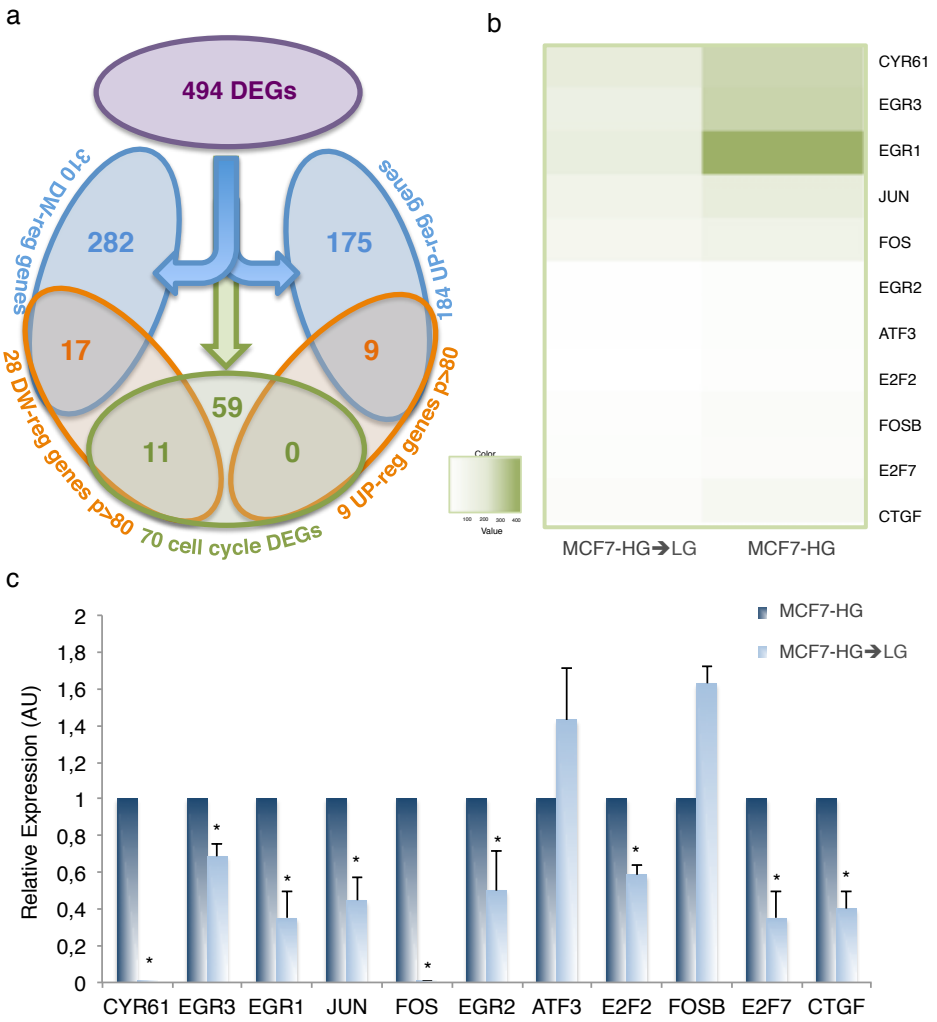

FIGURE 18: DEGs analysis and validation. *Venn diagram of DEGs showing the selection of DEGs involved in cell cycle with higher statistic probability of differential expression (Pr ≥ 0,8) (a). Heatmap showing 11 out of 70 cell cycle DEGs selected (b). Experimental validation by qReal-Time PCR has been performed using the expression of the housekeeping HPRT gene as internal control. Data have been reported as mean values and results analyzed by paired Student's t test. Asterisks denote statistically significant values (* $p < 0.05$; ** $p < 0.001$) (c).*

4.4 Human adipocyte conditioned medium induces *CTGF* gene expression in MCF7 cells

It has been demonstrated, by using either conditioned media either co-colture system, that adipose-derived factors impair MCF7 cell responsiveness to 4-OHT in HG medium (Paragraph 4.2). In order to investigate whether adipocyte released factors in HG medium may affect the expression of *CTGF* and *CYR61* genes, conditioned media obtained from differentiated Ad-MSCs have been collected (see Paragraph 3.4) and applied onto MCF7-HG for 4 days in presence of E_2. As control, MCF7 cells have been treated with E_2 in serum-free RPMI 0,25 % BSA. *CTGF* and *CYR61* gene expression has been evaluated by qReal-Time PCR. Interestingly, hAdipo-CM significantly increases the expression of both *CTGF* and *CYR61* gene (Figure 19), indicating that adipocyte released factors in HG medium induce expression changes of *CTGF* and *CYR61* genes in MCF7 cells.

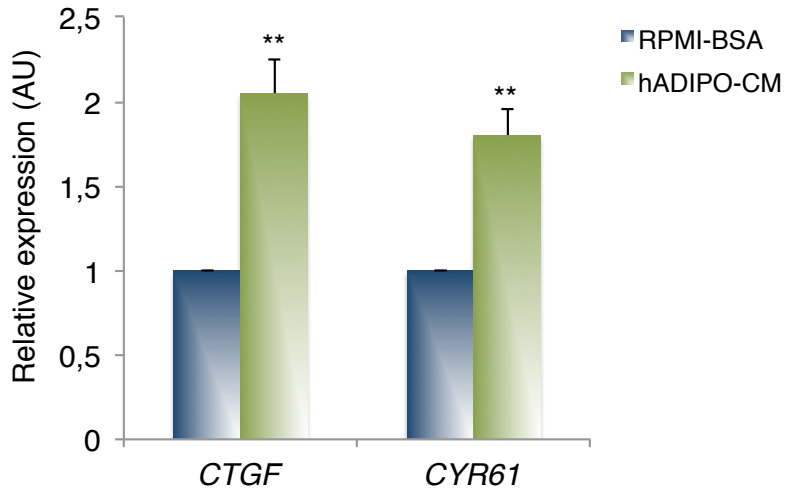

FIGURE 19: CTGF and CYR61 gene expression in MCF7 exposed to hAdipo-CM. *MCF7-HG cells have been cultured in RPMI 10 % C/S FBS red phenol free for 48 hours. Then, they have been incubated with RPMI 0,25 % BSA (RPMI-BSA) or adipocyte conditioned medium (hADIPO-CM) when treated 100 nM E_2. After 4 days, CTGF and CYR61 gene expression has been evaluated by qReal-Time PCR. The expression of the housekeeping HPRT gene has been used as internal control. Asterisks denote statistically significant values (** $p < 0.001$).*

4.5 *CTGF* silencing increases MCF7 responsiveness to 4-OHT treatment

Since glucose and adipocyte-released factors reduced MCF7 sensitivity to Tamoxifen and modify different genes in cancer cells, among which *CTGF* and *CYR61*, we wondered whether these genes might be involved in drug responsiveness. Therefore, MCF7-HG cells were transfected with three different anti-*CTGF* or anti-*CYR61* DsiRNAs to setup the correct experimental conditions to induce gene silencing. The cells were transfected with 10 nM of each DsiRNA. Gene silencing was evaluated by qReal-Time PCR (see Paragraph 3.9). As shown in Figure 20a, both DsiRNA 2 and DsiRNA 3 induced *CTGF* gene silencing of about 60 % upon 48 hours transfection. DsiRNA 2 was able to silence *CTGF* gene already after 24 hours of transfection (Figure 20b).

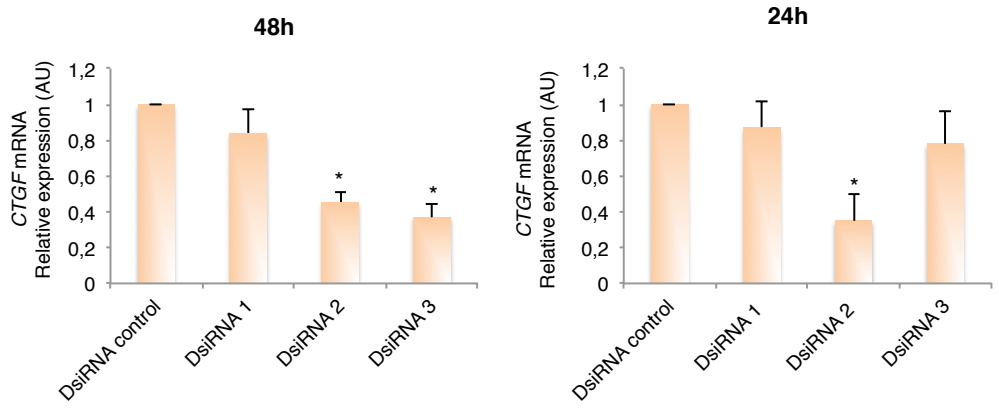

FIGURE 20: DsiRNA anti-CTGF selection. *MCF7-HG cells have been transfected with 10 nM of each DsiRNA recognizing CTGF gene, in RPMI without serum and antibiotics. After 6 hours, the transfection medium has been removed and replaced with RPMI 10 % C/S FBS red phenol free. After 48 hours and 24 hours gene silencing has been evaluated by qReal-Time PCR. The expression of the housekeeping HPRT gene has been used as internal control.*

Both 5 nM and 10 nM DsiRNA anti-*CYR61* displayed a toxic effect on MCF7 cells (data not shown). Thus, the transfection was performed with 1 nM DsiRNA. As shown in Figure 21, either upon 48 hours (a) and 24 hours (b) of transfection, only DsiRNA 3 was able to induce a marked reduction (about 50 %) of *CYR61* expression.

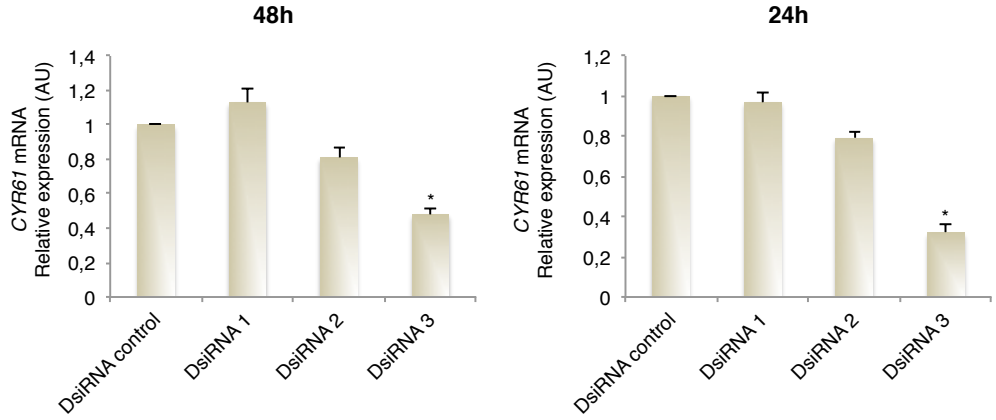

FIGURE 21: DsiRNA anti-CYR61 selection. *MCF7-HG cells have been transfected with 1 nM of each DsiRNA recognizing CYR61 gene, in RPMI without serum and antibiotics. After 6 hours, the transfection medium has been removed and replaced with RPMI 10 % C/S FBS red phenol free. After 48 hours and 24 hours gene silencing has been evaluated by qReal-Time PCR. The expression of the housekeeping HPRT gene has been used as internal control.*

Therefore, in order to investigate the role of *CTGF* and *CYR61* genes on MCF7-HG responsiveness to 4-OHT, the cells have been transfected with DsiRNA anti-*CTGF 2* or DsiRNA anti-*CYR61* 3. As control, MCF7 cells have been transfected with DsiRNA control. After 6 hours, the cells have been treated with 5 μM 4-OHT in presence of E_2. As positive control, the cells have been treated with E_2. After 24 hours, cell viability has been assessed by sulforhodamine assay (Paragraph 3.3). Of note, *CTGF* gene silencing induced a significant reduction of about 40 % of viable MCF7 upon treatment with 4-OHT compared to cells transfected with DsiRNA control – resembling the effect of glucose concentration reduction (Figure 22). On the opposite, *CYR61* gene silencing did not affect the response of MCF7-HG to 4-OHT treatment (Figure 22).

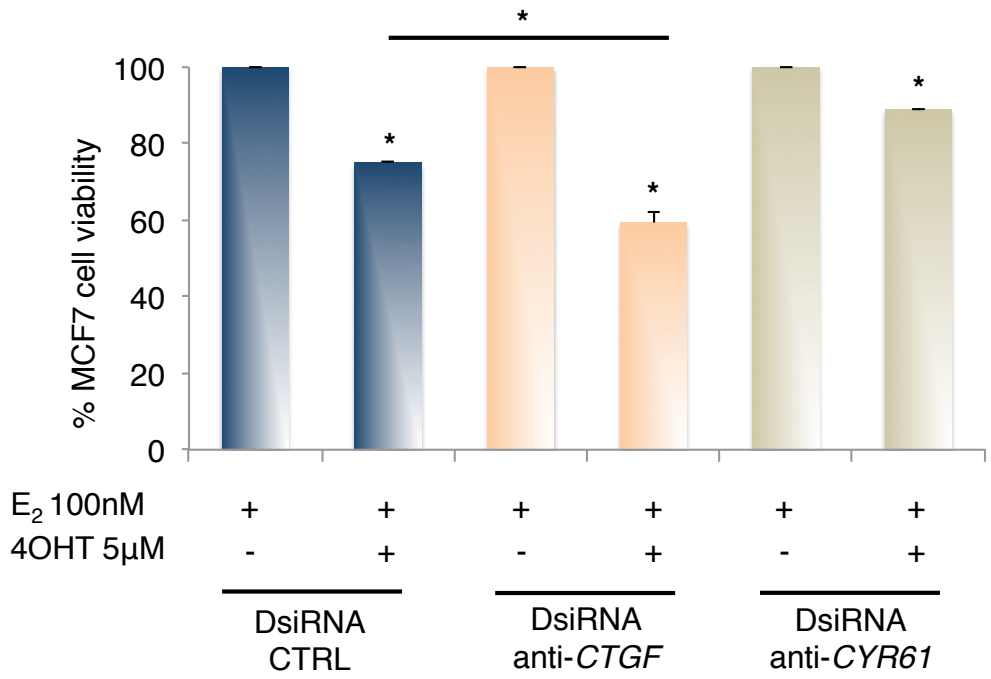

FIGURE 22: Effect of CTGF and CYR61 silencing on MCF7-HG cells' responsiveness to Tamoxifen. *MCF7-HG cells have been transfected with 10 nM DsiRNA recognizing CTGF gene or 1 nM DsiRNA recognizing CYR61 in RPMI without serum and antibiotics. After 6 hours, the transfection medium has been removed and replaced with RPMI 10 % C/S FBS red phenol free. The cells have been treated with 5 µM 4-OHT in presence of 100 nM E_2. After 24 hours, cell viability has been assessed by sulforhodamine assay. The results have been reported as percentage of viable cells compared with cells treated with E_2 alone, considered as 100 % viable cells. Asterisks denote statistically significant values (* $p < 0.05$).*

In parallel, mRNA levels of the other DEGs genes obtained by RNA-Seq experiment have been measured in MCF7 cells transfected with DsiRNA anti-*CTGF* gene. Interestingly, the expression of these genes did not change after *CTGF* silencing in MCF7-HG cells (data not shown) suggesting that the effect on 4-OHT responsiveness is largely due to the silencing of *CTGF* gene.

5. DISCUSSION

Chronic hyperglycaemia is the most important metabolic dysregulation associated with diabetes and contributes to long-term complications of diabetes such as nephropathy, retinopathy and neuropathy. Convincing evidence indicates that diabetes is also associated with increased incidence and mortality related to several type of cancer, including breast cancer. Although a number of studies strongly support the association of diabetes with a higher risk and a poor prognosis in women with breast cancer (Zeng et al. 2010), the effects of glucose on cancer cell phenothype, and in particular on drug response, still remains to be determined. Besides acting on cancer cells, glucose may well affect surrounding cells as well as distant cells, which in turn may interfere with cancer phenotype. Breast cancer cells grow and metastasize to a predominantly adipocyte-dominated host environment (Calle and Kaaks 2004). Adipocytes may integrate metabolic derangements that are typical of T2D, such as hyperglycaemia, and may drive an indirect influence on several aspects of tumorigenesis. Indeed, adipocyte-released factors can induce cell proliferation, promote local invasion, angiogenesis, metastasis and drug resistance. Of note, despite the proven survival benefit of systemic adjuvant chemotheraphy in patients with breast cancer, a significant number of them still develops metastatic disease and responds only transiently to conventional treatment. The significant reduction of the mortality due to breast cancer during the last decade is thought to be attributable to the widespread use of Tamoxifen (Yi et al. 2013). It has been shown to greatly prolong disease-free survival and induce remission in more than half of all patients with estrogen dependent metastatic disease (Knowlden et al. 2003; Gutierrez et al. 2005). Unfortunately, despite the its indisputable benefits, resistance to Tamoxifen is the underlying cause of treatment failure in a significant number of patients with breast cancer, also contributing to an enhanced aggressive tumor phenotype and transition toward a mesenchymal phenotype (Yi et al. 2013). To be able to overcome cancer chemoresistance, a more comprehensive understanding of the molecular mechanisms and pathways underlying intrinsic and acquired resistance to Tamoxifen is of huge clinical importance. In this PhD thesis, it has first been investigated the effect of glucose on breast cancer cell response to Tamoxifen treatment. I have shown that cells treated in a glucose concentration resembling hyperglycaemia in humans are less sensitive to Tamoxifen compared to cells grown in a concentration corresponding to normal fasting glucose levels in humans. Thus, it is necessary to use a higher concentration of drug to reduce the viability of cells growing in a high-sugar environment. Interestingly, the reduction of glucose concentration significantly ameliorates breast cancer cell sensitivity to Tamoxifen. Therefore, I demonstrated that glucose directly affect breast cancer cell response to Tamoxifen treatment. To better understand the effect of glucose on breast cancer cells, I investigated whether reduced glucose levels may induce significant changes in the expression profile of breast cancer cells, potentially

explaining their increased sensitivity to Tamoxifen treatment. Thus, using RNA-Sequencing on a Next Generation Sequencing platform I was able to investigate the entire cell transcriptome of these cells under different glucose concentrations. In particular, as describe in the Results, the reduction of glucose levels determines to a statistically significant down-regulation of several genes involved in cell cycle. Among them, some encode transcription factors, including those belonging to the EGR family, and two- *CTGF* and *CYR61* - belonging to the "CCN family of immediate-early genes". CCN proteins are known to regulate adhesion, apoptosis, extracellular matrix production, migration, proliferation, differentiation, survival and gene expression (Brigstock 2003). *CYR61* gene encodes a known pro-angiogenic factor named cysteine-rich 61. It is overexpressed in invasive and metastatic human breast cancer cells and tumor biopsies and is able to promote invasiveness *in vitro* and tumorigenesis *in vivo* (Tsai et al. 2002a; Tsai et al. 2002b). *CTGF* gene encodes connective tissue growth factor. Among its various functions, it is involved in tumor development and progression (Shi-Wen et al. 2008). Consistently with its induction by estrogen, CTGF expression is high in different cancers including steroid-dependent breast tumors (Xie et al. 2001; Brigstock 2003). Particularly, CTGF enhances clonogenic ability, cell viability and migration in breast cancer cells (Chien et al. 2011). Since a previous study showed that glucose enhance the ability of adipocytes to produce factors involved in the control of breast cancer cell phenotype (D'Esposito et al. 2012), I hypothesized that adipocytes could integrate metabolic input (i.e. hyperglycaemia) and in turn affect drug response. Thus, I investigated the effect of adipocytes released factors in high glucose concentration on breast cancer cell response to Tamoxifen. In the present thesis, I have shown that adipocyte-released factors reduce breast cancer cell responsiveness to Tamoxifen, indicating that the tumor microenvironment, and in particular adipocytes integrate metabolic input and interfere with cancer cell drug response. Starting from RNA-Seq data, I investigated the role of *CTGF* and *CYR61* in Tamoxifen response, evaluating their expression in breast cancer cells exposed to adipocytes' released factors. Consistently, I found that these factors induce a significantly over-expression of *CTGF* and *CYR61* genes in breast cancer cells, that in turn may explain their reduced sensibility to Tamoxifen. Given previous considerations and in line with obtained data, I hypothesized that *CTGF* and *CYR61* genes might exert a possible role in breast cancer cell responsiveness to Tamoxifen. Accordingly, *CTGF* gene silencing induces a significant increase in Tamoxifen sensitivity in breast cancer cell grown in high glucose medium. The cells reach a drug sensitivity similar to those obtained for cells cultured in lower glucose concentrations. It strongly suggests that the effect of glucose concentration on breast cancer cells' sensitivity to Tamoxifen is altered by *CTGF* gene. In particular, based on these data, I hypothesize that the reduction of glucose levels induces a down-regulation of *CTGF* gene that in turn increases breast cancer cells sensibility to Tamoxifen. In summary, the major finding described

in this PhD thesis is that hyperglycaemia significantly reduces Tamoxifen sensitivity of human breast cancer cells and that this effect is worsened in presence of adipocytes-released factors. Moreover, by using NGS technology to profile the entire cell transcriptome, this study revealed that the altered sensitivity to Tamoxifen response is associated to the deregulation of specific gene pathways. Combining NGS data to gene silencing I could demonstrate that such effects are likely to be mediated by the reduced expression of C*TGF* gene. Previous studies have shown that CTGF is critical in tumor development, progression as well as in tumor survival (Shi-Wen et al. 2008). Moreover, it confers resistance to doxorubicin- and paclitaxel- induced apoptosis in breast cancer cells (Wang et al. 2009). In line with these data, I have shown that Tamoxifen response in breast cancer cells correlates with *CTGF* gene expression, providing additional clues to the hypothesis that CTGF is one of the most relevant contributors to chemotheraphy sensitivity in breast cancer. Interestingly, a higher expression of CTGF has been also shown in diabetes (Brigstock 2003). Hence, CTGF may be a novel predictive marker for chemo-sensitivity and could be considered as a potential therapeutic target in novel strategies to overcome Tamoxifen resistance further improving survival of diabetic patients affected by breast cancer.

6. CONCLUSION

In this PhD thesis I have described that high glucose levels, that mimic hyperglycaemia in humans, are able to dramatically impair breast cancer cell sensitivity to Tamoxifen, a drug widely used to treat estrogen-sensitive cancers. Reducing glucose concentrations, to levels corresponding to normal fasting glucose in humans, it is possible to rescue breast cancer cell sensitivity to this drug. I also found that adipocyte-released factors impair Tamoxifen responsiveness of breast cancer cells, indicating the crucial role of the tumor microenvironment in cancer drug responsiveness. *CTGF* gene was experimentally demonstrated to be a potential contributor to the onset of Tamoxifen resistance in breast cancer cells.

Hence, the results obtained in this PhD project, strongly support the hypothesis of CTGF as a therapeutic target in novel strategies to overcome Tamoxifen resistance in breast cancer. These findings also suggest that the expression of this gene in breast biopsies may represent a potential novel predictive marker for chemo-sensitivity, even though further studies are needed to confirm this hypothesis.

The identification of CTGF as a potential gene responsible of breast cancer sensitivity to Tamoxifen, is likely to represent a solid starting point to design new adjuvant therapeutic strategies to overcome tamoxifen resistance, particularly in presence of metabolic comorbidities.

The results of my PhD project also highlight the relevant role of hyperglycemia and of adipocyte-released factors in the onset of drug resistance. It indicates that the glycemic control in diabetic women affected from breast cancer is of primary importance for the effectiveness of chemotherapy.

7. ACKNOWLEDGMENT

…grazie a tutte le persone che hanno fatto parte di questo percorso…e grazie alle persone che solo per breve tempo l'hanno incrociato…perche tutti hanno contribuito a renderlo speciale e soprattutto hanno contibuito alla mia crescita personale e professionale…

…grazie a tutti…da chi mi ha insegnato a chi mi ha messo alla prova, da chi mi ha dato consigli a chi mi ha semplicemente regalato un sorriso…

…grazie a chi, nonostante la mia assenza, non ha mai smesso di considerarmi e tenermi presente come parte del gruppo…e grazie a che mi ha accolta, ha imparato a conoscermi e fin da subito mi ha fatta sentire a casa…

…grazie a Pietro, per me esempio di intelligenza, correttezza ed umiltà… oltre che di entusiasmo ed amore per la ricerca…lo ringrazio per avermi concesso di far parte del suo gruppo di lavoro…per avermi dato fiducia…e per essere stato sempre disponibile nonostante i suoi mille impegni…

…grazie al Prof. Alfredo Ciccodicola, per avermi dato la fiducia e l'opportunità di realizzare questo progetto di tesi, per l'affetto e per essere sempre stato esempio di professionalità e serietà…

…grazie al Prof. Francesco Beguinot, i cui consigli sono stati fondamentali per la buona riuscita di questo progetto di tesi…

…grazie a Vittoria…anche se non credo potrei mai trovare le parole adatte per ringraziare la persona che, forse più di tutti, e talvolta più di me stessa, ha creduto in me…che, sempre paziente e disponibile, è stata parte di questo percorso dall'inizio alla fine…che con me ha affrontato dubbi e difficoltà…che insieme a me ha condiviso ogni soddisfazione e sorriso…che mi ha insegnato, consigliato e supportato…e che oggi è per me un'amica prima di ogni altra cosa…

…grazie a Mimmo…perchè come un padre ha saputo essere preciso nei suoi insegnamenti e severo nei suoi richiami, ma non ha mai saputo nascondere la tenerezza nei suoi occhi…

...grazie a Valerio…per i suoi consigli, i suoi suggerimenti e le sue critiche…per avermi sempre tenuta in considerazione dimostrandomi stima e fiducia...per aver contribuito alla mia crescita professionale e personale con affetto e premura…

…grazie a Marianna…un dolce tesoro nel lavoro e nella vita…

…grazie a Giusy, Ale e Francy perchè mi hanno insegnato che la complicità è un qualcosa di innato tra le persone e per avermi dato prova che "l'unione" fa davvero "la forza"!!!

…grazie a Daniela…per le chiacchiere infinite…per gli sfoghi e le confidenze che ha saputo accogliere e soprattutto per il coraggio e la forza che ha saputo trasmettermi…

…grazie alla mia famiglia…in particolare alla mia mamma ed al mio papa…perchè ancora una volta hanno sostenuto le mie scelte senza mai mancare di incondizionato supporto, attenzione e soprattutto amore…

…grazie a Peppe…per essere il mio sicuro rifugio…perchè con tutto il suo amore (e spesso tanta pazienza) è sempre al mio fianco…

…infine grazie a chi, purtroppo, non è più qui…ma ha vegliato e veglia sempre su di me…

…grazie a tutti coloro che non ho avuto modo di citare ma che hanno contribuito a rendere questi anni più lieti…

…perchè se potessi tornare indietro non c'è nessuno che non vorrei aver incontrato…perchè ciascuno mi ha regalato "un pezzetto" di sè contribuendo a rendermi la persona che sono oggi!

…davvero un grazie di cuore a tutti!!!!

8. REFERENCES

Aronson D. Hyperglycemia and the pathobiology of diabetic complications. Adv Cardiol 2008; 45:1-16.

Balkwill FR, Capasso M, Hagemann T. The tumor microenvironment at a glance. J Cell Sci 2012; 125(Pt 23):5591-6.

Baron JA, Weiderpass E, Newcomb PA, Stampfer M, Titus-Ernstoff L, Egan KM, Greenberg ER. Metabolic disorders and breast cancer risk (United States). Cancer Causes and Control 2001; 12:875–880.

Barone BB, Yeh HC, Snyder CF, Peairs KS, Stein KB, Derr RL, Wolff AC, Brancati FL. Postoperative mortality in cancer patients with preexisting diabetes: systematic review and meta-analysis. Diabetes Care 2010; 33(4): 931-9.

Bartella V, De Marco P, Malaguarnera R, Belfiore A, Maggiolini M. New advances on the functional cross-talk between insulin-like growth factor-I and estrogen signaling in cancer. Cell Signal 2012; 24(8):1515-21.

Bissell MJ, Hines WC. Why don't we get more cancer? A proposed role of the microenvironment in restraining cancer progression. Nat Med 2011; 17(3): 320-9.

Borena W, Stocks T, Jonsson H, Strohmaier S, Nagel G, Bjørge T, Manjer J, Hallmans G, Selmer R, Almquist M, Häggström C, Engeland A, Tretli S, Concin H, Strasak A, Stattin P, Ulmer H. Serum triglycerides and cancer risk in the metabolic syndrome and cancer (Me-Can) collaborative study. Cancer Causes Control 2011; 22(2):291-9.

Brigstock DR. The CCN family: a new stimulus package. J Endocrinol 2003; 178(2):169-75.

Calle EE, Kaaks R. Overweight, obesity and cancer: epidemiological evidence and proposed mechanisms. Nat Rev Cancer 2004; 4:579-91.

Cariou S, Donovan JC, Flanagan WM, Milic A, Bhattacharya N, Slingerland JM. Down-regulation of p21WAF1/CIP1 or p27Kip1 abrogates antiestrogen-mediated cell cycle arrest in human breast cancer cells. Proc Natl Acad Sci USA 2000; 97(16):9042-6.

Carroll KK. Dietary factors in hormone-dependent cancers. Curr Concepts Nutr 1977; 6:25-40.

Chiba K., Kawakami K., Tohyama K. Simultaneous evaluation of cell viability by neutral red, MTT and crystal violet staining assays of the same cells. Toxicol In Vitro 1998; 12(3), 251-258.

Chien W, O'Kelly J, Lu D, Leiter A, Sohn J, Yin D, Karlan B, Vadgama J, Lyons KM, Koeffler HP. Expression of connective tissue growth factor (CTGF/CCN2) in breast cancer cells is associated with increased migration and angiogenesis. Int J Oncol 2011; 38(6):1741-7.

Chocarro-Calvo A, García-Martínez JM, Ardila-González S, De la Vieja A, García-Jiménez C. Glucose-induced β-catenin acetylation enhances Wnt signaling in cancer. Mol Cell 2013; 49(3):474-86.

Clemmons DR. Role of insulin-like growth factor binding proteins in controlling IGF actions. Mol Cell Endocrinol 1998; 140:19–24.

Coebergh JW, Janssen-Heijnen ML, Post PN, Razenberg PP. Serious co-morbidity among unselected cancer patients newly diagnosed in the southeastern part of The Netherlands in 1993–1996. Journal of Clinical Epidemiology 1999; 52 1131–1136.

Coughlin SS, Calle EE, Teras LR, Petrelli J, Thun MJ. Diabetes mellitus as a predictor of cancer mortality in a large cohort of US adults. American Journal of Epidemiology 2004; 159 1160–1167.

D'Esposito V, Passaretti F, Hammarstedt A, Liguoro D, Terracciano D, Molea G, Canta L, Miele C, Smith U, Beguinot F, Formisano P. Adipocyte-released insulin-like growth factor-1 is regulated by glucose and fatty acids and controls breast cancer cell growth in vitro. Diabetologia 2012; 55(10):2811-22.

Djiogue S, Nwabo Kamdje AH, Vecchio L, Kipanyula MJ, Farahna M, Aldebasi Y, Seke Etet PF. Insulin resistance and cancer: the role of insulin and IGFs. Endocr Relat Cancer 2013; 20(1):R1-R17.

El-Serag HB, Hampel H, Javadi F. The association between diabetes and hepatocellular carcinoma: a systematic review of epidemiologic evidence. Clin Gastroenterol Hepatol 2006; 4(3):369-80.

Feng YH, Velazquez-Torres G, Gully C, Chen J, Lee MH, Yeung SC. The impact of type 2 diabetes and antidiabetic drugs on cancer cell growth. J Cell Mol Med 2011; 15(4):825-36.

Flier JS. Clinical review 94: What's in a name? In search of leptin's physiologic role. J Clin Endocrinol Metab 1998; 83(5):1407-13.

Friberg E, Orsini N, Mantzoros CS, Wolk A. Diabetes mellitus and risk of endometrial cancer: a meta-analysis. Diabetologia 2007; 50(7):1365-74.

Frühbeck G, Gómez-Ambrosi J, Muruzábal FJ, Burrell MA. The adipocyte: a model for integration of endocrine and metabolic signaling in energy metabolism regulation. Am J Physiol Endocrinol Metab 2001; 280(6):E827-47.

Galic S, Oakhill JS, Steinberg GR. Adipose tissue as an endocrine organ. Mol Cell Endocrinol 2010; 316(2):129-39.

Gallagher EJ, LeRoith D. Epidemiology and molecular mechanisms tying obesity, diabetes, and the metabolic syndrome with cancer. Diabetes Care. 2013; 36 Suppl 2:S233-9.

García-Jiménez C, García-Martínez JM, Chocarro-Calvo A, De la Vieja A. A new link between diabetes and cancer: enhanced WNT/β-catenin signaling by high glucose. J Mol Endocrinol. 2013; 52(1):R51-66.

Giaccone G, Pinedo HM. Drug Resistance. Oncologist 1996; 1(1 & 2):82-87.

Giovannucci E, Harlan DM, Archer MC, Bergenstal RM, Gapstur SM, Habel LA, Pollak M, Regensteiner JG, Yee D. Diabetes and cancer: a consensus report. CA Cancer J Clin 2010; 60(4):207-21.

Gutierrez MC, Detre S, Johnston S, Mohsin SK, Shou J, Allred DC, Schiff R, Osborne CK, Dowsett M. Molecular changes in tamoxifen-resistant breast cancer: relationship between estrogen receptor, HER-2, and p38 mitogen-activated protein kinase. J Clin Oncol 2005; 23(11):2469-76.

Hanahan D, Weinberg RA. Hallmarks of cancer: the next generation. Cell. 2011; 144(5):646-74.

Harding JL, Shaw JE, Peeters A, Cartensen B, Magliano DJ. Cancer risk among people with type 1 and type 2 diabetes: disentangling true associations, detection bias, and reverse causation. Diabetes Care 2015; 38(2):264-70.

Harrison. Principi di Medicina Interna. Il Manuale 17/ed 2009.

Hems G. The contributions of diet and childbearing to breast-cancer rates. Br J Cancer 1978; 37 974-982.

Huber-Keener KJ, Liu X, Wang Z, Wang Y, Freeman W, Wu S, Planas-Silva MD, Ren X, Cheng Y, Zhang Y, Vrana K, Liu CG, Yang JM, Wu R. Differential gene expression in tamoxifen-resistant breast cancer cells revealed by a new analytical model of RNA-Seq data. PLoS One 2012; 7(7):e41333.

Huxley R, Ansary-Moghaddam A, Berrington de González A, Barzi F, Woodward M. Type-II diabetes and pancreatic cancer: a meta-analysis of 36 studies. Br J Cancer 2005; 92(11):2076-83.

International Diabetes Federation. IDF Diabetes Atlas, 6th edn. Brussels, Belgium: International Diabetes Federation, 2013.

Isakson P, Hammarstedt A, Gustafson B, Smith U. Impaired preadipocyte differentiation in human abdominal obesity: role of Wnt, tumor necrosis factor-alpha, and inflammation. Diabetes 2009; 58(7):1550-1557.

Iyengar P, Combs TP, Shah SJ, Gouon-Evans V, Pollard JW, Albanese C, Flanagan L, Tenniswood MP, Guha C, Lisanti MP, Pestell RG, Scherer PE. Adipocyte-secreted factors synergistically promote mammary tumorigenesis through induction of anti-apoptotic transcriptional programs and proto-oncogene stabilization. Oncogene 2003; 22(41)

Johnson JA, Pollak M. Insulin, glucose and the increased risk of cancer in patients with type 2 diabetes. Diabetologia 2010; 53(10):2086-8.

Johnston SR, Dowsett M. Aromatase inhibitors for breast cancer: lessons from the laboratory. Nat Rev Cancer 2003; 3(11):821-31.

Khandekar MJ, Cohen P, Spiegelman BM. Molecular mechanisms of cancer development in obesity. Nat Rev Cancer 2011; 11(12):886-95.

Kim S, Moustaid-Moussa N. Secretory, endocrine and autocrine/paracrine function of the adipocyte. J Nutr 2000; 130(12):3110S-3115S.

Knowlden JM, Hutcheson IR, Jones HE, Madden T, Gee JM, Harper ME, Barrow D, Wakeling AE, Nicholson RI. Elevated levels of epidermal growth factor receptor/c-erbB2 heterodimers mediate an autocrine growth regulatory pathway in tamoxifen-resistant MCF-7 cells. Endocrinology 2003; 144(3):1032-44.

Krone CA, Ely JT. Controlling hyperglycemia as an adjunct to cancer therapy. Integr Cancer Ther 2005; 4:25-31.

Landa MC, Frago N, Tres A. Diet and the risk of breast cancer in Spain. European Journal of Cancer Prevention 1994; 3:313–320.

Larsson SC, Orsini N, Wolk A. Diabetes mellitus and risk of colorectal cancer: a meta-analysis. J Natl Cancer Inst 2005; 97(22):1679-87.

Larsson SC, Orsini N, Brismar K, Wolk A. Diabetes mellitus and risk of bladder cancer: a meta-analysis. Diabetologia 2006; 49(12):2819-23.

Larsson SC, Mantzoros CS, Wolk A. Diabetes mellitus and risk of breast cancer: a meta-analysis. International Journal of Cancer 2007; 121:856–862.

Lubin JH, Burns PE, Blot WJ, Ziegler RG, Lees AW, Fraumeni JF Jr. Dietary factors and breast cancer risk. International Journal of Cancer 1981; 28:685–689.

Macciò A, Madeddu C, Mantovani G. Adipose tissue as target organ in the treatment of hormone-dependent breast cancer: new therapeutic perspectives. Obes Rev 2009; 10(6):660-70.

Makino T, Noguchi Y, Yoshikawa T, Doi C, Nomura K. Circulating interleukin 6 concentrations and insulin resistance in patients with cancer. Br J Surg 1998; 85(12):1658-62.

Masur K, Vetter C, Hinz A, Tomas N, Henrich H, Niggemann B, Zänker KS. Diabetogenic glucose and insulin concentrations modulate transcriptome and protein levels involved in tumour cell migration, adhesion and proliferation. Br J Cancer 2011; 104(2):345-52.

McCall JL, Tuckey JA, Parry BR. Serum tumour necrosis factor alpha and insulin resistance in gastrointestinal cancer. Br J Surg 1992; 79(12):1361-3.

Michels KB, Solomon CG, Hu FB, Rosner BA, Hankinson SE, Colditz GA, Manson JE. Type 2 diabetes and subsequent incidence of breast cancer in the Nurses' Health Study. Diabetes Care 2003; 26:1752–1758.

Mojarrad M, Momeny M, Mansuri F, Abdolazimi Y, Tabrizi MH, Ghaffari SH, Tavangar SM, Modarressi MH. Autocrine human growth hormone expression leads to resistance of MCF-7 cells to tamoxifen. Med Oncol 2010; 27(2):474-80.

Moreno-Navarrete JM, Fernández-Real JM. Adipocyte Differentiation. In: Symonds ME, editor. Adipose Tissue Biology. New York: Springer; 2012. p. 17-38

Nieman KM, Romero IL, Van Houten B, Lengyel E. Adipose tissue and adipocytes support tumorigenesis and metastasis. Biochim Biophys Acta 2013; 1831(10):1533-41.

Niemelä S, Miettinen S, Sarkanen JR, Ashammakhi N. Adipose Tissue and Adipocyte Differentiation: Molecular and Cellular Aspects and Tissue Engineering. Ashammakhi N, Reis R, Chiellini F, editors. Applications Topics in Tissue Engineering, Vol. 4. Oulu, Finland: University of Oulu; 2008. p. 1-26

Noto H, Osame K, Sasazuki T, Noda M. Substantially increased risk of cancer in patients with diabetes mellitus: a systematic review and meta-analysis of epidemiologic evidence in Japan. J Diabetes Complications 2010; 24(5):345-53.

Novosyadlyy R, LeRoith D. Hyperinsulinemia and type 2 diabetes: impact on cancer. Cell Cycle 2010; 9(8):1449-50.

O'Mahony F, Razandi M, Pedram A, Harvey BJ, Levin ER. Estrogen modulates metabolic pathway adaptation to available glucose in breast cancer cells. Mol Endocrinol 2012; 26(12):2058-70.

Onitilo AA, Engel JM, Glurich I, Stankowski RV, Williams GM, Doi SA. Diabetes and cancer II: role of diabetes medications and influence of shared risk factors. Cancer Causes Control 2012; 23(7):991-1008.

Osborn O, Olefsky JM. The cellular and signaling networks linking the immune system and metabolism in disease. Nat Med 2012; 18(3):363-74.

Park J, Morley TS, Kim M, Clegg DJ, Scherer PE. Obesity and cancer-mechanisms underlying tumour progression and recurrence. Nat Rev Endocrinol 2014; 10(8):455-65.

Peifer C, Alessi DR. New anti-cancer role for PDK1 inhibitors: preventing resistance to tamoxifen. Biochem J 2009; 417(1):e5-7.

Potischman N, Coates RJ, Swanson CA, Carroll RJ, Daling JR, Brogan DR, Gammon MD, Midthune D, Curtin J, Brinton LA. Increased risk of early-stage breast cancer related to consumption of sweet foods among women less than age 45 in the United States. Cancer Causes and Control 2002; 13:937–946.

Poulos SP, Hausman DB, Hausman GJ. The development and endocrine functions of adipose tissue. Mol Cell Endocrinol 2010; 323(1):20-34.

Quail DF, Joyce JA. Microenvironmental regulation of tumor progression and metastasis. Nat Med 2013; 19(11):1423-37.

Rajala MW, Scherer PE. Minireview: The adipocyte--at the crossroads of energy homeostasis, inflammation, and atherosclerosis. Endocrinology 2003; 144(9):3765-73.

Renehan AG, Yeh HC, Johnson JA, Wild SH, Gale EA, Møller H; Diabetes and Cancer Research Consortium. Diabetes and cancer (2): evaluating the impact of diabetes on mortality in patients with cancer. Diabetologia 2012; 55(6):1619-32.

Russo F, Angelini C. RNASeqGUI: a GUI for analysing RNA-Seq data. Bioinformatics 2014; 30(17):2514-6.

Ryu TY, Park J, Scherer PE. Hyperglycemia as a risk factor for cancer progression. Diabetes Metab J 2014; 38(5):330-6.

Seshasai SR, Kaptoge S, Thompson A, Di Angelantonio E, Gao P, Sarwar N, Whincup PH, Mukamal KJ, Gillum RF, Holme I, Njølstad I, Fletcher A, Nilsson P, Lewington S, Collins R, Gudnason V, Thompson SG, Sattar N, Selvin E, Hu FB, Danesh J. Diabetes mellitus, fasting glucose, and risk of cause-specific death. N Engl J Med 2011; 364(9):829-41.

Shafie SM & Grantham FH. Role of hormones in the growth and regression of human breast cancer cells (MCF-7) transplanted into athymic nude mice. Journal of the National Cancer Institute 1981; 67:51–56.

Shang Y. Molecular mechanisms of oestrogen and SERMs in endometrial carcinogenesis. Nat Rev Cancer 2006; 6(5):360-8.

Shi Y, Hu FB. The global implications of diabetes and cancer. Lancet 2014; 383(9933):1947-8.

Shi-Wen X, Leask A, Abraham D. Regulation and function of connective tissue growth factor/CCN2 in tissue repair, scarring and fibrosis. Cytokine Growth Factor Rev 2008; 19(2):133-44.

Silvera SA, Jain M, Howe GR, Miller AB, Rohan TE. Dietary carbohydrates and breast cancer risk: a prospective study of the roles of overall

glycemic index and glycemic load. International Journal of Cancer 2005; 114:653–658.

Srokowski TP, Fang S, Hortobagyi GN, Giordano SH. Impact of diabetes mellitus on complications and outcomes of adjuvant chemotherapy in older patients with breast cancer. J Clin Oncol. 2009; 27(13):2170-6.

Talamini R, Franceschi S, Favero A, Negri E, Parazzini F, La Vecchia C. Selected medical conditions and risk of breast cancer. British Journal of Cancer 1997; 75:1699–1703.

Tarazona S, Garcia-Alcalde F, Dopazo J, Ferrer A, Conesa A. Differential expression in RNA-seq: a matter of depth. Genome research 2011; 21(12), pp. 4436.

Tavani A, Giordano L, Gallus S, Talamini R, Franceschi S, Giacosa A, Montella M, La Vecchia C. Consumption of sweet foods and breast cancer risk in Italy. Annals of Oncology 2006; 17:341–345.

Tsai MS, Bogart DF, Li P, Mehmi I, Lupu R. Expression and regulation of Cyr61 in human breast cancer cell lines. Oncogene 2002; 21(6):964-73 (a).

Tsai MS, Bogart DF, Castañeda JM, Li P, Lupu R. Cyr61 promotes breast tumorigenesis and cancer progression. Oncogene 2002; 21(53):8178-85 (b).

Vigneri P, Frasca F, Sciacca L, Pandini G, Vigneri R. Diabetes and cancer. Endocr Relat Cancer 2009; 16(4):1103-23.

Wang MY, Chen PS, Prakash E, Hsu HC, Huang HY, Lin MT, Chang KJ, Kuo ML. Connective tissue growth factor confers drug resistance in breast cancer through concomitant up-regulation of Bcl-xL and cIAP1. Cancer Res 2009; 69(8):3482-91.

Weiderpass E, Gridley G, Persson I, Nyren O, Ekbom A, Adami HO. Risk of endometrial and breast cancer in patients with diabetes mellitus. International Journal of Cancer 1997; 71:360–363.

Wideroff L, Gridley G, Mellemkjaer L, Chow WH, Linet M, Keehn S, Borch-Johnsen K, Olsen JH. Cancer incidence in a population-based cohort of patients hospitalized with diabetes mellitus in Denmark. Journal of the National Cancer Institute 1997; 89:1360–1365.

Wotton CJ, Yeates DG, Goldacre MJ. Cancer in patients admitted to hospital with diabetes mellitus aged 30 years and over: record linkage studies. Diabetologia 2011; 54(3):527-34.

Xie D, Nakachi K, Wang H, Elashoff R, Koeffler HP. Elevated levels of connective tissue growth factor, WISP-1, and CYR61 in primary breast cancers associated with more advanced features. Cancer Res 2001; 61(24):8917-23.

Yancik R, Wesley MN, Ries LA, Havlik RJ, Edwards BK, Yates JW. Effect of age and comorbidity in postmenopausal breast cancer patients aged 55 years and older. Journal of the American Medical Association 2001; 285:885–892.

Yi EH, Lee CS, Lee JK, Lee YJ, Shin MK, Cho CH, Kang KW, Lee JW, Han W, Noh DY, Kim YN, Cho IH, Ye SK. STAT3-RANTES autocrine signaling is essential for tamoxifen resistance in human breast cancer cells. Mol Cancer Res 2013; 11(1):31-42.

Youlden DR, Cramb SM, Dunn NA, Muller JM, Pyke CM, Baade PD. The descriptive epidemiology of female breast cancer: an international comparison of screening, incidence, survival and mortality. Cancer Epidemiol 2012; 36(3):237-48.

Zeng L, Biernacka KM, Holly JM, Jarrett C, Morrison AA, Morgan A, Winters ZE, Foulstone EJ, Shield JP, Perks CM. Hyperglycaemia confers resistance to chemotherapy on breast cancer cells: the role of fatty acid synthase. Endocr Relat Cancer 2010; 17(2):539-51.

Zimmet P, Alberti KG, Shaw J. Global and societal implications of the diabetes epidemic. Nature 2001; 414(6865):782-7.

Zuk PA, Zhu M, Ashjian P, De Ugarte DA, Huang JI, Mizuno H, Alfonso ZC, Fraser JK, Benhaim P, Hedrick MH. Human adipose tissue is a source of multipotent stem cells. Mol Biol Cell 2002; 13(12): 4279-95.

Curr Tran Geriatr Gerontol Rep (2012) 1:219–228
DOI 10.1007/s13670-012-0023-4

FROM GENETICS TO EPIGENETICS: IMPLICATIONS IN NEURODEGENERATIVE DISORDERS (P JIN, SECTION EDITOR)

Non-coding RNA in Neurodegeneration

Alfredo Ciccodicola · Maria Rosaria Ambrosio · Margherita Scarpato · Valerio Costa

Published online: 8 September 2012

Abstract Aging-associated chronic diseases, such as neurodegenerative disorders, have a dramatic impact on healthcare systems. Despite progresses in understanding their etiology, unsolved questions still exist. These complex disorders share a common inflammatory *status* and are influenced by common post-transcriptional mechanisms of gene regulation. MicroRNAs, key players in modulating gene expression, and other non-coding RNAs have specific spatial-temporal expression in the brain, and a critical role in neurogenesis and neurodegenerative diseases. Here, we review the emerging impact of non-coding RNAs in their pathogenesis, also performing a computational analysis on microRNAs and target genes. Our findings strengthen the notion of an inflammatory-related component in neurodegenerative disorders, confirming the contribution of microRNA-dependent gene expression regulation in the etiology of such diseases.

Keywords Non-coding RNA · miRNAs · Neurodegeneration · Inflammation · Down syndrome · Epigenetics mechanisms · RNA-Seq

A. Ciccodicola (✉) · M. R. Ambrosio · M. Scarpato · V. Costa
CNR, Institute of Genetics and Biophysics
"A. Buzzati-Traverso" (IGB),
Via P. Castellino 111,
80131 Naples, Italy
e-mail: alfredo.ciccodicola@igb.cnr.it

M. R. Ambrosio
e-mail: ambrosi@igb.cnr.it

M. Scarpato
e-mail: scarpato@igb.cnr.it

V. Costa
e-mail: valerio.costa@igb.cnr.it

Introduction

Life expectancy has greatly increased worldwide during the last decades, due to the fact that the elderly population (60 y.o. or over) has tripled over the last 50 years and it is expected to triple again over the next 50 years [1]. Along with the increasing number of elderly persons, aging-associated chronic diseases are assuming a significant relevance. In particular, the prevalence of neurodegenerative disorders (NDs), which rises in step with the aging of the population, is having a broad impact on healthcare systems and is predicted to worsen in the near future [2]. A growing number of studies focusing on NDs are still in progress to understand the pathogenesis and the molecular mechanisms underlying these disorders, with the aim to develop effective programs for prevention and therapy. Nevertheless, many questions remain unanswered and much can still be brought to light.

NDs constitute a wide class of disorders, including Alzheimer's, Parkinson's and Huntington's diseases (AD, PD and HD, respectively), frontotemporal dementia (FTD), amyotrophic lateral sclerosis (ALS), spinocerebellar ataxia (SCA), and Prion diseases. In addition, young individuals with Down syndrome (DS) develop an early impairment of cognitive functions with Alzheimer-like phenotype [3]. These conditions are all - except DS - characterized by a progressive loss of neuronal cells in adulthood [4]. Neurodegeneration is initially limited to a specific cell type in the central nervous system (CNS), in line with the heterogeneity of clinical symptoms. Cortical and hippocampal regions are affected in AD, dopaminergic neurons in the *substantia nigra* in PD, frontal and/or temporal lobes in FTD, motor neurons in the brain and spinal chord in ALS, the basal ganglia in HD [5]. In later stages, neuronal cell death progressively extends to wider CNS regions, gradually leading to a severe physical and cognitive disability, frequently including loss of body control, speech impairment and dementia [6].

Although their etiology is not fully understood, the presence of intracellular or extracellular aggregates of misfolded proteins in the brain is a common feature. Amyloid plaques, consisting of deposits of β-amyloid protein - a fragment derived from altered processing of amyloid protein precursor (APP) - in extracellular parenchyma, and intracellular neurofibrillary tangles, containing aggregation of hyperphosphorylated tau protein, represent histopathological signatures of AD [7]. Tau aggregates are also observed in FTD [8], whereas TDP-43 inclusions are common in frontotemporal lobar degeneration (FTLD) and in ALS [9]. In PD, dopaminergic neurons are characterized by cytoplasmic inclusions of α-synuclein, known as Lewy bodies [10]. Protein aggregates, due to polyglutamine expansion in huntingtin and ataxin proteins, are detected in HD and SCA, respectively [11, 12]. Moreover, Prion diseases are characterized by the accumulation of conformationally-modified glycoprotein PrP [13]. Since the deposits of abnormal proteins are a distinctive feature of all NDs, it is reasonable to assume that protein misfolding and the aggregation process represent a crucial step in neurodegenerative mechanisms [14]. Although each ND shows a different histological phenotype, the abnormal protein accumulation triggers the activation of inflammatory and oxidative-stress pathways. Thus, a chronic inflammatory state has a relevant impact on neuronal cell death, consistent with the "age-based theory" of neurodegeneration's pathogenesis, since the levels of oxidative damage increase with aging and, conversely, the anti-oxidative defenses decrease [15].

Most of the molecular causes underlying NDs are still unclear, although in the last three decades the application of molecular cell biology's techniques to CNS study has improved our knowledge about neurodegenerative processes [16]. In the "pre-genomic era", the genetic bases of NDs have been investigated by linkage analyses, and a restricted subset of causative genes identified by positional cloning. So, more than 200 disease-causing mutations have been identified in three different genes, *APP* (amyloid precursor protein), *PSEN1* (presenilin1) and *PSEN2* (presenilin2), associated with AD [17], whereas more than 300 pathogenic mutations have been identified in five genes, α-synuclein (*SNCA*), parkin (*PARK2*), PTEN-induced putative kinase 1 (*PINK1*), DJ-1 (*PARK7*), and Leucine-rich repeat kinase 2 (*LRRK2*) in PD families [18]. Moreover, five established genes for Mendelian forms of FTD and thirteen for ALS have been identified [4]. In addition, hereditary forms of Prion diseases, such as Creutzfeld-Jacob disease, have been associated to mutations in the gene encoding PrP (*PRNP*) [5].

Despite the impact of their genetic component, NDs are complex traits and only few cases can be explained by a typical Mendelian inheritance. More than 90 % of cases, defined as "sporadic" or "idiopathic" forms, appear to be regulated by an intricate network of genes and environmental factors. Particularly, the recent application of genome-wide association studies (GWAS) has led to the identification of many single nucleotide polymorphisms (SNPs) in susceptibility genes, associated with the etiology of NDs, i.e. APOE-ε4 in AD [17]. However, for all human diseases it has been estimated that about 90 % of currently identified disease-associated SNPs are intronic or intergenic, and GWAS explain only a small percentage of NDs cases [19]. Therefore, a significant portion of "missing hereditability" remains. Moreover, variation in gene expression has recently been shown to affect susceptibility to complex diseases [20], such as the Alzheimer-like dementia occurring in DS individuals, strictly linked to the presence of an extra copy of critical genes on chromosome 21 [21].

Changes in gene expression occur during aging, and these are accelerated in some forms of neurodegeneration [22••]. Epigenetic mechanisms dynamically regulate gene expression, acting at several levels. In this scenario, other contributors are the non-coding RNAs (ncRNAs) - transcribed from DNA regions considered for a long time to be evolutionary debris and junk sequences - which represent a major portion of transcriptome acquiring an emerging pivotal role as determinants of gene expression regulation, revealing an unexpected involvement in human diseases [23••]. Evidences show the contribution of ncRNAs in complex regulatory networks of differentiation and development, acting through chromatin modification, transcription, RNA modification, splicing, mRNA translation and RNA stability [24]. Moreover, it should also be considered that some classes of ncRNAs have specific spatial-temporal patterns of expression in CNS, suggesting a role in neurogenesis and neuronal functions and, consequently to their deregulation, in neuronal pathological processes [25]. Among them, miRNAs are becoming major players in shaping cell functionality, as well as in determining cell fate. Indeed, they are crucial factors in cell differentiation, and in many other cell processes fundamental for neurons, such as neurotransmission and synaptic plasticity [26••]. In addition, several long non-coding RNAs (lncRNAs) display specific localization limited to restricted brain regions, particular neuronal cell-type or subcellular compartments, suggesting their deregulation might contribute to NDs' onset [27].

Therefore, given the inability to explain all NDs cases by a typical Mendelian inheritance, and also considering the potential impact of ncRNAs on gene expression and on disease onset/progression, it is reasonable to speculate ncRNAs might be involved in their pathogenesis.

Neurodegeneration and Non-coding RNA

Only 2–4 % of the mammalian genome encodes mRNAs. The ncRNA fraction has been long considered non-functional, with the exception of the common infrastructural

RNAs involved in protein synthesis, transport and splicing [28]. However, researchers have increasingly focused their attention on the part of human genome transcribed and never translated, trying to clarify the genetic information contained therein, and its functions [26••, 29, 30]. In recent years, interesting results have been obtained, challenging the traditional view of RNA as a simple intermediary between DNA and protein, and thus showing that the vast majority of the genome encodes functional RNA species [24].

A large variety of ncRNAs has been progressively identified in the CNS, and their roles in neurogenesis, neural stem cell maintenance, synaptic and neural network connectivity and plasticity have been highlighted [25]. These evidences suggest a strong connection between the regulatory potential of ncRNAs and CNS complexity [31]. Consequently, it is intuitive that altered expression and function of ncRNAs may be directly linked to the onset of CNS disorders.

The most widely studied class of small-ncRNAs (<400 nucleotides) is microRNAs (miRNAs), highly conserved molecules of 20–22 nucleotides in length, found in almost all eukaryotic cells [32•]. Mature miRNAs are generated through a multi-step process. They are post-transcriptional regulators of gene expression which, binding to complementary sequences, downregulate target mRNAs' levels, causing the degradation of related transcripts or the inhibition of their translation [23••, 33–35]. Whereas some miRNAs regulate specific individual targets, others can function as master regulators of a process, or through the simultaneous regulation of hundreds of genes, or acting cooperatively on target genes [31, 36].

miRNAs are involved in numerous biological processes, including cell proliferation, development, stress responses and apoptosis [36]. In mammals, they are predicted to control the activity of more than 50 % of all protein-coding genes [33]. About 70 % of miRNAs are expressed in specific brain regions, and experimental evidences have shown their role in terminal differentiation and maintenance of many neuronal types, suggesting a relevant functional role in brain activities [31, 36, 37]. A growing number of reports have shown that miRNA deregulation is associated with the pathogenesis of human NDs [38]. For instance, altered miRNA levels have been directly linked to AD pathogenesis [39••]. Analyses performed on the brains of AD patients, with deregulated levels of β-site APP cleaving enzyme (encoded by *BACE1*), have displayed a significant alteration in miRNA expression. BACE1 contributes to the accumulation of toxic Aβ fragment, and is a target of several miRNAs [40–43].

In addition, it is reasonable to speculate that miRNAs may represent a crucial regulatory mechanism also linking AD and DS pathogenesis. Indeed, both the overexpression of specific genes located on chromosome 21 (HSA21) - such as *APP* - and HSA21 miRNAs have been reported in DS patients. The simultaneous downregulation of their target genes has suggested a relevant role for HSA21 miRNAs on their expression during DS pathological processes. Therefore, these molecules may represent good candidates for the onset of the Alzheimer's-like dementia occurring in young DS individuals, as well as for other NDs [44, 45]. Interestingly, accumulating evidences of miRNAs' role have been reported also in PD. Two miRNAs (miR-7 and miR-153) have been demonstrated to inhibit *SNCA* - encoding α-synuclein - crucially related to PD pathogenesis [46]. Furthermore, expression profiling of miRNAs in adult PD vs. normal midbrain, revealed the downregulation of miR133b - normally enriched in the midbrain - possibly acting as negative regulator in dopaminergic neuron maturation, targeting the transcription factor (TF) Pitx3 [39••].

The evidence of direct and indirect roles of miRNAs has also been progressively suggested in other NDs, such as in HD onset. Patients affected by HD show a pathogenic polyglutamine expansion in huntingtin, responsible for disrupted interaction with the transcription factor REST that, in normal neurons, is sequestered in the cytoplasm by the protein huntingtin. In HD, its aberrant nuclear-cytoplasmic trafficking is promoted, and the expression of its target genes is deregulated. REST target genes include not only protein-coding, but also miRNAs and other ncRNAs [39••]. Interestingly, REST regulates the expression levels of miR9 and miR9*, which in turn can regulate REST itself, suggesting a negative feedback loop during HD development [47, 48]. ALS is another member of NDs in which miRNAs play a critical role. Notably, mutations in the components of Drosha microprocessor complex - involved in biogenesis of miRNAs - cause up to 50 % of familiar cases of ALS [49].

Although experimental evidences have shown the relevant role of miRNAs in ND pathogenesis, further studies have gradually highlighted the involvement of other ncRNAs in their onset. Among them, lncRNAs (>400 nucleotides) represent one of the most abundant classes [26••, 50]. They derive from genomic *loci* proximal to protein-coding genes, and are usually regulated by the same transcriptional and epigenetic mechanisms. These transcripts are fundamental in a plethora of subcellular processes, including formation of cellular structural compartments, neuronal differentiation, hippocampal development and oligodendrocyte myelination [51•]. Indeed, their expression is largely reported in the brain and, interestingly, some of them have been shown to interact with promoter elements and TFs, critically modulating the transcriptional activity. For instance, the Sox2OT lncRNA may have a regulatory effect on Sox2, a TF required for neural induction and maintenance of neural stemness [52]. Similarly, Nkx2.2AS lncRNA modulates the expression of Nkx2 and other factors involved in oligodendocyte lineage specification [53].

Furthermore, lncRNAs can regulate post-transcriptional mRNA processing and translation by interacting with specific sequences [54] and modulating the epigenetic *status* of protein-coding genes through *cis* and *trans* mechanisms. In addition, lncRNAs may be the precursor of small ncRNAs, such as miRNAs [55]. Interestingly, a large number of studies have revealed a very dynamic profile of expression - and functions - for lncRNAs during the development of adult tissues, including brain and several neural cell subtypes [51•]. Deregulation of lncRNAs has been associated with the pathogenesis of different NDs, including *ATXN80S* in SCA8 [56–58], *BACE1-AS* and *BC200* in AD [59, 60]. Moreover, further findings have suggested that some lncRNAs might be involved in molecular mechanisms underlying ALS and HD [51•].

Our recent transcriptome analysis in DS has revealed lncRNAs' deregulation in trisomic vs. euploid cells, suggesting their involvement in some pathological features typical of DS [61]. Finally, it is reasonable to assume many disease-associated SNPs, identified in intronic and intergenic regions in patients affected by NDs, are likely to fall in previously unannotated non-coding transcripts, such as lncRNA, possibly contributing to the disease.

It should be mentioned that another class of ncRNAs, the small nucleolar RNAs (snoRNAs), has been directly linked to Prader-Willi syndrome characterized by neonatal muscular hypotonia, obesity, hypogonadism, behavioral problems and mental retardation. In particular, HBII-52 snoRNA, which regulates alternative splicing of 5-HT_{2C}R mRNA, is silenced in patients, leading to the production of different isoforms compared to healthy individuals [62].

In light of these evidences, studying the function, spatial-temporal localization and regulation of ncRNAs in neurons is becoming essential to understanding physiological neurogenesis and neural plasticity, as well as to disclose the molecular bases of neurodegenerative processes occurring in patients' brains.

miRNAs in Neurodegeneration

As mentioned above, miRNAs represent the major and better-studied class of ncRNAs involved in neurodegenerative processes. Given their relevant contribution to ND onset and severity, and also considering the large amount of molecular data available from gene expression studies, and consequently, the growing number of well-curated miRNA databases, we focused our analysis on this ncRNA species.

In particular, after browsing commonly used databases, we collected from miRWalk [63] and mir2disease [64] all miRNAs with a proven involvement in NDs and neurodegenerative processes (listed in Table 1). miRBase was also used to retrieve additional information about the selected miRNAs [65].

The newly developed miRWalk algorithm was used to predict miRNA binding sites within the complete set of annotated human genes, particularly those implicated in crucial biological pathways. Unlike other algorithms producing prediction of miRNAs binding sites within 3'UTRs of target genes, the "Validated Targets module" of miRWalk provides information on experimentally validated miRNA-gene interactions, dramatically reducing the rate of false positive sites. Such analysis was performed by pooling - for each disease - miRNAs retrieved by both miRWalk and mir2disease databases. The number of identified target genes is also indicated in Table 1. The PANTHER (Protein ANalysis THrough Evolutionary Relationships) tool was used to classify target gene lists according to their molecular function as well as their involvement in specific cellular pathways [66]. Notably, as shown in the bar graphs (Fig. 1), the most recurrent pathways for almost all examined NDs were inflammation, integrin, interleukin and Wnt signaling, angiogenesis and apoptosis pathways. These findings are of particular interest since chronic inflammatory state is a common feature in NDs (as discussed in detail in "Neurodegeneration and Inflammation"). Intersection among the lists of miRNAs' target genes for each disease was performed with a custom Matlab script in order to explore all possible combinations (schematically shown in Fig. 1). A significant overlap of genes among some NDs was disclosed, as indicated by the heat map in Fig. 1. In addition, by using the Genetic Association Database [67], an archive of human genetic association studies for complex diseases, we identified - as expected - that a significant fraction of common genes is associated with aging, neurological and psychiatric disorders (pie charts in Fig. 1).

Neurodegeneration and Inflammation

Neurodegenerative process is characterized by unremitting activation of the inflammatory response, which might trigger neuronal cell death [68•]. Enduring inflammation implies the persistence of the inflammatory *stimulus*, which may consist of environmental (exogenous) factors or endogenous molecules perceived by the immune system as "stranger" or "danger" signals. Therefore, it is reasonable that in each ND, misfolded proteins accumulated in cytoplasm or parenchyma of specific brain regions are recognized as "non-self" by the immune system [69••]. Thus, a chronic inflammatory state might be a direct consequence of the inflammatory response triggered by abnormal protein deposits, a common feature of NDs. Moreover, the age advancement is associated with increased levels of oxidative stress and reduced effectiveness of antioxidative defense mechanisms, in line with the late onset of such diseases [70]. Both evidences could explain the typical alterations in inflammatory *status* observed during neurodegenerative

Table 1 Deregulated miRNAs in neurodegenerative diseases

Disease	miR2Disease db		miRWalk db	N° target genes	Ref
AD	↑ miR125b, miR-128a, miR-146, miR-146a, miR-197, miR-320, miR-511, miR-9	N/A	miR-101, miR-146a, miR-146a*, miR-298, miR-29a, miR-29a*, miR-29b, miR-29b-1*, miR-29b-2*, miR-29c, miR-29c*, miR-328, miR-338-3p, miR-34a, miR-34a*	1025	[40–43] [88–91]
	↓ let-7i, miR-101, miR-106b, miR-107, miR-124a, miR15a, miR-181c, miR-210, miR-22, miR-26b, miR-298, miR-29a, miR-29b-1, miR-328, miR-34a, miR-363, miR-9, miR-93				
PD	↑ miR-433	N/A	miR-30a, miR-30a*, miR-30b, miR-30b*, miR-30c, miR-30c-1*, miR-30c-2*, miR-30d, miR-30d*, miR-30e, miR-30e*, miR-433	622	[37] [92–94]
	↓ miR-133b, miR-64, miR-65, miR-7				
HD	↑ miR-29a, miR-330 ↓ miR-128, miR-22, miR-132, miR-9, miR-9*			320	[99] [100] [47]
FTLD		N/A	let-7b, let-7b*, miR-663	628	
FTD	↑ miR-659	N/A	miR-107, miR-29b, miR-29b-1*, miR-29b-2*, miR-659	153	[96]
ALS		N/A	let-7b, let-7b*, miR-206, miR-29a*, miR-29a, miR-29b, miR-338-3p, miR-663	804	
SCA	↑ miR-144, miR-144* ↓ miR-101, miR-130, miR-19	N/A	miR-144, miR-144*	112	[97, 98]
DS	↑ let-7c, miR-125b-2, miR-155, miR-802, miR-99a	N/A	let-7c, miR-125b-2, miR-155, miR-802, miR-99a let7c*, miR-125b, miR-125b-2*, miR-155*, miR-99a*	967	[45]
Prion	↑ miR-342-3p	N/A	miR-342-3, miR-494	40	[95]

HD, Huntington's disease; PD, Parkinson's disease; AD, Alzheimer's disease; FTLD, Frontotemporal Lobar Degeneration; FTD, Frontotemporal dementia; SCA, spinocerebellar ataxia; DS, Down Syndrome; ALS, Amyotrophic Lateral Sclerosis; Prion, Prion diseases.↑ , ncRNAs upregulated and ↓, downregulated

processes. Indeed, a wide spectrum of studies has highlighted the involvement of activated microglia and reactive astrocytes in NDs [71]. Inflammatory response activation implies the synthesis of a wide range of proinflammatory mediators and the production of free radicals and oxygen/nitrogen reactive species (ROS and RNS), increasing the oxidative damage and determining a positive feedback [72]. In addition, dysfunctions of mitochondria, involved in the defense mechanisms against oxidative stress, occur in all major NDs [73]. Notably, mutations in *SOD1* gene - encoding for the superoxide dismutase enzyme responsible for destroying toxic superoxide radicals - is associated with ALS [74] and evidence of altered expression of the *SOD1* gene has been reported in DS for several cells/tissues [75, 76]. Definitively, the immune response to chronic inflammatory state might play a pivotal role in synaptic dysfunction and selective neuronal loss, strongly contributing to the onset and progression of neurodegeneration.

Recent evidence shows that miRNAs have a determinant function in modulating immune response in NDs. For instance, miR-125b, miR-146a and miR-155 downregulate the Complement Factor H encoding gene (*CFH*) in AD e DS [77]. In addition, miR-146a overexpression in Prion diseases is involved in microglia activation [78], whereas miR-101 contributes to the regulation of the *APP* gene in response to the proinflammatory cytokine interleukin-1β (IL-lβ) [79].

Such findings stimulate further research aimed at the comprehension of the connection among the three elements of the triad ncRNAs-inflammation-neurodegeneration.

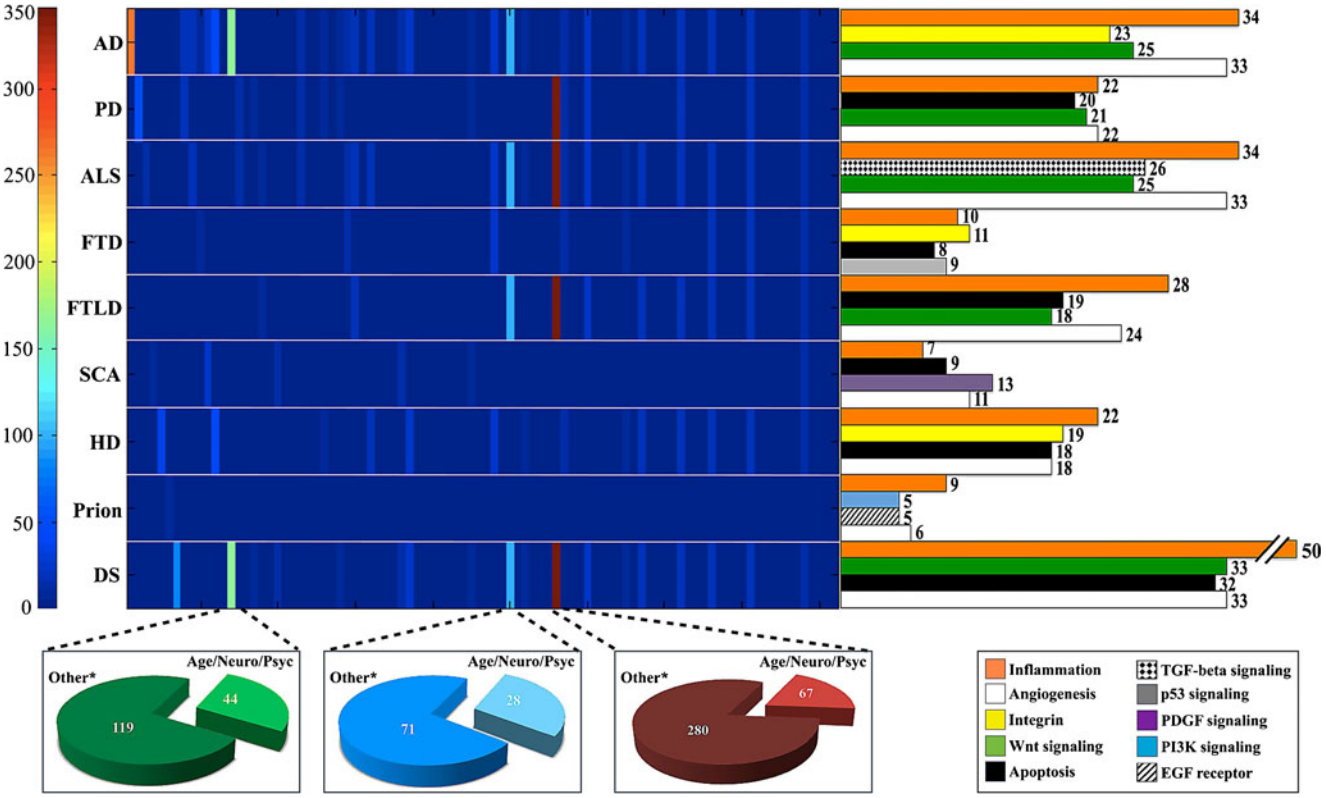

Fig. 1 Graphical representation of target genes of miRNAs involved in all examined NDs. The matrix, shown on a blue background, was built considering "disease-specific" target genes and all combinations of those genes shared by two or more NDs. Color intensity of vertical blocks indicates the number of common genes, according to the heat map (on the left). NDs are indicated in the rows and, on the right, the bar graphs show the most recurrent pathways in each disease. For the most numerous sets of shared target genes, pie charts (on the bottom) display the percent of common genes associated with aging, neurological and psychiatric disorders according to the Genetic Association Database

Inflammation-Related miRNAs and Genes: A Bridge to Neurodegeneration?

NDs display different histological phenotypes and clinical symptoms, although the production of abnormal proteins and their pathological accumulation into cellular aggregates are common features [12]. Such events, as above described, have been correlated with a chronic inflammatory state, and consequently to neuronal cell death [15]. The finding that a significant fraction of genes targeted by ND-related miRNAs belongs to inflammatory-related pathways (described in "miRNAs in Neurodegeneration"; Fig. 1) further suggests a direct, and perhaps strong, impact of inflammation in the etiology of NDs. Thus, to observe the extent of such overlap we first catalogued annotated human genes involved in inflammatory-related pathways (retrieved by PANTHER) and then identified the validated miRNAs that regulate them (mirWalk).

Interestingly, as shown in Table 2, the examined NDs - except DS - share a very significant fraction of "disease-associated" miRNAs with analyzed inflammatory-related genes, with, on average, 84 % of common miRNAs. These data further support the notion that an altered expression of inflammation-related genes, possibly due to miRNA deregulation and thus a chronic activation of the inflammatory cascade, may significantly contribute to neurodegenerative

Table 2 Disease- vs. Inflammation- specific miRNAs

Disease	Validated miRNAs		
	Disease-specific	Common	Inflammation-specific
AD	5	29 (85,3 %)	351
PD	2	14 (87,5 %)	366
ALS	0	8 (100,0 %)	372
FTD	1	4 (80,0 %)	376
FTLD	0	3 (100,0 %)	377
SCA	2	3 (60,0 %)	377
HD	1	6 (85,7 %)	374
Prion	1	2 (66,7 %)	378
DS	8	2 (20,0 %)	378

AD, Alzheimer's Disease; PD, Parkinson's Disease; ALS, Amyotrophic Lateral Sclerosis; FTD, Frontotemporal Dementia; FTLD, Frontotemporal Lobar Degeneration; SCA, Spinocerebellar Ataxia; HD, Huntington's disease; Prion, Prion Diseases; DS, Down Syndrome

processes, possibly triggering the onset (or determining the severity) of NDs, in line with previous findings [68•].

RNA-Seq: A Promising Tools for Transcriptome Profiling in NDs

NDs have been widely studied from a "DNA perspective." The search for causative mutations in few disease-causing genes or for SNPs and *loci* associated with disease susceptibility have only partially explained NDs inheritance and the molecular causes of such diseases. In the last decade, gene expression studies have gradually been employed to investigate many human genetic disorders, including NDs [80••]. Transgenic animal models, *post-mortem* brains and patient-derived cell lines have been frequently used for gene expression analyses [81•].

Most of the gene expression studies performed so far, mainly on microarray platforms, have focused on PD, AD and HD, although conflicting results have been reported. Technological drawbacks [82], the variable quality/integrity of RNAs and the fragile nature of RNA samples from brains have been reported as the main causes of such discrepancies [81•].

Sequencing-based assays, such as Serial and Cap Analysis of Gene Expression have been successfully used in PD, AD and DS [83]. The introduction of NGS platforms for high-resolution analyses, and particularly of accurate methods for massive-scale transcriptomics (RNA-Seq), allows exploration of such NDs from a different perspective [84]. Indeed, RNA-Seq has been revealed to be a promising tool to study human diseases and to analyze transcriptomics' changes, also in NDs' patients [85]. Nonetheless, to date, only one group has employed RNA-Seq on AD patients' brains [86••]. In particular, they observed significant differences in the expression, and promoter usage, for different *APOE* splice isoforms in normal vs. AD brains, indicating that alternative splicing plays a crucial role in the progression of neurodegeneration in AD patients.

Of note, another group has profiled human neurons derived from induced pluripotent stem cells proposing a model to study defective neurogenesis [87]. In addition, our group has recently analyzed by RNA-Seq the transcriptome of endothelial progenitor cells - impaired in DS - showing that coupling a protocol of rRNA depletion to RNA-Seq allows investigation of transcriptome in pathological conditions [61].

Conclusions

In recent years, the increased prevalence of NDs is having a dramatic impact on healthcare systems worldwide. Despite steps taken toward an understanding of the etiology behind neurodegenerative processes, there are still many molecular aspects to clarify. Studies aimed at identifying disease-causing mutations in the Mendelian forms of NDs and large-scale GWAS have only partially explained their pathogenesis, showing a substantial lack of knowledge. Gene expression studies, particularly those investigating the role of ncRNAs, have started to highlight the contribution of these molecules to ND pathogenesis. Particularly, miRNAs and lncRNAs are showing relevant roles in neural cell plasticity and in neurodegenerative processes [39••].

Moreover, it has been recognized that despite having different histological phenotypes, distinction in brain areas affected, and varying clinical symptoms, there are distinctive common features among NDs. Pathological deposits of misfolded proteins are the first step toward formation of cell aggregates [14], and activation of inflammatory and oxidative-stress pathways, possibly leading to neuronal cell death, are common characteristics of these diseases [16].

Our analysis of miRNAs and their target genes retrieved interesting results, confirming that recurrent pathways for all examined NDs are inflammation-mediated by chemokines and cytokines, integrin and Wnt signaling, angiogenesis and apoptosis pathways. Moreover, a significant fraction of miRNA target genes common to more NDs was associated to aging, neurological and psychiatric disorders according to the Genetic Association Database.

Such observations further strengthen the evidence of an inflammatory-related component in NDs, confirming the relevant contribution of miRNA-dependent gene expression regulation in the etiology of such diseases.

However, functional studies are needed to validate such findings, and large-scale expression analyses of ncRNAs in these diseases will surely provide a significant contribution. Despite the fact that NGS application to NDs is still in its infancy, and few groups have currently employed RNA-Seq to profile the transcriptome of neuronal cells [87, 88], we expect it will rapidly reveal its great potential, generating a major improvement in the knowledge of the molecular etiology of many neurodegenerative disorders.

Disclosures No potential conflicts of interest relevant to this article were reported.

References

Papers of particular interest, published recently, have been highlighted as:
- • Of importance
- •• Of major importance

1. Population Division, DESA, United Nations: World Population Ageing 1950–2050. Available at http://www.un.org/esa/population/publications/worldageing19502050/index.htm. United Nations New York, 2001.

2. World Health Organization and Alzheimer's Disease International: Dementia: a public health priority. Available at http://www.who.int/mentalhealth/publications/dementiareport2012. Accessed August 2012.
3. Lockrow JP, Fortress AM, Granholm AC. Age-related neurodegeneration and memory loss in Down syndrome. Curr Gerontol Geriatr Res. 2012;2012:463909.
4. Lill CM, Bertram L. Towards unveiling the genetics of neurodegenerative diseases. Semin Neurol. 2011;31:531–41.
5. Bertram L, Tanzi RE. The genetic epidemiology of neurodegenerative disease. J Clin Invest. 2005;115:1449–57.
6. Mayeux R. Epidemiology of neurodegeneration. Annu Rev Neurosci. 2003;26:81–104.
7. Luan K, Rosales JL, Lee KY. Viewpoint: crosstalks between neurofibrillary tangles and amyloid plaque formation. Ageing Res Rev 2012; In press.
8. Sydow A, Van der Jeugd A, Zheng F, et al. Reversibility of Tau-related cognitive defects in a regulatable FTD mouse model. J Mol Neurosci. 2011;45:432–7.
9. Lagier-Tourenne C, Polymenidou M, Cleveland DW. TDP-43 and FUS/TLS: emerging roles in RNA processing and neurodegeneration. Hum Mol Genet. 2010;19:R46–64.
10. Yanamandra K, Gruden MA, Casaite V, et al. α-synuclein reactive antibodies as diagnostic biomarkers in blood sera of Parkinson's disease patients. PLoS One. 2011;6:e18513.
11. Weiss KR, Kimura Y, Lee WC, Littleton JT. Huntingtin aggregation kinetics and their pathological role in a Drosophila Huntington's disease model. Genetics. 2012;190:581–600.
12. Ross CA, Poirier MA. Protein aggregation and neurodegenerative disease. Nat Med. 2004;10(Suppl):S10–7.
13. Saborio GP, Permanne B, Soto C. Sensitive detection of pathological prion protein by cyclic amplification of protein misfolding. Nature. 2001;411:810–3.
14. Soto C, Estrada LD. Protein misfolding and neurodegeneration. Arch Neurol. 2008;65:184–9.
15. Herrup K. Reimagining Alzheimer's disease–an age-based hypothesis. J Neurosci. 2010;30:16755–62.
16. Cowan WM, Kandel ER. Prospects for neurology and psychiatry. JAMA. 2001;285:594–600.
17. Bertram L, Lill CM, Tanzi RE. The genetics of Alzheimer disease: back to the future. Neuron. 2010;68:270–81.
18. Nuytemans K, Theuns J, Cruts M, Van Broeckhoven C. Genetic etiology of Parkinson disease associated with mutations in the SNCA, PARK2, PINK1, PARK7, and LRRK2 genes: a mutation update. Hum Mutat. 2010;31:763–80.
19. Freedman ML, Monteiro AN, Gayther SA, et al. Principles for the post-GWAS functional characterization of cancer risk loci. Nat Genet. 2011;43:513–21.
20. Cookson W, Liang L, Abecasis G, et al. Mapping complex disease traits with global gene expression. Nat Rev Genet. 2009;10:184–94.
21. Antonarakis SE, Lyle R, Dermitzakis ET, Reymond A, Deutsch S. Chromosome 21 and down syndrome: from genomics to pathophysiology. Nat Rev Genet. 2004;5:725–38.
22. •• Cao K, Chen-Plotkin AS, Plotkin JB, Wang LS. Age-correlated gene expression in normal and neurodegenerative human brain tissues. PLoS One. 2010; 5. *This study establishes a quantitative scale for measuring premature aging in neurodegenerative disease cohorts. It identifies specific physiological mechanisms common to aging and some forms of neurodegeneration.*
23. •• Esteller M. Non-coding RNAs in human disease. Nat Rev Genet. 2011;12:861–74. *This review summarizes the most well-characterized classes of ncRNAs and focuses on their contribution to the genesis and the progression of neurological, cardiovascular, developmental and other human disease. It also discusses novel therapeutic approaches.*
24. Taft RJ, Pang KC, Mercer TR, et al. Non-coding RNAs: regulators of disease. J Pathol. 2010;220:126–39.
25. Mehler MF, Mattick JS. Noncoding RNAs and RNA editing in brain development, functional diversification, and neurological disease. Physiol Rev. 2007;87:799–823.
26. •• Salta E, De Strooper B. Non-coding RNAs with essential roles in neurodegenerative disorders. Lancet Neurol. 2012;11:189–200. *This review discusses the advances in understanding of the function of ncRNAs in the CNS, focusing on the potential involvement of specific species, such as miRNAs, in various neurodegenerative disorders.*
27. Niland CN, Merry CR, Khalil AM. Emerging roles for long non-coding RNAs in cancer and neurological disorders. Front Genet 2012; In press.
28. Mattick JS, Makunin IV. Non-coding RNA. Hum Mol Genet. 2006;1:R17–29.
29. Cho WC. Grand challenges and opportunities in deciphering the role of non-coding RNAs in human diseases. Front Genet 2011; In press.
30. Lindberg J, Lundeberg J. The plasticity of the mammalian transcriptome. Genomics. 2010;95:1–6.
31. Cao X, Yeo G, Muotri AR, et al. Noncoding RNAs in the mammalian central nervous system. Annu Rev Neurosci. 2006;29:77–103.
32. • Bian S, Sun T. Functions of noncoding RNAs in neural development and neurological diseases. Mol Neurobiol. 2011;44:359–73. *This review highlights the discoveries of ncRNA functions in neural development and neurological disease.*
33. Krol J, Loedige I, Filipowicz W. The widespread regulation of microRNA biogenesis, function and decay. Nat Rev Genet. 2010;11:597–610.
34. Khraiwesh B, Arif MA, Seumel GI, et al. Transcriptional control of gene expression by microRNAs. Cell. 2010;140:111–22.
35. Pratt AJ, MacRae IJ. The RNA-induced silencing complex: a versatile gene-silencing machine. J Biol Chem. 2009;284:17897–901.
36. Persengiev SP, Kondova II, Bontrop RE. The impact of MicroRNAs on brain aging and neurodegeneration. Curr Gerontol Geriatr Res. 2012;2012:359369.
37. Kim J, Inoue K, Ishii J, et al. A microRNA feedback circuit in midbrain dopamine neurons. Science. 2007;317:1220–4.
38. Nelson PT, Wang WX, Rajeev BW. MicroRNAs (miRNAs) in neurodegenerative diseases. Brain Pathol. 2008;18:130–8.
39. •• Junn E, Mouradian MM. MicroRNAs in neurodegenerative disorders. Cell Cycle. 2010;9:1717–21. *This report provides experimental evidence of miRNA-mediated function in neuronal dysfunction and death characterizing neurodegenerative disorders.*
40. Boissonneault V, Plante I, Rivest S, Provost P. MicroRNA-298 and microRNA-328 regulate expression of mouse beta-amyloid precursor protein-converting enzyme 1. J Biol Chem. 2009;284:1971–81.
41. Wang WX, Rajeev BW, Stromberg AJ, et al. The expression of microRNA miR-107 decreases early in Alzheimer's disease and may accelerate disease progression through regulation of beta-site amyloid precursor protein-cleaving enzyme 1. J Neurosci. 2008;28:1213–23.
42. Hebert SS, Horre K, Nicolai L, et al. Loss of microRNA cluster miR-29a/b-1 in sporadic Alzheimers disease correlates with increased BACE1/beta-secretase expression. Proc Natl Acad Sci USA. 2008;105:6415–20.
43. Lukiw WJ. Micro-RNA speciation in fetal, adult and Alzheimers disease hippocampus. Neuroreport. 2007;18:297–300.
44. Elton TS, Sansom SE, Martin MM. Trisomy-21 gene dosage over-expression of miRNAs results in the haploinsufficiency of specific target proteins. RNA Biol. 2010;7:540–7.
45. Kuhn DE, Nuovo GJ, Martin MM, et al. Human chromosome 21-derived miRNAs are overexpressed in down syndrome brains and hearts. Biochem Biophys Res Commun. 2008;370:473–7.
46. Doxakis E. Post-transcriptional regulation of alpha-synuclein expression by mir-7 and mir-153. J Biol Chem. 2010;285:12726–34.

47. Packer AN, Xing Y, Harper SQ, et al. The bifunctional microRNA miR-9/miR-9* regulates REST and CoREST and is downregulated in Huntington's disease. J Neurosci. 2008;28:14341–6.
48. Conaco C, Otto S, Han JJ, Mandel G. Reciprocal actions of REST and a microRNA promote neuronal identity. Proc Natl Acad Sci U S A. 2006;103:2422–7.
49. Ling SC, Albuquerque CP, Han JS, et al. ALS-associated mutations in TDP-43 increase its stability and promote TDP-43 complexes with FUS/TLS. Proc Natl Acad Sci USA. 2010;107:13318–23.
50. Mercer TR, Dinger ME, Mariani J, et al. Noncoding RNAs in long-term memory formation. Neuroscientist. 2008;14:434–45.
51. • Qureshi IA, Mattick JS, Mehler MF. Long non-coding RNAs in nervous system function and disease. Brain Res. 2010;1338:20–35. *This review summarizes the emerging evidence that highlights the expression and the function of lncRNAs in CNS processes, suggesting the relevant role of their deregulation in CNS pathologies.*
52. Amaral PP, Neyt C, Wilkins SJ, et al. Complex architecture and regulated expression of the Sox2ot locus during vertebrate development. RNA. 2009;15:2013–27.
53. Tochitani S, Hayashizaki Y. Nkx2.2 antisense RNA overexpression enhanced oligodendrocytic differentiation. Biochem Biophys Res Commun. 2008;372:691–6.
54. Beltran M, Puig I, Pena C, et al. A natural antisense transcript regulates Zeb2/Sip1 gene expression during Snail1-induced epithelial-mesenchymal transition. Genes Dev. 2008;22:756–69.
55. Mattick JS, Makunin IV. Small regulatory RNAs in mammals. Hum Mol Genet. 2005;14:R121–32.
56. Daughters RS, Tuttle DL, Gao W, et al. RNA gain-of-function in spinocerebellar ataxia type 8. PLoS Genet. 2009;5:e1000600.
57. Lee JE, Cooper TA. Pathogenic mechanisms of myotonic dystrophy. Biochem Soc Trans. 2009;37:1281–6.
58. Moseley ML, Zu T, Ikeda Y, et al. Bidirectional expression of CUG and CAG expansion transcripts and intranuclear polyglutamine inclusions in spinocerebellar ataxia type 8. Nat Genet. 2006;38:758–69.
59. Faghihi MA, Modarresi F, Khalil AM, et al. Expression of a noncoding RNA is elevated in Alzheimer's disease and drives rapid feed-forward regulation of beta-secretase. Nat Med. 2008;14:723–30.
60. Mus E, Hof PR, Tiedge H. Dendritic BC200 RNA in aging and in Alzheimer's disease. Proc Natl Acad Sci U S A. 2007;104:10679–84.
61. Costa V, Angelini C, D'Apice L, et al. Massive-scale RNA-Seq analysis of non ribosomal transcriptome in human trisomy 21. PLoS One. 2011;6:e18493.
62. Kishore S, Stamm S. The snoRNA HBII-52 regulates alternative splicing of the serotonin receptor 2C. Science. 2006;311:230–2.
63. Dweep H, Sticht C, Pandey P. Gretz N: miRWalk—database: prediction of possible miRNA binding sites by "walking" the genes of 3 genomes. J Biomed Inform. 2011;44:839–47.
64. Jiang Q, Wang Y, Hao Y, et al. miR2Disease: a manually curated database for microRNA deregulation in human disease. Nucleic Acids Res. 2009;37:D98–104.
65. Kozomara A, Griffiths-Jones S. miRBase: integrating microRNA annotation and deep-sequencing data. NAR. 2011;39(Database Issue):D152–7.
66. Paul DT, Anish K, Michael JC, et al. PANTHER: a browsable database of gene products organized by biological function, using curated protein family and subfamily classification. Nucleic Acids Res. 2003;31:334–41.
67. Becker KG, Barnes KC, Bright TJ, Wang SA. The genetic association database. Nat Genet. 2004;36:431–2.
68. • Khandelwal PJ, Herman AM, Moussa CE. Inflammation in the early stages of neurodegenerative pathology. J Neuroimmunol. 2011;238:1–11. *This is a review on inflammation in the early stages of neurodegeneration.*
69. •• Glass CK, Saijo K, Winner B, et al. Mechanisms underlying inflammation in neurodegeneration. Cell. 2010;140:918–34. *This review discusses several aspects of neuroinflammation that contribute to neuronal dysfunction and death.*
70. Nunomura A, Moreira PI, Castellani RJ, et al. Oxidative damage to RNA in aging and neurodegenerative disorders. Neurotox Res 2012; In press.
71. Griffin WS. Inflammation and neurodegenerative diseases. Am J Clin Nutr. 2006;83:470S–4.
72. Medzhitov R. Origin and physiological roles of inflammation. Nature. 2008;24:428–35.
73. Lin MT, Beal MF. Mitochondrial dysfunction and oxidative stress in neurodegenerative diseases. Nature. 2006;443:787–95.
74. Brown JA, Min J, Staropoli JF, et al. SOD1, ANG, TARDBP and FUS mutations in amyotrophic lateral sclerosis: a United States clinical testing lab experience. Amyotroph Lateral Scler. 2012;13:217–22.
75. Costa V, Sommese L, Casamassimi A, et al. Impairment of circulating endothelial progenitors in Down syndrome. BMC Med Genom. 2010;3:40.
76. Esposito G, Imitola J, Lu J, et al. Genomic and functional profiling of human Down syndrome neural progenitors implicates S100B and aquaporin 4 in cell injury. Hum Mol Genet. 2008;17:440–57.
77. Lukiw WJ, Dua P, Pogue AI, et al. Upregulation of micro RNA-146a (miRNA-146a), a marker for inflammatory neurodegeneration, in sporadic Creutzfeldt-Jakob disease (sCJD) and Gerstmann-Straussler-Scheinker (GSS) syndrome. J Toxicol Environ Health A. 2011;74:1460–8.
78. Saba R, Gushue S, Huzarewich RL, et al. MicroRNA 146a (miR-146a) is over-expressed during prion disease and modulates the innate immune response and the microglial activation state. PLoS One. 2012;7:e30832.
79. Vilardo E, Barbato C, Ciotti M, et al. MicroRNA-101 regulates amyloid precursor protein expression in hippocampal neurons. J Biol Chem. 2010;285:18344–51.
80. •• Costa V, Aprile M, Esposito R, Ciccodicola A. RNA-Seq and human complex diseases: recent accomplishments and future perspectives. Eur J Hum Genet 2012; In press. *This is the only review that describes the RNA-Seq approach to studying complex human diseases, considering its advantages over conventional technologies for studying cancer and ND.*
81. • Courtney E, Kornfeld S, Janitz K, Janitz M. Transcriptome profiling in neurodegenerative disease. J Neurosci Methods. 2010;193:189–202. *This review discusses the technologies involved transcriptome studies and the related literature on Alzheimer's disease, Parkinson's disease and Huntington's disease.*
82. Costa V, Angelini C, De Feis I, Ciccodicola A. Uncovering the complexity of transcriptomes with RNA-Seq. J Biomed Biotechnol. 2010;2010:853916.
83. Horan MP. Application of serial analysis of gene expression to the study of human genetic disease. Hum Genet. 2009;126:605–14.
84. Ozsolak F, Milos PM. RNA sequencing: advances, challenges and opportunities. Nat Rev Genet. 2011;12:87–98.
85. Sutherland GT, Janitz M, Kril JJ. Understanding the pathogenesis of Alzheimer's disease: will RNA-Seq realize the promise of transcriptomics? J Neurochem. 2011;116:937–46.
86. •• Twine NA, Janitz K, Wilkins MR, Janitz M. Whole transcriptome sequencing reveals gene expression and splicing differences in brain regions affected by Alzheimer's disease. PLoS One. 2011;6:e16266. *This study provides, for the first time, transcriptomic analysis for distinct regions of the AD brain using RNA-Seq next-generation sequencing technology.*
87. Lin M, Pedrosa E, Shah A, et al. RNA-Seq of human neurons derived from iPS cells reveals candidate long non-coding RNAs involved in neurogenesis and neuropsychiatric disorders. PLoS One. 2011;6:e23356.

88. Hébert SS, Horré K, Nicola L, et al. MicroRNA regulation of Alzheimer's Amyloid precursor protein expression. Neurobiol Dis. 2009;33:422–8.
89. Li YY, Cui JG, Hill JM, et al. Increased expression of miRNA-146a in Alzheimer's disease transgenic mouse models. Neurosci Lett. 2011;487:94–8.
90. Lukiw WJ, Zhao Y, Cui JG. An NF-kB-sensitive microRNA-146a-mediated inflammatory circuit in Alzheimer's disease and in stressed human brain cells. J Biol Chem. 2008;283:31315–22.
91. Wang X, Liu P, Zhu H, et al. miR-34a, a microRNA up-regulated in a double transgenic mouse model of Alzheimer's disease, inhibits bcl2 translation. Brain Res Bull. 2009;80:268–73.
92. Wang G, van der Walt JM, Mayhew G, et al. Variation in the miRNA-433 binding site of FGF20 confers risk for Parkinson disease by overexpression of alpha-synuclein. Am J Hum Genet. 2008;82:283–9.
93. Asikainen S, Rudgalvyte M, Heikkinen L, et al. Global microRNA expression profiling of Caenorhabditis elegans Parkinson's disease models. J Mol Neurosci. 2010;41:210–8.
94. Junn E, Lee KW, Jeong BS, et al. Repression of alpha-synuclein expression and toxicity by microRNA-7. Proc Natl Acad Sci U S A. 2009;106:13052–7.
95. Montag J, Hitt R, Opitz L, et al. Upregulation of miRNA hsa-miR-342-3p in experimental and idiopathic prion disease. Mol Neurodegener. 2009;4:36.
96. Rademakers R, Eriksen JL, Baker M, et al. Common variation in the miR-659 binding-site of GRN is a major risk factor for TDP43-positive frontotemporal dementia. Hum Mol Genet. 2008;17:3631–42.
97. Lee Y, Samaco RC, Gatchel JR, et al. miR-19, miR-101 and miR-130 co-regulate ATXN1 levels to potentially modulate SCA1 pathogenesis. Nat Neurosci. 2008;11:1137–9.
98. Persengiev S, Kondova I, Otting N, et al. Genome-wide analysis of miRNA expression reveals a potential role for miR-144 in brain aging and spinocerebellar ataxia pathogenesis. Neurobiol Aging. 2011;32:2316.e17–27.
99. Lee ST, Chu K, Im WS, et al. Altered microRNA regulation in Huntington's disease models. Exp Neurol. 2011;227:172–9.
100. Johnson R, Zuccato C, Belyaev ND, et al. A microRNA-based gene dysregulation pathway in Huntington's disease. Neurobiol Dis. 2008;29:438–45.

Database, Vol. 2014, Article ID bau009, doi:10.1093/database/bau009

Original article

AnaLysis of Expression on human chromosome 21, ALE-HSA21: a pilot integrated web resource

Margherita Scarpato[1,†], Roberta Esposito[1,2,†], Daniela Evangelista[3,4,†], Marianna Aprile[1], Maria Rosaria Ambrosio[1], Claudia Angelini[3,‡], Alfredo Ciccodicola[1,*,‡] and Valerio Costa[1,*]

[1]Institute of Genetics and Biophysics 'Adriano Buzzati-Traverso', National Research Council, Naples, Italy, [2]Department of Pharmaceutical Sciences, University of Salerno, National Research Council, Fisciano, Salerno, Italy, [3]Istituto per le Applicazioni del Calcolo 'Mauro Picone', National Research Council, Naples, Italy and [4]Department of Biochemistry and Biophysics, Second University of Naples (SUN), Naples, Italy

***Corresponding author:** Valerio Costa. Tel: +39 0816132258; Fax: +39 0816132617; Email: valerio.costa@igb.cnr.it
Correspondence may also be addressed to Alfredo Ciccodicola. Tel: +39 0816132259; Fax: +39 0816132617; Email: alfredo.ciccodicola@igb.cnr.it.
Claudia Angelini. Tel: +39 0816132393; Fax: +39 081 6132597; Email: c.angelini@iac.cnr.it

[†]The authors contributed equally to this work.

[‡]The laboratories contributed equally to this work.

Submitted 5 August 2013; Revised 16 January 2014; Accepted 21 January 2014

Citation details: Scarpato,M., Esposito,R., Evangelista,D., *et al*. AnaLysis of expression on human chromosome 21, ALE-HSA21: a pilot integrated web resource. *Database* (2014) Vol. 2014: article ID bau009; doi:10.1093/database/bau009.

Transcriptome studies have shown the pervasive nature of transcription, demonstrating almost all the genes undergo alternative splicing. Accurately annotating all transcripts of a gene is crucial. It is needed to understand the impact of mutations on phenotypes, to shed light on genetic and epigenetic regulation of mRNAs and more generally to widen our knowledge about cell functionality and tissue diversity. RNA-sequencing (RNA-Seq), and the other applications of the next-generation sequencing, provides precious data to improve annotations' accuracy, simultaneously creating issues related to the variety, complexity and the size of produced data. In this 'scenario', the lack of user-friendly resources, easily accessible to researchers with low skills in bioinformatics, makes difficult to retrieve complete information about one or few genes without browsing a jungle of databases. Concordantly, the increasing amount of data from 'omics' technologies imposes to develop integrated databases merging different data formats coming from distinct but complementary sources. In light of these considerations, and given the wide interest in studying Down syndrome—a genetic condition due to the trisomy of human chromosome 21 (HSA21)—we developed an integrated relational database and a web interface, named ALE-HSA21 (AnaLysis of Expression on HSA21), accessible at http://bioinfo.na.iac.cnr.it/ALE-HSA21. This comprehensive and user-friendly web resource integrates—for all coding and noncoding transcripts of chromosome 21—existing gene annotations and transcripts identified *de novo* through RNA-Seq analysis with predictive computational analysis of regulatory sequences. Given the role of noncoding RNAs and untranslated regions of coding genes in key regulatory mechanisms, ALE-HSA21 is also an interesting web-based platform to investigate such processes. The 'transcript-centric' and easily-accessible nature of ALE-HSA21 makes this resource a valuable tool to rapidly retrieve data at the isoform level, rather than at gene level, useful to investigate any disease, molecular pathway or cell process involving chromosome 21 genes.

Database URL: http://bioinfo.na.iac.cnr.it/ALE-HSA21/

Database, Vol. 2014, Article ID bau009, doi:10.1093/database/bau009

Introduction

In the past years, transcriptome studies have largely shown the pervasive nature of transcription in living organisms (1–4). In particular, the GENCODE Consortium, by combining computational analysis, manual curation and experimental validations, has identified a plethora of new coding and noncoding RNA transcripts expressed in human cells (5). Altogether these studies demonstrate that a significant fraction of transcribed regions stands outside known genes and most of them undergo alternative splicing (AS). Therefore, defining a curated and validated gene annotation is difficult, even though crucial for several reasons. For instance, annotating all the transcripts of a given gene is strictly necessary to postulate the functional impact of nucleotide variations, particularly those located in genomic regions till now recognized as 'nongenic'. The most striking evidence is mutations accounting for Mendelian disorders (6) or common variants associated to complex traits and diseases (7). Moreover, a correct annotation of mRNAs' untranslated regions (UTRs) would significantly help to investigate their role in the regulation of transcription and translation (8). Finally, identifying novel tissue or cell-specific coding and noncoding transcripts would significantly improve the knowledge of cell functionality.

Large-scale data sets produced by RNA-sequencing (RNA-Seq), an application of the next-generation sequencing, are revealing an optimal source to improve the accuracy of gene annotations (9). However, the variety, the complexity and the size of available data have exponentially increased, making them difficult to handle, analyze, store, share and integrate with those stored in existing databases (10). It is common for research groups—and/or large consortia—to annotate the same transcript, gene or protein isoform using different identifiers (id), often confounding unskilled users. For this reason, comparing and combining these data from different resources still represent a difficult task.

Another hurdle to overcome is data dispersion. For instance, having a complete landscape of regulatory molecules for a specific transcript of interest is challenging, as most of the available resources are difficult to browse without any expertise in bioinformatics, and often they appear too specialized. Several Web sites and tools have been specifically developed for the 'sequence-based' predictions of transcription factors' or microRNAs' binding sites but, to the best of our knowledge, such information has not been systematically integrated into already existing genomic resources. Such issues often limit the access to complete information for a transcript, gene or protein of interest without browsing different databases. Therefore, given the substantial lack of comprehensive and user-friendly Web sites for researchers or medical geneticists with low experience in bioinformatics, it is crucial to implement easy-to-use web resources. Concordantly, the massive production of 'omics' data makes urgent the need to develop integrated databases.

In light of these considerations, and given our interest in studying the expression of genes mapping on human chromosome 21 (HSA21)—whose triplication causes Down Syndrome (DS)—we developed an open-access integrated relational database and a web interface, ALE-HSA21 (AnaLysis of Expression on HSA21; http://bioinfo.na.iac.cnr.it/ALE-HSA21). Because RNA-Seq studies have indicated the need to investigate biological processes and disease mechanisms at isoform level, rather than at gene level, we designed our database as a 'transcript-centric' web portal.

It integrates—for all transcripts generated by AS from HSA21 genes—nucleotide sequences and exon/intron structures with data about regulatory sequences. The latter consist of computational predictions for canonical and noncanonical regulatory motifs within promoters, exons, introns and 3′ UTRs. Links to widely used genotype and phenotype databases are also integrated in ALE-HSA21, avoiding the user to browse different resources over the web. Finally, it contains a set of *de novo* discovered transcripts, identified through a robust computational analysis of our recently published RNA-Seq data sets (11).

This web portal clearly represents an estimable source of information for researchers and clinicians interested in studying DS. Given the proven role of HSA21 genes' dosage imbalance in DS clinical outcomes (11), having a comprehensive set of information about all HSA21 genes, and their alternative transcripts, is of major interest for researchers studying DS. The database is also a valuable resource for medical geneticists interested in other HSA21-related diseases. Disruption or alteration of binding sites for auxiliary splicing factors as well as of other gene regulatory regions—promoter and 3′ UTR—may affect mRNA transcription, processing and translation, in turn playing a pathological role.

This kind of information is available in ALE-HSA21 through an easily accessible web interface, designed to rapidly provide heterogeneous data in a scientifically rigorous—even though user-friendly—way.

Materials and Methods

Links to the external databases, files and software (with version and parameters) are shown in Supplementary File S1.

RNA-Seq data processing and gene annotations

Raw files containing short reads of 50 bp (.csfasta and .ual formats from SOLiD v3) originated by the massive-scale sequencing of endothelial progenitor cells (11), were filtered out for quality values, homology to adapters and rRNA sequences. Filtered reads were aligned with TopHat software version 1.1.4 (12) against the reference human genome (release hg19). Without providing annotated gene models,

splice junctions were *de novo* determined by the software, and reported as a list in a standard tabular format (BED). Reads uniquely mapped on the reference genome—extracted from the output alignment file (BAM)—and junctions supported by at least three high-quality reads were used. For further analyses we extracted only HSA21 mapping reads. A coverage file (BEDGRAPH format) for HSA21 was created and loaded into an open-access session of University of California Santa Cruz (UCSC) Genome Browser, named ALE-HSA21. The track 'Comprehensive Gene Annotation Set GENCODE Version 12' was downloaded from Table Browser of UCSC in GTF format. The exact number and the category of HSA21 transcripts considered in our further analyses, and reported in ALE-HSA21, are listed in Supplementary Table S1. Manual curation was used—in some cases—to correctly assign, if any, the corresponding RefSeq ID to annotated GENCODE transcripts.

Discovery of intronic and intergenic transcription

To identify potentially new exons and/or transcripts in introns and intergenic intervals, uniquely mapped reads were converted into sorted files in BED format using SAMtools and BEDtools (13, 14). Results were visualized in UCSC Genome Browser to assess the quality and the consistency of the mapping analysis. A customized workflow was built to extract the genomic coordinates of intronic and intergenic HSA21 transcripts from GENCODE annotation, as well as reads mapping within these regions. In detail, we divided intronic and intergenic intervals in windows of 200 and 500 bp, respectively, and we counted the number of reads falling within such windows. Putative windows were reported as potential new transcribed regions if the number of mapped reads was sufficiently large. Signal enrichment was evaluated by using a Poisson test similar in the spirit to MACS (15). The background (no-signal) intensity, λ, was independently estimated for intronic and intergenic regions by maximum likelihood approach. In particular, a subset of intergenic regions—>1 Mb and 10 kb distant from gene boundaries—was used to estimate $\lambda_{intergenic}$. For the estimation of $\lambda_{intronic}$ we used intronic intervals >300 kb and 1 kb away from exon boundaries. Poisson *P*-values computed in each window underwent Benjamini and Hochberg False Discovery Rate correction (16). Significant windows were merged in larger genomic regions when the distance among them was smaller or equal to the window size. Transcriptionally active regions were defined 'high coverage peaks' (HCPs). In addition, to assess the transcription upstream transcription start sites, and downstream the last nucleotide of annotated transcripts, we used windows of variable size (50–1000 bp). Coverage was evaluated by counting the number of reads mapping within these windows. We selected the transcripts to experimentally validate after the intersection with genomic coordinates of expressed sequence tags and gene predictions (AceView database), as well as by visual inspection in UCSC and Integrative Genomic Viewer.

Computational analysis of splicing isoforms

The output of TopHat, i.e. the list of *de novo* determined splice junctions, was used to infer the evidence of unannotated isoforms generated by AS for each HSA21 gene. Each junction (j) consists of two connected blocks, left (L_j) and right (R_j). The length of each block, here defined as MOL_j and MOR_j, is given by the Maximal Overhang (MO) over all reads mapping within L_j and R_j, respectively (12).

The genomic coordinates (i.e. the starting and ending sites, S and E, respectively) of L_j and R_j were defined as follows:

$$L_j = [SL_j, EL_j] \text{ and } R_j = [SR_j, ER_j]$$

where

$$SL_j(5'\ start) = S_j \text{ and } EL_j(3'\ end) = S_j + MOL_j$$

and

$$SR_j(5'\ start) = E_j - MOR_j \text{ and } ER_j(3'\ end) = E_j$$

For the 'plus' strand, S_j is the 5′ start genomic and E_j is the 3′ end coordinate of *j*. *Vice versa*, for the 'minus' strand, S_j is the 3′ end genomic coordinate of junction *j* and E_j is the 5′ start coordinate of *j*. Thus, we independently intersected intervals L_j and R_j with the genomic coordinates of all exons of the HSA21 GENCODE v12 annotation by using the *intersectBed* function of BEDtools (13). Seven different categories of junctions were defined through this analysis (schematized in Supplementary Figure S1): (i) 'annotated' and (ii) 'exon skipping' if L_j and R_j map to consecutive or nonconsecutive exons on the same transcript, respectively; (iii) 'only one side', if only L_j or R_j map to one exon of a transcript and the other does not; (iv) 'intra-exonic' if both L_j and R_j map within the same exon; (v) 'different transcripts' if L_j maps to an exon of a transcript and R_j maps to an exon of another transcript belonging to the same gene; (vi) 'trans-splicing' if L_j and R_j map to exons of two different (adjacent) genes and (vii) 'intronic/intergenic' if both L_j and R_j do not map to any exon of an annotated transcript. Because a splice junction may belong to multiple categories (i.e. it may be 'annotated' for a given transcript but 'exon skipping' for another), we established a junction hierarchy (from category 1 to 7) in which junctions assigned to a category cannot be assigned to the next one.

Finally, each HSA21 GENCODE transcript was associated to a known official gene symbol to identify potentially new splice isoforms.

Computational prediction of regulatory sequences

Nucleotide sequences for each promoter, exon, intron and 3′ UTR were downloaded in FASTA format from UCSC database. In detail, of 1702 HSA21 protein-coding transcripts,

Database, Vol. 2014, Article ID bau009, doi:10.1093/database/bau009

1295 were exclusively annotated in the 'Comprehensive Gene Annotation Set from GENCODE Version 12', 139 only in RefSeq (release 56) and 268 in both of them. Simultaneously, 462 HSA21 noncoding transcripts were divided in 10 classes according to GENCODE v12 (Supplementary Table S1 and illustrated in the right panel of Figure 1B). For miRNAs, a comprehensive list of 30 entries was created merging information from different databases (GENCODE, RefSeq, Ensembl and miRBase). For the other noncoding transcripts, we retrieved from the 'Comprehensive Gene Annotation Set from GENCODE v12' a list of 220 long intergenic noncoding RNAs (lincRNAs), 24 pseudogenes, 15 sense-intronic transcripts, 80 antisense transcripts, 40 processed transcripts, 21 small nuclear RNAs, 19 small nucleolar RNAs (snoRNAs), 5 rRNAs and 8 miscellaneous RNA. Promoters' sequences (±1 kb from transcription start site) of coding transcripts were scanned for the presence of TF binding sites using the 'matrix scan' option of Regulatory Sequence Analysis Tools (RSAT) web server (17). Position weight matrices of 78 human transcription factors (TFs) were downloaded from JASPAR database. The 'DNA pattern' tool of RSAT web server was used to determine the presence of 'consensus' sequences for 106 exonic splicing enhancer and 50 silencer (ESE/ESS), 54 intronic splicing enhancer and 32 silencer (ISE/ISS). Regulatory sequences were downloaded from RegRNA web server (18). The number of analyzed exons and introns is shown in Table 1.

For the identification of miRNA responsive elements (MREs) within the mRNA 3′ UTRs, the complete list of 6121 mammalian miRNAs of TargetScan database was filtered for 4582 nonhuman miRNAs. Thus, targetscan_60.pl script downloaded from TargetScan was used to analyze 1201 3′UTRs of protein-coding transcripts, searching for binding sites of 1539 miRNAs. Of note, the number of 3′UTRs analyzed for the presence of MREs is smaller than the total number of transcripts because some of them lack UTR in the GENCODE annotation or are annotated as 'processed transcripts', 'retained introns' and other categories lacking the typical 3′UTR.

The same analysis was performed also to predict MREs within the entire nucleotide sequences of 220 lincRNAs' and 24 pseudogenes' transcripts mapping on HSA21.

RNAfold web server, with default parameters (19), was used to predict—and visualize—the secondary structure of 19 snoRNA and 30 pre-miRNA sequences (figures available on ALE-HSA21). Such analysis represents predictions of secondary structures based on minimum free energy and partition functions, and the images do not represent *in vivo* structures.

For the 19 HSA21 miRNAs annotated in miRBase (20), the mature miRNA sequence was also highlighted in such drawings. miRNA target genes (MiTGs) were predicted by miRWalk [using algorithms both for 'validated' and 'predicted' genes; (21)] and CoMeTa databases (22). Complete data were available for five miRNAs (miR99a, miR125b, miR155, miR802 and let-7 c). Finally, the three lists of MiTGs were intersected to determine a common pool using Venny (23).

Database development and description

ALE-HSA21 is a database-driven Web site, more properly driven on a Relational Database Management System. It allows to structure the information contained in the web portal and to display them in tables. Overall, the database contains 534 HSA21 genes, consisting of 33.394 different genomic elements (Table 1). Database was implemented using server version 5.1.67—10.04.1 (Ubuntu)—and a web server Apache/2.2.14 (Ubuntu). MySQL client version 5.1.67—10.04.1 (Ubuntu)—and the free tool phpMyAdmin version 3.3.2 deb1ubuntu were used to handle the administration of MySQL over the World Wide Web.

ALE-HSA21 Web site

The web-oriented side was created using the scripting language PHP. The Javascript technology for dynamic contents, the markup language HTML for static contents and style sheet CSS 2.0 were also used. All 3D images have been implemented using the 'clickable image maps' method, thus making only a certain portion of the image sensitive to mouse clicks, linking to different destinations and contents. The ALE-HSA21 code is validated according to the standard web of the international community W3C (World Wide Web Consortium: http://www.w3.org/) and therefore, although optimized for Mozilla Firefox, it is easily visible and accessible by all browsers and smartphones.

The web resource will be regularly updated on the basis of the progress of our study.

Results

Global organization of ALE-HSA21 web portal

ALE-HSA21 is an open-access user-friendly web resource built on a relational database. This web portal is a comprehensive 'transcript-centric' database for HSA21, in which data from different sources are dynamically integrated (Figure 1A). ALE-HSA21 contains 2164 annotated transcripts, generated through AS from 534 genes. Particularly, 1702 transcripts derive from 238 protein-coding genes and 462 from 296 noncoding genes (Table 1; Supplementary Figure S2). Moreover, ALE-HSA21 also collects 11 transcripts (of protein-coding genes) identified—and validated—through the computational reanalysis of our RNA-Seq data sets.

The web resource consists of five main sections, schematically shown in the block diagram of Supplementary Figure S3 and in the 'Sitemap' of ALE-HSA21. The core is

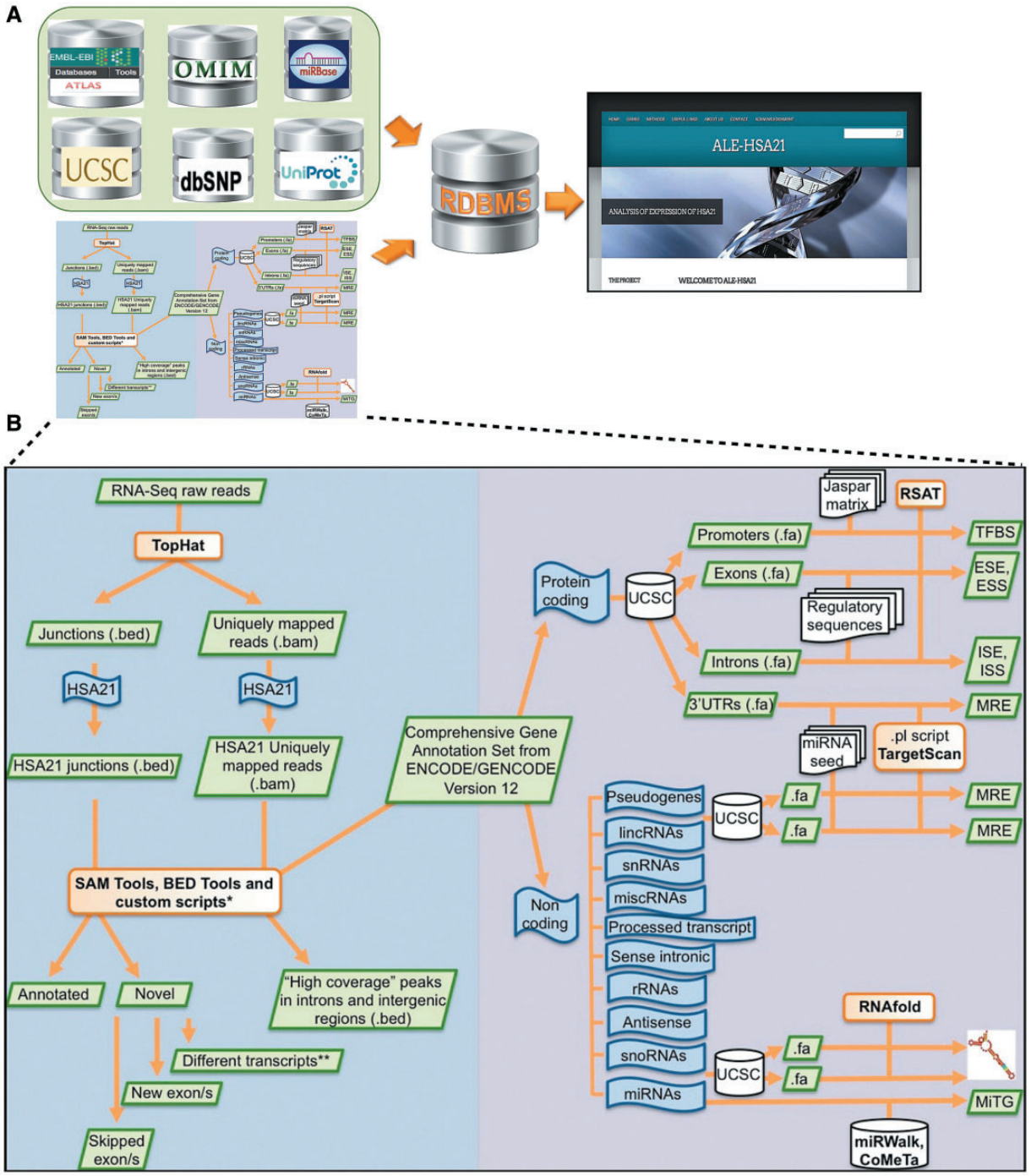

Figure 1. Schematic overview of data collected in ALE-HSA21 and of the computational analysis. Panel (**A**) shows a list of open-access databases used to retrieve information and the cartoon of the computational workflow used to analyze the data. Data derived from these sources were collected and integrated into our relational database and its web interface, represented on the right by the Homepage of ALE-HSA21. On the left part of panel (**B**) is schematically illustrated the computational approach used to analyze RNA-Seq data sets. In the right part it is depicted the workflow of the *in silico* analysis performed on the regulatory sequences for both coding and noncoding transcripts of chromosome 21. Green boxes indicate data files; in orange are indicated the computational tools used to perform the analysis; in blue are indicated the 'features' of interest; in white are indicated the databases and the regulatory data sets retrieved from them.

Database, Vol. 2014, Article ID bau009, doi:10.1093/database/bau009

Table 1. Number of analyzed gene elements collected in ALE-HSA21 database

	Genes	Transcripts	Promoters	Exons	Introns	3′ UTR
Coding	238	1713	1713	14 177	12 454	1201[a]
Noncoding	296	462				244[b]
Total	534	2175	1713	14 177	12 454	1445

[a]The number of 3′ UTRs analyzed for the presence of MREs is smaller than the total number of transcripts because some of them lack UTR in the GENCODE annotation or are currently annotated as 'processed transcripts', 'retained introns' and other categories lacking a typical 3′ UTR.
[b]For noncoding RNAs, the entire sequences of 220 lincRNAs and 24 pseudogenes have been analyzed for the presence of MREs.

represented by the sections 'Coding genes'—divided in 'Annotated' and 'Novel'—and 'Noncoding genes'. The 'Novel' subsection hosts transcripts identified *de novo* by the analysis of our RNA-Seq data sets by merging custom computational workflows to open source tools and public databases (Figure 1B). In this subsection, only experimentally validated new HSA21 transcripts are reported. For all of them, sequences have been submitted and approved by EMBL Nucleotide Sequence Database.

Both sections, 'Coding genes' and 'Noncoding genes', contain two types of data: genomic/structural and regulatory. In particular, for all HSA21 transcripts, ALE-HSA21 provides a brief gene/category description, sequences in FASTA format and 3D structures. These dynamic images are linked to the regulatory data, consisting of computationally predicted motifs within nucleotide sequences. In addition, for coding genes, this web resource integrates links to public repositories of expression data, gene networks and ontologies, nucleotide variations, proteins and association to disease (Gene Expression Atlas, Gene Networks, dbSNP, UniProt and OMIM, respectively).

In silico identification and experimental validation of novel HSA21 transcripts

Our RNA-Seq data sets (11) were reanalyzed using a custom computational workflow (see 'Materials and Methods' section; schematized in Figure 1B). Through this *in silico* approach we identified different intronic/intergenic regions possibly representing novel transcripts (Supplementary File S2). Additionally, we checked the presence/absence of intronic/intergenic HCPs in two independent RNA-Seq data sets from HeLa and K562 cell lines (24) and tumor samples (manuscript in preparation), observing these are not cell-specific. Similarly, for known HSA21 genes putative extended UTRs and novel splice junctions—according to our categorization method—were also detected (Supplementary Files S3 and S4). Filtering out signals (i.e. mapped reads) from pre-mRNAs and repeats, and considering their overlap with AceView predictions and/or expressed sequence tags, we confirmed the presence of 11 novel transcripts arising from six HSA21 genes (Table 2). Their *bona fide* was confirmed in progenitor cells used in our previous study (11), as well as in other cell lines (data not shown). Nucleotide sequences of these new transcripts were submitted to the EMBL Nucleotide Archive, and accession numbers are listed in Table 2. Newly identified transcripts were added to ALE-HSA21 database and included in the computational analyses, further described.

Of note, potentially new transcripts reported in the Supplementary Files S2–S4, not yet validated by reverse transcriptase-polymerase chain reaction and Sanger sequencing, are, however, supported by RNA-Seq data (HCPs with uniquely mapped reads and/or a sufficient number of reads mapping on the splice junctions). However, as RNA-Seq data sets come from fragment libraries of 50 bp reads, and given the heuristic nature of algorithms for reads' alignment, despite our checks, false-positive alignments may have occurred.

Computational analysis of regulatory sequences in protein-coding transcripts

Predictive *in silico* analysis of regulatory sequences within gene promoters, exons, introns and 3′ UTRs was performed for both annotated and newly identified HSA21 protein-coding transcripts (Table 1). The 'consensus' sequences for 78 human TFs were predicted within gene promoters. Similarly to the RSAT output, the results are provided to the final user as tables with a 'weight score' column measured by the 'Background model estimation method' (17). Such tables, dynamically integrated on the web portal, can be accessed through the clickable '*Promoter*' button in the 3D structure of each transcript (Figure 2C and D). In addition, to provide the users with ChIP-Seq (chromatin immunoprecipitation followed by massive sequencing) data for TFs of the ENCODE project, we also integrated a clickable button linked to these tracks, loaded into an open-access custom session of UCSC Genome Browser. This kind of approach, based both on computational predictions of TFs' binding motifs and experimental large-scale data, represents a starting point to investigate differential TFs' binding among distinct genes and, more interestingly, among different transcripts of the same gene.

Moreover, as 'noncanonical' exonic and intronic sequences are known to affect splicing—and mutations herein can cause monogenic or can be associated to complex disorders—we computationally predicted ESE/ESS and ISE/ISS within all exons/introns of each HSA21 transcript. Similar to the predictive analysis of TFs' binding sites, data in tabular format were included within ALE-HSA21 and dynamically integrated in 3D transcripts' models. The user can access these results by clicking the exon/intron of interest on the 3D structures (Figure 2C and D).

Table 2. Novel transcripts identified by RNA-Seq analysis

Gene symbol	Transcript	Accession number	Primer sequence (5′–3′)	
			Forward primer	Reverse primer
IFNAR2	IFNAR2_var1	HG380509	CTGGGAGTCCGCTTTCGTT	GGAGACTTTATTACTGCTTGC
MCM3AP	MCM3AP_HF584748	HF584748	AGTGCTGAGCGAACCGGAAG	GGCTCAACAGGAAATGGTAAA
NRIP1	NRIP1_HF584749	HF584749	GAGAGCTGCTGAAGAAGTAG	TAAATGAGAAAAAATGCATTGTC
NRIP1	NRIP1_HF584750	HF584750	GAGAGCTGCTGAAGAAGTAG	TAAATGAGAAAAAATGCATTGTC
POFUT2	POFUT2_var1	HG380510	GGGCCATGGCGACACTCA	TGTGTTTCTCAGCAGCAGGG
POFUT2	POFUT2_var2	HG380511	GGGCCATGGCGACACTCA	TTTATCCCTGGCGCTGCAC
SAMSN1	SAMSN1_all_skip	HG380514	GCACACTGCTGACTGTTTTC	ATCTTCCTCTCCTATTTGACG
SAMSN1	SAMSN1_var1	HG380512	GCACACTGCTGACTGTTTTC	ACTATAGAAGTGCTTGGTACT
SAMSN1	SAMSN1_var2	HG380513	GCACACTGCTGACTGTTTTC	ATCTTCCTCTCCTATTTGACG
DYRK1A	DYRK1A_var1	HF584751	TGTTATAGTTTTGCCGCTGGA	CTGTTGGTCACTTATGTTTGG
DYRK1A	DYRK1A_var2	HF584752	TGTTATAGTTTTGCCGCTGGA	CTGTTGGTCACTTATGTTTGG

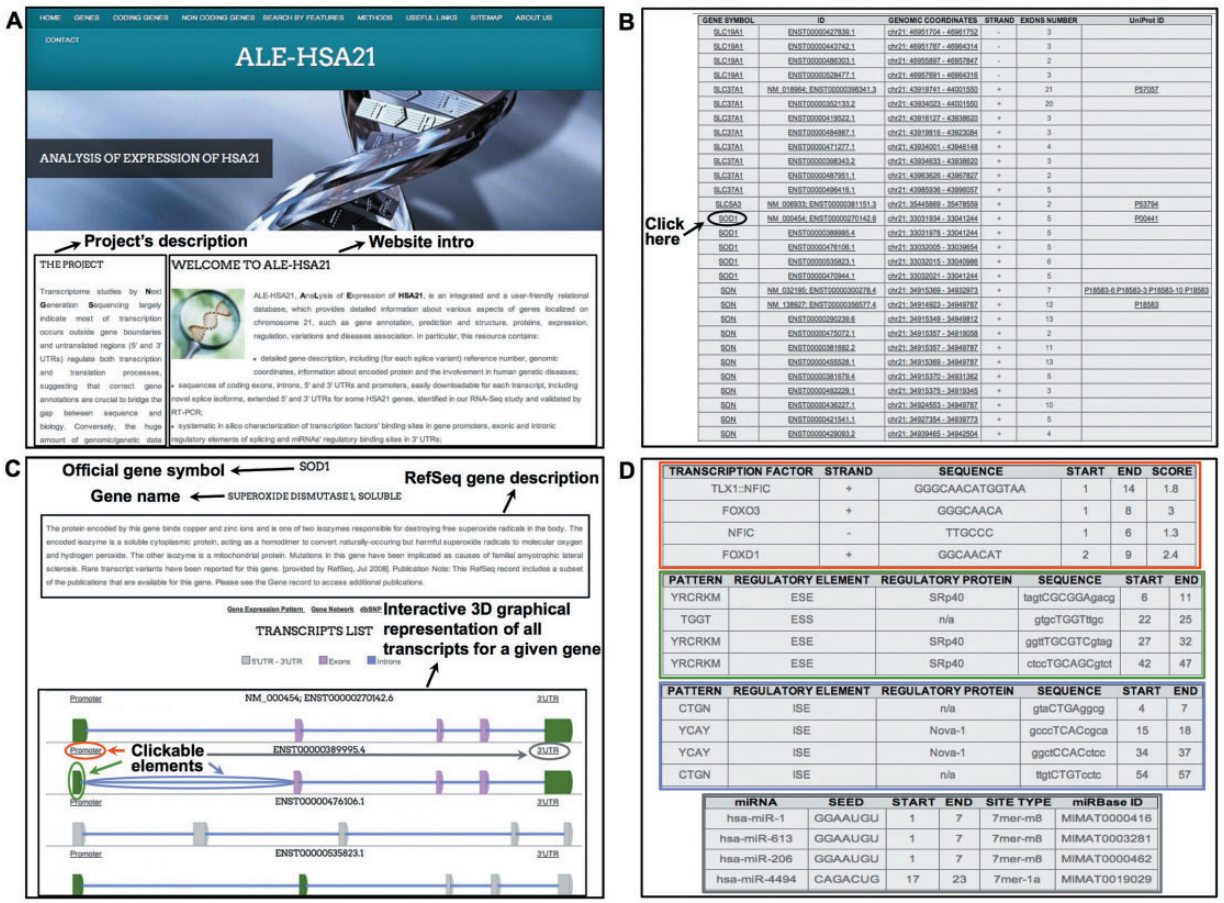

Figure 2. Screenshots from ALE-HSA21 web resource. Panel (**A**) shows the Homepage with Navigation Bar; panel (**B**) shows the list of HSA21 transcripts in the 'Coding genes' section in tabular format. Official gene symbol, ID, genomic coordinates, the sense of transcription, the number of exons and UniProt IDs are reported. The Black arrow and circle indicate an example of a clickable item (*SOD1* gene in the example). By clicking there, the users access the Gene Description page, depicted in Panel (**C**). Interactive 3D graphical representation for each transcript is embedded in this web page. Each gene element is linked to results of *in silico* analysis. Colored circles—red for 'Promoter', green for 'exons', light blue for 'introns' and gray for '3′ UTRs'—correspond to the clickable elements of the 3D images. The same color scheme is used in panel (**D**) to indicate the relative results for the computational analyses of those elements.

Database, Vol. 2014, Article ID bau009, doi:10.1093/database/bau009

In addition, given the crucial role of miRNAs in the posttranscriptional regulation of mRNAs through their binding to 3′ UTRs (25, 26), we added to our resource this layer of gene regulation. Particularly, we computationally predicted the binding sites of all annotated human miRNAs within 3′ UTRs sequences of HSA21 mapping mRNAs. Results of such predictive analysis can be accessed through the '3′ UTR' button integrated within the 3D graphical representation of each transcript (Figure 2C and D). Predicting the presence of differential MREs within distinct transcripts of the same gene can be rapidly and easily assessed browsing data of our computational analyses integrated in ALE-HSA21.

Computational analysis for noncoding transcripts

Recent evidences have shown that pseudogenes sequester miRNAs and act as competitive endogenous RNAs, and a similar mechanism has been proposed for lincRNAs (27). The role of these transcripts as miRNAs' sponges has been directly linked to carcinogenesis and muscle differentiation (28–30), and proposed for the onset of neurodegenerative diseases (31). Given these considerations, using prediction algorithms we searched for MREs in HSA21 lincRNAs and pseudogenes. The results were dynamically integrated in tabular format within the 'Noncoding genes' section of ALE-HSA21, accessible by clicking the 'miRNA binding sites' button located in the web page of the related transcript. In addition, using three different prediction algorithms, we also independently predicted—for the five HSA21 miRNAs available in CoMeTa and miRWalk databases—the putative MiTGs, not limiting such analysis to HSA21 genes. Data integrated in the web portal are provided in tabular format (Figure 3A). Moreover, the intersections between the three above-mentioned lists of computationally predicted MITGs—one for each prediction algorithm used—are shown as Venn diagrams (Figure 3B). These data allow rapidly observing a common pool of target genes, possibly regulated by the same HSA21 miRNA. Finally, as miRNAs and snoRNAs have a peculiar folding, which in turn determines their biological functions, we predicted their secondary structures and integrated these data as static images within ALE-HSA21 (Figure 3C). More in detail, in each miRNA and snoRNA drawing, nucleotides are colored by the base-pair probabilities, according to local measures of reliability, as described in (32). For all 19 HSA21 miRNAs, currently annotated in miRBase, we highlighted the nucleotide sequences corresponding to the mature—and functional—form of these miRNAs.

Exploring ALE-HSA21

The intuitive interface of ALE-HSA21 makes this web resource an easy and fast—although scientifically accurate, comprehensive and updated—tool to retrieve, in few clicks, relevant information about HSA21 genes and transcripts. A detailed user's guide on how to browse ALE-HSA21 and how to extract useful information is provided as Supplementary File S5 and also available on the web portal. The homepage is shown in Figure 2A. From the navigation bar the user can access to the different sections of the portal. Within the 'Coding genes' section there is the complete and updated list of HSA21 transcripts, both known and newly identified in this study, in a user-friendly tabular format (Figure 2B). For each transcript, there is the official gene symbol, ID (NM and/or ENST according to the RefSeq and the GENCODE annotations), the genomic coordinates with a link to an open-access session of UCSC Genome Browser, ad hoc created with chromosome 21 coverage files, the sense of transcription (indicated by '+/-' strand), the number of exons and the corresponding, if any, UniProt IDs. Each feature has a link to other sections of the web portal as well as to other external widely used databases. From the gene list table (Figure 2B) the user can easily access an interactive 3D graphical representation of all the transcripts. A 'Search by Gene' button allows a direct and quick access to all information for a given gene of interest. For each gene, such information consist of (i) full gene name and gene symbol, (ii) brief gene description with eventual literature references, (iii) links to gene expression data, gene networks and ontologies, (iv) single-nucleotide polymorphisms, (v) involvement in human diseases and (vi) 3D structures of all transcripts generated by AS (Figure 2C). In the 3D structures, each gene element (i.e. promoter, exons, introns and 3′ UTR) is clickable, allowing to directly access the results of our *in silico* analysis of regulatory sequences. As previously described, these data are provided in easily comprehensible tabular format, as illustrated in Figure 2D. In addition, for each element, below the results table, the nucleotide sequences are viewable and downloadable (FASTA format).

The 'Noncoding genes' section contains the comprehensive list of all HSA21 noncoding transcripts, divided in 10 categories, as depicted in Figure 1B. Similar to the 'Coding genes' section, by clicking on a specific transcript ID, the users can retrieve structural and regulatory data, described in the previous paragraph. In particular, for lincRNAs and pseudogenes, clickable 'miRNA binding sites' button allows accessing a complete list of predicted MREs in tabular format. Furthermore, the 'Target genes' button, included within the web pages dedicated to miRNAs, is directly linked to the results of our analysis on genes predicted to be targets of the selected miRNA.

Finally, a 'Search by Features' section has been implemented to ease the browsing ALE-HSA21 for specific features of interest, such as Gene Symbol, Transcript ID and UniProt ID.

Conclusion

RNA-Seq studies have clearly shown that the vast majority of—if not all—human genes undergo AS, generating

A

Validated	Predicted	Co-expressed
AADACL1	7A5	AAK1
AARSD1	A2BP1	ABAT
ABCF2	A4GALT	ABCA1
ABHD10	AADAC	ABCC5
ABHD11	AADACL1	ABCD2
ACP2	AAK1	ABHD10
ADAM11	AASDHPPT	ABHD2
ADM	AASS	ABHD6
ADPGK	ABAT	ABT1
ADSS	ABBA-1	ACBD3
AGMAT	ABCA1	ACP2
AGRN	ABCA13	ACRV1
AGTR1	ABCA5	ACSL5
AHSA1	ABCA9	ACTA1
AICDA	ABCB1	ACVR2A
AKAP8	ABCC4	ACVR2B
AKT1	ABCC9	ADAMTS5

B

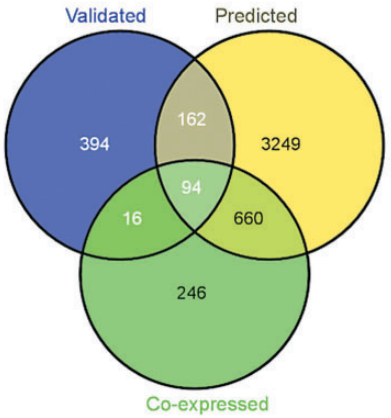

C

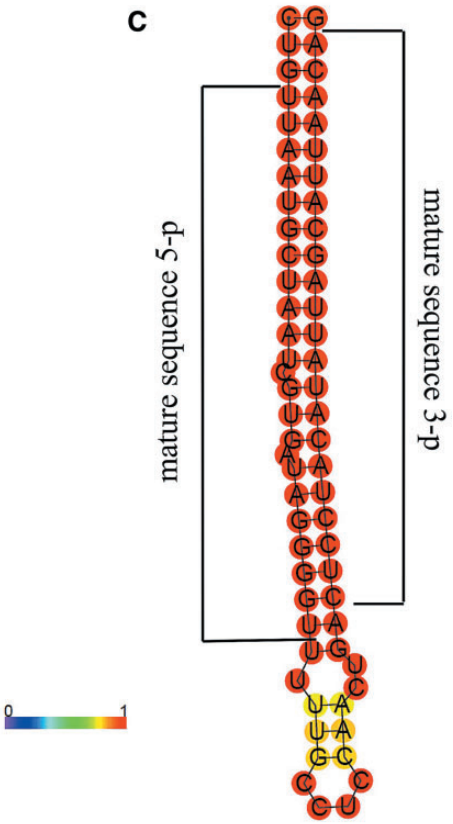

Figure 3. Example of the data provided for miRNAs in ALE-HSA21 web portal. In panel (**A**) and (**B**) are shown the results of the computational prediction of MiTGs in tabular format and Venn diagrams, respectively. Such data are accessible by clicking the 'Target genes' button embedded within miRNA web pages. 'Validated', 'predicted' and 'co-expressed' correspond to the target genes according to miRWalk and CoMeTa databases. Panel (**C**) shows a prediction of the secondary pre-miRNA structure obtained by RNAfold. Mature miRNA sequences are indicated by black brackets.

different transcripts (33, 34). These can be transcribed from alternative promoters and may possibly be regulated by different TFs as well as epigenetic factors (i.e. methylation and/or histone modifications). Transcripts with alternative 3′ UTRs may also undergo different co- and posttranscriptional regulation by miRNAs. In light of this, ALE-HSA21 is designed to provide, at the transcript level, computational predictions of TFs' binding sites in promoters as well as MREs in 3′ UTRs. Nonetheless, the presence of *in silico* predicted binding motifs does not guarantee a specific regulatory factor will bind that sequence. Future studies, based on ChIP-Seq data sets for TFs and sequencing of small RNAs, will surely allow us to improve the accuracy of this analysis. Understanding if alternative transcripts may be targets of different miRNAs, or if their transcription may be triggered by the same TFs, is clearly important to address their differential regulation, both in physiological and pathological conditions.

Moreover, it is known that different transcripts can arise from the same gene through the usage of alternative canonical splice sites, as well as noncanonical splicing enhancer/silencer sequences. Mutations within these regions affect splicing, causing diseases (35). Among them, familial isolated growth hormone deficiency type II is caused by different mutations occurring in the 5′ splice site, ISE and ESE that increase splicing of the exon 3 of *GH1* gene (36–38). In addition, aberrant splicing events—such as those caused by mutations in *WT1* gene in Frasier syndrome—may alter isoform abundance, affecting several cell processes (39–41). Thus, cataloguing the predicted binding sites for auxiliary splicing factors within all the splicing isoforms of a gene is an added value for clinicians studying human diseases.

Moreover, incomplete annotation of transcripts can lead to misinterpret the effect of nucleotide variations, both mutations and single-nucleotide polymorphisms. On the opposite, the exact knowledge of all splicing isoforms is crucial for clinicians to identify disease-causing mutations. The discovery of a 3′ terminal exon of *RPGR* gene—mutated in 60% of X-linked retinitis pigmentosa patients—is one of the first and most convincing examples of the link between AS and human diseases (6).

Such evidence highlights the importance to study at the isoform level, rather than at gene level, both physiological processes and disease mechanisms. The recently developed DataBase of Alternative Transcripts Expression (DBATE), valuable source of expression data for AS variants, is a good example (42).

In this 'scenario', our pilot transcript-centric database represents a fast and intuitive resource for medical geneticists interested in HSA21-related pathologies (such as DS), as well as for researchers investigating any molecular pathway or cell process involving HSA21 genes. Because ALE-HSA21 is an easy-to-use resource, it is accessible to all scientists with low experience in computational biology or informatics. ALE-HSA21 has been conceived to simply and rapidly provide the user with data usually dispersed in distinct databases or accessible by independently using different computational tools. The presence of genomic data, as well as of *in silico* predictions of regulatory sequences, links to gene expression, mutation and gene network databases in a unique Web site is an added value of ALE-HSA21.

Finally, our resource is in line with the growing interest for ncRNAs—supported by the wide diffusion of databases such as miRBase (20), miRWalk (21), lncRNome (43), lncRNA db (44), NONCODE (45) and Pseudofam (46). ALE-HSA21 provides open-access computational predictions about the presence of regulatory sequences for pseudogenes, lncRNAs and miRNAs, known to be involved in several biological processes.

This study is likely to represent an interesting proof-of-concept and a starting point for implementing similar resources with the aim to integrate information available in different databases to 'omics' data, generated by next-generation sequencing (RNA-Seq, ChIP-Seq and MeDIP-Seq) or by other large-scale technologies.

Acknowledgements

We thank Luciano De Leo for technical assistance to the web portal and Manuela Marescotti for reading the manuscript. We also thank the anonymous reviewers for the helpful comments and suggestions. We also acknowledge the ComBOlab (Computational & Biology Open laboratory).

Funding

This work was funded by the FLAGSHIP ''InterOmics'' Project (PB.P05) to A.C. and C.A., supported by the Italian MIUR and CNR organizations. Both laboratories are members of the COST-Action (BM1006) ''Next-Generation Sequencing Data Analysis Network'' funded by the EU.

Conflict of interest. None declared.

References

1. Kapranov,P., Cheng,J., Dike,S. *et al*. (2007) RNA maps reveal new RNA classes and a possible function for pervasive transcription. *Science*, **316**, 1484–1488.
2. Birney,E.J., Stamatoyannopoulos,A., Dutta,A. *et al*. (2007) Identification and analysis of functional elements in 1% of the human genome by the ENCODE pilot project. *Nature*, **447**, 799–816.
3. Jacquier,A. (2009) The complex eukaryotic transcriptome: unexpected pervasive transcription and novel small RNAs. *Nat. Rev. Genet.*, **10**, 833–844.
4. Clark,M.B., Amaral,P.P., Schlesinger,F.J. *et al*. (2011) The reality of pervasive transcription. *PLoS Biol.*, **9**, e1000625.
5. Harrow,J., Frankish,A., Gonzalez,J.M. *et al*. (2012) GENCODE: the reference human genome annotation for The ENCODE project. *Genome Res.*, **9**, 1760–1774.
6. Vervoort,R., Lennon,A., Bird,A.C. *et al*. (2000) Mutational hot spot within a new RPGR exon in X-linked retinitis pigmentosa. *Nat. Genet.*, **25**, 462–466.
7. Liu,G., Mattick,J.S. and Taft,R.J. (2013) A meta-analysis of the genomic and transcriptomic composition of complex life. *Cell Cycle*, **12**, 2061–2072.
8. Barrett,L.W., Fletcher,S. and Wilton,S.D. (2012) Regulation of eukaryotic gene expression by the untranslated gene regions and other non-coding elements. *Cell Mol. Life Sci.*, **69**, 3613–3634.
9. Yandell,M. and Ence,D. (2012) A beginner's guide to eukaryotic genome annotation. *Nat. Rev. Genet.*, **13**, 329–342.
10. Costa,V., Angelini,C., De Feis,I. *et al*. (2010) Uncovering the complexity of transcriptomes with RNA-Seq. *J. Biomed. Biotechnol.*, **2010**, 853916.
11. Costa,V., Angelini,C., D'Apice,L. *et al*. (2011) Massive-scale RNA-Seq analysis of non ribosomal transcriptome in human trisomy 21. *PLoS One*, **6**, e18493.
12. Trapnell,C., Pachter,L. and Salzberg,S.L. (2009) TopHat: discovering splice junctions with RNA-Seq. *Bioinformatics*, **25**, 1105–1111.
13. Quinlan,A.R. and Hall,I.M. (2010) BEDTools: a flexible suite of utilities for comparing genomic features. *Bioinformatics*, **26**, 841–842.
14. Li,H., Handsaker,B., Wysoker,A. *et al*. (2009) The Sequence alignment/map format and SAMtools. *Bioinformatics*, **25**, 2078–2079.
15. Zhang,Y., Liu,T., Meyer,C.A. *et al*. (2008) Model-based analysis of ChIP-Seq (MACS). *Genome Biol.*, **9**, R137.
16. Benjamini,Y. and Hochberg,Y. (1995) Controlling the false discovery rate: a practical and powerful approach to multiple testing. *J. R. Stat. Soc. Ser. B*, **57**, 289–300.
17. van Helden,J. (2003) Regulatory sequence analysis tools. *Nucleic Acids Res.*, **31**, 3593–3596.

18. Huang,H.Y., Chien,C.H., Jen,K.H. *et al*. (2006) RegRNA: an integrated web server for identifying regulatory RNA motifs and elements. *Nucleic Acids Res.*, **34**, W429–W434.
19. Hofacker,I.L. (2003) Vienna RNA secondary structure server. *Nucleic Acids Res.*, **31**, 3429–3431.
20. Griffiths-Jones,S., Grocock,R.J., van Dongen,S. *et al*. (2006) miRBase: microRNA sequences, targets and gene nomenclature. *Nucleic Acids Res.*, **34**, D140–D144.
21. Dweep,H., Sticht,C., Pandey,P. and Gretz,N. (2011) miRWalk–database: prediction of possible miRNA binding sites by ''walking'' the genes of three genomes. *J. Biomed. Inform.*, **44**, 839–847.
22. Gennarino,V.A., D'Angelo,G., Dharmalingam,G. *et al*. (2012) Identification of microRNA-regulated gene networks by expression analysis of target genes. *Genome Res.*, **22**, 1163–1172.
23. Oliveros,J.C. (2007) VENNY. An interactive tool for comparing lists with Venn Diagrams. http://bioinfogp.cnb.csic.es/tools/venny/index.html.
24. Tilgner,H., Raha,D., Habegger,L. *et al*. (2013) Accurate identification and analysis of human mRNA isoforms using deep long read sequencing. *G3 (Bethesda)*, **3**, 387–397.
25. Bartel,D.P. (2009) MicroRNAs: target recognition and regulatory functions. *Cell*, **136**, 215–233.
26. Guo,H., Ingolia,N.T., Weissman,J.S. *et al*. (2010) Mammalian microRNAs predominantly act to decrease target mRNA levels. *Nature*, **466**, 835–840.
27. Salmena,L., Poliseno,L., Tay,Y. *et al*. (2011) A ceRNA hypothesis: the Rosetta stone of a hidden RNA language? *Cell*, **146**, 353–368.
28. Cesana,M., Cacchiarelli,D., Legnini,I. *et al*. (2011) A long noncoding RNA controls muscle differentiation by functioning as a competing endogenous RNA. *Cell*, **147**, 358–369.
29. Karreth,F.A., Tay,Y., Perna,D. *et al*. (2011) In vivo identification of tumor-suppressive PTEN ceRNAs in an oncogenic BRAF-induced mouse model of melanoma. *Cell*, **147**, 382–395.
30. Tay,Y., Kats,L., Salmena,L. *et al*. (2011) Coding-independent regulation of the tumor suppressor PTEN by competing endogenous mRNAs. *Cell*, **147**, 344–357.
31. Costa,V., Esposito,R., Aprile,M. *et al*. (2012) Non-coding RNA and pseudogenes in neurodegenerative diseases: ''The (un)Usual Suspects''. *Front. Genet.*, **3**, 231.
32. Gruber,A.R., Lorenz,R., Bernhart,S.H. *et al*. (2008) The Vienna RNA websuite. *Nucleic Acids Res.*, **36**, W70–W74.
33. Pan,Q., Shai,O., Lee,L.J. *et al*. (2008) Deep surveying of alternative splicing complexity in the human transcriptome by highthroughput sequencing. *Nat. Genet.*, **40**, 1413–1415.
34. Keren,H., Lev-Maor,G. and Ast,G. (2010) Alternative splicing and evolution: diversification, exon definition and function. *Nat. Rev. Genet.*, **11**, 345–355.
35. Kornblihtt,A.R., Schor,I.E., Alló,M. *et al*. (2013) Alternative splicing: a pivotal step between eukaryotic transcription and translation. *Nat. Rev. Mol. Cell Biol.*, **14**, 153–165.
36. Binder,G., Brown,M. and Parks,J.S. (1996) Mechanisms responsible for dominant expression of human growth hormone gene mutations. *J. Clin. Endocrinol. Metab.*, **81**, 4047–4050.
37. Moseley,C.T., Mullis,P.E., Prince,M.A. *et al*. (2002) An exon splice enhancer mutation causes autosomal dominant GH deficiency. *J. Clin. Endocrinol. Metab.*, **87**, 847–852.
38. Faustino,N.A. and Cooper,T.A. (2003) Pre-mRNA splicing and human disease. *Genes Dev.*, **17**, 419–437.
39. Barbaux,S., Niaudet,P., Gubler,M.C. *et al*. (1997) Donor splice-site mutations in WT1 are responsible for Frasier syndrome. *Nat. Genet.*, **17**, 467–470.
40. Hossain,A. and Saunders,G.F. (2001) The human sex-determining gene SRY is a direct target of WT1. *J. Biol. Chem.*, **276**, 16817–16823.
41. Wilhelm,D. and Englert,C. (2002) The Wilms tumor suppressor WT1 regulates early gonad development by activation of Sf1. *Genes Dev.*, **16**, 1839–1851.
42. Bianchi,V., Colantoni,A., Calderone,A. *et al*. (2013) DBATE: database of alternative transcripts expression. *Database (Oxford)*, **2013**, bat050.
43. Bhartiya,D., Pal,K., Ghosh,S. *et al*. (2013) lncRNome: a comprehensive knowledgebase of human long noncoding RNAs. *Database (Oxford)*, **2013**, bat034.
44. Amaral,P.P., Clark,M.B., Gascoigne,D.K. *et al*. (2011) lncRNAdb: a reference database for long noncoding RNAs. *Nucleic Acids Res.*, **39**, D146–D151.
45. Bu,D., Yu,K., Sun,S. *et al*. (2012) NONCODE v3.0: integrative annotation of long noncoding RNAs. *Nucleic Acids Res.*, **40**, D210–D215.
46. Lam,H.Y., Khurana,E., Fang,G. *et al*. (2009) Pseudofam: the pseudogene families database. *Nucleic Acids Res.*, **37**, D738–D743.

Hindawi Publishing Corporation
PPAR Research
Volume 2014, Article ID 537865, 11 pages
http://dx.doi.org/10.1155/2014/537865

Research Article

PPARG in Human Adipogenesis: Differential Contribution of Canonical Transcripts and Dominant Negative Isoforms

M. Aprile,[1] M. R. Ambrosio,[1,2] V. D'Esposito,[2] F. Beguinot,[2,3] P. Formisano,[2,3] V. Costa,[1] and A. Ciccodicola[1]

[1] *Institute of Genetics and Biophysics "Adriano Buzzati-Traverso", National Research Council, 80131 Naples, Italy*
[2] *Department of Translational Medical Sciences, University of Naples "Federico II", 80131 Naples, Italy*
[3] *Institute of Experimental Endocrinology and Oncology, National Research Council, 80131 Naples, Italy*

Correspondence should be addressed to V. Costa; valerio.costa@igb.cnr.it

Received 25 November 2013; Revised 3 February 2014; Accepted 5 February 2014; Published 23 March 2014

Academic Editor: Guangrui Yang

The nuclear receptor PPARγ is a key regulator of adipogenesis, and alterations of its function are associated with different pathological processes related to metabolic syndrome. We recently identified two *PPARG* transcripts encoding dominant negative PPARγ isoforms. The existence of different *PPARG* variants suggests that alternative splicing is crucial to modulate PPARγ function, underlying some underestimated aspects of its regulation. Here we investigate *PPARG* expression in different tissues and cells affected in metabolic syndrome and, in particular, during adipocyte differentiation of human mesenchymal stem cells. We defined the transcript-specific expression pattern of *PPARG* variants encoding both canonical and dominant negative isoforms and identified a novel *PPARG* transcript, γ1ORF4. Our analysis indicated that, during adipogenesis, the transcription of alternative *PPARG* variants is regulated in a time-specific manner through differential usage of distinct promoters. In addition, our analysis describes—for the first time—the differential contribution of three ORF4 variants to this process, suggesting a still unexplored role for these dominant negative isoforms during adipogenesis. Therefore, our results highlight crucial aspects of *PPARG* regulation, suggesting the need of further investigation to rule out the differential impact of all *PPARG* transcripts in both physiologic and pathologic conditions, such as metabolism-related disorders.

1. Introduction

Peroxisome proliferator-activated receptors (PPARs, also known as nuclear receptor family 1C, NR1C) are ligand-dependent transcription factors belonging to the nuclear hormone receptor superfamily. Three members of the PPAR family—known as PPARα, PPARβ/δ, and PPARγ—encoded by different genes located on different chromosomes have been identified [1–3].

Undoubtedly, PPARγ is the most extensively studied and characterized member of PPARs, given its involvement in several physiological states, as well as pathological conditions. Indeed, it modulates the expression of several genes that play a central role in glucose, lipid and cholesterol metabolism, inflammation, angiogenesis, proliferation, and differentiation [4–7]. In particular, PPARγ is the master regulator of adipogenesis, since it regulates the transcription of a wide number of genes involved in cellular differentiation and lipid accumulation [8, 9]. Defects in PPARγ, signaling its altered expression and/or activation, as well as polymorphisms/mutations, are implicated in different pathological conditions occurring in metabolic syndrome, such as insulin resistance, obesity [10], dyslipidemia, and hypertension, that markedly increase the risk of type 2 diabetes [11–13], as well as cardiovascular diseases and cancer [3, 4, 14–17].

The prevalence of metabolic syndrome is increasing to epidemic proportions and, to date, an adequate therapy has not been yet established. Of great clinical interest, synthetic ligands of PPARγ, belonging to the class of thiazolidinediones (TZDs), such as troglitazone, pioglitazone, and rosiglitazone, function as insulin sensitizers and are used for treating hyperglycemia in patients with type 2 diabetes [7, 18–20].

Nevertheless, their use in type 2 diabetes therapy has been limited by untoward effects. Thus, a better understanding of PPARγ signaling is crucial to develop more effective and targeted therapeutic strategies to treat metabolic syndrome and its complications.

However, to fully define the landscape of PPARγ activity, some relevant aspects need to be taken into account. One of the most relevant features is the ability of *PPARG* gene to give rise to different transcripts. Indeed, the human *PPARG* gene consists of nine exons and—by differential promoter's usage and alternative splicing—generates at least four main splice variants (i.e., PPARG1, PPARG2, PPARG3, and PPARG4). These transcripts display different 5′ untranslated regions (UTRs), followed by six coding exons. However, despite the presence of such a variable number of *PPARG* transcripts, this gene encodes only two protein isoforms. Indeed, PPARG1, PPARG3, and PPARG4 encode the same protein PPARγ1—localized in the adipose tissue, liver, heart, and skeletal muscle—whereas PPARG2 yields a protein with 28 additional amino acids at the N-*terminus*, known as PPARγ2, exclusively localized in the adipose tissue [21–23].

Different ability to induce adipogenesis has been shown for PPARγ1 and PPARγ2, indicating a more relevant adipogenic activity for PPARγ2. Although both isoforms are thought to be essential during adipocyte differentiation, their relative contribution is not yet well clarified [24–27].

More recently, our group identified in sporadic colorectal cancers two novel *PPARG* transcripts harboring a read-through in intron 4, named γ2ORF4 and γ3ORF4, displaying the same 5′UTRs of PPARG2 and PPARG3, respectively [28]. The protein products lack the ligand binding domain (LBD) and act as dominant negative toward PPARγ. Although it has been shown that γORF4 plays a role in pathogenesis of colorectal cancer, its presence and expression levels have not yet been investigated in other cells and/or tissues.

To date, accurate analyses of the expression pattern of each *PPARG* transcript are still missing. For instance, to the best of our knowledge, this consideration holds true particularly for the adipogenesis, in which PPARγ is the main driver [4, 7, 29]. Alterations of adipocyte differentiation are strictly associated with obesity and metabolism-related disorders and therefore intimately linked to the physiopathology of the metabolic syndrome [30, 31]. Describing in detail the relative contribution of all currently known *PPARG* transcripts—and its dominant negative isoforms—in adipogenesis, as well as in tissues and cells related to processes altered in metabolic syndrome, will provide a solid basis to rule out if, and how, they may account for metabolism-related diseases.

Here we describe a complete expression analysis of all annotated *PPARG* transcripts—PPARG1, PPARG2, PPARG3, and PPARG4—as well as its dominant negative isoform γORF4 in human tissues and cells affected in metabolic syndrome. In particular, we focus on their differential expression during human adipogenesis, using human mesenchymal stem cells (hMSCs) isolated from the stromal vascular fraction of adipose tissue [32]. After *in vitro* differentiation of hMSCs in adipose cells, by using transcript-specific RT-PCR and Quantitative Real-Time PCR assays, we measured the expression of *PPARG* transcripts at various time points from the induction of adipocyte differentiation, demonstrating the differential contribution of each alternative splice variant. A similar pattern of expression was also observed for total PPARγ and γORF proteins. In addition, here we describe, for the first time, a novel transcript of *PPARG*, named γ1ORF4, similar to the dominant negative γ2ORF4 and γ3ORF4, previously identified [28]. Finally, we evaluated the abundance of all ORF4 variants during adipocytes' differentiation, also suggesting—for the first time—the involvement of these dominant negative isoforms in human adipogenesis.

2. Materials and Methods

2.1. Cell Cultures. Media, sera, and antibiotics for cell culture were from Lonza (Basel, Switzerland). Human Embryonic Kidney 293 cells (HEK239) were cultured in Dulbecco's modified Eagle's medium (DMEM) supplemented with 10% fetal bovine serum (FBS), 2 mmol/L glutamine, 100 units/mL penicillin, and 100 units/mL streptomycin.

Human Mesenchymal Stem Cells (hMSCs) were obtained by abdominal biopsy and cultures established as described previously [33]. The cells were grown in DMEM-F12 (1 : 1) with 10% FBS, 2 mmol/L glutamine, 100 units/mL penicillin, and 100 units/mL streptomycin. Cultures were maintained in a humidified atmosphere of 95% air and 5% CO_2 at 37°C.

2.1.1. Adipocyte Differentiation. Adipocyte differentiation was achieved as previously described [34]. Briefly, hMSCs were seeded (10,000 cells/cm^2) and cultured in six-well plates until confluence. Adipocyte differentiation was induced with a differentiation cocktail consisting of 850 nmol/L insulin, 10 μmol/L dexamethasone, 0.5 mmol/L IBMX (isobutylmethylxanthine), 10 μmol/L pioglitazone, 33 μmol/L biotin, and 17 μmol/L pantothenate in DMEM-F12 (1 : 1) supplemented with 3% FBS, 2 mmol/L glutamine, and antibiotics. After 3 days, the medium was changed to a medium containing only insulin and pioglitazone in DMEM-F12 (1 : 1) supplemented with 10% FBS, glutamine, and antibiotics. Culture medium was then changed every 2 days for another 8 days up to obtain a complete adipocyte differentiation of hMSCs. Lipid accumulation was determined by Oil Red O staining as described by Isakson and colleagues [34]. Adipocyte differentiation from hMSCs was performed in triplicate.

2.2. RNA Extraction and RT-PCR Assays. Total RNA was isolated from HEK239 and hMSCs at different stages of adipocyte differentiation, using TRIzol solution (Invitrogen) according to the manufacturer's instructions. RNA extracted from the other human tissues, heart, liver, and thyroid, and cells, human colon carcinoma, endothelial progenitor (EPCs), macrophages, and breast cancer (MCF7), employed in our analysis, was obtained in previous studies [28, 33, 35, 36]. For each sample, total RNA (1000 ng) was reverse transcribed using "high-capacity cDNA reverse-transcription kit" (Applied Biosystems, Foster City, CA). cDNAs obtained from human tissues and cells were used as template for RT-PCR assays. PCR amplification with specific primer

Table 1: Primer pairs for canonical and dominant negative *PPARG* variants.

Transcript	Oligonucleotide pairs		Size (bp)
	Forward	Reverse	
tPPARG	GAGAAGGAGAAGCTGTTGGC	ATGGCCACCTCTTTGCTCT	272
PPARG1	CGAGGACACCGGAGAGGG	TGTGGTTTAGTGTTGGCTTCTT	69
PPARG2	TTTTAACGGATTGATCTTTTGC	AGGAGTGGGAGTGGTCTTCC	255
PPARG3	TTCTGCTTAATTCCCTTTCC	AGGAGTGGGAGTGGTCTTCC	194
PPARG1/4	CGAGGACACCGGAGAGGG	AGGAGTGGGAGTGGTCTTCC	211/137
tORF4	CTTGCAGTGGGGATGTCTCA	AAACCCAAAACAACTTCCCG	279
γ1ORF4	CGAGGACACCGGAGAGGG	AAACCCAAAACAACTTCCCG	906
γ2ORF4	TTTTAACGGATTGATCTTTTG	AAACCCAAAACAACTTCCCG	950
γ3ORF4	TTCTGCTTAATTCCCTTTCC	AAACCCAAAACAACTTCCCG	889

pairs—designed using Oligo 4.0 and listed in Table 1—was performed using 1 μL of the reverse transcription reaction as template in PCR reactions set up with AmpliTaq Gold (Perkin Elmer). PCR assays have been performed using these amplification conditions: 95°C for 10 minutes, followed by 35 cycles at 95°C for 40 sec, 60°C for 40 sec, 72°C for 30 sec, and 70°C for 7 min. RT-PCR products were of expected length (see Table 1). In each experiment, a sample without reverse transcriptase was used as negative control and it was amplified under the same conditions as the reverse-transcribed RNA.

2.3. Cloning and Sequencing. The multiple PCR products (of about 211 and 137 bp, resp.), obtained in RT-PCR assays of PPARG1/PPARG4, have been cloned into Topo Vector II (Invitrogen) according to the manufacturer's instructions. Clones and other RT-PCR products were directly sequenced by Sanger method, confirming the specificity of reactions.

2.4. Real-Time PCR. Quantitative Real-Time PCRs were performed on cDNA samples of hMSCs and undifferentiated at different stages of adipocyte differentiation (6 hours, 12 hours, 24 hours, 2 days, 4 days, 7 days, and 10 days after induction of the process). Amplification reaction mix contained 1x SYBR Green PCR master mix (Applied Biosystems), 160 nM of each primer, and 50 ng of cDNA (RNA equivalent) as template. Quantitative Real-Time PCR assays were performed in according to the manufacturer's instructions for the 7900HT Real-Time PCR system (Applied Biosystems) in the same conditions described in [37]. Each assay for the 5 analyzed transcripts was performed in three biological replicates for all the time points. For each cell replicate, Real-Time assays were performed in two duplicated wells. Relative gene expression was measured by using $2^{-\Delta\Delta Ct}$ method. For each assay, expression levels were normalized for the reference values (time point at 0 hours or 6 hours) using glyceraldehyde 3-phosphate dehydrogenase (GAPDH) as housekeeping gene. qRT-PCRs data were reported as mean values and standard deviation of three biological replicates and results analyzed by paired Student t test. P value < 0.05 was considered statistically significant.

2.5. Immunoblot Procedure. Total cell lysates were obtained and separated by sodium dodecyl sulfate—polyacrylamide gel electrophoresis (SDS-PAGE) as previously described [38]. Briefly, hMSCs undifferentiated and at different stages of adipocyte differentiation (2 and 10 days) were solubilized for 2 hours at 4°C with lysis buffer containing 50 mM HEPES, 150 mM NaCl, 10 mM EDTA, 10 mM $Na_4P_2O_7$, 2 mM sodium orthovanadate, 50 mM NaF, 1 mM phenyl-methyl-sulfonyl fluoride, 10 μg/mL aprotinin, 10 μg/mL leupeptin, pH 7.4, and 1% (v/v) Triton X-100 (all reagents for lysis buffer were from Sigma-Aldrich, St Louis, MO, USA). The lysates were clarified by centrifugation at 12,000 rpm for 20 min at 4°C. Proteins were separated by SDS-PAGE (Bio-Rad Hercules, CA, USA) and blotted on Immobilon-P membranes (Millipore, Billerica, MA). Membranes were incubated with a polyclonal antibody directed against the N-terminal domain of PPARγ (Santa Cruz Biotechnology, CA, USA) and with antiactin antibodies (Santa Cruz Biotechnology, CA, USA). Detection of blotted proteins was performed by enhanced chemiluminescence (ECL, Amersham Biosciences, Arlington Heights, IL, USA) according to the manufacturer's instructions. Densitometric analysis was performed using Image Lab Software (Bio-Rad, Hercules, CA, USA). For each protein isoform (PPARγ and γORF4), data are shown as pixel density ratio versus control protein (actin).

3. Results

3.1. Expression Profile of PPARG Transcripts. Four main *PPARG* transcripts are currently known, as described by Costa et al. [3]. Additionally, our group has recently identified two isoforms acting asdominant negative toward PPARγ [28], transcribed by the same promoters of PPARG2 and PPARG3 transcripts, respectively (details in Figure 1).

Using specific primers pairs (Table 1), we performed an extensive expression analysis of PPARG1, PPARG2, PPARG3, PPARG4, and ORF4 in tissues and cells related to complications of metabolic syndrome—such as altered glucose and lipids' metabolism (liver), increased inflammatory response (macrophages), atherosclerosis (EPCs, heart, and macrophages), cancer (colon carcinoma and MCF7), and thyroid dysfunction (thyroid)—and in a widely used cell

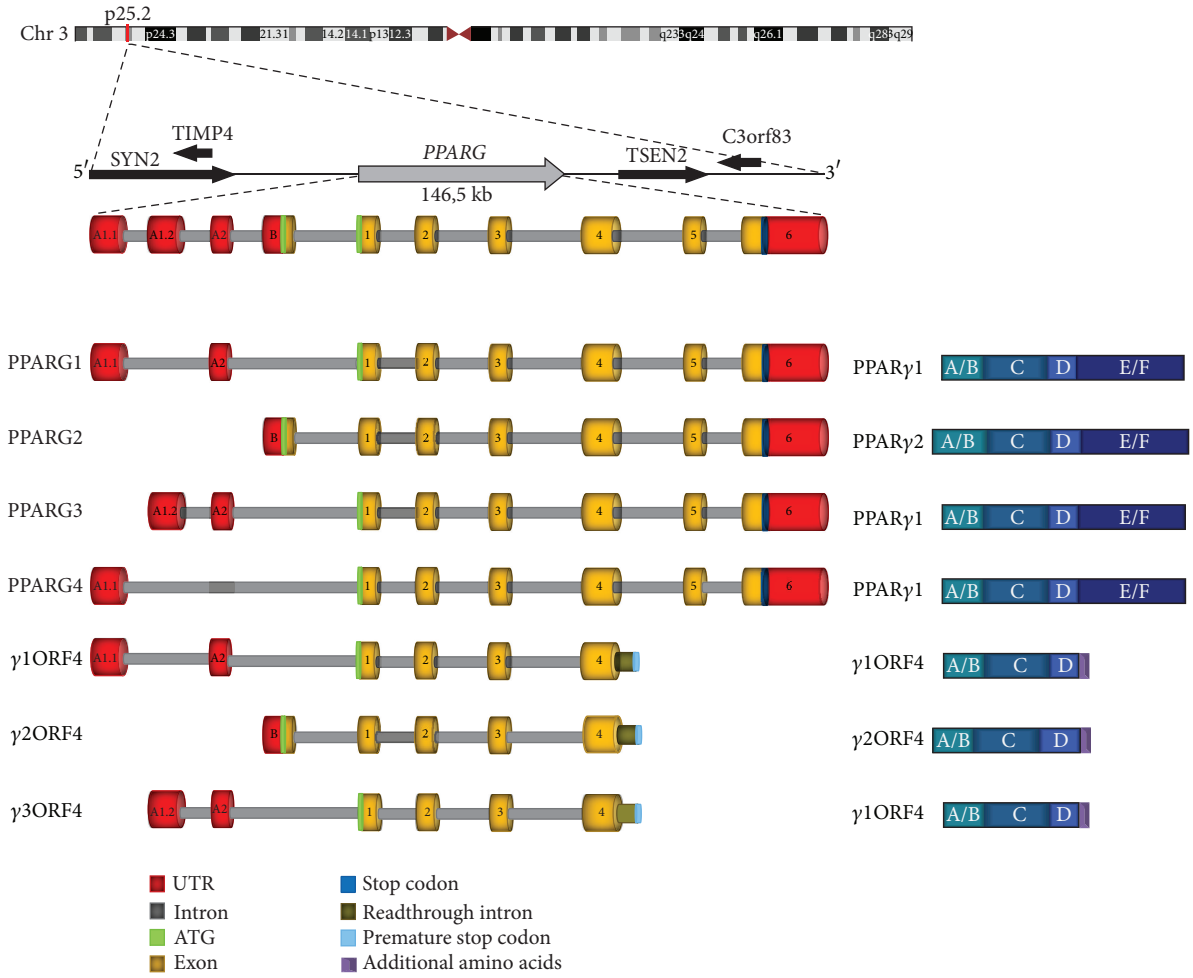

Figure 1: Schematic representation of human *PPARG* gene, transcripts, and protein isoforms. In the upper part the genomic localization of *PPARG* gene is indicated, with chromosome indication, cytogenetic band, and surrounding genes. Below is depicted the exon/intron structure of *PPARG* gene with transcribed splicing variants. Transcripts encoding both the canonical and dominant negative proteins are illustrated in the left panel. The right panel shows a schematic representation of the encoded proteins with the functional domains.

model, HEK293 [3, 6, 17, 39, 40]. Given the high similarity between the 5′UTRs of PPARG1 and PPARG4 transcripts, the primers employed to analyze PPARG4 amplify both variants (distinguishable as PCR products of different size), whereas we could design PPARG1 specific primers.

The tissue-specific expression pattern of *PPARG* alternative variants, including also transcripts encoding the same protein (PPARG1, PPARG3, and PPARG4), is shown in Figure 2. Such analysis revealed that PPARG1 transcript is expressed in all analyzed tissues and cell lines, confirming that it is abundantly and almost ubiquitously expressed in human tissues [21]. Similarly, PPARG4—which is transcribed from the same promoter—is expressed in almost all analyzed samples, albeit at lower levels than PPARG1. Therefore, we demonstrated that, in most of examined samples, PPARG1 and PPARG4 contribute to the translation of PPARγ1 protein, whereas PPARG3 is expressed at low levels only in EPCs and heart. Noteworthy, also PPARG2 transcript is expressed in EPCs, as well as in the heart, whereas its expression is undetectable in other examined tissues and cell lines. This finding—possibly correlated to the anti-inflammatory role of this nuclear receptor in the cardiovascular system [41–43]—suggests that PPARγ2 is predominantly expressed in these adult tissues. Surprisingly, the dominant negative isoform γORF4, till now associated with tumor pathogenesis, is expressed in all analyzed tissues and cell lines, suggesting a not negligible contribute to *PPARG* activity also in other physiologic and pathological cell processes. Of note, the results shown in Figure 2 refer to ORF4 transcripts' total expression.

3.2. Expression of PPARG Variants during Adipogenesis. After *in vitro* induction of hMSCs toward adipogenic differentiation (see Methods), we selected seven different time points (Figure 3). In particular, we investigated the "early stages" of adipocyte differentiation (6, 12, and 24 hours after induction), an intermediate time point (2 days), and "late stages" (4 and 7 days) according to visible changes in cell morphology and an endpoint at 10 days when cells differentiate into adipocytes (Figure 3).

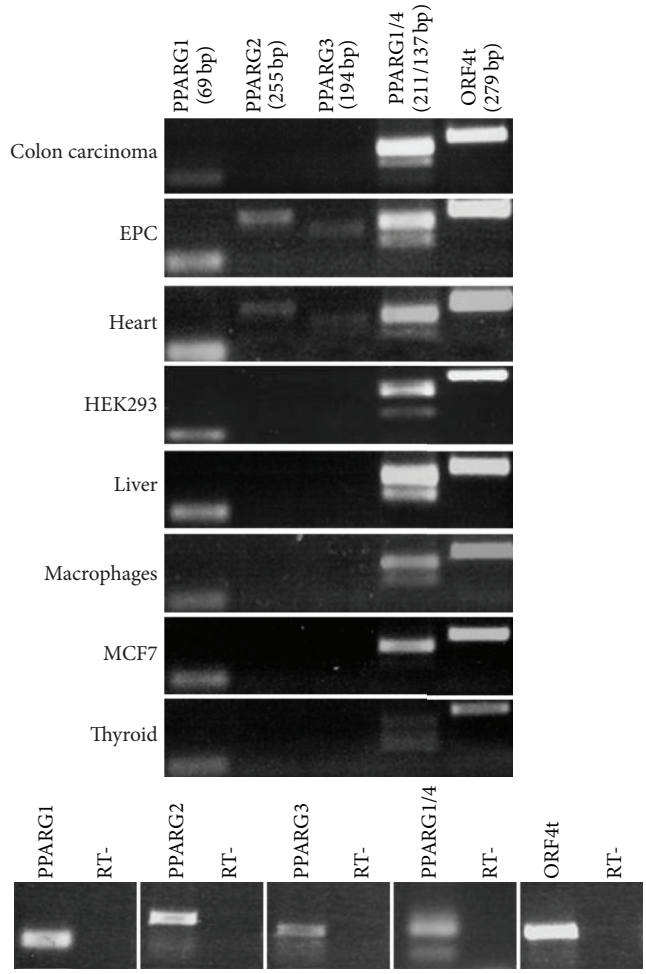

Figure 2: Expression pattern of *PPARG* variants in tissues and cells affected in the metabolic syndrome. For each *PPARG* transcript, specific primer pairs were used for PCR reactions. Given the similarity between PPARG1/4 5′UTRs primers amplifies both variants (distinguishable as PCR products of different sizes). "ORF4t" indicates the entire pool of ORF4 transcripts. Amplicons' sizes are shown (in bp) below transcripts' names. On the bottom panel, negative PCR controls are shown for each primer pair.

RT-PCR assay revealed that, first of all, total *PPARG* expression (i.e., of the entire pool of canonical *PPARG* transcripts) is very high throughout the process. In detail, using variant-specific primers we observed that all *PPARG* transcripts are expressed—albeit at variable levels—in the examined differentiation stages (Figure 4(a)). Interestingly, PPARG2 is not expressed in hMSCs, whereas its expression is remarkably higher in the early stages after induction toward adipocyte differentiation. Particularly, as shown in Figure 4(a), this transcript reaches its highest expression after 2 days from the induction and is completely silenced at the end of the process. Similarly, PPARG3 has a mild but detectable expression only in the intermediate and late stages of cells' differentiation, with its highest expression at 2 days. This analysis revealed that PPARG1 and PPARG4 are the only canonical transcripts contributing to the final expression of PPARγ protein in undifferentiated hMSCs and therefore that these cells express only PPARγ1 isoform. In particular, PPARG1 is expressed at much higher levels than PPARG4 variant and, given the absence of the PPARG3 splice variant, it can be considered as the main contributor to the synthesis of functional PPARγ1 protein in undifferentiated cells (Figure 4(a)).

However, PPARG1 and PPARG4 are expressed also throughout the adipocyte differentiation, although the former is the most expressed *PPARG* transcript at all the stages.

3.2.1. Identification of γ1ORF4 and Analysis of PPARG Dominant Negative Transcripts. Given the existence of two different isoforms of γORF4, previously described as dominant negative of PPARγ [28], we asked whether other ORF4 variants may be transcribed from the promoter upstream the $A_{1.1}$ exon of *PPARG* gene. Thus, using specific primers pairs (described in Table 1), we were able to identify in hMSCs a novel ORF4 variant, named γ1ORF4 (accession number still in process; see Figure 1 for details). Similarly to PPARG1, its 5′UTR consists of $A_{1.1}$ and A_2 exons, whereas its coding region extends from exon 1 to 4, with a read-through in intron 4, identical to the other ORF4 transcripts (structural details in Figure 1).

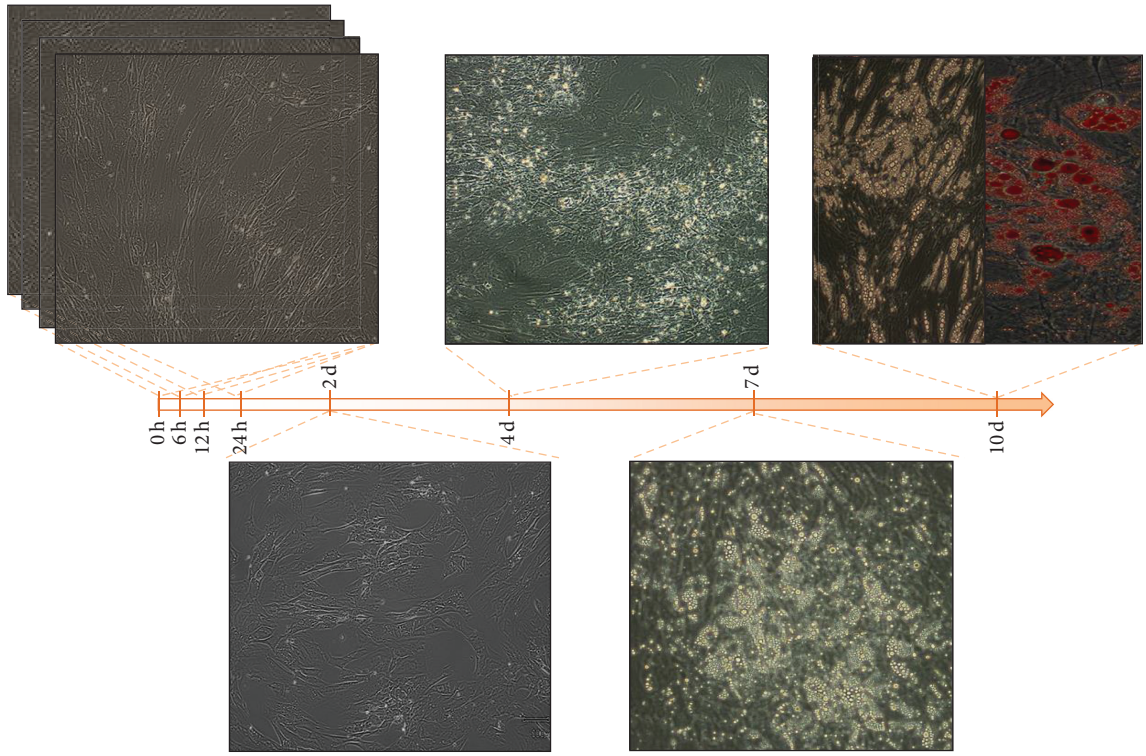

Figure 3: Phenotypic characteristics of undifferentiated, differentiating, and differentiated hMSCs (h = hours; d = days). Adipocyte differentiation was determined at 10 days from adipogenesis induction by Oil Red O staining of lipids vacuoles, as shown.

Given the discovery of such new transcript in hMSCs, we decided to investigate the expression of the entire pool of ORF4 variants (ORF4t in Figure 4(b)) during *in vitro* adipogenesis. Of note, RT-PCR assay revealed that these variants are expressed along adipocytes' differentiation and particularly in the crucial stages of this process (24 hours, 2 and 4 days). Subsequent independent analysis of the three ORF4 transcripts revealed that γ3ORF4 variant is expressed throughout the process, whereas γ2ORF4 mRNA undergoes a dramatic increase at 2 days from differentiation's induction. Noteworthy, the novel variant γ1ORF4—identified in undifferentiated hMSCs—is expressed at variable levels during adipogenesis, although it is undetectable at some stages (Figure 4(b)).

3.3. Quantitative Analysis of Canonical and Dominant Negative PPARG Splice Variants during Adipogenesis. To have a quantitative estimate of *PPARG* transcripts after induction of the adipogenic process, we performed Quantitative Real-Time analysis with specific primer pairs at the time points above described. Such quantitative analysis confirmed the findings of RT-PCR assay, showing that the expression of total *PPARG* increases up to 2 days by adipogenesis induction. Indeed, at this stage, total *PPARG* expression is about 20-fold increase compared to undifferentiated cells and it linearly decreases after 7 days, reaching expression levels comparable to undifferentiated cells (Figure 5(a)).

However, the most relevant findings derive from the canonical transcript-specific analysis. Indeed, it revealed that all PPARG canonical transcripts have a similar trend of expression but exhibit different fold increase during the process (Figure S1 see supplementary materials available online at http://dx.doi.org/10.1155/2014/537865). For PPARG2 and PPARG3 the expression values at 6 hours were used as baseline, since they are not expressed in undifferentiated hMSCs (Figure 5(a)). However, despite their low expression levels, these transcripts exhibit an increase of expression considerably higher than PPARG1. Indeed, at 2 days by differentiations' induction, the expression of PPARG2 and PPARG3 raises of about 110- and 45-fold, respectively, whereas PPARG1 increase is of about 10-fold (Figure 5(a)).

To quantitatively study ORF4 transcripts, the only way to discriminate among the different variants is through the analysis of large PCR amplicons (about 900–1000 bp, Figure 4(b)), unfeasible with qRT-PCR. Thus, quantitative data for ORF4, shown in Figure 5(a), refer to the pool of ORF4 transcripts. Particularly, we observed, for these variants, a different trend of expression throughout the process compared to *PPARG* canonical transcripts, confirming RT-PCR assays (Figure 4(b)). Indeed, ORF4 total expression is significantly downregulated in early stages of differentiation and reaches its highest values at 2 days. Nonetheless, its increase is considerably lower than the canonical transcripts (fold increase = 4; Figure 5(a)).

Finally, pairwise comparison of fold changes' variation, that is, between two subsequent time points, revealed that the most significant increase of the expression values occurs in the transition from day 1 to day 2 upon induction of adipocyte

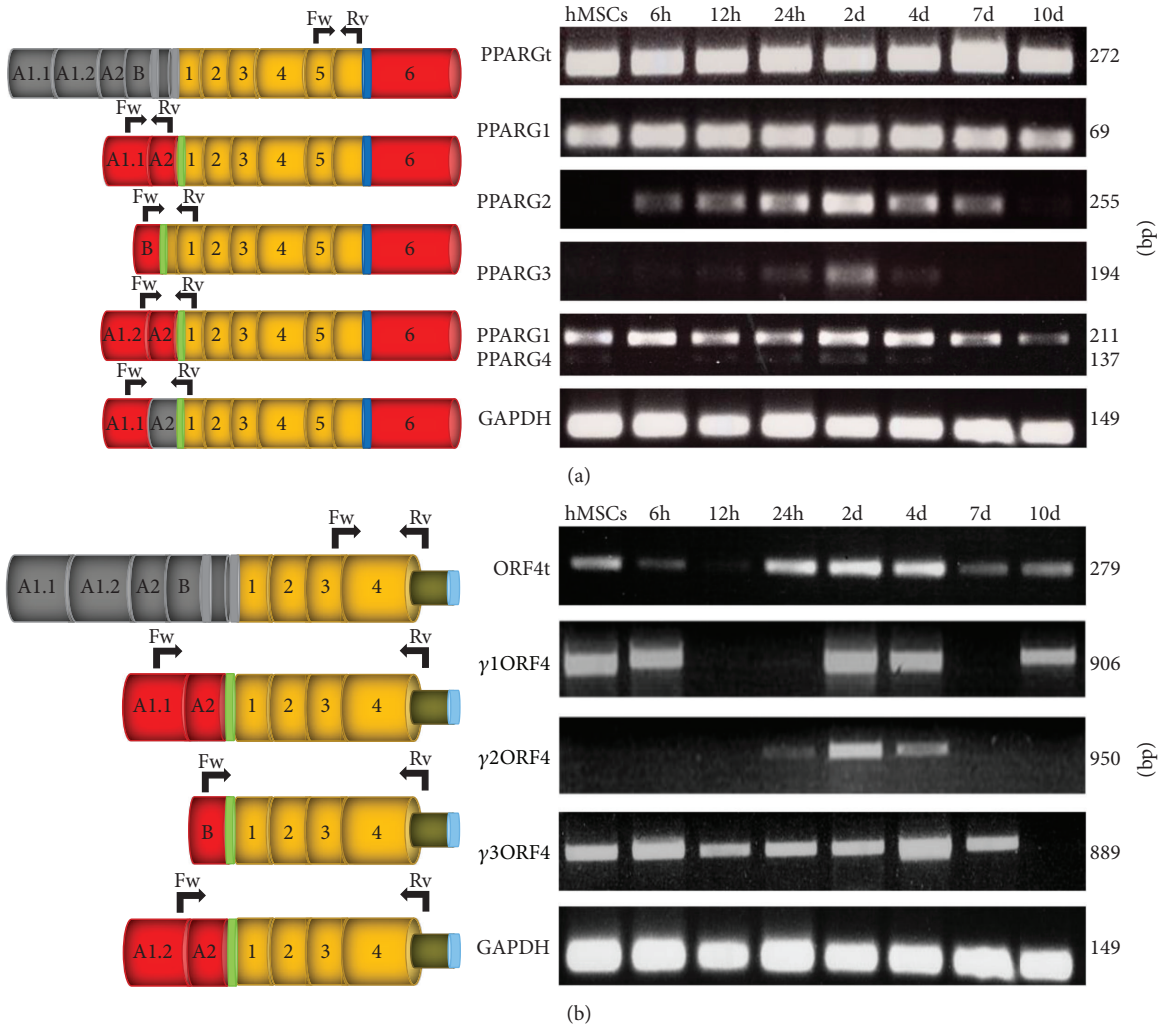

Figure 4: Transcript-specific RT-PCR assays for *PPARG* canonical transcripts (panel (a)) and ORF4 variants (panel (b)) at different time points of the adipogenesis (indicated on the top). On the left, the different *PPARG* transcripts are schematically shown; on the right the related PCR amplicons and their sizes (in bp) are illustrated. "PPARGt" and "ORF4t" indicate the entire pool of canonical *PPARG* and ORF4 transcripts, respectively. Transcript-specific exons are shown in grey and common exons are coloured. Black arrows indicate the specific primer pairs used in this analysis (Fw, forward; Rv, reverse). *GAPDH* was used as internal control.

differentiation (Figure S1). Notably, the most striking increase has been observed for PPARG2 and PPARG3 variants (about 90 and 40 fold, resp.), suggesting the inducible nature of their promoters during this process. On the opposite, highly significant decreases were observed—for these two splice variants—immediately after day 2 from the induction of the process. A common behavior was observed for PPARG1 and ORF4 transcripts. In particular, these variants undergo mild expression changes in the transitions among the stages, showing a quite constant basal expression throughout the adipogenic process (Figure 5(a) and S1). Since the most evident changes in *PPARG* transcripts' abundance were detected after 2 days by differentiation induction, we investigated protein levels on three time points, day 0 (undifferentiated cells), day 2 (i.e., the highest peak of *PPARG* expression), and day 10 (i.e., differentiated cells). As no commercially available antibodies exist for ORF4 protein, we used a polyclonal antibody directed against the N-terminal domain, able to recognize both the canonical and the shortest *PPARG* isoforms. We detected canonical PPARγ at 67 kDa and immunoreactive bands at 40 kDa, the predicted weight of ORF4 protein isoform. As expected, consistently with the changes in mRNA levels, after 2 days by differentiation induction, the expressions of PPARγ—and of the shortest isoforms—were higher compared to both undifferentiated and completely differentiated cells (Figure 5(b)).

4. Conclusions

Epidemiological studies demonstrate that the prevalence of the metabolic syndrome is increasing in the Western world and developing countries, and to date an adequate therapy has not been yet established [17, 44].

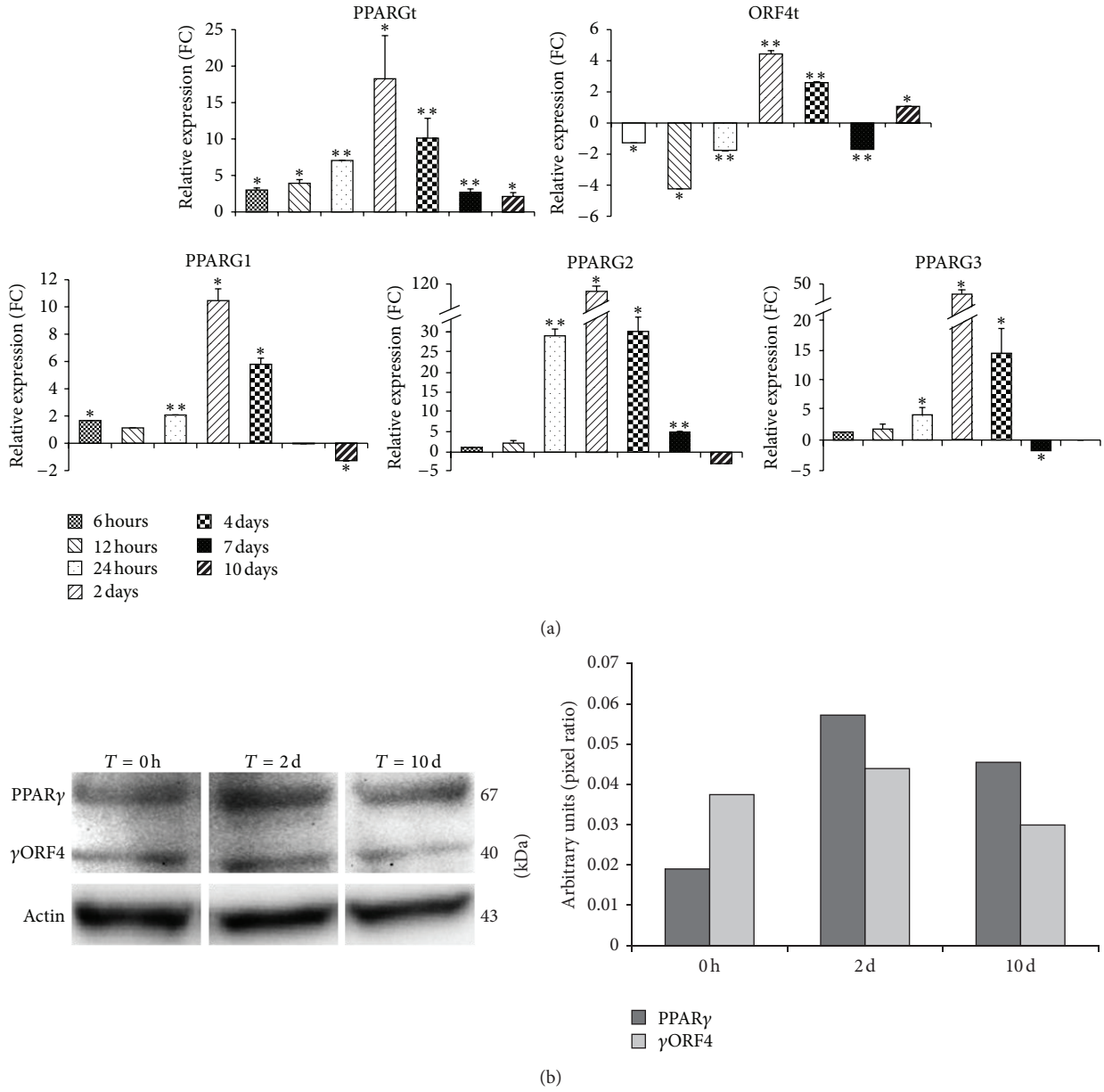

Figure 5: For each analyzed *PPARG* variant, bar graphs in the Panel (a) indicate the relative expression levels at different time points after i*n vitro* adipocyte differentiation. For each assay, expression is normalized for reference samples (time point at 0 or 6 hours) using *GAPDH* as housekeeping gene. Data are reported as mean values, and error bars are also reported. P values < 0.05 are considered statistically significant and indicated by an asterisk. Double asterisks indicate P values < 0.001. In panel (b), total cell lysates of hMSC at day 0, day 2, and day 10 by differentiation induction blotted with anti-PPARγ antibody are shown. To ensure equal protein transfer, membranes were blotted with antiactin antibody. Bar graph indicates the pixel intensity ratio between PPARγ isoforms and actin protein levels, reported as arbitrary units over basal (day 0).

Undoubtedly, *PPARG* is one of the most studied genes accounting for metabolic disorders. Indeed, it modulates the expression of several genes with a crucial role in glucose, lipid and cholesterol metabolism, insulin signaling, and adipokines' production, whose imbalance leads to insulin resistance, obesity, type 2 diabetes, and cardiovascular diseases [3, 4, 7, 14]. PPARγ is also a drug target and, currently, its synthetic ligands are used to treat hyperlipidemia and as insulin-sensitizing antidiabetic agents [18]. Thus, defining *PPARG* activity in tissues and cells related to energy metabolism may provide useful insights to develop new and effective therapeutic strategies to treat the metabolic syndrome and its complications.

It is currently known that—by different promoter usage and alternative splicing—the human *PPARG* gene generates multiple variants encoding two proteins, PPARγ1 and

PPARγ2. Since different *PPARG* splice variants encode the same protein isoform, their differential expression, both spatial and temporal, may reflect a different regulation, translation, mRNA stability, and/or localization. To complicate the picture, the recent identification of γORF4 isoform—able to act as dominant-negative and with a tumorigenic effect [28]—suggests that PPARγ activity is modulated through transcript-specific regulation.

Therefore, our effort has been to investigate *PPARG* expression in different tissues and cells—affected in metabolic syndrome—and during hMSCs' adipocyte differentiation. Other than focusing on canonical *PPARG* transcripts, a particular emphasis was posed toward defining the expression pattern of its variants encoding dominant negative isoforms. In our study we identified γ1ORF4, a novel *PPARG* transcript that, similarly to the previously described γ2ORF4 and γ3ORF4 [28], may act as dominant negative toward PPARγ.

Our expression analysis has clearly demonstrated that the different promoters of *PPARG* have a peculiar transcriptional activity. Such finding is particularly relevant in the adipocyte differentiation, in which PPARγ is a key player [4, 9, 29]. The almost ubiquitous PPARG1/PPARG4 expression, particularly throughout adipogenesis, indicates a more pronounced activity of their promoter compared to the others, suggesting it as the main contributor to PPARγ protein synthesis. Furthermore, the mild expression changes of PPARG1 along adipocyte differentiation strengthen the hypothesis that its promoter provides constitutive levels of *PPARG* messengers. On the opposite, the tissue- and stage-specific PPARG2 expression, as well as its dramatic variations throughout the adipogenesis, clearly demonstrate its inducible nature.

Interestingly, the almost ubiquitous expressions of ORF4 variants in tissues and cells, as well as during adipogenesis, support the hypothesis that *PPARG* regulates itself through dominant negative isoforms. Furthermore, our results suggest that similarly to *PPARG* canonical transcripts, the three ORF4 variants give a different contribution to PPARγ activity. Indeed, whereas γ1ORF4 and γ2ORF4 exhibit stage-specific expression, γ3ORF4 is constantly expressed along adipocyte differentiation but not in mature adipose cells. These findings, strictly correlated with those regarding the canonical isoforms, suggest that (1) the promoter upstream exon B is inducible for both the canonical and ORF4 variants, (2) constitutive levels of *PPARG* variants, encoding dominant negative isoforms, are provided throughout differentiation by the promoter upstream noncoding exon $A_{1.2}$, and (3) it almost exclusively transcribes γ3ORF4 rather than the canonical PPARG3. Therefore, such evidences suggest a relevant—if not exclusive—role of promoter of γ3ORF4 and PPARG3 variants in negative PPARγ regulation. In addition, protein analysis confirmed that after 2 days by differentiation induction PPARγ protein has a higher expression compared to undifferentiated and completely differentiated cells. Moreover, we observed the same trend of expression also for a shorter protein of 40 kDa, corresponding to the predicted weight of ORF4 isoform.

Although the results described herein represent only a starting point to understand the impact of *PPARG* transcripts along human adipogenesis, they support the notion that this generegulates such crucial process through balancing the levels of its different splicing variants. Further studies—particularly taking into account *PPARG* protein products—are strictly required to definitely establish the role of all splicing variants in adipocyte differentiation. Notably, our results shed light on previously underestimated aspects of *PPARG* regulation and propose a yet unexplored role of its dominant negative isoforms during adipogenesis. Indeed, the finding that—during a crucial process in which *PPARG* is a "master gene"—both the transcripts and the proteins encoding dominant negative isoforms are constitutively expressed and/or can be modulated similarly to the canonical *PPARG* variants, enforces the need to investigate toward this direction. Understanding more about *PPARG* activity in the adipogenic process is directly linked to its possible contribution to the onset and progression of metabolism-related pathologies, including the metabolic syndrome and its complications.

Finally, we cannot exclude that the presence of transcripts encoding *PPARG* dominant negative proteins in other human tissues may underlie their interesting roles in physiological processes as well as in other pathological conditions.

Conflict of Interests

The authors declare that there is no conflict of interests regarding the publication of this paper.

Authors' Contribution

M. Aprile and M. R. Ambrosio contributed equally to this work.

Acknowledgments

The authors thank the FLAGSHIP "InterOmics" Project (PB.P05) to A. Ciccodicola, funded and supported by the Italian MIUR and CNR organizations and the Italian Ministry of Education, University and Research (MIUR) Project National Operational Programme for "Research and Competitiveness" 2007–2013 PON01 02460 to A. Ciccodicola, P. Formisano and F. Beguinot. The financial support through the projects ORTO11TSM3 to F. Beguinot and the FIRB project RBNE08NKH7 (MERIT initiative) to F. Beguinot and P. Formisano is gratefully acknowledged. M. Aprile is PhD student in molecular and cellular biotechnology at the Department of Environmental Sciences and Technologies, biological, and pharmaceutical "DISTABiF" at Second University of Naples. M. R. Ambrosio is PhD student in Molecular Oncology and Endocrinology at the Department of Translational Medical Sciences, University of Naples "Federico II".

References

[1] T. M. Willson, P. J. Brown, D. D. Sternbach, and B. R. Henke, "The PPARs: from orphan receptors to drug discovery," *Journal of Medicinal Chemistry*, vol. 43, no. 4, pp. 527–550, 2000.

[2] M. C. Cho, K. Lee, S. G. Paik, and D. Y. Yoon, "Peroxisome proliferators-activated receptor (PPAR) modulators and metabolic disorders," *PPAR Research*, vol. 2008, Article ID 679137, 14 pages, 2008.

[3] V. Costa, M. A. Gallo, F. Letizia, M. Aprile, A. Casamassimi, and A. Ciccodicola, "PPARG: gene expression regulation and next-generation sequencing for unsolved issues," *PPAR Research*, vol. 2010, Article ID 409168, 17 pages, 2010.

[4] E. D. Rosen and B. M. Spiegelman, "PPARγ: a nuclear regulator of metabolism, differentiation, and cell growth," *Journal of Biological Chemistry*, vol. 276, no. 41, pp. 37731–37734, 2001.

[5] W. Ahmed, O. Ziouzenkova, J. Brown et al., "PPARs and their metabolic modulation: new mechanisms for transcriptional regulation?" *Journal of Internal Medicine*, vol. 262, no. 2, pp. 184–198, 2007.

[6] L. Széles, D. Töröcsik, and L. Nagy, "PPARγ in immunity and inflammation: cell types and diseases," *Biochimica et Biophysica Acta—Molecular and Cell Biology of Lipids*, vol. 1771, no. 8, pp. 1014–1030, 2007.

[7] M. Ahmadian, J. M. Suh, N. Hah et al., "PPARγ signaling and metabolism: the good, the bad and the future," *Nature Medicine*, vol. 19, no. 5, pp. 557–566, 2013.

[8] Y. Barak, M. C. Nelson, E. S. Ong et al., "PPARγ is required for placental, cardiac, and adipose tissue development," *Molecular Cell*, vol. 4, no. 4, pp. 585–595, 1999.

[9] E. D. Rosen, P. Sarraf, A. E. Troy et al., "PPARγ is required for the differentiation of adipose tissue in vivo and in vitro," *Molecular Cell*, vol. 4, no. 4, pp. 611–617, 1999.

[10] Y. L. Muller, C. Bogardus, B. A. Beamer, A. R. Shuldiner, and L. J. Baier, "A functional variant in the peroxisome proliferator—activated receptor γ2 promoter is associated with predictors of obesity and type 2 diabetes in Pima Indians," *Diabetes*, vol. 52, no. 7, pp. 1864–1871, 2003.

[11] D. Altshuler, J. N. Hirschhorn, M. Klannemark et al., "The common PPARγ Pro12Ala polymorphism is associated with decreased risk of type 2 diabetes," *Nature Genetics*, vol. 26, no. 1, pp. 76–80, 2000.

[12] H. Mori, H. Ikegami, Y. Kawaguchi et al., "The Pro12 → Ala substitution in PPAR-γ is associated with resistance to development of diabetes in the general population: possible involvement in impairment of insulin secretion in individuals with type 2 diabetes," *Diabetes*, vol. 50, no. 4, pp. 891–894, 2001.

[13] V. Costa, A. Casamassimi, K. Esposito et al., "Characterization of a novel polymorphism in PPARG regulatory region associated with type 2 diabetes and diabetic retinopathy in italy," *Journal of Biomedicine and Biotechnology*, vol. 2009, Article ID 126917, 7 pages, 2009.

[14] J. I. Odegaard, R. R. Ricardo-Gonzalez, M. H. Goforth et al., "Macrophage-specific PPARγ controls alternative activation and improves insulin resistance," *Nature*, vol. 447, no. 7148, pp. 1116–1120, 2007.

[15] S. Azhar, "Peroxisome proliferator-activated receptors, metabolic syndrome and cardiovascular disease," *Future Cardiology*, vol. 6, no. 5, pp. 657–691, 2010.

[16] I. Barroso, M. Gurnell, V. E. F. Crowley et al., "Dominant negative mutations in human PPARγ associated with severe insulin resistance, diabetes mellitus and hypertension," *Nature*, vol. 402, no. 6764, pp. 880–883, 1999.

[17] D. Capaccio, A. Ciccodicola, L. Sabatino et al., "A novel germline mutation in peroxisome proliferator-Activated Receptor γ gene associated with large intestine polyp formation and dyslipidemia," *Biochimica et Biophysica Acta—Molecular Basis of Disease*, vol. 1802, no. 6, pp. 572–581, 2010.

[18] A. Raji and J. Plutzky, "Insulin resistance, diabetes, and atherosclerosis: thiazolidinediones as therapeutic interventions," *Current Cardiology Reports*, vol. 4, no. 6, pp. 514–521, 2002.

[19] M. C. Bragt and H. E. Popeijus, "Peroxisome proliferator-activated receptors and the metabolic syndrome," *Physiology and Behavior*, vol. 94, no. 2, pp. 187–197, 2008.

[20] H. Shahbazian, S. M. Latifi, M. T. Jalali et al., "Metabolic syndrome and its correlated factors in an urban population in South West of Iran.," *Journal of Diabetes & Metabolic Disorders*, vol. 12, no. 1, p. 11, 2013.

[21] L. Fajas, D. Auboeuf, E. Raspé et al., "The organization, promoter analysis, and expression of the human PPARγ gene," *Journal of Biological Chemistry*, vol. 272, no. 30, pp. 18779–18789, 1997.

[22] L. Fajas, J. C. Fruchart, and J. Auwerx, "PPARγ3 mRNA: a distinct PPARγ mRNA subtype transcribed from an independent promoter," *FEBS Letters*, vol. 438, no. 1-2, pp. 55–60, 1998.

[23] C. Knouff and J. Auwerx, "Peroxisome proliferator-activated receptor-γ calls for activation in moderation: lessons from genetics and pharmacology," *Endocrine Reviews*, vol. 25, no. 6, pp. 899–918, 2004.

[24] A. Werman, A. Hollenberg, G. Solanes, C. Bjørbæk, A. J. Vidal-Puig, and J. S. Flier, "Ligand-independent activation domain in the N terminus of peroxisome proliferator-activated receptor γ (PPARγ). Differential activity of PPARγ1 and -2 isoforms and influence of insulin," *Journal of Biological Chemistry*, vol. 272, no. 32, pp. 20230–20235, 1997.

[25] D. Ren, T. N. Collingwood, E. J. Rebar, A. P. Wolffe, and H. S. Camp, "PPARγ knockdown by engineered transcription factors: Exogenous PPARγ2 but not PPARγ1 reactivates adipogenesis," *Genes and Development*, vol. 16, no. 1, pp. 27–32, 2002.

[26] S. Yu, N. Viswakarma, S. K. Batra, M. Sambasiva Rao, and J. K. Reddy, "Identification of promethin and PGLP as two novel up-regulated genes in PPARγ1-induced adipogenic mouse liver," *Biochimie*, vol. 86, no. 11, pp. 743–761, 2004.

[27] E. Powell, P. Kuhn, and W. Xu, "Nuclear receptor cofactors in PPARγ-mediated adipogenesis and adipocyte energy metabolism," *PPAR Research*, vol. 2007, Article ID 53843, 11 pages, 2007.

[28] L. Sabatino, A. Casamassimi, G. Peluso et al., "A novel peroxisome proliferator-activated receptor γ isoform with dominant negative activity generated by alternative splicing," *Journal of Biological Chemistry*, vol. 280, no. 28, pp. 26517–26525, 2005.

[29] A. Chawla, E. J. Schwarz, D. D. Dimaculangan, and M. A. Lazar, "Peroxisome proliferator-activated receptor (PPAR) γ: adipose-predominant expression and induction early in adipocyte differentiation," *Endocrinology*, vol. 135, no. 2, pp. 798–800, 1994.

[30] R. M. Evans, G. D. Barish, and Y. X. Wang, "PPARs and the complex journey to obesity," *Nature Medicine*, vol. 10, no. 4, pp. 355–361, 2004.

[31] S. Kersten, B. Desvergne, and W. Wahli, "Roles of PPARS in health and disease," *Nature*, vol. 405, no. 6785, pp. 421–424, 2000.

[32] A. Armani, C. Mammi, V. Marzolla et al., "Cellular models for understanding adipogenesis, adipose dysfunction, and obesity," *Journal of Cellular Biochemistry*, vol. 110, no. 3, pp. 564–572, 2010.

[33] V. D'Esposito, F. Passaretti, A. Hammarstedt et al., "Adipocyte-released insulin-like growth factor-1 is regulated by glucose and fatty acids and controls breast cancer cell growth in vitro," *Diabetologia*, vol. 55, no. 10, pp. 2811–2822, 2012.

[34] P. Isakson, A. Hammarstedt, B. Gustafson, and U. Smith, "Impaired preadipocyte differentiation in human abdominal obesity: role of Wnt, tumor necrosis factor-α, and inflammation," *Diabetes*, vol. 58, no. 7, pp. 1550–1557, 2009.

[35] V. Costa, I. Conte, C. Ziviello et al., "Identification and expression analysis of novel Jakmip1 transcripts," *Gene*, vol. 402, no. 1-2, pp. 1–8, 2007.

[36] V. Costa, L. Sommese, A. Casamassimi et al., "Impairment of circulating endothelial progenitors in Down syndrome," *BMC Medical Genomics*, vol. 3, article 40, 2010.

[37] V. Costa, C. Angelini, L. D'Apice et al., "Massive-scale rna-seq analysis of non ribosomal transcriptome in human trisomy 21," *PLoS ONE*, vol. 6, no. 4, Article ID e18493, 2011.

[38] A. T. Alberobello, V. D'Esposito, D. Marasco et al., "Selective disruption of insulin-like growth factor-1 (IGF-1) signaling via phosphoinositide-dependent kinase-1 prevents the protective effect of IGF-1 on human cancer cell death," *Journal of Biological Chemistry*, vol. 285, no. 9, pp. 6563–6572, 2010.

[39] S. B. Park, H. C. Choi, and N. S. Joo, "The relation of thyroid function to components of the metabolic syndrome in Korean men and women," *Journal of Korean Medical Science*, vol. 26, no. 4, pp. 540–545, 2011.

[40] H. P. Koeffler, "Peroxisome proliferator-activated receptor γ and cancers," *Clinical Cancer Research*, vol. 9, no. 1, pp. 1–9, 2003.

[41] M. D. Rollins, S. Sudarshan, M. A. Firpo et al., "Anti-inflammatory effects of PPAR-γ agonists directly correlate with PPAR-γ expression during acute pancreatitis," *Journal of Gastrointestinal Surgery*, vol. 10, no. 8, pp. 1120–1130, 2006.

[42] R. B. Clark, "The role of PPARs in inflammation and immunity," *Journal of Leukocyte Biology*, vol. 71, no. 3, pp. 388–400, 2002.

[43] N. Marx, B. Kehrle, K. Kohlhammer et al., "PPAR activators as antiinflammatory mediators in human T lymphocytes: implications for atherosclerosis and transplantation-associated arteriosclerosis," *Circulation Research*, vol. 90, no. 6, pp. 703–710, 2002.

[44] N. Gupta, K. Goel, P. Shah, and A. Misra, "Childhood obesity in developing countries: epidemiology, determinants, and prevention," *Endocrine Reviews*, vol. 33, no. 1, pp. 48–70, 2012.

Platelet-rich plasma increases growth and motility of adipose tissue-derived mesenchymal stem cells and controls adipocyte survival and secretory function.

Vittoria D'Esposito[1], Federica Passaretti[1], Giuseppe Perruolo[2], Maria Rosaria Ambrosio[1], Rossella Valentino[2], Francesco Oriente[1], Gregory A. Raciti[2], Cecilia Nigro[2], Claudia Miele[2], Gilberto Sammartino[3], Francesco Beguinot[1,2], Pietro Formisano*[1,2]

[1]Department of Translational Medicine, Federico II University of Naples, Naples, Italy. [2]Institute of Experimental Endocrinology and Oncology, National Council of Research (CNR), Naples, Italy. [3]Department of Neurosciences, Reproductive and Odonto-stomatological Sciences, Federico II University of Naples, Naples, Italy.

*Corresponding author:

Prof. Pietro Formisano

Department of Translational Medicine, Federico II University of Naples, Naples, Italy

Via Pansini 5, 80131 Naples, Italy

Tel. +39-0817464450

FAX +39-0817464334

e-mail: fpietro@unina.it

Running head: Platelet factors and Mesechymal stem cells

Keywords: **Growth Factors, Tissue regeneration, Adipose tissue, Cytokines**

Total number of text figures: 4
Total number of tables: 3
Contract grant sponsor: Associazione Italiana per la Ricerca sul Cancro (AIRC), European Foundation for the Study of Diabetes (EFSD), Italian Minisrtry of Education (MIUR)
Contract grant number: AIRC n. IG 12136; EFSD Diabetes and Cancer Programme 2011 #; MIUR – PRIN n.2010MCLBCZ; MIUR - FIRB MERIT n. RBNE08NKH7

ABSTRACT

Adipose tissue-derived mesenchymal stem cells (Ad-MSC) and platelet derivatives have been used alone or in combination to achieve regeneration of injured tissues. We have tested the effect of platelet-rich plasma (PRP) on Ad-MSC and adipocyte function. PRP increased Ad-MSC viability, proliferation rate and G1- S cell cycle progression, by at least 7-, 2-, and 2.2-fold, respectively. Higher PRP concentrations or PRPs derived from individuals with higher platelet counts were more effective in increasing Ad-MSC growth. PRP also accelerated cell migration by at least 1.5-fold. However, PRP did not significantly affect adipocyte differentiation and expression levels of PPAR-γ and AP-2 mRNAs, while it increased leptin production by 3.5-fold. Interestingly, Ad-MSC-derived adipocytes displayed increased viability and cell size following exposure to PRP. PRP treatment of mature adipocytes also enhanced the release of Interleukin (IL)-6, IL-8, IL-10, Interferon-γ and Vascular Endothelial Growth Factor. At variance, Platelet-derived Growth Factor, IL-4 and the chemokine CCL5/RANTES, which were mainly released by platelets, were reduced in the media of PRP-treated adipocytes. Thus, data are consistent with a stimulatory effect of platelet derivatives on Ad-MSC growth and motility. Moreover, PRP sustained adipocyte survival and release of pro-angiogenic factors, which may facilitate tissue regeneration processes.

INTRODUCTION

The use of platelet derivatives represents a novel approach in tissue regeneration (Burnouf et al., 2013). Although the mechanisms involved are still poorly understood, the relative ease and safety of application of platelet products in clinical practice and the potential beneficial outcomes, including regeneration of bone and soft tissues, reduction of bleeding, and acceleration or promotion of wound healing, hold promise for new therapeutic approaches (Burnouf et al., 2013; Lacci and Dardik, 2010; Nikolidakis and Jansen, 2008).

The rationale for the use of platelet products is mostly based on the production and release of multiple growth factors upon platelet activation. Primary factors associated with platelets include Platelet Derived Growth Factor (PDGF) and Transforming Growth Factor β (TGF-β), which have been mostly involved in cell proliferation, chemotaxis and extracellular matrix production/angiogenesis (Burnouf et al., 2013; Lubkowska et al., 2012). Other growth factors discharged from the platelets are Fibroblast Growth Factors (FGF) 1 and 2 and Vascular Endothelial Growth Factor (VEGF) which play critical roles in the hemostasis, proliferative, and remodeling phases of wound healing (Demidova-Rice et al., 2012; Intini, 2009; Lacci and Dardik, 2010; Lubkowska et al., 2012). More than 95% of the pre-synthesized growth factors are secreted within 1 h from the beginning of the clotting process. After the initial burst, the platelets secrete additional growth factors for the remaining 7 days of their life span (Marx RE, 2004). Platelet degranulation also leads to the release of cytokines and chemokines, further contributing to the healing process (Demidova-Rice et al., 2012; Passaretti et al., 2014).

Several technical procedures have been developed to obtain platelet concentrates (Dohan Ehrenfest et al., 2009). Different procedures lead to variable yield of platelets and may contain different cellular components (Cieslik-Bielecka et al., 2012; Prakash and Thakur, 2011). Consistently, they also differ for the qualitative and quantitative release of growth factors, cytokines and chemokines and may find different indications (Galliera et al., 2012; Lubkowskaet al., 2012; Passaretti et al., 2014). Attention has also been given to the clinical utilization of individual growth factors. However, the overall experience has not been satisfactory, most likely since wound healing and tissue repair are outcomes of an intricate network of circulating and tissue elements. Combination of multiple growth factors, timing of their release, and cell-specific response to individual growth factors are indeed essential requirements for a successful wound healing (Giacco et al., 2006).

Auto-transplantation of adipose tissue is commonly used for the treatment of tissue defects in plastic and reconstructive surgery. The reduced survival of the transplanted adipose tissue remains an unsolved issue. This is due, at least in part, to accelerated apoptosis of the implanted pre-adipocytes. Several reports have indicated that application of Platelet-Rich Plasma (PRP) may improve the outcome of adipose tissue transplantation (Cervelli et al., 2009; Fukaya et al., 2012). The molecular mechanisms may possibly involve interactions of PRP factors with either adipocytes and mesenchymal stem cells, which are embedded within adipose tissue (Ad-MSC) (Liuet al., 2008). MSCs are multipotent, non hematopoietic stem cells that are typically obtained from bone marrow but can also be isolated from several other tissues such as umbilical cord and adipose tissue (de Girolamo et al., 2013). Human Ad-MSCs are attractive candidates for clinical use because of their ease of isolation, extensive proliferation and differentiation capacity, and hypoimmunogenic nature. Ad-MSCs display the ability to differentiate into multiple mesoderm-derived cells, such as adipocytes, osteocytes, and chondrocytes, but they may also give rise to cells of nonmesodermal origin, such as hepatocyte-like and neuronal-like cells. The multilineage capacity of Ad-MSC offers the potential to repair, maintain or enhance regeneration of various tissues (Kocaoemeret al., 2007; Phinneyand Prockop, 2007; Schäffler and Büchler, 2007; Tran and Kahn, 2010). However, the poor viability of Ad-MSCs at the transplanted site often decreases their therapeutic potential (Nakamuraet al., 2013). Thus, it is important to improve Ad-MSC survival and enhance their biological functions.

The combined use of PRP and Ad-MSC offers the advantage that they both could be autologous products, prepared from the patient's own tissues, thereby eliminating concerns about immunogenic reactions and disease transmission. Nevertheless, in some cases, preparations from donors could be needed (Everts, 2007; Liuet al., 2008).

Despite the large utilization of platelet derivatives as therapeutic tools in conditions requiring tissue repair, little has been reported about the molecular

mechanisms elicited by PRP on adipose tissue function. In this paper, we have described that PRP affects Ad-MSC growth and migration without interfering with their ability to differentiate into mature adipocytes. Moreover, the exposure to PRP sustains adipocyte viability and increases adipocyte size and production of specific factors, thereby contributing to the induction of tissue repair processes.

MATERIALS AND METHODS

Materials. Media, sera, and antibiotics for cell culture were from Lonza (Lonza Group Ltd, Basel, Switzerland). Antibodies against phospho-Ser_{473}PKB/Akt1, ERK and actin were purchased from Santa Cruz Biotechnology (Santa Cruz Biotechnology, Santa Cruz, CA, USA). Phospho-Thr_{202}/Tyr_{204}ERK, phosphor-Ser15 p53 and p53 antibodies were obtained from Cell Signaling Technology (Danvers, MA, USA). PKB/Akt antibody was from Millipore (Millipore, Billerica, MA, USA). Sodium dodecyl sulfate-polyacrylamide gel electrophoresis (SDS-PAGE) reagents from Bio-Rad (Bio-Rad, Hercules, CA, USA). All the other chemicals were from Sigma-Aldrich (Sigma-Aldrich, St. Louis, MO, USA).

Subject recruitment and Platelet-Rich plasma (*PRP) preparation.* 10 subjects undergoing biliary surgery (M/F:4/6; age 24 – 40) were enrolled in the study. All were non-smokers, non-obese (BMI range: 20.4- 28.3) and with a platelet count >180.000/mm^3. None of them were under any medication for the last 21 days. Informed consent was obtained from every subject before the surgical procedure. This procedure was approved by the ethical committee of the University of Naples.

Blood was drawn from each subject and was collected in a Vacutainer tube (Vacutainer; Becton Dickinson, East Rutherford, NJ, USA) containing 10% trisodium citrate anticoagulant solution for the preparation of Platelet-Rich plasma (PRP). Tubes were centrifuged at 350 g for 15 min. The upper fraction containing platelet-poor plasma (PPP) was discarded and the preparation

procedure for PRP were performed as previously described (Passaretti et al., 2014).

For platelet gel preparations, autologous thrombin (0.1 NIH unit/ml final concentration) and calcium gluconate (10 mg/ml final concentration) were added to PRP for 5 min at room temperature to allow clot formation (Giacco et al., 2006).

Human adipose tissue-derived mesenchymal stem cell culture, growth and viability. Human adipose tissue biopsies were digested with collagenase and Mesenchymal Stem Cells (Ad-MSC) were isolated and differentiated as previously reported (D'Esposito et al., 2012). For growth evaluation, Ad-MSCs were seeded in 6-well culture plates in a complete medium. The following day, the cells were starved in serum-free DMEM (Dulbecco's modified Eagle's Medium) -F12 (1:1) 0.25% BSA for 16 h and incubated with PRP gel, obtained as described above, for different times. Cell count was performed either by Bürker chamber and with the TC10^{TM} Automated Cell Counter (Bio-Rad, Hercules, CA, USA) according to the manufacturer's protocol. Sulforhodamine assay was used for cell viability determination (Chiba et al., 1998); cells were fixed with 10% trichloroacetic acid for at least 2 h at 4 C and then washed 5 times with distilled and de-ionized water. After air drying, sulforhodamine was added to the cells and incubated for 30 min. Cells were then washed with 1% acetic acid 5 times. After air drying, 10 mmol/l Tris solution (pH 7.5) was added to dissolve the bound dye. Cell viability was assessed by optical density (OD) determination at 510 nm using a microplate reader. Three replicate wells were used for each data point.

Cell cycle analysis. Ad-MSCs were seeded in 10 cm^2 culture plates in a complete medium. The following day, the cells were starved in serum-free DMEM F12 (1:1) 0.25% BSA for 16 h and incubated with PRP gel obtained as described above. Bromodeoxyuridine (BrdU)/Propidium Iodide (PI) analysis was performed as previously reported (Ma, Y et al, 2013). Briefly, cells were labeled with 10 μM BrdU for 30 min and fixed over-night in ice-cold 70%

ethanol at -20 C. Cells were then washed once with PBS and incubated for 15 min at room temperature with 2N HCl. Next, cells were washed with PBT (0.5% BSA, 0.1% Tween20 in PBS) and resuspended in PBT containing anti-BrdU antibody (1:40, Dako, Carpinteria CA, USA). After 30 min, cells were washed twice with PBT and then resuspended in PBT containing Alexa488 anti-mouse (1:100, Life Technologies, Carlsbad, CA, USA) in the dark for 30 min. Cells were washed twice with PBS, resuspended in Propidium Iodide (PI) 0.015 M (Sigma-Aldrich) in PBS for 20 min and analyzed for the emission in FL1 and FL3 channels. The samples were acquired by a BD LSRFortessa (BD Biosciences, San Jose, CA, USA) and analyzed using BD FACSDiva Software.

Cell migration. Cell migration was performed using 8-μm pore polycarbonate membranes (Costar, Cambridge, MA, USA). Ad-MSCs were loaded at 50,000 cells per insert (upper chamber) and PRP gel was added to the lower chamber in DMEM F12 (1:1) 0.25% BSA. The cells were allowed to migrate into the lower chamber at 37 C in a 5% CO_2 atmosphere saturated with H_2O for 24 h. At the end of incubation, cells that had migrated to the lower side of the filter were fixed with 11% glutaraldehyde for 15 min at room temperature, washed three times with PBS, and stained with 0.1% crystal violet-20% methanol for 20 min at room temperature. After three PBS washes and complete drying at room temperature, the crystal violet was solubilized by immersing the filters in 10% acetic acid. The concentration of the solubilized crystal violet was evaluated as absorbance at 540 nm.

Adipocyte differentiation markers and real-time RT-PCR analysis. Adipocyte differentiation was assessed by the analysis of real-time RT-PCR of adipocyte-specific (aP2 or PPARγ) mRNAs (see below) and by lipid accumulation using Oil Red O staining, as described by Ramirez-Zacarias et al. (1992). Total RNA was isolated from either undifferentiated Ad-MSC and differentiated adipocytes, after removal of PRP gels, by using the RNeasy Kit (Qiagen, Valencia, CA, USA) according to the manufacturer's instruction. For real-time RT-PCR analysis, 1μg cell RNA was reverse transcribed using SuperScript III

Reverse Transcriptase (Life Technologies, Carlsbad, CA, USA). PCR were analyzed using SYBR Green mix (Bio-Rad, Hercules, CA, USA). Reactions were performed using Platinum SYBR Green Quantitative PCR Super-UDG using an iCycler IQ multicolor Real-Time PCR Detection System (Bio-Rad, Hercules, CA, USA). All reactions were performed in triplicate and β-actin was used as an internal standard. Primer sequences are described in Table 1.

Immunoblot procedure. Total cell lysates were obtained and separated by SDS-PAGE as previously described (Alberobello et al., 2010). Briefly, cells were solubilized for 20 min at 4 C with lysis buffer containing 50 mM HEPES, 150 mM NaCl, 10 mM EDTA, 10 mM $Na_4P_2O_7$, 2 mM sodium orthovanadate, 50 mM NaF, 1 mM phenylmethylsulfonyl fluoride,10 µg/ml aprotinin, 10 µg/ml leupeptin, pH 7.4, and 1% (v/v) Triton X-100. Lysates were clarified by centrifugation at 12,000g for 20 min at 4 C. Proteins were separated by SDS-polyacrylamide gel electrophoresis and blotted on Immobilon-P membranes (Millipore, Billerica, MA, USA). Membranes were blocked for 1 h in TBS (10 mM Tris-HCl, pH 7.4, and 140 mM NaCl) containing 3% (w/v) bovine serum albumin and then incubated with the indicated antibodies. Detection of blotted proteins was performed by ECL according to the manufacturer's instruction. Densitometric analysis was performed using Image Lab software (Bio-Rad, Hercules, CA, USA).

Conditioned media collection. Adipocytes were incubated with PRP gels, obtained as described above, for 24 h. Next, PRP gels were removed and the cells were starved in serum-free DMEM F12 (1:1) 0.25% BSA. As control, PRP gels, without cells, were maintained in serum-free DMEM F12 (1:1) 0.25% BSA. After 24 h media were collected and centrifuged at 14,000g to remove cellular debris and analyzed for cytokines and growth factor content, as described below.

Determination of cytokine and growth factor release. PRP and adipocyte conditioned media were screened for the concentration of IL-2, IL-4, IL-6, IL-8, IL-10, GM-CSF, IFN-γ, MIP-1α, MIP-1β, RANTES, TNF-α, bFGF, PDGF,

VEGF using the Bioplex multiplex Human Cytokine and Growth factor assay kit (Bio-Rad, Hercules, CA, USA) according to the manufacturer's protocol.

Statistical analysis. Data were analyzed with Statview software (Abacus Concepts Piscataway, NJ, USA) by one-factor analysis of variance. *p* values of less than 0.05 were considered statistically significant.

RESULTS

PRP promotes Ad-MSC growth, survival and migration. We have first analyzed the impact of PRP-released factors on human Mesenchymal Stem Cells isolated from stromal-vascular fraction of subcutaneous adipose tissue biopsies (Ad-MSC). PRP was activated with thrombin and applied onto cultured human Ad-MSCs as PRP gel. PRP gels were applied onto cells isolated either from the same donor (autologous PRP; n=5) or from other individuals (homologous PRP; n=5). The application of both autologous and homologous PRP gel to the Ad-MSC cultures was capable to induce cell growth in the absence of serum in a concentration dependent fashion (Fig. 1a). Ad-MSC growth in the presence of 20% PRP was comparable to that achieved with 10% FBS medium (Fig. 1a).

To further investigate whether PRP growth promoting action was dependent on blood platelet count, Ad-MSCs derived from one subject were incubated with PRP gels obtained from grouped subjects according to concentration of blood platelets; those with "low" (200,000 - 300,000/μl) platelet count (n=5) and those with "high" (400,000 - 500,000/μl) platelet count (n=5). Ad-MSC growth was significantly higher upon incubation with the PRP obtained from individuals with a higher concentration of platelets (Fig. 1b).

As assessed by sulforhodamine assay, Ad-MSC viability was strongly increased in presence of 5% or 20% PRP gel, compared to that measured in serum deprivation and was about 3- and 4-fold higher, respectively, compared to cells cultured in 10% FBS (Fig. 1c).

Moreover, BrdU/PI staining revealed that both 5% and 20% PRP gel addition increased the amount of Ad-MSCs in S-phase, compared to cells cultured in serum-free medium without PRP (Fig. 1d). PRP gel reduced the number of cells in G1 phase without affecting G2-M and sub G1 phases (Supplementary Online Table).

To investigate whether PRP could also ameliorate Ad-MSC migration, cells were placed in the upper chamber of a transwell system, while the lower chamber was filled up with PRP-gel in serum-free medium. Cells that migrated across the filter were detected and quantified. 5% and 20% PRP increased Ad-MSC migration by 1.5- and up to 2-fold (Fig.2a-b).

We next tested whether PRP could activate intracellular signaling pathways involved in cell survival and growth. To this aim, Ad-MSC were incubated with PRP gel for 12 h. Western blot analysis with phospho-specific antibodies revealed that 5% and 20% PRP increased PKB/AKT, ERK and p53 phosphorylation compared to the control untreated cells (Fig. 2c).

PRP does not interfere with Ad-MSC adipogenic differentiation, survival and function. Ad-MSCs readily differentiate into cells of the adipocyte lineage and retain differentiation potential through multiple passages (Schäfflerand Büchler, 2007). In order to evaluate whether PRP treatment may interfere with adipocyte differentiation, Ad-MSC were incubated with PRP along with the induction of the differentiation procedure as described in Materials and Methods. Adipogenesis was assessed by analysis of lipid accumulation using oil red O staining (Fig. 3a) and by the expression of adipocyte-specific genes (aP2 and Peroxisome Proliferator-Activated Receptor γ –PPARγ) (Fig. 3b). Ad-MSC differentiation in presence of 20%PRP was comparable to that observed for cells differentiated with the standard procedures (Fig. 3a and b), with a slight increase of cell size.

In addition, we have tested the effect of PRP on mature adipocytes. Sulforhodamine assay revealed that 20% PRP gels lightly increased adipocyte

viability (Fig. 3c). Interestingly, leptin expression was 3-fold higher in differentiated adipocytes exposed to PRP (Fig. 3d).

Release of cytokines/chemokines and growth factors by human adipocytes upon PRP stimulation. As previously reported, PRP released a variety of cytokines/chemokines and growth factors (Passaretti, F. et al., 2014). Here, we have shown that PRP secreted IL-4, IL-8, CCL5/RANTES and PDGF in a concentration dependent fashion (Table 2). IL-6 and INF-γ were found only in conditioned media from 20% PRP. No statistically significant differences were observed for the amount of VEGF between 5% PRP and 20% PRP medium (Table 2). We have therefore investigated whether PRP may affect the ability of human adipocytes to release cytokines/chemokines and growth factors. As expected, several inflammatory cytokines and growth factors were detected in the medium of untreated adipocytes. Interestingly, the amount of IL-6, IL-8, IL-10, IFN-γ and VEGF was significantly increased in PRP-treated adipocytes. However, while the increase of IFN-γ and VEGF levels was consistent with an additive release by PRP and adipocytes separately, the increase of IL-6, IL-8 and IL-10 was likely due to the PRP stimulation of release by adipocytes. Moreover, the concentrations of IL-4, PDGF and CCL5/RANTES were significantly reduced in PRP-treated adipocyte medium, compared to PRP alone, suggesting a consumption of those platelet-released factors by the adipocytes (Fig. 4).

DISCUSSION

Platelet derivatives are widely used in regenerative medicine (Burnouf et al, 2013; Lacci and Dardik, 2010; Nikolidakis and Jansen, 2008). For instance, the simultaneous application of fat explants and PRP has hold a great deal of promise to ameliorate “lipofilling” procedures and the outcome of fat engraftment (Kølle et al., 2013; Nakamura et al., 2010). Indeed, one of the main limitations of adipose tissue transfer is the rapid loss of fat at the site of

engraftment (Nakamura et al., 2010). This is possibly due to several factors: i) very low capability of adipose tissue to engraft and to repopulate at the site of implantation; ii) reduced life span of terminally differentiated mature adipocytes; iii) reduced blood supply mainly due to insufficient tissue-driven angiogenesis.

Here, we have tested the effect of PRP-released factors on Ad-MSCs and on mature adipocytes in cultured models. PRP-released factors had an incremental effect on Ad-MSCs, since they improved cell viability, induced S-phase and increased cell number. This is consistent with previous reports indicating a positive effect of PRP on growth of mesenchymal stem cell, either from adipose tissue (Kocaoemer et al., 2007) and from bone marrow (Murphy et al., 2012), as well as of other cultured cell types (Gassling et al., 2009; Giacco et al., 2006; Kakudo et al., 2008; Lucarelli et al., 2003; Passaretti et al., 2014). The molecular mechanisms responsible for increased cell growth likely involve PKB/Akt and ERK (Fig. 2) activation by platelet released growth factors and the potential regulation of apoptosis-related genes, such as p53 (Fig. 2), as also recently described (Fukaya et al., 2012).

Growth effect on Ad-MSC is not limited to the exposure to autologous PRP, but is also elicited by PRPs obtained from different donors. Moreover, Ad-MSC growth is elicited at higher levels by PRP preparations from donors with higher platelet count. Thus, as also previously suggested (Lucarelli et al., 2003), the concentration of platelet factors may be crucial in inducing cell proliferation. Indeed, Murphy and coworkers (2012) have recently described that PRP obtained by umbilical cord (uc-PRP) is more potent than that obtained by peripheral blood in inducing BM-MSC growth. This is possibly due to the release of higher concentrations of specific growth factors by uc-PRP. Nevertheless, growth effect is most likely cell-specific, since different types of platelet preparations release different amount of growth factors and cytokines/chemokines (Passaretti et al., 2014).

We have now provided further evidence that PRP can exert a chemo-attractant action on Ad-MSCs. Increased motility could also be driven by PKB/Akt activation (Bulj et al., 2013). Other mechanisms however could not be excluded. One might argue that PRP increases cellularity at the site of implant, both by inducing proliferation and recruiting more Ad-MSC. The higher amount of precursor cells may then lead to increased tissue formation, thereby contributing to improve the outcome of fat transplantation. Furthermore, our data provided, at the best of our knowledge, the first evidence that PRP increased viability of mature adipocytes, whose improved survival might be beneficial for the stability of fat tissue, reducing fat loss at the site of engraftment.

Thus, PRP treatment of adipose tissue may facilitate the recruitment of Ad-MSCs and induce their proliferation, and may increase, as well, the survival of mature adipocytes. The combination of these effects supports the hypothesis of a beneficial action of PRP products in adipose tissue regeneration and filling procedures.

Based on morphological data and on expression of specific markers, PRP-treated Ad-MSCs retain their ability to differentiate into adipocytes, as well as into osteogenic lineage (data not shown; Tavakolinejad et al., 2014), at least in cultured models. These data suggested that the adipose tissue obtained in the presence of platelet factors preserved its architecture and its functional features. Slightly higher cell size and lipid content were observed for PRP-treated adipocytes. Interestingly, however, we also detected an increase of leptin in PRP-treated differentiated adipocytes and increased levels of VEGF, IL-6, IL-8, IL-10 and IFN-γ in the conditioned media. In particular, the increase of IL-6, IL-8 and IL-10 levels are more than additive and likely results from PRP stimulation of adipocyte release. On the other end, PDGF, IL-4 and CCL5/RANTES, which are robustly produced by platelets, were reduced in the medium of PRP-treated adipocytes. Thus, it could be hypothesized that PRP-released factors (i.e. PDGF) are taken and consumed by adipocytes, which in

turn release more pro-angiogenic factors (i.e. VEGF and IL-6), thereby facilitating new vessel formation and further contributing to the stabilization of the transplanted fat. Alternatively, a bi-directional cross talk could be envisioned, by which adipocytes enhance degradation or inhibit production of platelet factors, although the latter appears as a less likely possibility.

Platelet secretome analysis has released a very large amount of proteins, which may independently ad coordinately act on processes involved in wound healing and tissue repair (Demidova-Rice et al., 2012; Intini, 2009; Lacci and Dardik, 2010; Lubkowska et al., 2012). Different procedures of platelet preparations may vary in the abundance of growth factors and cytokines (Horn et al., 2010; Passaretti et al., 2014), and this may be taken into account for the variability of the outcomes of platelet-based therapies (Prakash and Thakur, 2011). The use of individual factors, such as PDGF for example, has proven largely unsuccessful (Park et al., 2014). More recently, peptides derived from human PRP have been isolated and tested for promoting cutaneous wound healing in animal models (Demidova-Rice et al., 2012).

We have now provided evidence that PRP may elicit chemo-attractant and proliferative effects on Ad-MSC, as well as survival effect on mature adipocytes. PRP-treated adipocytes may then become more potent in secreting pro-angiogenic factors, including leptin and VEGF, and ameliorate the outcome of autologous fat implants. More studies are needed to elucidate the individual factors involved in the intricate cross-talk among cell types responsible for wound healing and tissue regeneration.

ACKNOWLEDGEMENTS

Vittoria D'Esposito and Federica Passaretti equally contributed to this work. The authors are grateful to Dr. C. Passaro for technical help with cytofluorimetric assays and to Dr. D. Liguoro for technical help and advice on cell cultures. The authors also wish to thank Prof. G. Molea for the valuable help with adipose tissue specimens. This study was supported in part by:

Associazione Italiana per la Ricerca sul Cancro - AIRC (IG 12136), European Foundation for the Study of Diabetes (EFSD Diabetes and Cancer Programme 2011), MIUR - PRIN (prot.2010MCLBCZ), MIUR - FIRB MERIT (RBNE08NKH7), P.O.R. Campania FSE 2007-2013, Project CREMe. All authors have no conflict of interest.

LITERATURE CITED

Alberobello AT, D'Esposito V, Marasco D, Doti N, Ruvo M, Bianco R, Tortora G, Esposito I, Fiory F, Miele C, Beguinot F, Formisano P. 2010. Selective disruption of insulin-like growth factor-1 (IGF-1) signaling via phosphoinositide-dependent kinase-1 prevents the protective effect of IGF-1 on human cancer cell death. J BiolChem 285:6563-6572.

Bulj Z, Duchi S, Bevilacqua A, Gherardi A, Dozza B, Piccinini F, Adalgisa Mariani G, Lucarelli E, Giannini S, Donati D, Marmiroli S. 2013. Protein kinase B/AKT isoform 2 drives migration of human mesenchymal stem cells. Int J Oncol 42:118-126.

Burnouf T, Goubran HA, Chen TM, Ou KL, El-Ekiaby M, Radosevic M. 2013. Blood-derived biomaterials and platelet growth factors in regenerative medicine. Blood Rev 27:77-89.

Cervelli V, Gentile P, Scioli MG, Grimaldi M, Casciani CU, Spagnoli LG, Orlandi A. 2009. Application of platelet-rich plasma in plastic surgery: clinical and in vitro evaluation. Tissue Eng. Part C Methods. 15:625-634.

Chiba K, Kawakami K, Tohyama K. 1998. Simultaneous evaluation of cell viability by neutral red, MTT and crystal violet staining assays of the same cells. Toxicol Vitro 12:251-258.

Cieslik-Bielecka A, Choukroun J, Odin G, DohanEhrenfest DM. 2012. L-PRP/L-PRF in esthetic plastic surgery, regenerative medicine of the skin and chronic wounds. CurrPharmBiotechnol 13:1266-1277.

D'Esposito V, Passaretti F, Hammarstedt A, Liguoro D, Terracciano D, Molea G, Canta L, Miele C, Smith U, Beguinot F, Formisano P. 2012. Adipocyte-released insulin-like growth factor-1 is regulated by glucose and fatty acids and controls breast cancer cell growth in vitro. Diabetologia 55:2811-2822.

de Girolamo L, Lucarelli E, Alessandri G, Avanzini MA, Bernardo ME, Biagi E, Brini AT, D'Amico G, Fagioli F, Ferrero I, Locatelli F, Maccario R, Marazzi M, Parolini O, Pessina A, and Torre ML. 2013. Mesenchymal stem/stromal cells: a new "cells as drugs" paradigm. Efficacy and critical aspects in cell therapy. Curr Pharm Des. 19:2459-2473.

Demidova-Rice TN, Wolf L, Deckenback J, Hamblin MR, Herman IM. 2012. Human platelet-rich plasma- and extracellular matrix-derived peptides promote impaired cutaneous wound healing in vivo. PLoS One 7:e32146.

DohanEhrenfest DM, Rasmusson L, Albrektsson T. 2009. Classification of platelet concentrates: from pure platelet-rich plasma (P-PRP) to leucocyte- and platelet-rich fibrin (L-PRF). Trends Biotechnol 27:158-167.

Everts PA, Overdevest EP, Jakimowicz JJ, Oosterbos CJ, Schönberger JP, Knape JT, van Zundert A. 2007. The use of autologous platelet-leukocyte gels to enhance the healing process in surgery, a review. SurgEndosc. 21:2063-2068.

Fukaya Y, Kuroda M, Aoyagi Y, Asada S, Kubota Y, Okamoto Y, Nakayama T, Saito Y, Satoh K, Bujo H. 2012. Platelet-rich plasma inhibits the apoptosis of highly adipogenic homogeneous preadipocytes in an in vitro culture system. ExpMol Med 44:330-339.

Galliera E, Corsi MM, Banfi G. 2012. Platelet rich plasma therapy: inflammatory molecules involved in tissue healing. J BiolRegulHomeost Agents. 26:35S-42S.

Gassling VL, Açil Y, Springer IN, Hubert N, Wiltfang J. 2009. Platelet-rich

plasma and platelet-rich fibrin in human cell culture. OralSurgOralMedOralPatholOralRadiolEndod 108:48-55.

Giacco F, Perruolo G, D'Agostino E, Fratellanza G, Perna E, Misso S, Saldalamacchia G, Oriente F, Fiory F, Miele C, Formisano S, Beguinot F, Formisano P. 2006. Thrombin-activated platelets induce proliferation of human skin fibroblasts by stimulating autocrine production of insulin-like growth factor-1. FASEB J 20:2402-2404.

Horn P, Bokermann G, Cholewa D, Bork S, Walenda T, Koch C, Drescher W, Hutschenreuther G, Zenke M, Ho AD, Wagner W. 2010. Impact of individual platelet lysates on isolation and growth of human mesenchymal stromal cells. Cytotherapy 12:888-898.

Intini G. 2009. The use of platelet-rich plasma in bone reconstruction therapy. Biomaterials 30:4956-4966.

Kakudo N, Minakata T, Mitsui T, Kushida S, Notodihardjo FZ, Kusumoto K. 2008. Proliferation-promoting effect of platelet-rich plasma on human adipose-derived stem cells and human dermal fibroblasts. PlastReconstrSurg 122:1352-1360.

Kocaoemer A, Kern S, Klüter H, Bieback K. 2007. Human AB serum and thrombin-activated platelet-rich plasma are suitable alternatives to fetal calf serum for the expansion of mesenchymal stem cells from adipose tissue. Stem Cells 25:1270-1278.

Kølle SF, Fischer-Nielsen A, Mathiasen AB, Elberg JJ, Oliveri RS, Glovinski PV, Kastrup J, Kirchhoff M, Rasmussen BS, Talman ML, Thomsen C, Dickmeiss E, Drzewiecki KT. 2013. Enrichment of autologous fat grafts with ex-vivo expanded adipose tissue-derived stem cells for graft survival: a randomised placebo-controlled trial. Lancet 382:1113-1120.

Lacci KM, Dardik A. 2010. Platelet-rich plasma: support for its use in wound healing. Yale J Biol Med 83:1-9.

Liu Y, Zhou Y, Feng H, Ma GE, Ni Y. 2008. Injectable tissue-engineered bone composed of human adipose-derived stromal cells and platelet-rich

plasma. Biomaterials. 29:3338-3345.

Lubkowska A, Dolegowska B, Banfi G. 2012. Growth factor content in PRP and their applicability in medicine. J BiolRegulHomeost Agents 26:3S-22S.

Lucarelli E, Beccheroni A, Donati D, Sangiorgi L, Cenacchi A, Del Vento AM, Meotti C, Bertoja AZ, Giardino R, Fornasari PM, Mercuri M, Picci P. 2003. Platelet-derived growth factors enhance proliferation of human stromal stem cells. Biomaterials 24:3095-3100.

Ma Y, Li A, Faller WJ, Libertini S, Fiorito F, Gillespie DA, Sansom OJ, Yamashiro S, MacheskyLM. 2013. Fascin 1 is transiently expressed in mouse melanoblasts during development and promotes migration and proliferation. Development 140:2203-2211.

Marx RE. 2004. Platelet-rich plasma: evidence to support its use. J Oral Maxillofac. Surg 62:489-496.

Murphy MB, Blashki D, Buchanan RM, Yazdi IK, Ferrari M, Simmons PJ, Tasciotti E. 2012. Adult and umbilical cord blood-derived platelet-rich plasma for mesenchymal stem cell proliferation, chemotaxis, and cryo-preservation. Biomaterials 33:5308-5316.

Nakamura S, Ishihara M, Takikawa M, Murakami K, Kishimoto S, Nakamura S, Yanagibayashi S, Kubo S, Yamamoto N, Kiyosawa T. 2010. Platelet-rich plasma (PRP) promotes survival of fat-grafts in rats. Ann PlastSurg 65:101-106.

Nakamura Y, Ishikawa H, Kawai K, Tabata Y, Suzuki S. 2013. Enhanced wound healing bytopical administration of mesenchymal stem cells transfected with stromal cell-derived factor-1. Biomaterials 34:9393-9400.

Nikolidakis D, Jansen JA. 2008. The biology of platelet-rich plasma and its application in oral surgery: literature review. TissueEng Part B Rev 14:249-258.

Park SA, Raghunathan VK, Shah NM, Teixeira L, Motta MJ, Covert J,

Dubielzig R, Schurr M, Isseroff RR, Abbott NL, McAnulty J, Murphy CJ. 2014. PDGF-BB does not accelerate healing in diabetic mice with splinted skin wounds. PLoS One. Aug 14;9(8):e104447. doi: 10.1371/journal.pone.0104447. eCollection 2014.

Passaretti F, Tia M, D'Esposito V, De Pascale M, Del Corso M, Sepulveres R, Liguoro D, Valentino R, Beguinot F, Formisano P, Sammartino G. 2014. Growth-promoting action and growth factor release by different platelet derivatives. Platelets25:252-256.

Phinney DG, Prockop DJ. 2007. Concise review: mesenchymal stem/multipotent stromal cells: the state of transdifferentiation and modes of tissue repair-current views. Stem Cells 25:2896-2902.

Prakash S, Thakur A. 2011. Platelet concentrates: past, present and future. J Maxillofac Oral Surg. 10:45-49.

Ramírez-Zacarías JL, Castro-Muñozledo F, Kuri-Harcuch W. 1992. Quantitation of adipose conversion and triglycerides by staining intracytoplasmic lipids with Oil red O. Histochemistry 97:493-497.

Schäffler A, Büchler C. 2007. Concise review: adipose tissue-derived stromal cells--basic and clinical implications for novel cell-based therapies. Stem Cells 25:818-827.

Tavakolinejad S, Khosravi M, Mashkani B, EbrahimzadehBideskan A, SanjarMossavi N, Parizadeh MR, HamidiAlamdari D. 2014. The effect of human platelet-rich plasma on adipose-derived stem cell proliferation and osteogenic differentiation. Iran Biomed J 18:151-7.

Tran TT, Kahn CR. 2010. Transplantation of adipose tissue and stem cells: role in metabolism and disease. Nat Rev Endocrinol 6:195-213.

FIGURE LEGENDS

Figure 1. **Effect of PRP on Ad-MSC growth, survival and cell cycle.** a) Ad-MSCs isolated by adipose tissue biopsy (n=5) have been serum-starved for 18 h and then incubated for 24 h with PRP gel (5% or 20% vol/vol in DMEM F12 1:1) obtained from the same donor of adipose tissue (homologous PRP; n=5) or from other donors (autologous PRP; n=5). As a control, Ad-MSCs have been incubated with DMEM F12 (1:1) without serum supplementation (MEDIUM BSA) or with 10% fetal bovine serum (MEDIUM 10% FBS). Then, cells have been counted as described in Materials and Methods and the results have been reported as fold-increase over basal (cell count in MEDIUM BSA). * denote statistically significant values over basal (* $p<0.05$; ** $p<0.01$).# denote statistically significant differences of 20% autPRP vs 5% autPRP (# $p<0.05$)).§ denote statistically significant differences of 20% homPRP vs 5% homPRP (§ $p<0.05$). b) PRP gel (20% vol/vol in DMEM F12 1:1) obtained from donors with different hematic platelet counts (Low Platelet – LP:2-3 x 10^5 platelets per µl; High Platelet – HP:4-5 x 10^5 platelets perµl) were directly applied onto the culture plate containing serum-starved Ad-MSCs for 6, 12, 24 and 48h. As control, Ad-MSCs have been incubated with DMEM F12 (1:1) without serum supplementation (MEDIUM BSA) or with 10% fetal bovine serum (MEDIUM 10% FBS). Then, cells have been counted as described in Materials and Methods and the results have been reported as fold-increase over basal (cell count in MEDIUM BSA). * denote statistically significant values over basal (* $p<0.05$; ** $p<0.01$). # denote statistically significant differences of HP-PRP vs LP- PRP (# $p<0.05$). c) PRP gel (5% or 20% vol/vol in DMEM F12 1:1) has been added to serum-starved Ad-MSCs for 48 h. Cell viability has been assessed by sulforhodamine assay as described in Materials and Methods and the results reported as percentage of viable cells compared to cells in DMEM F12 10% FBS, considered as 100% viable cells.* denote statistically significant values over basal, considered as cells kept in 10% FBS medium

(*** p<0.001). # denote statistically significant differences of 20% PRP vs 5% PRP (# p <0.05).d) PRP gel (5% or 20% vol/vol in DMEM F12 1:1) has been added to serum-starved Ad-MSCs for 48 h. Cells have been pulse-labeled with BrdU for 30 min. FACS analysis of samples stained for BrdU and for propidium iodide, to quantify the amount of DNA, was performed. Numbers represent the percentage of BrdU positive cells ± SD.* denote statistically significant values over DMEM-BSA (* p<0.05). # denote statistically significant differences of 20% PRP vs 5% PRP (# p <0.05).

Figure 2. **Effect of PRP on Ad-MSC migration and intracellular pathway activation.** Ad-MSCs have been serum-starved for 18 h and then seeded on the polycarbonate membrane in the upper compartment of the transwell, whereas PRP gel (5% and 20% vol/vol in DMEM F12 1:1) has been added to the lower compartment in presence of DMEM F12 (1:1) without serum supplementation. As control, DMEM F12 (1:1) without serum supplementation (MEDIUM BSA) or with 10% fetal bovine serum (MEDIUM 10% FBS) has been added to the lower compartment. Migratory cells on the bottom of the polycarbonate membrane were stained (a) and quantified at OD 540 nm after extraction (b). Asterisks denote statistically significant values over basal (** p<0.01; *** p<0.001). c) Ad-MSCs were exposed to PRP (5% and 20% vol/vol in DMEM F12 1:1) for 24 h and then solubilized as described in Materials and Methods. Cell lysates (50 μg protein/sample) were blotted with phospho- Ser_{473}PKB/Akt, phospho-Thr_{202}/Tyr_{204}ERK and phospho-Ser15 p53 antibodies and then reblotted with anti-PKB/Akt, anti-ERK and anti p53 antibodies. To ensure the equal protein transfer, membranes were blotted with actin antibodies. The filters were revealed by ECL and autoradiography. The autoradiographs shown are representative of four independent experiments.

Figure 3. **Effect of PRP on adipocyte differentiation, viability and function.** Ad-MSCs have been differentiated in adipocytes as described in Materials and Methods, in presence or absence of PRP gel (20% vol/vol in DMEM F12 1:1). a) Lipid accumulation has been observed by Oil Red O staining

microscopically. mRNA levels of PPARγ, AP2 (b) and Leptin (d) were determined by real-time RT-PCR analysis on RNA preparations obtained from adipocytes after complete removal of PRP gels. Data have been normalized on β-actin as internal standard. Bars show the mRNA levels in these cells relative to those in Ad-MSCs differentiated without 20% PRP gel addition. c) Adipocyte viability has been assessed by sulforhodamine assay and the results reported as percentage of viable cells compared to cells differentiated without 20% PRP gel addition, considered as 100% viable cells.

Figure 5. **Effect of PRP on adipocyte-released cytokines and growth factors.** Human adipocytes have been incubated with PRP gel (20% vol/vol in DMEM F12 1:1) for 24 h. Media have been collected (CM) and tested by using the Bioplex multiplex Human Cytokine and Growth factor assay kit. Values ± SD are reported in the bar graph. Asterisks denote statistically significant values (* $p<0.05$; ** $p<0.01$; *** $p<0.001$).

.

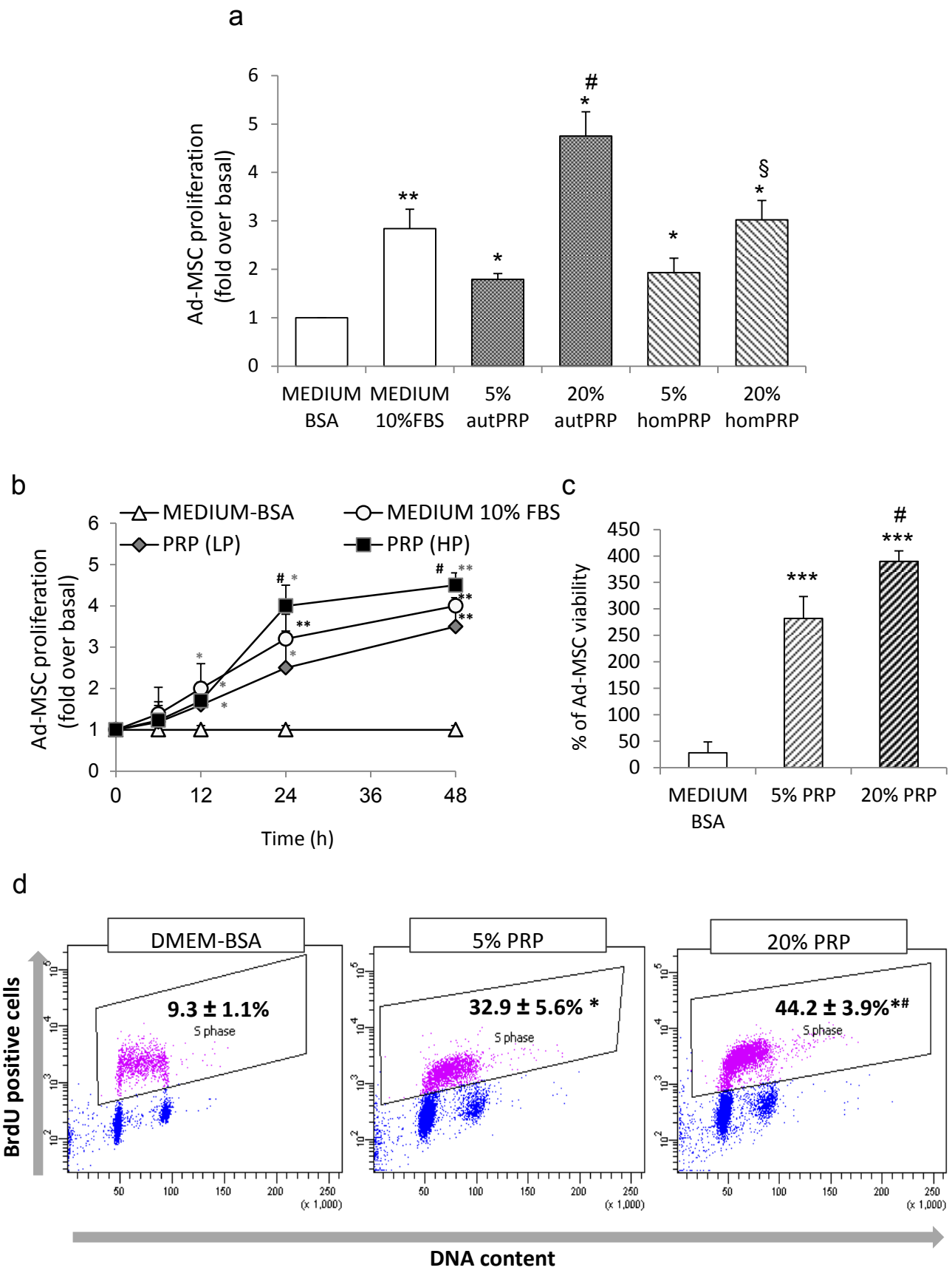
a
Ad-MSC proliferation (fold over basal)
MEDIUM BSA
MEDIUM 10%FBS
5% autPRP
20% autPRP
5% homPRP
20% homPRP
b
MEDIUM-BSA
MEDIUM 10% FBS
PRP (LP)
PRP (HP)
Ad-MSC proliferation (fold over basal)
Time (h)
c
% of Ad-MSC viability
MEDIUM BSA
5% PRP
20% PRP
d
DMEM-BSA
5% PRP
20% PRP
9.3 ± 1.1%
32.9 ± 5.6% *
44.2 ± 3.9%*#
S phase
BrdU positive cells
DNA content
(x 1,000)

Fig. 1

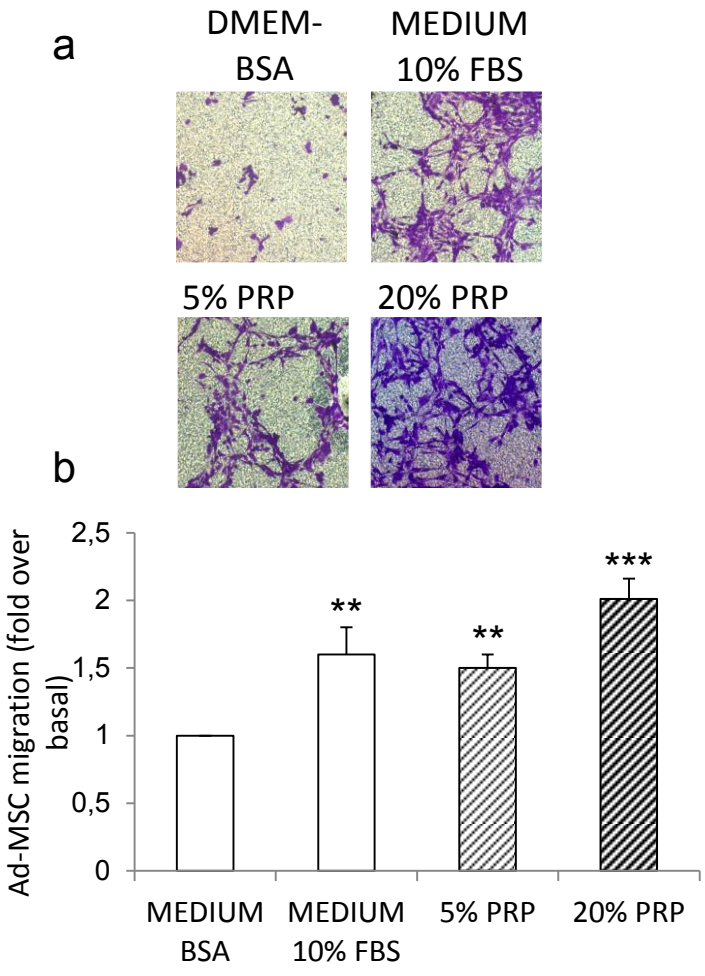
a
DMEM-
BSA
MEDIUM
10% FBS
5% PRP
20% PRP
b
Ad-MSC migration (fold over basal)
2,5
2
1,5
1
0,5
0
**
**
***
MEDIUM
BSA
MEDIUM
10% FBS
5% PRP
20% PRP

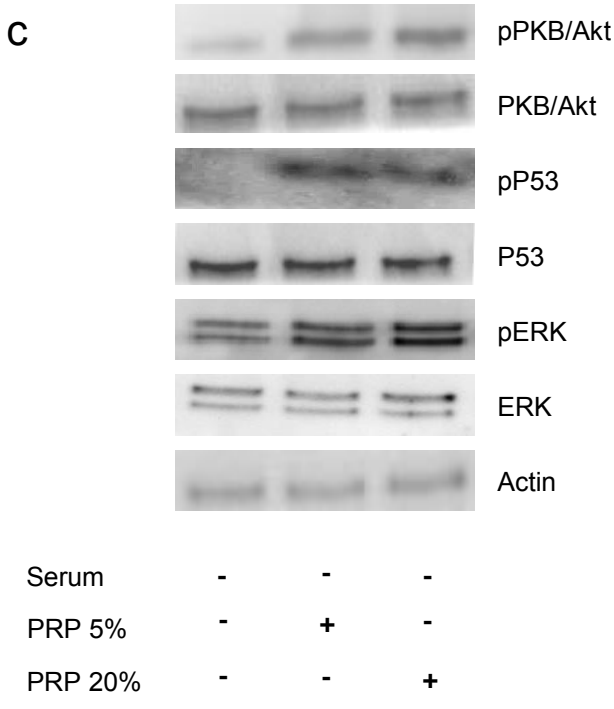
c
pPKB/Akt
PKB/Akt
pP53
P53
pERK
ERK
Actin
Serum - - -
PRP 5% - + -
PRP 20% - - +

Fig. 2

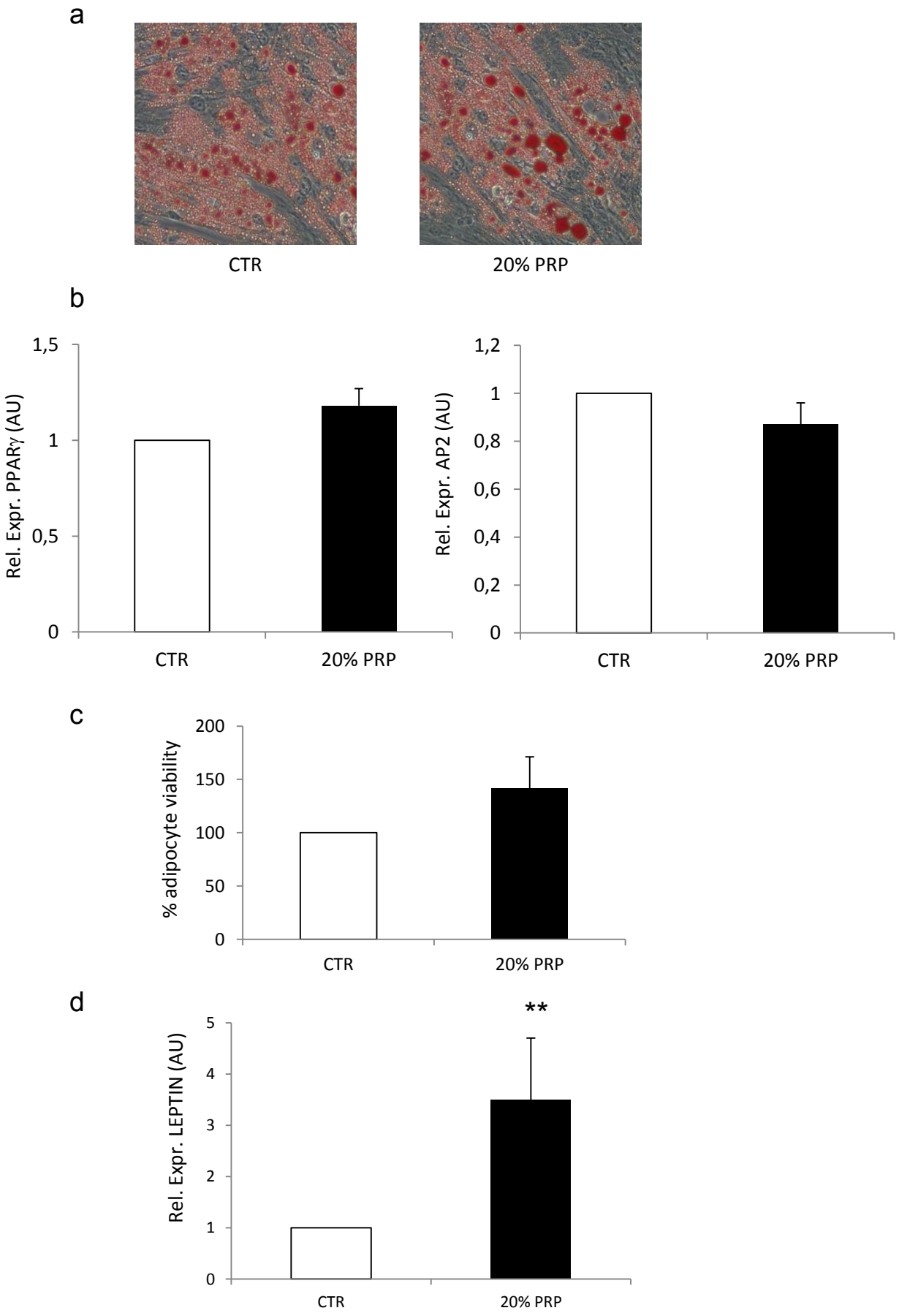
a
CTR
20% PRP
b
Rel. Expr. PPARγ (AU)
1,5
1
0,5
0
CTR
20% PRP
Rel. Expr. AP2 (AU)
1,2
1
0,8
0,6
0,4
0,2
0
CTR
20% PRP
c
% adipocyte viability
200
150
100
50
0
CTR
20% PRP
d
Rel. Expr. LEPTIN (AU)
**
5
4
3
2
1
0
CTR
20% PRP

Fig. 3

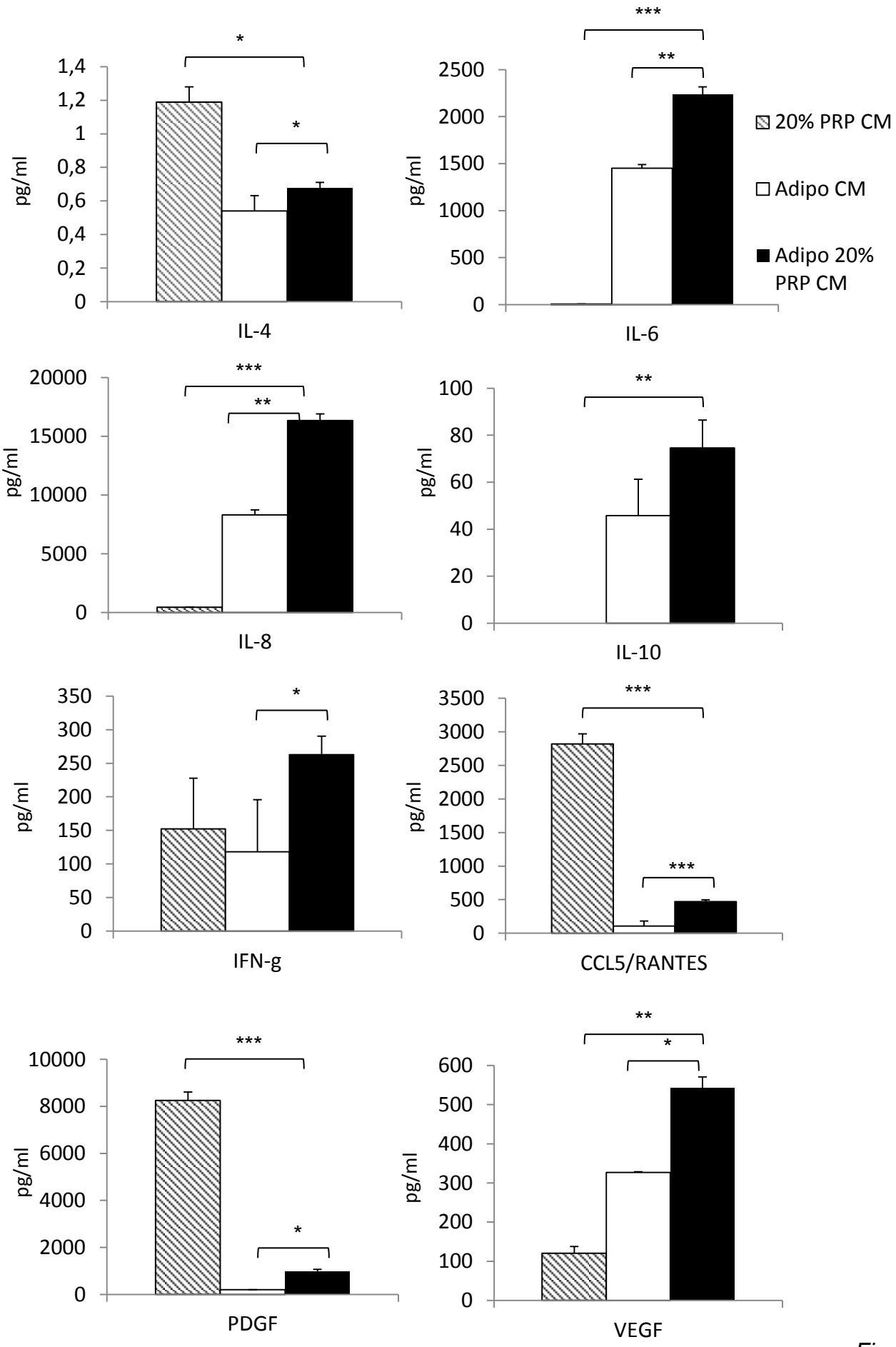
20% PRP CM
Adipo CM
Adipo 20% PRP CM
pg/ml
IL-4
IL-6
IL-8
IL-10
IFN-g
CCL5/RANTES
PDGF
VEGF

Fig. 4

Alginate-hyaluronan composite hydrogels accelerating wound healing process

O. Catanzano[1], V. D'Esposito[2], S. Acierno[3], C. De Caro[1], C. Avagliano[1], M.R. Ambrosio[2], P. Russo[4], R. Russo[1], A. Miro[1], F. Ungaro[1], A Calignano[1], P. Formisano[2], F. Quaglia[1*]

[1] Department of Pharmacy, University of Naples Federico II, Naples, Italy. [2] Department of Translational Medical Sciences, University of Naples Federico II, Napoli, Italy [3] Department of Engineering, University of Sannio, Benevento, Italy [4] Institute for Polymers, Composites and Biomaterials, National Research Council, Pozzuoli (NA), Italy

*Corresponding author:
Prof. Fabiana Quaglia
Department of Pharmacy, University of Naples Federico II, Naples, Italy
Tel/fax +39 81 678707
e-mail: Quaglia@unina.it

ABSTRACT

In this paper we propose polysaccharide hydrogels combining alginate (ALG) and hyaluronan sodium (HA) as biofunctional platform for dermal wound repair. Hydrogel produced by internal gelation were homogeneous and easy to handle. Rheological evaluation of gelation kinetics of ALG/HA mixtures at different ratios allowed understanding the HA effect on ALG gelation. Disk-shaped hydrogels, at different ALG/HA ratio, were characterised for morphology, homogeneity and mechanical properties. The *in vitro* activity of ALG/HA dressings were tested on adipose derived multipotent adult stem cells (Ad-MSC) and an immortalized keratinocyte cell line (HaCaT). Hydrogels did not interfere with cell viability in both cells lines, but significantly promoted wound closure at early (24 h) and later (5 days) stages as compared to hydrogels made of ALG alone. *In vivo* wound healing studies, conducted on rat dorsal wounds, indicated that after 5 days hydrogels could significantly accelerate wound healing process also in vivo. Overall results demonstrate that integration of HA in a physically cross-linked alginate hydrogels can be a versatile strategy to promote wound healing process that can be easily translated in a clinical setting.

INTRODUCTION

Wound repair is one of the most complex biological processes during witch various intracellular and intercellular pathways are activated to restore tissue integrity and homeostasis (Gurtner, Werner, Barrandon & Longaker, 2008). Dressings have been applied to open wounds for centuries to prevent further injury and bacteria invasion, but nowadays their design has evolved toward multifunctionality to better control potential infections and to aid healing process (Queen, Orsted, Sanada & Sussman, 2004). A key property of modern dressings is their ability to retain and create a moist environment around the wound to facilitate healing and at this purpose a number of new materials have been developed and tested. Amid modern dressings, hydrogels cover a large

area due to their well-recognized compatibility (Boateng, Matthews, Stevens & Eccleston, 2008) and the capacity to absorb the exuding liquids and debris from the wound area. Furthermore above their glass transition temperature, hydrogels are typically soft and elastic due to their thermodynamic compatibility with water (Peppas, Huang, Torres-Lugo, Ward & Zhang, 2000; Slaughter, Khurshid, Fisher, Khademhosseini & Peppas, 2009). Hydrogels have shown excellent potential in a variety of biomedical applications, including scaffolds for tissue engineering or carriers for drug delivery systems (Lee & Mooney, 2012). Alginates (ALGs), a whole family of water-soluble polysaccharides extracted from brown seaweed, are linear blocks copolymers composed of α-l-guluronate (GGGGGG), β-d-mannuronate (MMMMMM), or alternating M and G residues (GMGMGM) linked through (1,4) bonds. The proportional and sequential arrangements of the M and G residues depend upon the type of algae tissue from which the polysaccharide is extracted, as well as on the season in which the algae is collected (Tonnesen & Karlsen, 2002). Due to its biocompatibility and bioresorption properties, ALG has been widely used in regenerative medicine (Slaughter, Khurshid, Fisher, Khademhosseini & Peppas, 2009) and successfully applied to treat a wide variety of secreting lesions. The high water absorption limits wound secretions and minimizes bacterial contamination (Gilchrist & Martin, 1983). Furthermore, ALG dressings maintain a physiologically moist microenvironment that promotes healing and formation of granulation tissue. ALGs can be rinsed away from wound bed with saline irrigation, so that removal of the dressing does not interfere with healing granulation tissue and making dressing changes virtually painless. Another important aspect of ALG dressing is related to management of wound exudate, allowing significant limitation of maceration phenomena at wound periphery. ALG dressings can be designed to absorb large volumes of exudate, whilst continuing to provide a moist wound environment. ALG-based absorbent wound dressing may be used on multiple wound types, including but

not limited to diabetic wounds, venous wounds, pressure ulcers, cavity wounds, and some bleeding wounds.

Ionically cross-linked ALG hydrogels can be formed in the presence of several divalent cations such as Ca^{2+}, Ba^{2+}, Sr^{2+}, Zn^{2+}, Cu^{2+}, Cd^{2+}, and Co^{2+} (Morch, Donati, Strand & Skjak-Braek, 2006). Divalent cations allow ionic interactions between G-rich regions of adjacent polymer chains resulting in the formation of a bulk structure in a shape of an 'egg-box' (Grant, Morris, Rees, Smith & Thom, 1973). As the sequence patterns and lengths of ALG blocks heavily depend on the biological source, alginate hydrogels may possess a wide range of gel properties, such as final modulus and crosslinking kinetics.

Control over material properties of a hydrogel is crucial for many biomedical applications. Covalent crosslinking is an elective way to stabilize three dimensional polymer networks for a variety of applications and has also been used in hydrogel formation with permanent 3-D structures. However, chemical crosslinking reagents can show severe toxicity resulting in limited application in the biomedical field. Soluble calcium salts are widely employed to cross-link ALGs, but these methods typically lead to rapid and inadequately controlled gelation, resulting in the formation of hydrogels with scarce structural homogeneity and poor mechanical properties (Kuo & Ma, 2001) (Skjakbraek, Grasdalen & Smidsrod, 1989). To overcome this drawback, internal gelation of ALG through $CaCO_3$-GDL (D-glucono-δ-lactone) system has been proposed to obtain homogenous hydrogels useful as scaffolding materials for wound healing applications. The kinetics of the ALG gelation process has been studied extensively (Draget, Ostgaard & Smidsrod, 1989, 1990; Draget, Simensen, Onsoyen & Smidsrod, 1993), and the final properties of the hydrogels have proved to be affected by the M/G ratio, alginate concentration, and particle size of the calcium salts.

Hyaluronan sodium (HA) is a nonsulfated, linear glycosaminoglycan (GAG), consisting of repeating units of (β, 1–4) glucuronic acid and (β, 1-3)-N-acetyl glucosamine. HA is present in most living tissues as a high molecular mass

polymer (> 100 kDa) and in large amounts in the skin (dermis and epidermis), brain and central nervous system (Toole, 2004). Beyond the physical properties of a structural ECM molecule, it has become increasingly clear that HA provides cellular cues to regulate inflammation and tissue repair (Petrey & de la Motte, 2014). Several studies have shown that exogenous HA exerts beneficial effects on the wound-healing process (Frenkel, 2014). Topically applied HA has been shown to accelerate skin wound healing in rats (Foschi et al., 1990) and hamsters (King, Hickerson & Proctor, 1991). HA and its fragments may play crucial roles in the skin wound-healing process by modulating the expression of fibroblast genes involved in remodeling and repair of extracellular matrix (David-Raoudi et al., 2008). Furthermore, HA may also play a role in the control of angiogenesis during tissue repair (West, Hampson, Arnold & Kumar, 1985), and has been proposed that HA may protect granulation tissue from the deleterious effects of oxygen free radical by its ability to scavenge reactive oxygen species (ROS) (Trabucchi et al., 2002).

In the present study, we develop an ALG/HA hydrogel with enhanced wound healing activity potentially useful as platform for wound dressing. Internal gelation technique was used for cross-linking ALG/HA solutions at different HA ratio, and the resulting disk-shaped hydrogels were fully characterized. The gelation dynamics were monitored through rheological measurements to evaluate the influence of HA on the cross-linking process. Biocompatibility and wound healing potential of ALG/HA were evaluated on different cell lines. Human adipose-derived Mesenchymal Stem Cells (AdMSCs), a multipotent non hematopoietic stem cell line was selected due to its overwhelming interest in cell therapy and tissue engineering (Kocaoemer, Kern, Kluter & Bieback, 2007). Then, the effect on a human keratinocytes cell line HaCaT, a well-known systems modeling very closely the repairing process during re-epithelialization (Singer & Clark, 1999) (Gurtner, Werner, Barrandon & Longaker, 2008). In vivo wound healing activity of the most promising formulation has been evaluated in a rat model.

MATERIALS AND METHODS

Materials. Sodium alginate (ALG) (viscosity 360cps) was purchased from Farmalabor (Italy). Analysis-grade ethanol was purchased from Carlo Erba (Italy). Hyaluronic acid (HA) sodium salt from Streptococcus equi (1.5-1.8 * 10^6 Da), calcium carbonate, calcium chloride dihydrate ($CaCl_2$ * $2H_2O$), sodium chloride (NaCl), potassium chloride (KCl), sodium phosphate dibasic (Na_2HPO_4), D-glucono-δ-lactone (GDL) and all reagents used for sulforhodamine assay were obtained from Sigma-Aldrich (St. Louis, MO). Media, sera, and antibiotics for cell cultures were from Lonza (Lonza Group Ltd, Basel, Switzerland). Distilled water was used throughout this study.

ALG/HA hydrogel preparation. Structurally homogeneous ALG hydrogels were prepared according the Kuo and Ma method (Kuo & Ma, 2001). Briefly, ALG (1% w/v) was dissolved in deionized water and mixed with 30 mM calcium carbonate to form a suspension. A fresh aqueous 64 mM GDL solution was then added to the suspension and vortex-mixed to initiate gelation. A calcium carbonate to GDL molar ratio of 0.5 was maintained to achieve a neutral pH post-crosslinking. HA was dissolved directly in the alginate solution to obtain a 10% (ALG/HA10) and a 20% (ALG/HA20) w/w concentration. Solutions were cast in 96-well culture plate (50 µl, well size: 5 mm diameter, 20 mm height) or in 24-well culture plate (1 ml, well size: 15 mm diameter, 20 mm height) to form circular disk 2 mm in thickness and 5 mm in diameter and 5 mm in thickness and 15 mm in diameter, respectively. The well plate were capped, sealed with Parafilm®, and gelled on a level surface at room temperature for 24 h. After gelation the ALG disk were washed with water and stored at 4°C.

Hydrogel characterization. Homogeneity of the cylindrical ALG gels was evaluated from dry to wet weight ratios. Gels were cut perpendicular to the cylinder axis into 4 slices with approximately the same thickness. The slices were labeled 1-4 from top to bottom. After measuring their wet weights, the slices were dried at 45° C for 48 h. The specimens were weighed again and

their dry/wet weight ratio calculated. Gelation time and viscoelastic properties of gels were measured using a strain-controlled rotational rheometer (ARES, Rheometric Scientific Inc. USA) equipped with a dual-range force rebalance transducer (2KFRT). Measurements were performed using 25 mm parallel plates geometry and maintaining the samples at 22 °C. Cross-linking degree of the ALG hydrogels was evaluated by soaking the hydrogel gel disc in 15 mL of a 1, 3 or 5 mM calcium chloride solution to vary calcium ion concentrations. The swelling experiments were carried out at 37° C by keeping the samples in a thermostatic bath under gentle shaking. The medium was changed every day. At scheduled times, the specimens were retrieved and hydrogel surface was quickly blotted twice on a filter paper. The specimens were weighed on an analytical balance. The initial wet weight (W_0) was obtained after 24 h gelation. Wet weight (W) during immersion experiment was recorded at designated times. The swelling ratio was defined as W/W_0.

In vitro studies. Mesenchymal Stem Cells (Ad-MSCs) were isolated from human adipose tissue biopsies as previously described (D'Esposito et al., 2012). Cells were cultured at 37°C with Dulbecco's modified Eagle's medium (DMEM) and Ham's F12 (1:1) with 10% Fetal Bovine Serum (FBS), 2 mM glutamine, 100 IU/ml penicillin, and 100 IU/ml streptomycin. Cultures were maintained in humidified atmosphere of 95% air and 5% CO_2 at 37 °C. Immortalized keratinocyte cell line HaCaT (CRL2309) was obtained from American Type Culture Collection (Manassas, VA, USA). HaCaT were cultured in DMEM containing 10% FBS, penicillin/streptomycin (10.000 U/ml), L-glutamine (2 mM) and placed in a humidified incubator under of 95% air and 5% CO_2 at 37° C. Cells were passaged at confluence using a solution of 0.5% trypsin and 0.2% EDTA.

Evaluation of In vitro toxicity of hydrogels on Ad-MSCs. Ad-MSC viability was assessed using 24-transwell culture system 0.4-μm pore polycarbonate membranes (Costar, Cambridge, MA). Cells were loaded at 50,000 cells per insert in the lower chamber. The following day, the hydrogels were added to

the upper chamber in complete medium. Upon 24 h, sulforhodamine assay was used to determinate their viability (Chiba, Kawakami & Tohyama, 1998). Briefly, the upper chamber was removed and the cells were fixed with 50% trichloroacetic acid for at least 2 h at 4 °C. Then, cells were washed 5 times with distilled and de-ionized water. After air-drying, cells were stained for 30 min with 0.4% sulforhodamine dissolved in 1% acetic acid. Unbound dye was removed by five washes with 1% acetic acid. After air-drying, 10 mM Tris solution (pH 7.5) was added to dissolve the protein-bound dye. Cell survival was assessed by optical density (OD) determination at 510 nm using a microplate reader.

Cell motility - Wound healing Assay. For in vitro wound healing assay, HaCaT cells (50.000 cells/well) were seeded into 12-well plates in DMEM supplemented with 10% FBS and allowed to adhere for 24 h. Ad-MSCs were seeded into six-well microplates and grown in the same complete medium to a confluent monolayer. The monolayer was then carefully scratched with a sterile pipette tip, washed twice with sterile phosphate buffer saline (PBS) and incubated at 37 °C with a medium containing 1% FBS with or without the hydrogels. Reference points near the "scratch" were marked to guarantee the same area of image acquisition. Images of wound gap were taken at 0, 1 day and 5 days by a DFC295 camera (Leica) coupled to the microscope and the percentage of closure was calculated with NIH IMAGE J.

In vivo wound healing studies. A full-thickness excision wound model was used to monitor wound closure. Male Wistar albino rats weighing 300-350 g (Harlan, Italy) were housed singly to prevent fighting and attack on the wounds in Plexiglas cage for one week at temperature of 22 ± 1° C, with alternate cycle of 12 h of light and 12 h of dark. All animals received food and water ad libitum throughout the experimental period. All manipulations were performed using aseptic techniques. This study was carried out in strict accordance with the Institutional Guidelines and complied with the Italian D.L. no.116 of January 27, 1992 of Ministero della Salute and associated guidelines in the

European Communities Council Directive of November 24, 1986 (86/609/ECC). All the animals were anesthetized with ketamine hydrochloride (100 mg/kg body weight) and xylazine (5 mg/Kg) by intraperitoneal administration, and the dorsal hair was shaved using a shaving machine. The dorsal region was chosen to avoid animal access to their own wound and animals were housed one per box to prevent cross-access to the lesions. The surgical area was disinfected with Betadine R 10%. A full-thickness wound with a diameter of 2.5 cm was excised from the back of the rats using sterile scissors at the depth of loose subcutaneous tissues and the wounds were left open. Hemostasis was obtained by direct pressure using sterile gauze. Before hydrogel application the wound was moistened with 300 μL of saline. Animals (n=3) were divided into four groups and wounds were treated with a single application of hydrogels (ALG, ALG/HA20). Wound site was finally closed with Tegaderm^{TM} (3M, USA) to prevent the rats from removing the hydrogel. For wound closure study, changes in wound area were measured on day 1 and 5 and wound contraction was calculated according to equation:

$$\% \text{ Wound contraction} = \frac{A_0 - A_t}{A_0} X\ 100$$

Where A_0 is the initial wound area and A_t is the open area of wound at day 1 and 5 after biopsy.

RESULTS AND DISCUSSION

Internal gelation of ALG and ALG/HA hydrogels. Control over material properties of a hydrogel is crucial for many biomedical applications. Covalent crosslinking is an elective way to stabilize three dimensional polymer networks for a variety of applications and has also been used in hydrogel formation with permanent 3-D structures. However, chemical crosslinking reagents can show severe toxicity resulting in limited application in the biomedical field. As an alternative method, electrostatic cross-linking is a versatile and simple strategy to produce hydrogels for biomedical applications. In this case, the chemical

composition of ALG can greatly influence hydrogel properties. Indeed, the affinity of certain ions with the G units, the M/G ratio and the number of repeated sequential G and M units strongly affect the gelation process and, in turn, hydrogel physical structure (strength and porosity). Furthermore, it has been shown that ALG with a high G content have a high in vivo stability (Kong, Alsberg, Kaigler, Lee & Mooney, 2004), whereas ALGs with high M content were reported to show greater biocompatibility and recommended as suitable biomaterials for implants (Orive, Ponce, Hernandez, Gascon, Igartua & Pedraz, 2002). Although, M/G ratio of the raw ALG employed in this study was 1.54, a value corresponding reasonably well with those previously reported for ALG produced by Macrocystis pyrifera (Moe S.T., 1995), we tried to produce ALG/HA hydrogels with suitable mechanical properties through an internal gelation technique where the release of calcium ions directly in the ALG solution occurs (Draget, Ostgaard & Smidsrod, 1990).

As a first step of the study, we tried to evaluate if addition of HA could modify gelation properties of Alg. Indeed, Gelation time is an important variable in hydrogel formulation previous studies have shown that a fast gelation time can lead to a poorly homogeneous gel structure (Kuo & Ma, 2001). To determine the liquid-to-solid transition point (i.e., the so called “critical gel” state) samples were subjected to a continuous series of frequency sweeps (in the range 0.03–100 rad/s) and the gel time was determined as the instant where G’ and G’’ are parallel to each other or equivalently where the loss phase angle is frequency independent (Chambon & Winter, 1987). The time-evolution of viscoelastic moduli for the ALG/HA20 system is reported in Figure 1A. Other systems show similar behaviors and corresponding data are not shown. For times shorter than 3 minutes, the sample shows a liquid-like behavior with a viscous modulus (G’’) higher than the elastic component (G’) and a strong dependency upon frequency. At 7 minutes, the sample shows a critical gel behavior with G’ and G’’ parallel to one another and a power-law dynamics. At this condition the material behaves not as a liquid (as it has an infinite shear

viscosity) and not yet as a solid (as it has a null equilibrium modulus). At longer times (see for instance the curves referring to 21 minutes in Figure 2), the material shows a solid-like behavior with elastic modulus higher than viscous modulus and a less pronounced dependency upon frequency. Gelation time (left y-axis) and initial viscosity of the solutions (right y-axis) were plotted as a function of HA content (Figure 1B) where both data-sets show a monotonic increasing behavior. The gelation process is controlled by the mobility of G-blocks (of ALG chains) and calcium ions that interact to from cross-links and give rise to an "egg box" structure. In this view it is expected that an increase of the viscosity of the initial solution would result in a decreased mobility and, consequently, in a longer gelation time. These previsions are in line with the experimental data collected.

At the end of the gelation process, the resulting hydrogels have elastic shear moduli (G') of the order of a few kPa, viscous shear moduli (G'') about one order of magnitude smaller, and a weak frequency dependency. Furthermore, while viscoelastic properties of initial solution and of critical gels do strongly depend upon HA content (with higher contents corresponding to more elastic systems), after the gelation has completed all the systems have similar behavior and similar moduli. Compressive tests performed in quasi-static conditions confirm these observations (data not shown) with all samples showing similar (strain-hardening) behavior and stress at 10% deformation ranging between 200 and 300 Pa.

Uniform and transparent ALG hydrogels were easily obtained at calcium carbonate/GDL molar ratio of 2 (Figure 2), which guarantees also that pH of the final hydrogel is close to neutrality (Draget, Ostgaard & Smidsrod, 1989). One of the aims of this study was to formulate compact hydrogels able to remain intact after gelation and with sufficient strength to be easily placed on the wound bed during the dressing change. The investigated hydrogels showed sufficient strength to be handled, cut with scissors or packed without difficulties making them suitable as wound dressing.

Hydrogel homogeneity. Amid the large number of factors that can influence ALG gelation time (Alexander, Murphy, Gallagher, Farrell & Taggart, 2012), concentration of calcium carbonate in the polymer solution is of utmost importance since it controls availability of calcium ions for crosslinking. On the other hand, calcium carbonate is dispersed in polymer medium and can progressively accumulate at the bottom of recipient giving non-homogeneous cross-linking. It is worth of note that structural uniformity is crucial for biomedical applications not only from a drug delivery point of view to achieve uniform distribution of the drug in the matrix, but especially to get good material properties. To evaluate the homogeneity of hydrogels made with $CaCO_3$-GDL, cylindrical gels with varying compositions were prepared, sliced along the vertical axis and dry/wet ratio evaluated. Comparable homogeneity profiles of ALG gels at different HA concentrations indicated that the presence of HA did not affect gel homogeneity in the concentration range studied (Figure 3).

Cross-linking degree. The swelling behavior of ALG hydrogels is a function of crosslink density, ALG concentration and ALG chemical composition (Kuo & Ma, 2008). In particular, structural integrity and mechanical properties are highly dependent on crosslinking of G-blocks, that in presence of calcium ions form more highly ordered regions (Smidsrod & Skjak-Braek, 1990). During the internal gelation, calcium ions are released directly inside the ALG solution and, for this reason, their diffusion in the solution is essential to control cross-linking degree and in turn swelling. To determine whether hydrogels composition affected cross-linking degree, the effects of calcium chloride addition on equilibrium swelling (7 days) of different hydrogels were investigated (Figure 4). It was found that independently of the presence of HA all hydrogel gave a similar swelling behavior with a shrinking that directly depended from the calcium concentration in the medium. The W/W_0 ratio was similar for all the formulation suggesting that the presence of HA had a minimum influence on the crosslinking degree.

Biological evaluation of ALG and ALG/HA hydrogels. In order to evaluate the in vitro toxicity of hydrogels, Ad-MSCs previously isolated from subcutaneous adipose tissue biopsies (D'Esposito et al., 2012) were used. Indeed, in vitro predictive toxicological assays based on human stem cells and their derivatives offer significant vantages over animal models largely due to improved relevance and greater versatility. The use of human stem cell systems might dramatically increase the ability to predict toxic responses in humans while decreasing the need for extensive toxicity tests in animals (Liu, Deng, Liu, Gong & Deng, 2013). Ad-MSCs viability was investigated using a transwell system. The upper chamber was filled up with the hydrogels, while the lower chamber was loaded with a cell suspension in DMEM F12 (1:1) 10% FBS. Sulforhodamine assay revealed that Ad-MSC viability in the presence of ALG and ALG/HA hydrogels was comparable to that achieved in complete medium (Figure 5) indicating that hydrogels do not interfere with cell viability. Next, to investigate whether ALG and ALG/HA hydrogels could affect cell motility a wound healing assay was performed. On the basis of toxicity data, ALG/HA20 with the highest HA concentration was selected for further experiments. Ad-MSCs were scratched and incubated with ALG and ALG/HA20 hydrogels in medium without serum supplementation (DMEM F12 -0.25% BSA). Images were taken at 0 and 24 h after wounding. As shown in figure 6, serum induced an almost complete wound closure. Even in absence of serum, ALG and ALG/HA hydrogels significantly promoted wound closure as compared to serum-free medium. Results demonstrated that ALG/HA hydrogels do not impair Ad-MSC viability suggesting that combination of ALG and HA does not represent a toxic environment for Ad-MSCs. Interestingly, however, we observed an improvement of wound healing, which is most likely due to increased cell motility, rather than cell proliferation.

The same experiment was replicated using confluent monolayers of HaCaT allowing to extend the temporal window of wound closure assessment. In analogy to Ad-MSC, hydrogels did not interfere with HaCaT cell viability

(data not shown). Confluent monolayers of HaCaT were scratched and incubated with ALG and ALG/HA hydrogels in medium with 1% FBS. Images were taken at 0 h, 24 h (day 1) and 120 h (day 5) after wounding. As shown in figure 7, ALG and ALG/HA20 hydrogels significantly promoted wound closure at 24 h as compared to medium with 1% FBS. This effect was more significant at 120 h (day 5) and it is most likely due to increased cell motility, since the experiments were carried out with low serum concentrations, in order to reduce cell proliferation. These data support the hypothesis that ALG/HA hydrogels could potentiate regeneration of wounded tissues by stimulation of Ad-MSC and HaCaT motility and may be useful for tissue engineering procedures.

The wound healing effect of hydrogels was evaluated also *in vivo* using the full excision wound model in rats. ALG and ALG/HA hydrogels were applied on rat backs and the capacity of hydrogels to heal the wound was evaluated. As reported in figure 8, ALG/HA20 hydrogel induced a significant reduction of wound extension after 1 and 5 days from to application ($p<0.05$ and $p<0.01$, respectively) whereas, no evident effect was detectable using ALG alone.

CONCLUSIONS

Hydrogels based on ALG and HA, a polysaccharide with a crucial role in wound healing process, have been successfully produced and characterized. The internal gelation method allowed production of hydrogels with good handling characteristics and suitable mechanical properties as wound dressing. Although the presence of HA affected alginate gelation time, its limited influence on the overall properties of hydrogels was found. In vitro experiments on different cell lines highlighted that HA incorporation into ALG hydrogels promoted *in vitro* wound closure without affecting cell viability. Finally, a significant reduction of wound area in a excision wound model in rats at 1 day and more significantly at 5 days after skin application was found for a HA content of 20%. Taken together, these results demonstrate that

integration of HA in a physically cross-linked alginate matrix can be a simple and valid strategy to promote wound healing process and to translate in a clinical setting. Furthermore, these systems can be useful as potential platform for the release of drugs directly in the wound site avoiding systemic administration.

ACKNOWLEDGEMENTS

The authors wish to thank Prof. Alfonso Carotenuto and Dr. Antonio Limatola for NMR analysis of alginate. The financial support of Italian Ministry of University and Research (PRIN 2010H834LS) is gratefully acknowledged.

REFERENCES

Alexander, B. R., Murphy, K. E., Gallagher, J., Farrell, G. F., & Taggart, G. (2012). Gelation time, homogeneity, and rupture testing of alginate-calcium carbonate-hydrogen peroxide gels for use as wound dressings. *J Biomed Mater Res B Appl Biomater, 100*(2), 425-431.

Boateng, J. S., Matthews, K. H., Stevens, H. N., & Eccleston, G. M. (2008). Wound healing dressings and drug delivery systems: a review. *J Pharm Sci, 97*(8), 2892-2923.

Chambon, F., & Winter, H. H. (1987). Linear Viscoelasticity at the Gel Point of a Cross-Linking Pdms with Imbalanced Stoichiometry. *Journal of Rheology, 31*(8), 683-697.

Chiba, K., Kawakami, K., & Tohyama, K. (1998). Simultaneous evaluation of cell viability by neutral red, MTT and crystal violet staining assays of the same cells. *Toxicol In Vitro, 12*(3), 251-258.

D'Esposito, V., Passaretti, F., Hammarstedt, A., Liguoro, D., Terracciano, D., Molea, G., Canta, L., Miele, C., Smith, U., Beguinot, F., & Formisano, P. (2012). Adipocyte-released insulin-like growth factor-1 is regulated by glucose and fatty acids and controls breast cancer cell growth in vitro. *Diabetologia, 55*(10), 2811-2822.

David-Raoudi, M., Tranchepain, F., Deschrevel, B., Vincent, J. C., Bogdanowicz, P., Boumediene, K., & Pujol, J. P. (2008). Differential effects of hyaluronan and its fragments on fibroblasts: relation to wound healing. *Wound Repair Regen, 16*(2), 274-287.

Draget, K. I., Ostgaard, K., & Smidsrod, O. (1989). Alginate-Based Solid Media for Plant-Tissue Culture. *Applied Microbiology and Biotechnology, 31*(1), 79-83.

Draget, K. I., Ostgaard, K., & Smidsrod, O. (1990). Homogeneous Alginate Gels - a Technical Approach. *Carbohydrate Polymers, 14*(2), 159-178.

Draget, K. I., Simensen, M. K., Onsoyen, E., & Smidsrod, O. (1993). Gel Strength of Ca-Limited Alginate Gels Made in-Situ. *Hydrobiologia, 261*, 563-569.

Foschi, D., Castoldi, L., Radaelli, E., Abelli, P., Calderini, G., Rastrelli, A., Mariscotti, C., Marazzi, M., & Trabucchi, E. (1990). Hyaluronic acid prevents oxygen free-radical damage to granulation tissue: a study in rats. *Int J Tissue React, 12*(6), 333-339.

Frenkel, J. S. (2014). The role of hyaluronan in wound healing. *Int Wound J, 11*(2), 159-163.

Gilchrist, T., & Martin, A. M. (1983). Wound treatment with Sorbsan--an alginate fibre dressing. *Biomaterials, 4*(4), 317-320.

Grant, G. T., Morris, E. R., Rees, D. A., Smith, P. J. C., & Thom, D. (1973). Biological Interactions between Polysaccharides and Divalent Cations - Egg-Box Model. *Febs Letters, 32*(1), 195-198.

Gurtner, G. C., Werner, S., Barrandon, Y., & Longaker, M. T. (2008). Wound repair and regeneration. *Nature, 453*(7193), 314-321.

King, S. R., Hickerson, W. L., & Proctor, K. G. (1991). Beneficial actions of exogenous hyaluronic acid on wound healing. *Surgery, 109*(1), 76-84.

Kocaoemer, A., Kern, S., Kluter, H., & Bieback, K. (2007). Human AB serum and thrombin-activated platelet-rich plasma are suitable alternatives to fetal calf serum for the expansion of mesenchymal stem cells from adipose tissue. *Stem Cells, 25*(5), 1270-1278.

Kong, H. J., Alsberg, E., Kaigler, D., Lee, K. Y., & Mooney, D. J. (2004). Controlling Degradation of Hydrogels via the Size of Cross-Linked Junctions. *Adv Mater, 16*(21), 1917-1921.

Kuo, C. K., & Ma, P. X. (2001). Ionically crosslinked alginate hydrogels as scaffolds for tissue engineering: part 1. Structure, gelation rate and mechanical properties. *Biomaterials, 22*(6), 511-521.

Kuo, C. K., & Ma, P. X. (2008). Maintaining dimensions and mechanical properties of ionically crosslinked alginate hydrogel scaffolds in vitro. *Journal of Biomedical Materials Research Part A, 84A*(4), 899-907.

Lee, K. Y., & Mooney, D. J. (2012). Alginate: properties and biomedical applications. *Prog Polym Sci, 37*(1), 106-126.

Liu, W., Deng, Y., Liu, Y., Gong, W., & Deng, W. (2013). Stem cell models for drug discovery and toxicology studies. *J Biochem Mol Toxicol, 27*(1), 17-27.

Moe S.T., D. K. I., Skjåk-Bræk G., & Smidsrød O. . (1995). Alginate. *Food Polysaccharides and Their Applications*. New York: Dekker.

Morch, Y. A., Donati, I., Strand, B. L., & Skjak-Braek, G. (2006). Effect of Ca2+, Ba2+, and Sr2+ on alginate microbeads. *Biomacromolecules, 7*(5), 1471-1480.

Orive, G., Ponce, S., Hernandez, R. M., Gascon, A. R., Igartua, M., & Pedraz, J. L. (2002). Biocompatibility of microcapsules for cell immobilization elaborated with different type of alginates. *Biomaterials, 23*(18), 3825-3831.

Peppas, N. A., Huang, Y., Torres-Lugo, M., Ward, J. H., & Zhang, J. (2000). Physicochemical foundations and structural design of hydrogels in medicine and biology. *Annu Rev Biomed Eng, 2*, 9-29.

Petrey, A. C., & de la Motte, C. A. (2014). Hyaluronan, a crucial regulator of inflammation. *Front Immunol, 5*, 101.

Queen, D., Orsted, H., Sanada, H., & Sussman, G. (2004). A dressing history. *Int Wound J, 1*(1), 59-77.

Singer, A. J., & Clark, R. A. (1999). Cutaneous wound healing. *N Engl J Med, 341*(10), 738-746.

Skjakbraek, G., Grasdalen, H., & Smidsrod, O. (1989). Inhomogeneous Polysaccharide Ionic Gels. *Carbohydrate Polymers, 10*(1), 31-54.

Slaughter, B. V., Khurshid, S. S., Fisher, O. Z., Khademhosseini, A., & Peppas, N. A. (2009). Hydrogels in regenerative medicine. *Adv Mater, 21*(32-33), 3307-3329.

Smidsrod, O., & Skjak-Braek, G. (1990). Alginate as immobilization matrix for cells. *Trends Biotechnol, 8*(3), 71-78.

Tonnesen, H. H., & Karlsen, J. (2002). Alginate in drug delivery systems. *Drug Dev Ind Pharm, 28*(6), 621-630.

Toole, B. P. (2004). Hyaluronan: From extracellular glue to pericellular cue. *Nature Reviews Cancer, 4*(7), 528-539.

Trabucchi, E., Pallotta, S., Morini, M., Corsi, F., Franceschini, R., Casiraghi, A., Pravettoni, A., Foschi, D., & Minghetti, P. (2002). Low molecular weight hyaluronic acid prevents oxygen free radical damage to granulation tissue during wound healing. *Int J Tissue React, 24*(2), 65-71.

West, D. C., Hampson, I. N., Arnold, F., & Kumar, S. (1985). Angiogenesis Induced by Degradation Products of Hyaluronic-Acid. *Science, 228*(4705), 1324-1326.

FIGURE LEGENDS

Figure 1. **Rheological characterization of gelation process.** A) Viscoelastic moduli as a function of frequency for ALG/HA20 at different times after beginning of internal gelation process. B) Gelation time and initial viscosity of ALG/HA solutions at different HA concentration.

Figure 2. **ALG hydrogel obtained by internal gelation.**

Figure 3. **Dry/wet weight ratios of ALG hydrogel slices with varying ALG/HA concentrations** numbered 1-4, from top to bottom.

Figure 4. **Equilibrium swelling of ALG hydrogels** immersed for 7 days in medium containing different concentration of calcium chloride.

Figure 5. **Effect of ALG and ALG/HA hydrogels on Ad-MSCs viability.** ALG or ALG/HA hydrogels (ALG/HA10 - ALG/HA20) have been added in the upper chamber of the transwell in DMEM F12 (1:1) 10% FBS. Upon 24 hours, cell viability has been determined. The results have been reported as percentage of viable cells compared with cells incubated in DMEM F12 (1:1) 10% FBS in the absence of hydrogels (considered as 100% viable cells). Bars represent the mean ± SD of triplicate determination in three independent experiments.

Figure 6. **Effect of ALG and ALG/HA hydrogels on Ad-MSCs motility.** Confluent monolayers of Ad-MSCs have been subjected to scratch assays, washed twice with PBS and incubated at 37°C in presence of ALG or ALG/HA (ALG/HA20%) hydrogels in DMEM F12 (1:1) 0.25% BSA. Images of wound gap have been taken at 0 and 24 h by a digital camera coupled to the microscope and percentage of closure was calculated with NIH IMAGE J. The results are reported as percentage of wound distance at 24 h compared with the time 0. Bars represent the mean ± SD of triplicate determination in three independent experiments. Statistically significant differences respect to cells in DMEM F12 (1:1) 0.25% BSA (*$p < 0.05$; **$p < 0.01$; ***$p < 0.001$).

Figure 7. **Effect of ALG and ALG/HA20 hydrogels on HaCaT motility.** Confluent monolayers of HaCaT have been subjected to scratch assays, washed twice with PBS and incubated at 37°C in presence of ALG or ALG/HA20 hydrogels in DMEM with 1% FBS. Images of wound gap have been taken at 0 and 24 h and 120 h by a digital camera coupled to the microscope and percentage of closure was calculated with IMAGE J. The results have been reported as percentage of wound distance at 24 h (day 1) and 120 h (day 5)

compared with the starting point (time 0). Data are shown as mean ± SEM of triplicate determination in three independent experiments. *** $P<0.001$, and * $P<0.05$ vs. DMEM with 1% FBS; ### $P<0.001$ vs. ALG.

Figure 8. **Effects of ALG hydrogels on wound healing process in a rat wound model.** A full-thickness wound was excised from the back of the rats (n=3) using sterile scissors and the wounds were left open. Wounds were treated with hydrogels (ALG, ALG/HA20) and closed with TegadermTM. wound contraction on day 1 and 5. *$P<0.05$; **$P<0.001$ vs ALG hydrogel.

A

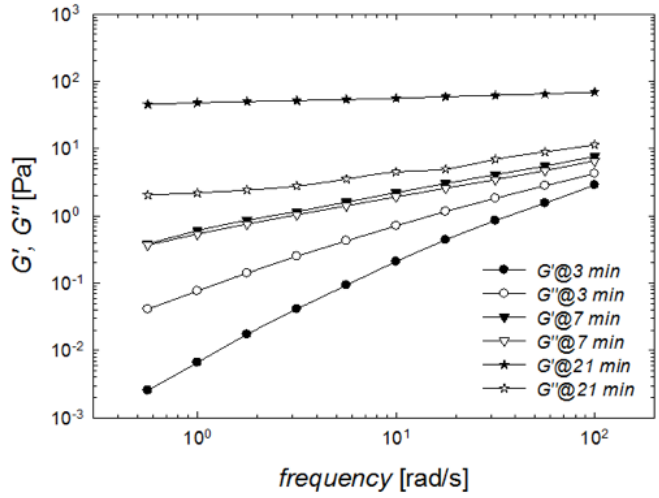
G', G'' [Pa]
frequency [rad/s]
G'@3 min
G''@3 min
G'@7 min
G''@7 min
G'@21 min
G''@21 min

B

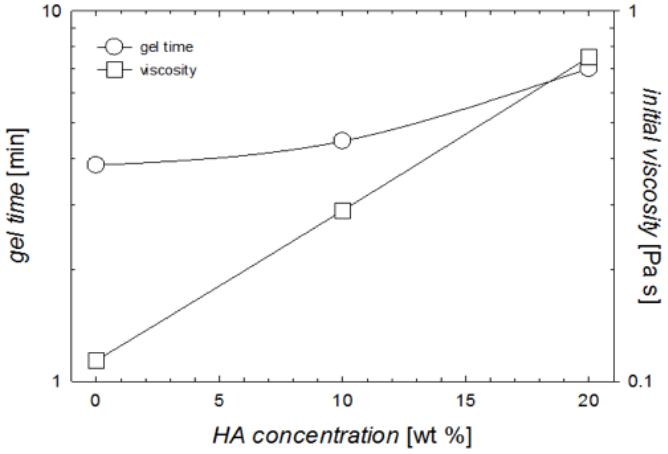
gel time
viscosity
gel time [min]
initial viscosity [Pa s]
HA concentration [wt %]

Fig.1

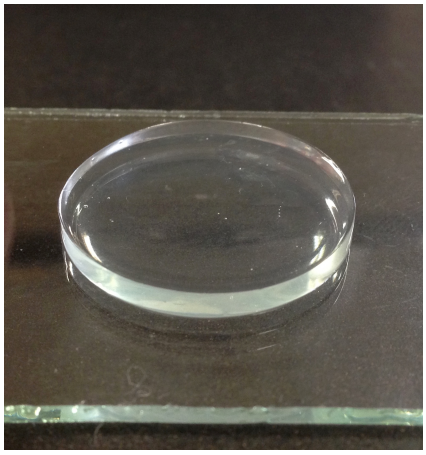

Fig.2

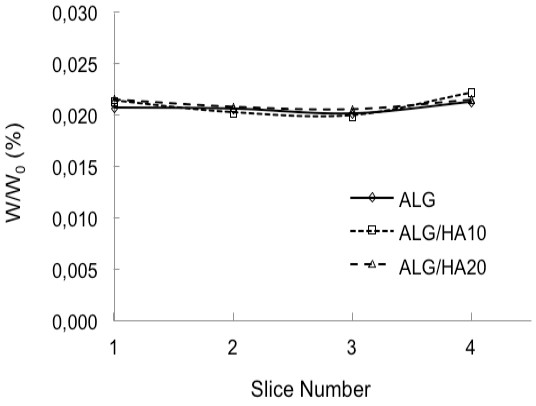

Fig.3

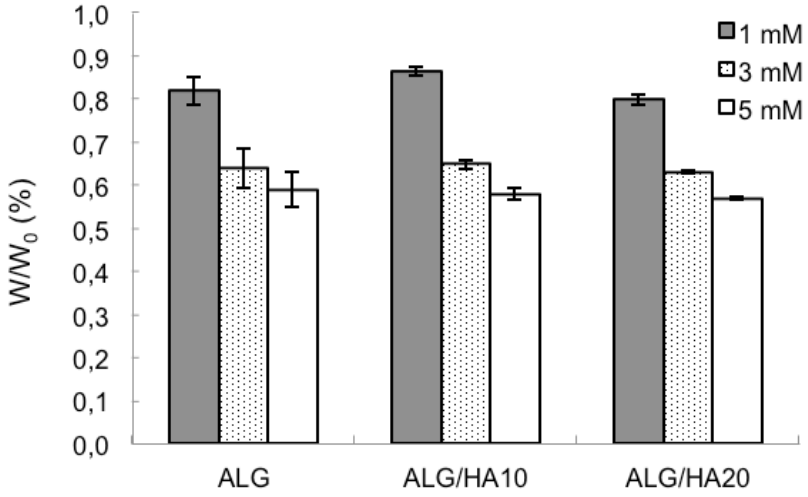

Fig.4

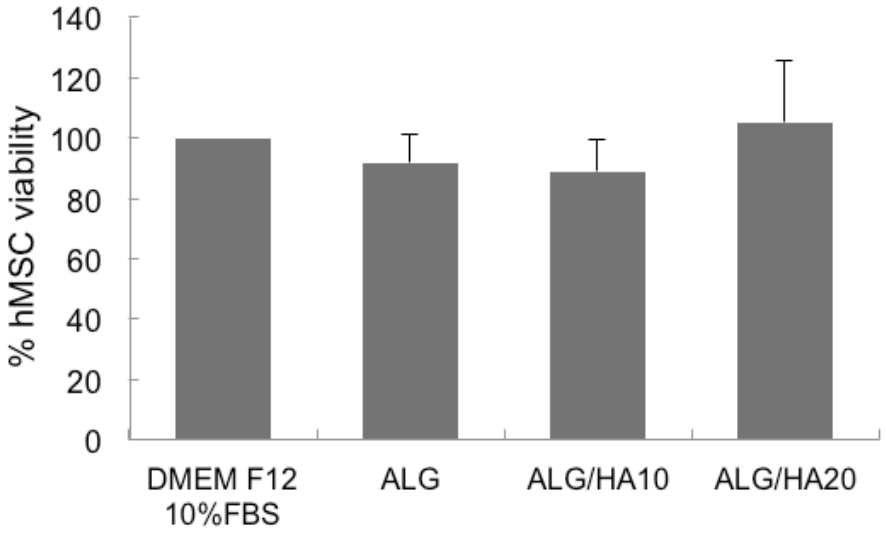
% hMSC viability
140
120
100
80
60
40
20
0
DMEM F12
10%FBS
ALG
ALG/HA10
ALG/HA20

Fig.5

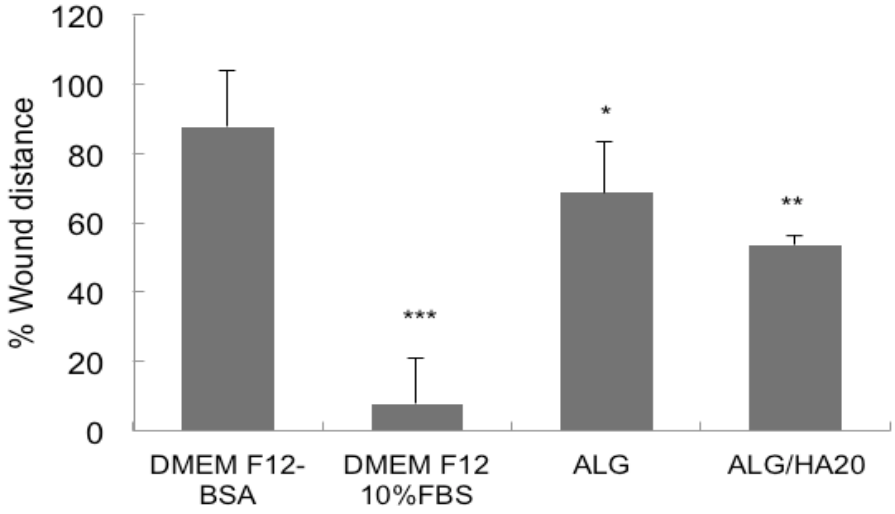
% Wound distance
120
100
80
60
40
20
0
***
*
**
DMEM F12-
BSA
DMEM F12
10%FBS
ALG
ALG/HA20

Fig.6

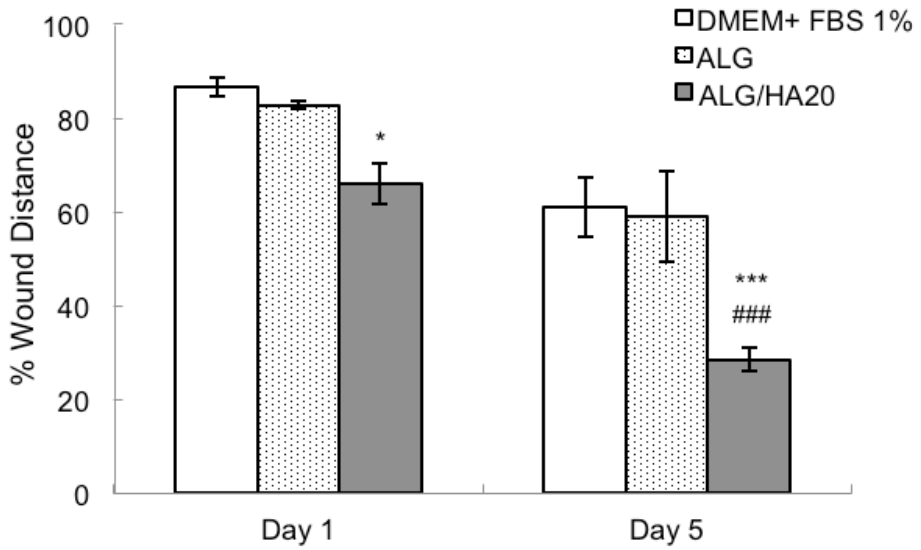
DMEM+ FBS 1%
ALG
ALG/HA20
% Wound Distance
100
80
60
40
20
0
*
***
###
Day 1
Day 5

Fig.7

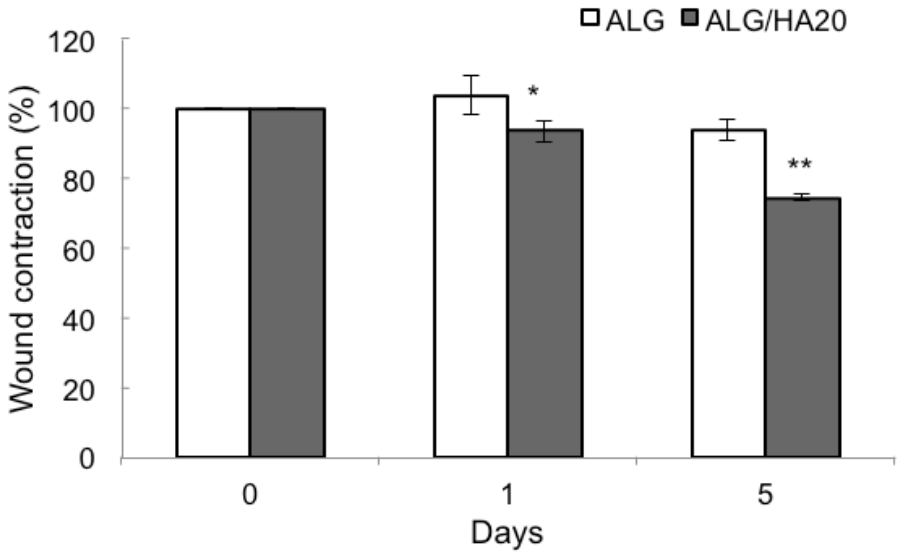
ALG
ALG/HA20
Wound contraction (%)
120
100
80
60
40
20
0
*
**
0
1
5
Days

Fig.8

Glucose-induced ccl5 release by human adipocytes promotes breast cancer invasiveness and distant metastasis

D'Esposito V, Liguoro D, Ambrosio MR, Cantile M, Collina F, Beguinot F, Di Bonito M, Franco R, Formisano P.

Type 2 diabetes (T2D) is associated with an excess risk of incidence and mortality for overall and a number of site-specific cancers. Women with (versus without) diabetes have a statistically significant 20% increased risk of breast cancer. Additionally, the patients with breast cancer and preexisting diabetes had an increased risk for distant metastasis and for all-cause mortality compared with their nondiabetic counterparts. Breast cancer grows and metastasizes to a predominantly adipocyte-dominated host environment. T2D associated derangements induce adipocyte alterations leading to an imbalanced adipokine production that in turn may promote cancer phenotypes. We have studied the mechanisms by which adipocytes integrate inputs from T2D-associated alterations and promote breast cancer cell motility and invasiveness. We have obtained evidence that human adipocytes grown in 25 mM glucose, a concentration corresponding to hyperglycemia in humans, significantly induced breast cancer cell proliferation, migration and invasion. Screening of several cytokines revealed that adipocytes cultured in high glucose medium (25 mM) released 1.5 and 2-fold higher amount of IGF1 and CCL5, respectively, compared to those cultured in low glucose medium (5.5 mM glucose). Moreover, adipocyte-released factors controlled IGF1, but not CCL5 expression in cancer cells. Inhibition of IGF-1 pathway almost completely prevented the effect of adipocytes on breast cancer cell growth but only slightly interfered with cancer cell motility. At variance, inhibition of CCL5 action by specific peptides and antibodies significantly reduced adipocyte promoting effect on breast cancer cell migration and invasion. Interestingly, CCL5/RANTES expression in peritumoral adipose tissue of women with Triple Negative Breast Cancer correlated with lymph node (p-value = 0.04)

and distant metastases (p-value=0.001). A positive trend with the presence of T2D was also observed. Finally, Kaplan-Meier curves showed a significant negative correlation between CCL5 staining in the peritumoral adipose tissue and overall survival of patients (p-value= 0.039). Hence, hyperglycemia induces adipocyte release of CCL5 that, in turn contributes to cancer cell motility, cancer lymph node and distant metastases, reducing the overall survival of patients.

New insights into PPARG regulation: the unexplored impact of alternative splicing on its function

Aprile M., Ambrosio M.R., D'Esposito V., Formisano P., Ciccodicola A., Costa V.

PPARγ is the most studied member of PPAR family. This nuclear receptor is a ligand-dependent transcriptional factor regulating the expression of a wide number of target genes. It represents the master regulator of adipocyte differentiation and metabolic processes. Indeed, defects in PPARγ signaling are implicated in metabolic syndrome and its complications. PPARγ synthetic ligands (including the class of thiazolidinediones) are used to treat hyperlipidemia and as insulin-sensitizing antidiabetic agents, although they produce adverse side effects. The existence of different isoforms, combined to the wide number of potential ligands, coregulators and target genes, determines the complexity of PPARγ biological role. In addition, by different promoter usage and alternative splicing the human PPARG gene generates at least four canonical transcript variants encoding two proteins, PPARγ1 and PPARγ2. Therefore, different PPARG splice variants encode the same protein isoform and, their differential spatial/temporal expression may reflect a different regulation, translation, mRNA stability and/or localization. To complicate the picture, the recent identification of γORF4 isoform – able to act as dominant-negative and with a tumorigenic effect – strengthen the hypothesis that PPARγ activity is modulated through transcript-specific regulation. However, the regulation of human PPARG gene – particularly through alternative splicing – still represents an unexplored aspect of PPARγ signalling. We identified, in normal cells and tissues, a new PPARG isoform, named γΔ5, that lacks the entire ligand binding domain. Similarly to γORF4 isoform, γΔ5 shows a reduced transactivation ability and an inhibitory activity toward PPARγ transcriptional activity. Whole-transcriptome analysis of cells overexpressing

γΔ5 revealed that this physiologically transcribed dominant negative isoform alters the expression of PPARγ target genes. The translation of protein isoforms lacking the ligand-binding domain, causing a reduction in the levels of functional PPARγ protein and a simultaneous increase in the levels of proteins with dominant negative effect, may be a new mechanism in self-regulatory loop of PPARγ activity. Interestingly, the activation of this negative-feedback on PPARγ activity could potentially determine unwanted side effects of the thiazolidinediones. Furthermore, the increased levels of γΔ5 mRNAs in patients with impaired glucose tolerance or type 2 diabetes suggest that they may contribute to the onset or worsen diseases in which PPARG is involved. This effect may be caused by a wide deregulation of alternative splicing mechanism in pathological conditions, that in turn may have a dramatic impact on PPARγ function. Targeted studies will potentially lead to refine the current therapies for metabolic syndrome and related complications, in which this gene is crucially involved.